

Université Joseph Fourier - Grenoble I
ECOLE DOCTORALE DE PHYSIQUE

THÈSE

présentée pour obtenir le titre de

Docteur en Sciences de l'Université Joseph Fourier

Spécialité : Physique théorique

par

Rimantas LAZAUSKAS

Etude de la diffusion de particules lourdes
sur des systèmes atomiques et nucléaires

Date de soutenance : 13 octobre 2003

Composition du Jury

J.	CARBONELL,	Directeur de Thèse
D.	DELANDE,	Examinateur
C.	GIGNOUX,	Co-directeur de Thèse
W.	GLÖCKLE,	Rapporteur
J.M.	RICHARD,	Président
M.	VIVIANI,	Rapporteur

Thèse préparée au sein de Laboratoire de Physique Subatomique et de Cosmologie
53, Avenue des Martyrs
38026 Grenoble Cedex

Remerciements

Je voudrais exprimer ma gratitude distinguée au personnel du LPSC et surtout aux membres du groupe de physique théorique qui m'ont accueilli et qui m'ont entouré d'une chaleur maternelle pendant mes trois années de thèse. Grâce à eux je me suis beaucoup enrichi sur le plan professionnel, mais aussi sur le plan humain.

Merci à mes tuteurs J. Carbonell et C. Cignoux pour leur patience et pour le nombre illimité d'heures qu'ils m'ont consacrées en me guidant dans les jungles de la science. Si cette thèse apporte des idées originales, je peux assurer que 99% d'entre elles appartiennent à Jaume et à Claude. J'ai eu beaucoup de chance de travailler avec Jaume. Son talent pédagogique m'a permis d'apprendre beaucoup, car son extraordinaire intuition physique m'a guidé vers des chemins scientifiques peu explorés et très prometteurs. Grâce à sa curiosité et sa vivacité, ce manuscrit de thèse inclut des discussions sur divers phénomènes physiques. D'un autre côté j'ai énormément profité en travaillant avec Claude. J'ai très vite compris que tous les problèmes difficilement résolubles ont la solution unique : "Il faut appeler Claude..."

J'exprime ma gratitude spécialement à Anne Delage-Wolfers, qui était la première à lire ce manuscrit, alors qu'il se trouvait dans un état très barbaresque et très peu compréhensible. Avec beaucoup de patience et de soin elle a corrigé de nombreuses fautes d'orthographe, de même qu'elle a réussi à polir son style très pointu.

Finalement je remercie les membres du jury d'avoir accepté d'évaluer ce travail de thèse : J. Carbonell, C. Gignoux, W. Glöckle, J.M. Richard, D. Delande et M. Viviani. Mes remerciements particuliers sont destinés aux rapporteurs W. Glöckle et M. Viviani qui ont eu beaucoup de courage d'accepter de lire mon manuscrit dans son état très raboteux et surtout pour leurs précieuses remarques.

Enfin, mes salutations au collectif des doctorants et à notre fameuse équipe de foot, équipe portant en elle un talent énorme lorsqu'il s'agit de perdre les matchs. Merci à vous, mes amis Rémy, Damian, Marciano, Rasa et Nico...

Contents

1 Formalism of a few-body scattering problem	9
1.1 Two-body scattering	9
1.1.1 Lippmann-Schwinger equation	11
1.1.2 Partial-wave series	12
1.1.3 The Coulomb problem	14
1.1.4 Integral representation of the phase shifts	15
1.1.5 Effective-range theory	16
1.1.6 Zero energy scattering	18
1.1.7 Integral representations of the scattering lengths	19
1.2 Basic concepts of a few-body problem	21
1.2.1 Multiparticle partitions. Jacobi coordinates	21
1.2.2 Faddeev equations	25
1.2.3 Faddeev-Yakubovsky equations	27
1.2.4 Identity of particles	29
1.2.5 Partial wave decomposition	31
1.3 Numerical Realization	39
1.3.1 Piecewise spline method	39
1.3.2 Numerical methods of linear algebra problems	44
1.3.3 Tensor inversion	52
2 Three-Body Coulomb Scattering	59
2.1 Merkuriev equations	62
2.2 Bound state calculations	66
2.2.1 Numerical tests	66
2.2.2 Results for X^+ -H system	67
2.3 Scattering problem	71
2.3.1 Modified boundary conditions	71
2.3.2 Synthesis of results	74
2.3.3 p ⁺ -H elastic scattering	79
3 Clusters of neutrons	93
3.1 Nucleon-nucleon interaction models	93
3.2 On the existence of bound neutron clusters	98
3.2.1 What do we know?	100
3.3 Borromean effect	101
3.4 Some results	104
3.4.1 Importance of \mathcal{P} -waves	108
3.4.2 Many nucleon force	111

3.5 Atomic ${}^3\text{He}$ against the neutrons	115
4 Four nucleon continuum states	125
4.1 Introduction	125
4.2 Coulomb interaction	128
4.3 Separating ${}^4\text{He}$ channels in the isospin formalism	130
4.4 Convergence	132
4.5 $n+{}^3\text{H}$ elastic cross sections	138
4.6 $p+{}^3\text{He}$ low energy scattering	144
4.7 $p+{}^3\text{H}$ scattering at very low energies	148
A Often used notations and abbreviations	163
B Transformation of Jacobi coordinates in arbitrary 4-body systems	167
B.1 Transformation between K -type coordinate sets	168
B.2 Transformation between H -type coordinate sets	169
B.3 Coordinate transformation between H and K Jacobi bases	169
C Three-body operators	171
C.1 Three-body transformation operator \hat{h}	171
C.2 Expectation value operator W	173
C.3 Case of the identical particles	174
D Four-body operators	175
D.1 Four-body basis transformation operators	175
D.1.1 Matrix elements of three-body permutation operator $\langle \alpha xyz P^+ \alpha' x' y' z' \rangle$	175
D.1.2 Permutation matrix $\langle \alpha xyz Q \alpha' x' y' z' \rangle = \langle K \varepsilon P_{34} K \rangle$ elements	176
D.1.3 Permutation operator $\langle \alpha xyz \tilde{P} \alpha' x' y' z' \rangle = \langle \alpha xyz P_{13} P_{24} \alpha' x' y' z' \rangle$	177
D.1.4 Transitions between the bases K and H	177
D.2 Double operators	178
D.2.1 Permutation operator $\langle H P^- Q P^- K \rangle = \langle H P_{13} P_{24} K \rangle$	179
D.2.2 Double operator $\langle \alpha xyz P^+ Q \alpha' x' y' z' \rangle = \varepsilon \langle \alpha xyz P_{12} P_{23} P_{34} \alpha' x' y' z' \rangle$	179
D.2.3 Double operator $\langle \alpha xyz P^+ \alpha' x' y' z' \rangle = \langle \alpha xyz P_{12} P_{23} \alpha' x' y' z' \rangle$	180
D.3 Four body W operators	181
E Spline interpolation	183
F Passing to spherical coordinates	187
G Implementing three-body force	191
G.1 Modified FY equations	191
G.2 Implementing UIX forces	192
G.2.1 Urbana IX model	192
G.2.2 Practical implementation	192
G.2.3 Explicit form of matrix elements	194
H The Scattering amplitude	197

Introduction en français

Ce travail de thèse s'inscrit dans le cadre de ce que l'on appelle la "Few-Body Physics", que l'on peut traduire par "Physique à petit nombre de corps". Elle a comme ambition d'obtenir les solutions exactes, au sens numérique, des problèmes quantiques "simples", la notion de "simplicité" ayant comme frontière – mobile! – le nombre de corps que l'on sait traiter au moment où on l'utilise.

Dans une vision un peu simplifiée de la physique théorique, la "Few-Body Physics" serait le partenaire exclusif de la "Many-Body Physics", approche complémentaire qui, consciente de la difficulté de la tâche au delà du problème à deux corps, renonce dès le départ aux solutions exactes et se donne comme but l'élaboration de modèles pertinents à une domaine de la phénoménologie.

Pour obtenir les solutions des équations de la Mécanique Quantique, le formalisme usuel de l'équation de Schrödinger est insuffisant. Il patit de plusieurs anomalies d'ordre formel ou/et pratique. Par exemple l'impossibilité de décrire avec une seule équation toute la riche variété des comportements asymptotiques que la physique autorise à partir de $N = 2$. Ou encore l'existence de solutions parasites pour les problèmes de diffusion. Le cadre formel adéquat a été établi par Faddeev pour un nombre de corps $N=3$ et fut ensuite étendu par Yakubovsky au cas N quelconque. Il offre une formulation mathématique rigoureuse du problème avec quelques questions qui demeurent ouvertes dans le cas des réactions de "break-up" coulombien, e.g. $e^- + H \rightarrow e^- + e^- + p^+$.

La Few-Body Physics est **par essence pluridisciplinaire**. Son domaine d'application, couvre différentes branches de physique atomique, moléculaire, nucléaire et hadronique. Branches dont les frontières n'existent, dans la majorité des cas, que pour satisfaire des besoins administratifs. Lorsque l'on étudie l'interaction forte nucléon-nucléon à 1 MeV, la répulsion coulombienne modifiera de façon substantielle les résultats; si l'on continue à descendre en énergie ce sont les incontournables électrons de la cible d'hydrogène qui vont déterminer le processus donnant lieu à des phénomènes très intéressants, de nature purement atomique, mais qui n'ont pas de ce seul fait pu arrêter notre curiosité. Par ailleurs, l'étude de la diffusion des anti-neutrons sur des cibles de deutérium peut tout aussi bien porter l'étiquette "Few-Body", "Nucléaire" ou "Antiprotons".

Ce mémoire présente donc tout naturellement plusieurs aspects de cette activité pluridisciplinaire. Son contenu est le reflet des aléas que le métier de chercheur comporte si l'on se donne comme objectif principal celui d'être attentif aux différentes voies de la découverte. Ils nous ont

mené à considérer des problèmes atomiques et moléculaires avec une attention bien plus grande que celle initialement prevue; puis des problèmes nucléaires dans un domaine – celui des clusters de neutrons – que l'on n'avait pas du tout envisagé au départ de ce travail. Son commun dénominateur reste notre attachement constant aux **solutions exactes de la Mécanique Quantique dans sa formulation non relativiste**.

Bien qu'il soit souvent question d'états liés, la thèse a été intitulée "**Diffusion de particules lourdes sur des systèmes atomiques et nucléaires**". Nous voulons signifier ainsi l'intérêt spécial que nous portons aux calculs des processus de diffusion. En effet, notre savoir faire actuel dans les problèmes de diffusion est limité à $N=4$. Il faut toutefois signaler que si l'on abandonne les techniques "analytiques" au bénéfice des calculs Montecarlo l'on peut accéder aux états liés de systèmes pouvant aller jusqu'à $N=12$. D'autre part, si l'on considère des systèmes purement coulombiens – comme en physique atomique ou moléculaire – le cas $N=3$ semble déjà extrêmement compliqué, avec des processus qui ne sont pas encore bien résolus ("break-up" coulombien).

Dans le **premier Chapitre** j'ai présenté un resumé des aspects formels et numériques permettant la résolution des équations pour les systèmes à $N=2,3,4$ corps en interaction. Elle contient des parties originales en ce qui concerne le traitement des forces à plusieurs corps et l'inclusion des forces de longue portée pour $N=3$ et 4. C'est une partie essentielle qui a été complétée par des nombreux appendices en fin du manuscrit.

Le **Chapitre 2** est consacré à l'étude de la diffusion purement coulombienne d'une particule lourde (comparée à l'électron) chargée positivement (X^+) sur un atome d'hydrogène (H). C'est la suite de mon travail de DEA. Il s'est avéré suffisamment fertile pour qu'il justifie une attention prolongée. Il aurait même pu faire l'objet de la thèse toute entière, au vu de l'intérêt des résultats obtenus et de tous les aspects qui n'ont pas encore pu être traités.

Cet étude permet aussi de comprendre l'influence des électrons de la cible – forcement atomique – lors des réactions nucléaires à la limite d'énergie nulle. Lorsque les énergies incidentes sont comparables aux énergies électroniques, le processus de diffusion est fortement influencé par la présence des électrons. Ses excitations virtuelles, dues à l'approche d'un projectile chargé, se traduisent par des forces $X^+ - H$ de longue portée et attractives qui génèrent une famille d'états liés et résonances et déterminent les propriétés de diffusion à basse énergie. Le cas que nous avons considéré est, malgré sa simplicité, le système le plus complexe que l'on puisse traiter exactement avec les techniques actuelles.

Nous avons étudié les propriétés de ces états en fonction de la masse m_X du projectile et mis en évidence l'existence d'un spectre très riche dont la complexité augmente avec m_X . Les valeurs correspondantes aux cas physiques ont fait l'objet d'une étude plus détaillée. Nous avons obtenu des prédictions pour les longueurs de diffusion des cas $\mu - H, \pi - H, p - H$ ainsi que des nombreuses résonances étroites dans différentes ondes partielles élevées.

Nous avons aussi prédit l'existence d'un nouvel état de l'ion moléculaire H_2^+ . Son énergie de liaison est extrêmement faible ($B \sim 10^{-9}$), ce qui se traduit par une longueur de diffusion $p - H$ de 750 a.u., valeur enorme qui conditionne toute la diffusion $p - H$ à très basse énergie. Un proton qui s'approche très lentement d'un atome d'H se comportera ainsi comme un objet de taille nanoscopique!

L'existence de cet état peut être déterminante pour expliquer l'abondance d'H moléculaire dans l'espace interstellaire. En effet son taux de formation par $e + H_2^+ \rightarrow H_2 + \gamma$ est déterminé par l'abondance de l'ion moléculaire H_2^+ , à son tour fortement dépendant du taux de réaction $p + H \rightarrow H_2^+ + \gamma$.

Il est remarquable que ce système, le plus simple après l'atome d'H, puisse encore produire de nouveaux résultats surprennantes. Nous voudrions rappeler¹ que l'ion moléculaire H_2^+ fit déjà l'objet au début du XX^{eme} siècle du travail de thèse de W. Pauli. Rappelons aussi, pour le plaisir de l'anecdote, que ce remarquable physicien conclut à l'impossibilité qu'un tel système puisse former des états liés. A tort ! ... il a, en fait, une vingtaine d'états liés (pour l'onde S seulement) et nous venons d'en découvrir un de nouveau. Ceci illustre la difficulté et la richesse du problème à trois corps, surtout lorsque des forces de longue portée sont en jeu.

Ces prédictions constituent des premières. Leur confirmation expérimentale s'avère être, autre nécessaire, très intéressante. Si une mesure directe de la section efficace pH à très faible énergie semble peu vraisemblable avec les techniques actuelles, on peut cependant accéder au continuum pH dans l'état final de la photodissociation de H_2^+ .

Le **Chapitre 3** est consacré à l'étude des systèmes de neutrons. Il a été motivé par l'annonce faite au GANIL [2] d'une possible mise en évidence d'un état lié à 3 ou 4 neutrons grâce à ses faisceaux de noyaux exotiques. Cette nouvelle récente remet en cause un certain nombre de résultats obtenus précédemment et relance l'intérêt, expérimental et théorique, dans l'étude d'un tel système. Nous nous sommes engagés dans un programme de recherches dont le but fut d'étudier dans quelle mesure les dernières versions des potentiels nucléon-nucléon qui brisent l'indépendance de charge, sont compatibles avec l'existence de tels objets, ainsi que d'étudier ses propriétés éventuelles (durée de vie, etc.) Il ne semble pas actuellement que les seules forces à deux corps neutron-neutron soient suffisantes à assurer sa liaison. Il faut pour cela faire appel aux forces à trois nucléons, indispensables pour reproduire l'énergie de liaison de la particule α .

Nous avons voulu mener cet étude en parallèle avec celui des atomes d'hélium 3 – un système fermionique similaire – et d'envisager la possibilité de structures plus grandes.

Finalement, le **Chapitre 4** contient ce qui aurait du constituer le corps principal de ce travail et qui en fut son point de départ. Il s'agit de la diffusion dans les systèmes à 4 nucléons.

¹voir e.g. le livre de Gutzwiller [1]

Après l'obtention, relativement récente, des résultats convergés pour l'état lié du noyau de ${}^4\text{He}$ [3] et les calculs Montecarlo de noyaux jusque $A=12$ [4, 5, 6], l'enjeu dans cette physique est la maîtrise du spectre continu. Celui-ci est particulièrement riche dans le cas $A=4$. Il représente, avec ses multiples résonances et seuils, une transition entre la relative simplicité des cas $A=2,3$ et la complexité des "vrais" noyaux. Il constitue en outre un sérieux défi pour l'approche traditionnelle de la physique nucléaire. On sait en effet, et c'est l'un des résultats majeurs de la Few-Body Physics, que le meilleur des potentiels NN est incapable de reproduire l'énergie de liaison du noyau de ${}^3\text{H}$. On s'en sort en invoquant l'existence des forces à trois corps (TNI) et, comme il s'agit de reproduire un nombre, il n'est pas étonnant d'y parvenir lorsque les forces invoquées disposent d'un ou plusieurs paramètres libres. Une force à trois corps bien paramétrée peut même arranger simultanément le manque de liaison pour $A=3$ et $A=4$.

Mais la grande nouveauté du cas $A=4$ est que lorsque l'on quitte l'énergie nulle, la physique est loin d'y être triviale. Il n'est pas du tout certain que le cadre conceptuel décrivant le noyau comme un ensemble de nucléons ponctuels intéragissant par un potentiel, soit encore valable dès que l'on atteint ce seuil.

Ainsi nous avons considéré par ordre de difficulté croissante les systèmes $n+{}^3\text{H}$, $p-{}^3\text{He}$ et $p-{}^3\text{H}$. Le cas $n+{}^3\text{H}$ est un état pur d'isopin $T=1$, sans la complication coulombienne, mais présente une résonance à basse énergie – la première résonance de la physique hadronique – que des travaux précédents ont eu beaucoup du mal à décrire. Nous avons considéré ensuite son partenaire "miroir par rapport à T_3 " et obtenu les observables de diffusion à basse énergie. Enfin le cas $p+t$ qui contient un couplage de deux états d'isospin et dont l'amplitude de diffusion est fortement déterminée par l'existence de la première excitation du noyau de ${}^4\text{He}$, qui se trouve expérimentalement seulement quelques 300 keV au dessus du seuil. **Nos calculs de diffusion à 4N sont pionniers dans ce domaine.**

La maîtrise des techniques Few-Body est difficile. Mais il est aussi difficile de pouvoir se passer en physique du contenu mathématique des solutions des équations que nous prétendons être les bonnes. Nos intuitions restent bien souvent en deca de ce que les solutions contiennent.

Les choses absolument nécessaires ne rentrent pas dans la catégorie des modes scientifiques. Ils n'ont pas lieu d'être à la mode car son intérêt est constant vital. Nous espérons contribuer modestement à depoussiérer cette évidence tout au long de ce travail.

Overview

Introduction

The most important experimental technique in quantum physics is the scattering experiment. Particle scattering experiments preceded such fundamental discoveries as atomic, nuclear, quark structure of the matter and determined the basic particle interaction properties as well. Scattering theory (theory describing particle collision experiments) is very rich in physical phenomenon and along further discussion one should recognize various possible divisions of the subject. In the first place there are the non-relativistic and relativistic theories. Second, there are the single-channel and multichannel parts of the theory. And third, there are time-dependent and time-independent parts. In this thesis only non-relativistic stationary scattering systems will be treated.

Practically, throughout whole physics, an understanding of the properties of the physical system is achieved by succeeding to represent the composite system as a one-body system. Examples of such reductions are the Hartree-Fock equations and the method of quasi-particles, Chew-Low equations in the field-theory describing πN interaction. However, attempts to achieve such simplified description are not always successful. The reason is that multiparticle systems may possess qualitative peculiarities going far beyond the simple one particle picture. Some examples of such properties are

1. The so-called Efimov effect [7] for a system of three particles interacting via short range potentials and when a system of two such particles has a bound state of zero (or close to zero) energy. In this case a situation can arise in which the levels of the system are pushed out of the potential well as its depth increases. Being in full contrast with the two-body case.
2. The Thomas effect [8]. The collapse occurring in a system of three particles interacting through a pair δ -like potentials. One can note that in two-particle systems nothing of the sort happens.
3. Off-mass-shell characteristics of the pair T-matrix, indicating that for a complete description of a system, consisting of three or more particles, it is not sufficient to know only the two-body scattering phases (or on-shell T matrix). Here one finds need to use new properties of pair interaction that are not observed in two-body problem.

On the other hand, in atomic-, nuclear- and elementary-particle physics a large number of states

and processes exist which need to be treated as a three- (four-) particle system. Such necessity occurs either when two-body experiments are not accessible or when exact treatment of the problem is required. Here are a few examples:

1. The scattering of electrons and other charged particles by hydrogen atoms. Such a system presents the simplest possible experimental setup for testing the Coulomb interactions at Rydberg energies.
2. Muonic, pionic atoms in order to study muon(pion) catalyzed fusion.
3. Propagation of antiprotons in gaseous media, their absorption by simplest neutral atomic systems (H and He).
4. To test the charge symmetry and isospin invariance of nuclear forces one needs data of neutron-neutron interaction. However, direct neutron-neutron scattering experiments are not available. Thus, one can attain this information only by treating the system of three and more nucleons.
5. Presence of collective forces between the nucleons, which appear only when more than two particles interact together. Existence of three-body, four-body nuclear forces.
6. Break-up reactions. Multichannel scattering.

All physical systems discussed above need the formalism of few-body scattering problem.

Layout

This thesis contains three chapters supported by the appendices. The first chapter is devoted to discuss the work underlying theory. The three following chapters employ theoretical ideas in practice by exploring real physical systems.

I will give a short description of their contains:

Chapter 1 reminds the basics of 2-body non-relativistic time-independent scattering theory. This theory is supplemented to treat three and four particle scattering as well as bound states. Corresponding three and four-body equations are developed in section 1.2.

Obtained equations are multidimensional coupled integro-differential equations. Their solution requires the application of powerful numerical methods. First differential equations are discretized using "the spline method", transforming them into corresponding linear algebra problem. However, resulting linear algebra systems are of very large size and still demand very special numerical treatment to be solved. Numeric technique related issues conclude the chapter of the formalism.

Chapter 2 deals with quantum three charged particle scattering. In particular, heavy positive charge particle (including e^+ , μ^+ , π^+ and p^+) scattering is studied on atomic hydrogen at energies below the first rearrangement and inelastic threshold. Predictions for the corresponding scattering lengths have been obtained.

Hence standard 3-body equations, as formulated by Faddeev[9], suppose particles interacting via short-range forces. Therefore they are not appropriate, when one deals with charged particles. The difficulty is overcome by reformulating these equations to treat Coulomb interaction in Merkuriev proposed way [10].

The most intriguing behavior is exhibited in $p^+ + H$ elastic scattering. Enormously large low energy scattering length found in this system have permitted to show the existence of weakly bound first excited H_2^+ σ_u symmetry state, as well as predict its binding energy. The H_2^+ formation rate, as well as the subsequent abundance of H_2 molecules, can be substantially influenced by this resonant p-H cross section.

Chapter 3 tries to discuss the possibility of the eventual existence of bound multineutron clusters. This work was inspired by the recent experiment at GANIL [2, 11], which once again raised doubts if bound few neutron systems can be formed. The most promising structure is the tetraneutron (bound state of 4 neutrons).

The aim of this chapter is to answer whether such systems (trineutron, tetraneutron) are compatible with our current knowledge of strong interaction, and what necessary corrections should be made to permit such an existence. Sensibility of ($n=2, 3, 4$) neutron systems to various modifications in nucleon-nucleon force have been studied, as well as effects of 3-4 Nucleon forces.

Neutron systems have been compared to other fermion system having resembling interaction, however eventually forming bound multifermion clusters (namely with clusters of He_3 molecules).

Chapter 4 deals with four nucleon elastic scattering problem. Three- and four-nucleon systems are the testing ground for studying the nuclear interaction. Whereas four-nucleon continuum states, being a challenge at present for few-body community, remains very scarcely explored. This study contributes to fill up this gap.

In order to treat all three experimentally available four-nucleon systems (namely $n-^3H$, $p-^3He$ and $p-^3H$) rigorously, Faddeev-Yakubovski equations have been modified to include Coulomb interactions. Eventual calculations were performed using semi-realistic and realistic nucleon-nucleon interaction models and also in conjunction with three nucleon force.

Chapter 1

Formalism of a few-body scattering problem

The formalism of three- and four-body scattering includes all the concepts of the two-body problem. Their basic ideas are shortly reviewed in the following section. For a more complete discussion, one could refer to classic textbooks like [12, 13, 14].

However, the general few-body problem goes far beyond the "ordinary" two-body scattering theory. One should recall that equations of motion for more than two particles are not integrable in the general case: Lippmann-Schwinger equation does not lead to one unique solution. Nevertheless this problem can be fixed by imposing mathematically rigorous constraints on the solution, which ensures correct boundary conditions. The underlying theory for three-particle scattering with short range interactions was formulated by L.D. Faddeev in 1960 [9]. Later on, this theory was generalized by O.A. Yakubovski [15] to any number of particles. Formalism developed by L.D. Faddeev and O.A. Yakubovski will be discussed in section 1.2. Finally, to put these ideas in practice, one should be able to solve the resulting integro-differential equations. In the general case, these many-dimensional equations do not have analytic solutions. In order to solve them, one should apply powerful numerical methods. The later issue will conclude this chapter.

1.1 Two-body scattering

Scattering experiments at the (sub)atomic level are performed by using particle sources and detectors which are both located at large (macroscopic) distances from the scattering region. The observed particles must be considered as propagating freely, i.e. with a motion governed by the free rather than the full Hamiltonian. Consequently, an experiment supplies data describing a relationship between free (or asymptotic) incoming and outgoing states, which can be expressed in the following way:

$$|\psi_{out}\rangle = S|\psi_{in}\rangle, \quad (1.1)$$

where S is quantum-mechanical scattering operator. A satisfactory scattering theory must be able to mimic this situation.

The starting point for developing our formalism is the time dependent Schrödinger equation:

$$i\hbar \frac{\partial}{\partial t} |\psi_t\rangle = H|\psi_t\rangle. \quad (1.2)$$

The general solution of this equation can be formally written in the form

$$|\psi_t\rangle = U(t)|\psi\rangle \equiv e^{-\frac{i}{\hbar}Ht}|\psi\rangle$$

where $U(t)$ is the so-called evolution operator. Let us suppose that the state $U(t)|\psi\rangle$ describes the evolution of some scattering experiment. By following this state back to a time well before the collision, one should trace the behavior of a free wave packet, described by the free evolution operator $U^0(t) \equiv e^{-\frac{i}{\hbar}H_0t}$, and thus expect:

$$U(t)|\psi\rangle \xrightarrow[t \rightarrow -\infty]{} U^0(t)|\psi_{in}\rangle. \quad (1.3)$$

Similarly, long after the collision, particles move freely and one expects:

$$U(t)|\psi\rangle \xrightarrow[t \rightarrow +\infty]{} U^0(t)|\psi_{out}\rangle. \quad (1.4)$$

This procedure can be successful only if there is a strict relation between incoming and outgoing states. In other words for any in- and any out- asymptote there exists one and only one state associated with them, and *vice versa*. It can be shown that for smooth, short ranged and – at the origin – non singular potentials, these conditions are satisfied¹. Once the strong limits for eq. (1.3-1.4) are satisfied², they guarantee the existence of the so-called Møller wave operator Ω_{\pm} :

$$\Omega_{\pm} = \lim_{t \rightarrow \mp\infty} U(t)^{\dagger} U_0(t). \quad (1.5)$$

The Møller operators are limits of the unitary operators and relate the asymptotes to the actual scattering states:

$$|\psi\rangle = \Omega_{+}|\psi_{in}\rangle = \Omega_{-}|\psi_{out}\rangle. \quad (1.6)$$

Since Møller operators are isometric they can be inverted to express Scattering operator:

$$S = \Omega_{-}^{\dagger} \Omega_{+}, \quad (1.7)$$

which on its turn is unitary. Its action on incoming plane wave can be expressed as a sum of free (non scattered) and scattered wave propagating from the center of interaction. In momentum space one has:

$$\langle \vec{k}' | S | \vec{k} \rangle = \delta(\vec{k}' - \vec{k}) - 2\pi i \delta(k'^2 - k^2) t(\vec{k}', \vec{k}). \quad (1.8)$$

¹It is worth noticing that Coulomb potential does not satisfy mentioned conditions. It falls too slow to permit asymptotic freedom of the particles and thus requires special treatment.

²In fact, conditions (1.3-1.4) are too weak, since both wave functions $U(t)|\psi\rangle$ and $U^0(t)|\psi_{in(out)}\rangle$ can tend pointwise to zero and in this case one cannot distinguish between different states $|\psi_{in(out)}\rangle$. Therefore, former conditions are reinforced by imposing strong limits for a difference of wave functions, ie: $\lim_{t \rightarrow \pm\infty} \|U(t)|\psi\rangle - U^0(t)|\psi_{in(out)}\rangle\| \rightarrow 0$

In this equation, the delta distributions express conservation of momentum and energy, respectively. The function $t(\vec{k}', \vec{k})$ is also known as the on-shell T-matrix (i.e. transition matrix). It differs from the well-known scattering amplitude $f(\vec{k}', \vec{k})$ only by a trivial factor:

$$f(\vec{k}', \vec{k}) = -\frac{m}{2\pi\hbar^2} t(\vec{k}', \vec{k}). \quad (1.9)$$

From eq. (1.8) one defines *the differential scattering cross section*:

$$\frac{d\sigma}{d\Omega}(\vec{k}', \vec{k}) = |f(\vec{k}', \vec{k})|^2, \quad (1.10)$$

whereas the total scattering cross section can be obtained after integrating over all possible directions of scattered beam:

$$\sigma(\vec{k}) = \int d\Omega_{k'} \frac{d\sigma}{d\Omega}(\vec{k}', \vec{k}). \quad (1.11)$$

1.1.1 Lippmann-Schwinger equation

The expression (1.5) for the Møller operator does not help much, as it stands, because we cannot carry out the time integral for non commuting operators $U(t)^\dagger$ and $U_0(t)$. But, since we are allowed to apply Møller operators on plane waves, we can write:

$$\begin{aligned} |\vec{k}\rangle^\pm &= \Omega_\pm |\vec{k}\rangle = \lim_{t \rightarrow \mp\infty} U(t)^\dagger U_0(t) |\vec{k}\rangle \\ &= \lim_{\varepsilon \rightarrow 0} \pm \frac{\varepsilon}{\hbar} \int_{\mp\infty}^0 dt e^{\pm \frac{\varepsilon}{\hbar} t} U(t)^\dagger U_0(t) |\vec{k}\rangle = \lim_{\varepsilon \rightarrow 0} \pm \frac{\varepsilon}{\hbar} \int_{\mp\infty}^0 dt e^{\frac{i}{\hbar}(H-E\mp i\varepsilon)t} |\vec{k}\rangle \\ &= \lim_{\varepsilon \rightarrow 0} \pm i\varepsilon(E \pm i\varepsilon - H)^{-1} |\vec{k}\rangle. \end{aligned} \quad (1.12)$$

Here we have obtained important relation between the scattering solutions $|\vec{k}\rangle^\pm$ and the resolvent, or Green's function:

$$G(z) = (z - H)^{-1}, \quad (1.13)$$

with $z = E \pm i\varepsilon$ and $E = \frac{\hbar^2 k^2}{2\mu}$, for a system with reduced mass μ . The relation (1.12) marks the transition from time-dependent to time-independent theory. Furthermore, by using the identity

$$G(z) = G_0(z) + G(z)VG_0(z) \quad (1.14)$$

$$= G_0(z) + G_0(z)VG(z), \quad (1.15)$$

with $G_0(z) = (z - H_0)^{-1}$ being the so-called free Green's function, equation (1.12) can be cast in a practical mathematical tool in order to obtain the scattering wave function:

$$\begin{aligned} |\vec{k}\rangle^\pm &= \lim_{\varepsilon \rightarrow 0} \pm \varepsilon [G_0(E \pm i\varepsilon) + G_0(E \pm i\varepsilon)VG(E \pm i\varepsilon)] |\vec{k}\rangle \\ &= |\vec{k}\rangle + G_0(E \pm i0)V|\vec{k}\rangle^\pm. \end{aligned} \quad (1.16)$$

This is the Lippmann-Schwinger (LS) equation, first formulated in [16, 17], for the scattering states $|\vec{k}\rangle^\pm$. The ε -limit, which has to be performed in Green's functions, is indicated by the notation $E \pm i0$. In configuration space representation [14], this limit leads to

$$\langle \vec{r}' | G_0(E \pm i0) | \vec{r} \rangle = -\frac{\mu}{2\pi\hbar^2} \frac{e^{\pm ik|\vec{r}' - \vec{r}|}}{|\vec{r}' - \vec{r}|}. \quad (1.17)$$

The free resolvent $G_0(E)$ has a cut along the positive real E-axis. The ε -limit tells us on which side of the cut we have to stay in order to fulfill the boundary condition. The + sign corresponds to the physical boundary condition.

By writing LS equation in configuration space representation

$$\langle \vec{r} | \psi_{out} \rangle = \langle \vec{r} | \vec{k} \rangle^+ = \langle \vec{r} | \vec{k} \rangle - \int d^3 \vec{r}' \frac{\mu}{2\pi\hbar^2} \frac{e^{\pm ik|\vec{r}' - \vec{r}|}}{|\vec{r}' - \vec{r}|} V(\vec{r}') \langle \vec{r}' | \vec{k} \rangle^+, \quad (1.18)$$

we see that the first term on the right hand side is a plane wave, and the second one is an outgoing spherical wave. The asymptotic conditions for outgoing state follows directly:

$$\psi_{out}(\vec{r}) \xrightarrow[r \rightarrow \infty]{} (2\pi)^{-\frac{3}{2}} \left(e^{i\vec{k} \cdot \vec{r}} + f(k\hat{r}, \hat{k}) \frac{e^{ikr}}{r} \right). \quad (1.19)$$

Here $f(k\hat{r}, \hat{k})$ is recognized as the *scattering amplitude*, which modulates the scattered wave in different directions, and therefore determines the amount of flux going in any direction. Equation (1.19) provides the boundary conditions necessary to uniquely specify the solution of the Schrödinger equation. Therefore one possible method of solving the scattering problem consists in solving

$$\left(-\frac{\hbar^2 \nabla^2}{2\mu} + V(\vec{r}) \right) \psi(\vec{r}) = E\psi(\vec{r}) \quad (1.20)$$

differential equation with eq. (1.19) as boundary conditions.

1.1.2 Partial-wave series

Equation (1.20), derived in preceding section is the proper ground for solving two-body scattering problem. However, in general, it is a three-dimensional and therefore not easy to solve directly.

For spherically symmetric potentials, considerable simplifications can take place. They have the property that the three-dimensional scattering equations reduce to a set of uncoupled one-dimensional equations in the partial-wave basis (PWB). In this case the scattering matrix commutes with both H_0 and \vec{L} (total angular momentum of the system) and therefore is diagonal in the PWB:

$$\langle k' l' m' | S | k l m \rangle = \delta(k' - k) \delta_{l'l} \delta_{m'm} s_l(k). \quad (1.21)$$

Because of unitarity of S-matrix, $s_l(k)$ should be unitary as well and therefore can be written in the following form:

$$s_l(k) = e^{2i\delta_l(k)}. \quad (1.22)$$

The real quantity $\delta_l(k)$ is known as the phase shift. The scattering amplitude $f(\vec{k}', \vec{k})$ can be expanded on the angular momentum basis by using polynomial functions of Legendre:

$$f(\vec{k}', \vec{k}) = \sum_{l=0}^{\infty} (2l+1) f_l(k) P_l(\hat{k}' \cdot \hat{k}), \quad (1.23)$$

whereas its partial-wave components $f_l(k)$ are directly related to the phase shift by

$$f_l(k) = \frac{s_l(k) - 1}{2ik} = \frac{e^{i\delta_l(k)} \sin \delta_l(k)}{k}. \quad (1.24)$$

Since Legendre polynomials are orthogonal functions, the total cross section is a sum of partial-wave cross sections $\sigma_l(k)$:

$$\sigma(k) = \sum_{l=0}^{\infty} \sigma_l(k) = 4\pi \sum_{l=0}^{\infty} (2l+1) |f_l(k)|^2 = 4\pi \sum_{l=0}^{\infty} (2l+1) \frac{\sin^2 \delta_l(k)}{k^2}. \quad (1.25)$$

Further as one develops scattering wave function into spherical waves

$$\psi_{l,k}(r) = \left(\frac{\pi}{2}\right)^{\frac{1}{2}} r \langle rlm | klm+ \rangle, \quad (1.26)$$

and obtains radial Schrödinger equation (1.20) for its components:

$$\left[\frac{\hbar^2}{2\mu} \frac{d^2}{dr^2} - \frac{\hbar^2}{2\mu} \frac{l(l+1)}{r^2} - V(r) + E \right] \psi_{l,k}(r) = 0. \quad (1.27)$$

Boundary conditions are obtained by performing a plane wave decomposition

$$\langle \vec{r} | \vec{k} \rangle = (2\pi)^{-\frac{3}{2}} \frac{1}{kr} \sum_{l=0}^{\infty} (2l+1) i^l \hat{j}_l(kr) P_l(\hat{r} \cdot \hat{k}), \quad (1.28)$$

including them into eq. (1.19) and regrouping the partial components of a given l . Boundary conditions to be implemented in PWB can be rewritten in several useful forms:

$$\begin{aligned} \psi_{l,k}(r) &\xrightarrow[r \rightarrow \infty]{} j_l(kr) + k f_l(k) e^{i(kr - l\pi/2)} \\ &\xrightarrow[r \rightarrow \infty]{} e^{i\delta_l(k)} \sin [kr - l\frac{\pi}{2} + \delta_l(k)] \\ &\xrightarrow[r \rightarrow \infty]{} \frac{i}{2} [\hat{h}_l^-(kr) - s_l(k) \hat{h}_l^+(kr)], \end{aligned} \quad (1.29)$$

where $\hat{j}_l(x)$ is the Riccati-Bessel function and $\hat{h}_l^\pm(x)$ are the Riccati-Hankel functions [18]. The second form of eq. (1.29) reveals the significance of the name phase shift. At large distances, the actual radial function is proportional to the free radial function $\hat{j}_l(kr) = \sin [kr - l\frac{\pi}{2}]$, except that the phase of its oscillations is shifted by an amount $\delta_l(k)$.

Conversely, the last expression is advantageous over the preceding one in the sense that the right-hand side of it is a solution of the free radial Schrödinger equation, which is the form taken by the wave function outside the range of the potential. This allows one to impose a cutoff radius of the order of the potential range, i.e., the differential equation has to be solved only in the interaction region. In what concerns applications of the first form, a very large cutoff radius should have to be used, since the free solutions converge to their asymptotic forms only as slow as $1/kr$.

1.1.3 The Coulomb problem

Up to now in our discussion, we were restricting to short range potentials, i.e. those which for $r \rightarrow \infty$ were falling quick enough to satisfy the strong limits of eq. (1.3) and eq. (1.4). Coulomb potential does not fulfill this condition. The reason is that the $1/r$ potential falls off so slowly that it continues to influence the particles even as they move apart. For instance, a scattering orbit never behaves freely even as $t \rightarrow \pm\infty$ and therefore asymptotic conditions do not hold on. In fact, when $r \rightarrow \infty$ solution of radial Schrödinger equation with $V(r) = Z_1 Z_2 e^2 / r$ potential, has asymptotic form [12, 19]:

$$\psi_{l,k}(r) \underset{r \rightarrow \infty}{\sim} \sin [kr - \gamma \ln 2kr + C], \quad (1.30)$$

where γ is a dimensionless quantity:

$$\gamma = \frac{Z_1 Z_2 \mu e^2}{\hbar^2 k} = \alpha \hbar c \sqrt{\frac{\mu}{2E\left(\frac{\hbar^2}{m}\right)}}, \quad (1.31)$$

μ is the reduced mass of scattered fragment and E - kinetic energy of the system in center of mass frame. One can see solution continuing to pick up phase logarithmically for large r . Therefore to get rid off divergent behavior of wave functions, which is purely due to Coulomb interaction, one separates contribution of short range potential by describing wave function as a superposition of incoming and outgoing Coulomb waves [19]:

$$|\psi_{l,k}(r)\rangle \underset{r \rightarrow \infty}{\longrightarrow} \left[u_l^-(r) - e^{i\delta_l} e^{i\sigma_l} u_l^+(r) \right]. \quad (1.32)$$

Here, δ_l is the phase shift associated with the distortion due to strong interaction, while σ_l – called Coulomb phase shift – is a quantity describing the strength of Coulomb interaction:

$$\sigma_l = \arg \Gamma(l + 1 + i\gamma). \quad (1.33)$$

It is worth noticing that eq. (1.32) is similar to the standard expression of asymptotic wave function for short range potential scattering eq. (1.29). The only difference is that Riccati-Hankel functions $\hat{h}_l^\pm(r)$ are replaced by appropriate Coulomb wave functions $u_l^\pm(r)$. On the other hand, the interpretation of the scattering parameters is not the same. The full scattering amplitude, when Coulomb potential is present, is separated in two terms. One is associated with strong interaction and the other one being the pure Coulomb part. Hence, total cross section now is:

$$\frac{d\sigma(\theta)}{d\Omega} = |f_C(\theta) + f_S(\theta)|^2. \quad (1.34)$$

The strong amplitude partial components are related to strong interaction phase shifts by standard relation, supplemented with additional Coulomb phase:

$$f_{S,l} = \frac{e^{i\delta_l} \sin \delta_l}{k} e^{2i\sigma_l}. \quad (1.35)$$

Complete amplitude in terms of its partial waves reads as

$$f_S(\theta) = \sum_{l=0}^{\infty} (2l+1) f_{S,l}(k) P_l(\cos \theta). \quad (1.36)$$

One can remark that the Coulomb term is non-isotropic and has an angular dependence in the following form:

$$f_C = -\frac{\gamma}{2k \sin^2 \frac{1}{2}\theta} \exp \left[-i\gamma \ln \left(\sin^2 \frac{1}{2}\theta \right) + 2i \arg \Gamma(1 + i\gamma) \right]. \quad (1.37)$$

1.1.4 Integral representation of the phase shifts

Certain properties or methods of calculating the phase shifts may be obtained by starting from their appropriate integral representations. Most of them are obtained by simply applying the Wronskian theorem to suitably defined solutions of corresponding radial equations. These integral methods can be very useful in numerical calculations. Contrary to phases extracted from the asymptotic form of the wave function – eq. (1.29)– their integral representation relies much more on the internal part of the wave function and thus provides an accurate alternative test of results.

We are seeking expression which compares the phase shifts $\delta_l(k)$ and $\tilde{\delta}_l(k)$, corresponding respectively to two different potentials $V(r)$ and $\tilde{V}(r)$ at the same given energy. We designate $\tilde{\psi}_{l,k}(r)$ the regular³ solution of the radial Schrödinger equation

$$\left[\frac{d^2}{dr^2} - \frac{l(l+1)}{r^2} - \frac{2\mu}{\hbar^2} (\tilde{V}(r) - E) \right] \tilde{\psi}_{l,k}(r) = 0, \quad (1.38)$$

while $\psi_{l,k}(r)$ designates the regular solution of the same equation with potential $V(r)$. Regular solutions have asymptotic expression

$$\tilde{\psi}_{l,k}(r) \underset{r \rightarrow \infty}{\sim} \sin \left[kr - l \frac{\pi}{2} + \tilde{\delta}_l(k) \right]. \quad (1.39)$$

The Wronskian $W[\psi_{l,k}(r), \tilde{\psi}_{l,k}(r)]$ is zero at the origin and asymptotically approaches the limit

$$\lim_{r \rightarrow \infty} W(\psi_{l,k}(r), \tilde{\psi}_{l,k}(r)) = k \sin [\delta_l(k) - \tilde{\delta}_l(k)]. \quad (1.40)$$

According to the Wronskian theorem:

$$\begin{aligned} \sin [\delta_l(k) - \tilde{\delta}_l(k)] &= \frac{W(\psi_{l,k}(r), \tilde{\psi}_{l,k}(r))|_0^\infty}{k} \\ &= -\frac{2\mu}{\hbar^2 k} \int_0^\infty \tilde{\psi}_{l,k}(r) (V(r) - \tilde{V}(r)) \psi_{l,k}(r) dr. \end{aligned} \quad (1.41)$$

This important relation is valid for any form of the potentials $V(r)$ and $\tilde{V}(r)$, provided that they vanish at infinity more rapidly than $1/r$ and that they have no singularity as strong as $1/r^2$ at the origin.

For $\tilde{V}(r) = 0$ one has $\tilde{\delta}_l(k) = 0$, whereas the regular solution for the free wave is described by $\tilde{\psi}_{l,k}(r) = \hat{j}_l(kr)$. Therefore eq. (1.41) becomes:

$$\sin \delta_l(k) = -\frac{2\mu}{\hbar^2 k} \int_0^\infty \hat{j}_l(kr) V(r) \psi_{l,k}(r) dr. \quad (1.42)$$

³Solution of the radial equation which vanishes at the origin is called regular. On the contrary, irregular is called the solution which is not zero at the origin.

Equation (1.41) allows to draw some conclusions concerning the effects on the phase shifts when the potential is changing. For infinitesimal changes one can neglect differences between the solutions $\psi_{l,k}(r)$ and $\tilde{\psi}_{l,k}(r)$ in the right-hand side of equation (1.42), whence

$$\Delta\delta_l(k) = -\frac{2\mu}{\hbar^2 k} \int_0^\infty \Delta V(r) \psi_{l,k}^2(r) dr. \quad (1.43)$$

In particular, if the variation of the potential $\Delta V(r)$ has the same sign over the entire interval $(0, \infty)$ the variation of the phase shift $\Delta\delta_l(k)$ has the opposite sign. Hence, any increase of the potential (greater repulsion) reduces the phase shift, while any decrease of the potential (greater attraction) enlarges it. This feature of the phase shifts, generalized for larger particle systems, will be of great service throughout this thesis.

1.1.5 Effective-range theory

The formulae (1.41) allows to study the variation suffered by the phase shift when one modifies the potential while keeping the energy constant. In practice, potentials are usually fixed by the nature of the interacting particles, while one wishes to know the phase shift variation as the function of the energy. It turns to be that in the low energy limit, useful relation can also be established.

We denote by $\phi(r)$ the regular solutions of radial Schrödinger equation (1.27). Let $\tilde{\phi}(r)$ be the irregular solution of eq. (1.38) corresponding to the same energy, having the same asymptotic form as $\phi(r)$ and the same normalization. Consider now two different energies E_1 and E_2 and their corresponding solutions. Following the Wronskian theorem:

$$\begin{aligned} W(\phi_1(r), \phi_2(r))|_a^b &= \frac{2\mu}{\hbar^2} (E_1 - E_2) \int_a^b \phi_1(r) \phi_2(r) dr \\ W(\tilde{\phi}_1(r), \tilde{\phi}_2(r))|_a^b &= \frac{2\mu}{\hbar^2} (E_1 - E_2) \int_a^b \tilde{\phi}_1(r) \tilde{\phi}_2(r) dr. \end{aligned} \quad (1.44)$$

As $b \rightarrow \infty$, since $\phi(r)$ and $\tilde{\phi}(r)$ have the same asymptotic form, the difference of the integrals in the right hand side of equations converge. Therefore the differences of two Wronskians of the left hand side evaluated at $b = \infty$ tends to zero. Since $\lim_{a \rightarrow 0} W(\phi_1(r), \phi_2(r)) = 0$ one obtains:

$$\lim_{a \rightarrow 0} \left[W(\tilde{\phi}_1(r), \tilde{\phi}_2(r)) + \frac{2\mu}{\hbar^2} (E_1 - E_2) \int_a^b (\tilde{\phi}_1(r) \tilde{\phi}_2(r) - \phi_1(r) \phi_2(r)) dr \right] = 0. \quad (1.45)$$

In the special case $\tilde{V} = 0$ and further restricting to the S -waves ($\ell = 0$) we denote functions $\tilde{\phi}(r)$ by $v(r)$. Choosing the normalization by the condition $v(0) = 1$

$$v(r) = \cos kr + \cot \delta \sin kr, \quad (1.46)$$

one obtains:

$$\begin{aligned} W(\tilde{\phi}_1(r), \tilde{\phi}_2(r)) &= k_1 \cot \delta_1(k_1) - k_2 \cot \delta_2(k_2) \\ &= \frac{2\mu}{\hbar^2} (E_1 - E_2) \int_a^b (v_1(r)v_2(r) - \phi_1(r)\phi_2(r)) dr. \end{aligned} \quad (1.47)$$

For short range potentials, when $V(r)$ falls to zero sufficiently rapidly as $r \rightarrow \infty$, integral in the right-hand side converges. We denote by $\phi_0(r)$ and $v_0(r)$ the functions $\phi(r)$ and $v(r)$ corresponding to zero energy. In this limit they read:

$$v_0(r) = 1 - \frac{r}{a_0} \quad \lim_{E \rightarrow 0} k \cot \delta(k) = -\frac{1}{a_0}, \quad (1.48)$$

where a_0 is the so-called *scattering length*, which measures the zero energy cross section ($\sigma(0) = 4\pi a_0^2$). By setting $E_1 = E$ and $E_2 = 0$ one obtains the well known *Bethe formula*:

$$k \cot \delta(k) = -\frac{1}{a_0} + \frac{2\mu}{\hbar^2} E \int (v(r)v_0(r) - \phi(r)\phi_0(r)) dr. \quad (1.49)$$

This relation is exact for any type of potential. However it becomes useful when the integral of the right hand side varies slowly as a function of the energy. This is the case for short range, exponentially decreasing, potentials, where the important contribution to the right hand side integral comes only from internal region of potential with $E \ll V(r)$. In this region $v(r) \approx v_0(r)$ and $\phi(r) \approx \phi_0(r)$, since they coincide at the origin and these functions have practically the same curvature ($\phi''(r)/\phi(r) \approx \frac{2\mu}{\hbar^2} V(r)$). One thus has in a very good approximation:

$$k \cot \delta(k) = -\frac{1}{a_0} + \frac{2\mu}{\hbar^2} E \int (v_0^2(r) - \phi_0^2(r)) dr. \quad (1.50)$$

The quantity $r_0 = 2 \int (v_0^2(r) - \phi_0^2(r)) dr$ is a characteristic parameter of the potential and is called *effective range of the interaction*. The two terms on right hand side of eq. (1.50) are the first two terms of $k \cot \delta$ expansion in a even series of momentum. This effective range formula can be generalized for any angular momentum partial waves:

$$k^{2l+1} \cot \delta_l(k) = -\frac{1}{a_l} + \frac{1}{2} r_{0,l} k^2 + o(k^4). \quad (1.51)$$

In contrast to S -wave case, where expansions parameters had clear physical meaning, the interpretation of a_l and $r_{0,l}$ for higher partial waves is less obvious.

For potentials which are not exponentially bounded, the effective-range function as defined in eq. (1.51) is not anymore an entire function of k^2 . The reason for this is that for such a potential the Jost function is analytic for $\text{Im}(k) > 0$ only. In fact, it has a branch-point singularity at $k = 0$, which gives rise to logarithms appearing in the expansion. For example, the S -wave expansion for a polarization potential with an r^{-4} tail, is [20]:

$$k \cot \delta_0(k) = -\frac{1}{a_0} + bk + ck^2 \ln k + o(k^2). \quad (1.52)$$

Nevertheless, one can usually define new effective-range functions, which are entire functions of k^2 . Even in case of Coulomb plus exponentially-bounded potential, for which a phase shift does not even exist in the usual sense, an analytic effective-range function can be defined. It is based on the *Coulomb-modified phase shift*, which does have an expansion in k^2 . For \mathcal{S} -wave, the effective-range function reads [21] [22]:

$$k [c_0^2 \cot \delta + 2\gamma h] \approx -\frac{1}{a} + \frac{1}{2} r_0 k^2 + \dots, \quad (1.53)$$

with

$$\begin{aligned} c_0^2 &= \frac{2\pi\gamma}{\exp(2\pi\gamma) - 1} \\ h &= \frac{1}{2} [\Psi(i\gamma) + \Psi(-i\gamma) - \ln(\gamma^2)] \end{aligned} \quad (1.54)$$

and Ψ is the digamma function [18].

1.1.6 Zero energy scattering

Let us consider the very low energy scattering. In this case, the incident wave becomes static and there is no anymore preferred direction of arriving particle. Therefore, the scattered wave should be isotropic in space and the scattering cross section is fully described by s-wave ($\ell = 0$). On the other hand from eq. (1.42) it follows that at zero energy all the partial phase shifts, as well as incident wave function $j_\ell(kr)$, fall to zero. Hence, all the asymptotic forms represented in eq. (1.29) tend to zero and can not serve as valid boundary conditions in numerical calculations. However, one can remark from eq. (1.51) that for s-wave phase shifts fall to zero linearly:

$$\lim_{k \rightarrow 0} \frac{\tan \delta_0(k)}{k} = -a_0 + o(k). \quad (1.55)$$

It means that scattering length can be extrapolated by studying low energy limit of the phase shifts. However, this kind of extrapolation becomes a subtle numerical task, since one must deal with quantities falling to zero. The more practical procedure relies on the fact that final limit for $\psi_{l=0,k}(r)/k$ exists:

$$\begin{aligned} \lim_{k \rightarrow 0} \frac{\psi_{l=0,k}(r)}{k} &= \lim_{k \rightarrow 0} \frac{j_l(kr) + kf_l(k)e^{i(kr-l\pi/2)}}{k} \Big|_{l=0} \\ &= \lim_{k \rightarrow 0} \frac{j_0(kr)}{k} + \lim_{k \rightarrow 0} \frac{e^{i\delta_0(k)} \sin \delta_0(k)}{k} e^{ikr} \\ &= r - a_0. \end{aligned} \quad (1.56)$$

This formula provides numerically correct boundary conditions for zero energy scattering by short range potential. Scattering length can be easily extracted from the tail of the numerical solution $f(r)$, representing the factorized wave function $\psi_{l=0,k}(r)/k$.

$$a_0 = r - \frac{f(r)}{f'(r)}. \quad (1.57)$$

When long range interaction is present, in particular Coulomb, things become more complicated. Of course one can use of effective range formulae (1.53) to extrapolate the scattering length from the low energy phase shifts. However this is an even more numerically unstable task than for the short range potentials, since Coulomb phase shifts fall to zero very rapidly, with an exponential factor proportional to $-1/k$ (see eq. 1.53).

The scattered S -wave, when Coulomb interaction is present, can be rewritten in alternative form to the expression (1.32):

$$\psi_{0,k}(r) \xrightarrow[r \rightarrow \infty]{} [F_0(kr, \gamma) + \tan \delta_0 G_0(kr, \gamma)]. \quad (1.58)$$

The Coulomb wave functions F_0, G_0 have exponentially singular behavior at the origin ($k = 0$). However when $kr \ll \gamma$, they can be expressed in terms of modified Bessel functions [18].

$$\begin{aligned} G_0(kr, \gamma) &\sim 2e^{\pi\gamma} \sqrt{\frac{kr}{\pi}} K_1(2\sqrt{2\gamma kr}), \\ F_0(kr, \gamma) &\sim e^{-\pi\gamma} \sqrt{\pi kr} I_1(2\sqrt{2\gamma kr}), \\ G'_0(kr, \gamma) &\sim -2ke^{\pi\gamma} \sqrt{\frac{2\gamma}{\pi}} K_0(2\sqrt{2\gamma kr}), \\ F'_0(kr, \gamma) &\sim e^{-\pi\gamma} k \sqrt{2\pi\gamma} I_0(2\sqrt{2\gamma kr}). \end{aligned} \quad (1.59)$$

Using eq. (1.53) one obtains:

$$\tan \delta(k \rightarrow 0) = -\frac{c_0^2 a_0 k}{2\gamma h a_0 k + 1} \rightarrow -2\pi\gamma a_0 k e^{-2\pi\gamma}. \quad (1.60)$$

By expressing the logarithmic derivative of Coulomb wave by means of eq. (1.60), one finally gets:

$$\frac{\psi'_{0,k}(r)}{\psi_{0,k}(r)} = \frac{I_0(2\sqrt{2\gamma kr}) + 4\gamma k a_0 K_0(2\sqrt{2\gamma kr})}{\sqrt{\frac{r}{2\gamma k}} I_1(2\sqrt{2\gamma kr}) - 2a_0 \sqrt{2\gamma kr} K_1(2\sqrt{2\gamma kr})}. \quad (1.61)$$

Now, scattering length can be obtained by just calculating logarithmic derivative of the zero energy solution at the extreme point of the grid and applying relation:

$$a_0 = \lim_{r \rightarrow \infty} \frac{r}{\kappa} \frac{\left(\frac{f'(r)}{f(r)} r\right) \frac{2I_1(\kappa)}{\kappa} - I_0(\kappa)}{\left(\frac{f'(r)}{f(r)} r\right) K_1(\kappa) + \frac{\kappa}{2} K_0(\kappa)}, \quad \text{with } \kappa = 2\sqrt{2\gamma kr} = 2\sqrt{\frac{2Z_1 Z_2 \mu e^2}{\hbar^2} r}. \quad (1.62)$$

1.1.7 Integral representations of the scattering lengths

In a previous section it has been demonstrated how to extract the scattering lengths from the asymptote of the wave function. Despite of being the most straightforward and simple method, it can be a risky practice in numerical calculations: one completely relies on the asymptote of the wave function, thus being not sure if the provided numerical solution describes well the internal part of the wave function. An alternative method can be developed using integral expressions of the phase shifts presented in subsection 1.1.4.

For short range interaction, the required expression follows by just inserting eq. (1.42) into eq. (1.50) and by searching the low energy limit. This leads to:

$$\begin{aligned}
 a_0 &= -\lim_{k \rightarrow 0} \frac{\tan \delta(k)}{k} = \lim_{k \rightarrow 0} \frac{2\mu}{\hbar^2} \int_0^\infty \frac{\hat{j}_l(kr)}{k} V(r) \frac{\psi_{l,k}(r)}{k} dr = \\
 &= \lim_{\substack{r_{\max} \rightarrow \infty \\ k \rightarrow 0}} \frac{2\mu}{\hbar^2} \int_0^{r_{\max}} r V(r) \left(f(r) \frac{\psi_{l,k}(r_{\max})}{k f(r_{\max})} \right) dr \\
 &= \lim_{r_{\max} \rightarrow \infty} \frac{2\mu r_{\max}}{\hbar^2 f(r_{\max})} \int_0^{r_{\max}} r V(r) f(r) dr
 \end{aligned} \tag{1.63}$$

Note that former expression is not applicable for the Coulomb (long range) scattering. In this case one should rely on scattering lengths extrapolated from the asymptote of wave function.

1.2 Basic concepts of a few-body problem

1.2.1 Multiparticle partitions. Jacobi coordinates

The Hamiltonian of a multiparticle system, with particles masses m_i ($i = 1, 2, \dots, N$) is:

$$H_N = -\sum_{i=1}^N \frac{\hbar^2}{2m_i} \Delta_i + \sum_{i < j} V_{ij}(r_i - r_j).$$

Here Δ_i denotes a three-dimensional Laplace operator in coordinates r_i , and $V_{ij}(r)$ are the pairwise interaction terms. However, general coordinates are not suited for solving the multiparticle problem, since they do not separate degrees of freedom describing conserved quantities of the system (such as the center of mass motion or projection of total angular momentum). Furthermore they are not suited for implementing boundary conditions.

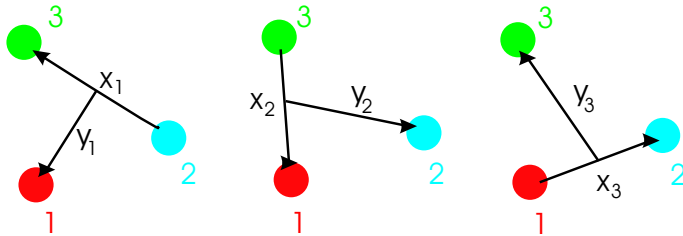


Figure 1.1: Three possible diagrams, together with associated Jacobi coordinates, for the three-body system

Dealing with multiparticle scattering problem, one should be easily able to divide the system into its subsystems, which describe the variety of all the possible outgoing channels, containing different particle sets. One makes use of concepts, first introduced by Yakubovski [15], of *partitions* and *chain of partitions*. The distribution of N particles into a groups is called partition a . A partition is described in detail by explicitly providing the subsystems it contains. For example the symbol

$$a_3 = (132)(4)(65)$$

means the subdivision of a six particle system into three groups (132) , (4) and (65) . Within these groups, only those particles occurring in parentheses interact with each other. Let us remark that the partition a_{N-1} is uniquely determined by the specifying the pair of particles (ij) joined in the group a_2 and furthermore cannot be subdivided into smaller groups.

In the case of two partitions a and α , the symbol (a, α) will be called a chain of partitions. The symbol $a \supset \alpha$ indicates that the partition α is obtained from the partition a by partitioning one or more of its subsystems. The chain can be pictured as a "tree". Every branch of this tree switches on an interaction between the particles.

For a three-particle system there is only one type of partition (tree): $a_2 = (ij)k$. By renumbering

the branches of this tree⁴, one obtains three diagrams corresponding to the same type of partition (see Fig. 1.1).

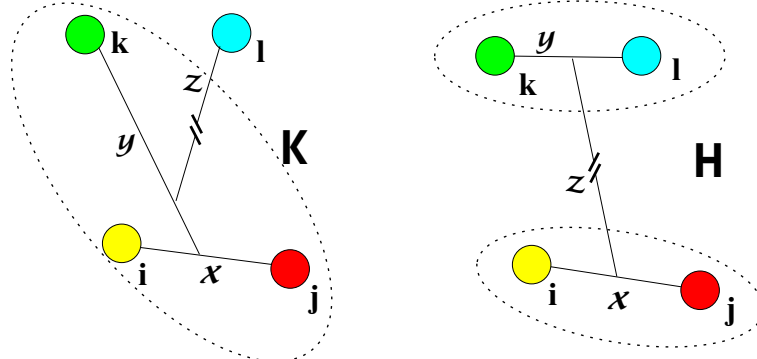


Figure 1.2: Two different partitions for four-body system

There are two ways of dividing four particle system in two groups $(ijk)l$ and $(ij)(kl)$. The $(ijk)l$ type partition is represented by so-called diagram K-type, whereas diagrams identifying partition $(ij)(kl)$ are called H-type (Fig. 1.2). In total, there are twelve trees of the first type and six trees of the second one (they correspond to the different renumbering of particles (1234) in $(ijkl)$).

For each subsystem $\varpi_i(n_1, n_2, \dots)$ contained in one of the parentheses of some partition, one has a corresponding Hamiltonian operator:

$$H_{\varpi_i} = - \sum_{i=1}^N \frac{\hbar^2}{2m_{n_i}} \Delta_{n_i} + \sum_{n_i < n_j} V_{n_i n_j} (r_{n_i} - r_{n_j}), \quad (1.64)$$

which depends only on the particle coordinates of this subsystem. For the partition a_k , one can decompose the space of states $L(R^{3N})$ in a tensor product of spaces $L(R^{3\varpi_i})$, which describes the states of the subsystems of a_k :

$$L(R^{3N}) = \prod_{j=1}^k \otimes L(R^{3\varpi_i}). \quad (1.65)$$

In accordance with this expression, we define the Hamiltonian of a partition as being the sum of Hamiltonians of its subsystems:

$$H_{a_k} = \sum_{j=1}^k H_{\varpi_i}. \quad (1.66)$$

Reduced coordinates

Let us introduce the coordinates related to the partition trees discussed above. First of all one can single out the degrees of freedom which describe the center of mass motion of the system as a

⁴Or, that is identical, by interchanging indexes (ijk) . These indexes represent any combination obtained by cyclic permutations of (123) .

whole. We denote by a vector \vec{R} its position:

$$\vec{R} = \frac{\sum_{i=1}^N m_i \vec{r}_i}{\sum_{i=1}^N m_i}. \quad (1.67)$$

Other coordinates are related to the branches of the partition. For two particle cluster (ij) one uses scaled *Jacobi* vector (these vectors are scaled to remove the masses from kinetic energy operator):

$$\vec{x}_{ij} = \sqrt{2\mu_{ij}}(\vec{r}_j - \vec{r}_i), \quad (1.68)$$

with μ_{ij} being the reduced mass of two particles $\mu_{ij} = \frac{m_i m_j}{m_i + m_j}$. The coordinate which joins two subsystems (let designate them $\varpi_i(n_{i_1}, n_{i_2}, \dots)$ and $\varpi_j(n_{j_1}, n_{j_2}, \dots)$) in the same partition is defined by using the following strategy:

1. One finds the center of masses \vec{r}_{ϖ_i} , \vec{r}_{ϖ_j} and reduced mass μ_{ϖ_i, ϖ_j} of these two subsystems

$$\vec{r}_{\varpi_i} = \frac{\sum_k m_{n_{i_k}} \vec{r}_{n_{i_k}}}{\sum_k m_{n_{i_k}}}, \quad \vec{r}_{\varpi_j} = \frac{\sum_k m_{n_{j_k}} \vec{r}_{n_{j_k}}}{\sum_k m_{n_{j_k}}}, \quad (1.69)$$

$$\mu_{\varpi_i, \varpi_j} = \frac{\sum_k m_{n_{i_k}} \sum_k m_{n_{j_k}}}{\sum_k m_{n_{i_k}} + \sum_k m_{n_{j_k}}}. \quad (1.70)$$

2. The required coordinate $\vec{x}_{\varpi_i, \varpi_j}$ is the reduced *Jacobi* coordinate which joins the centers of mass of these two subsystems:

$$\vec{x}_{\varpi_i, \varpi_j} = \sqrt{2\mu_{\varpi_i, \varpi_j}}(\vec{r}_{\varpi_j} - \vec{r}_{\varpi_i}). \quad (1.71)$$

The coordinate basis, obtained as described above, is orthogonal and has invariant norm (the sum of squares of these coordinates is partition and renumbering invariant):

$$\rho^2 = \sum_{\varpi_i < \varpi_j} \vec{x}_{\varpi_i, \varpi_j}^2. \quad (1.72)$$

Other major advantage of these coordinates is the trivial form of the kinetic energy (or Laplace) operator, which simply becomes:

$$\Delta = \sum_{\varpi_i < \varpi_j} \frac{\partial^2}{\partial \vec{x}_{\varpi_i, \varpi_j}^2} \quad (1.73)$$

and holds the same form for any partition and any renumbering of particles inside the given partition.

Three-body Jacobi coordinates

One can easily apply the definitions, introduced in the previous subsection, to write down Jacobi coordinates associated with the three-body partition $(jk)i$ (see Fig. 1.1):

$$\begin{aligned}\vec{x}_i &= -\sqrt{\frac{2m_j m_k}{m_j + m_k}}(\vec{r}_k - \vec{r}_j), \\ \vec{y}_i &= -\sqrt{\frac{2m_i(m_j + m_k)}{m_i + m_j + m_k}}(\vec{r}_i - \frac{m_k \vec{r}_k + m_j \vec{r}_j}{m_j + m_k}).\end{aligned}\quad (1.74)$$

The Jacobi vectors of the partitions having different indexes are related by an orthogonal transformation:

$$\begin{aligned}\vec{x}_j &= c_{ji} \vec{x}_i + s_{ji} \vec{y}_i, \\ \vec{y}_j &= -s_{ji} \vec{x}_i + c_{ji} \vec{y}_i,\end{aligned}\quad (1.75)$$

where the coefficients are expressed through the masses of the particles:

$$c_{ji} = -\left[\frac{m_j m_i}{(M - m_j)(M - m_i)}\right]^{\frac{1}{2}} \quad s_{ji} = (-1)^{j-i} \operatorname{sgn}(i - j) (1 - c_{ji}^2)^{\frac{1}{2}}. \quad (1.76)$$

Four-body Jacobi coordinates

In a four-body system, one can construct 48 distinct sets of Jacobi coordinates, since there are 2 types of partitions (see Fig. 1.2) and furthermore there are $4!$ possible rearrangements of the 4 particles. Definitions of these coordinates are as follows:

$$\begin{aligned}K \text{ type partition } (ij, kl) &\quad \left\{ \begin{array}{lcl} \vec{x}_{ij} &= \sqrt{2\mu_{ij}}(\vec{r}_j - \vec{r}_i) \\ \vec{y}_{ij,k} &= \sqrt{2\mu_{ij,k}}(\vec{r}_k - \frac{m_i \vec{r}_i + m_j \vec{r}_j}{m_i + m_j}) \\ \vec{z}_{ijk,l} &= \sqrt{2\mu_{ijk,l}}(\vec{r}_l - \frac{m_i \vec{r}_i + m_j \vec{r}_j + m_k \vec{r}_k}{m_i + m_j + m_k}) \end{array} \right. \\ H \text{ type partition } (ij)(kl) &\quad \left\{ \begin{array}{lcl} \vec{x}_{ij} &= \sqrt{2\mu_{ij}}(\vec{r}_j - \vec{r}_i) \\ \vec{y}_{kl} &= \sqrt{2\mu_{kl}}(\vec{r}_l - \vec{r}_{ki}) \\ \vec{z}_{ij,kl} &= \sqrt{2\mu_{ij,kl}}(\frac{m_k \vec{r}_k + m_l \vec{r}_l}{m_k + m_l} - \frac{m_i \vec{r}_i + m_j \vec{r}_j}{m_i + m_j}) \end{array} \right.. \end{aligned}\quad (1.77)$$

Relation between the different sets of Jacobi coordinates is less trivial than in three-body case. It can be written in general matrix form:

$$\begin{pmatrix} \vec{x}' \\ \vec{y}' \\ \vec{z}' \end{pmatrix} = [M_{3 \times 3}] \begin{pmatrix} \vec{x} \\ \vec{y} \\ \vec{z} \end{pmatrix}. \quad (1.78)$$

Due to orthogonality of Jacobi coordinates and the fact that the norm $\rho^2 = x^2 + y^2 + z^2$ is conserved, coordinate transformation matrices M are unitary. The practical realization of the passage between different sets of coordinates is explained in Appendix B.

1.2.2 Faddeev equations

The simplest technique to solve Lippmann-Schwinger (LS) equation is to iterate its kernel $K(z) = G(z)V$, which leads to the *Born series*:

$$K(z) = G_0(z)V + G_0(z)VG_0(z)V + \dots \quad (1.79)$$

Although its simplicity makes this technique an attractive one, in practical use it is limited even in two-body case, since Born series may diverge. In fact, it will diverge at the bound-state energy, if a bound state is supported, since K matrix will have a pole there. This pole is not present in any of the terms of the Born series (in this case the series will diverge for a range of positive energies as well [12]).

For a three-body system, LS equation is not able at all to ensure a unique solution, since its kernel becomes not square integrable. This can be easily demonstrated using graphical representation of operator $G_0(z)V$ (see Fig. 1.3). Only two particles interact in each term, while the third one moves freely, which means that there is a δ -function in the momentum space. When looking for useful integral equations, one should thus try to avoid disconnected parts in the kernel [23, 24].

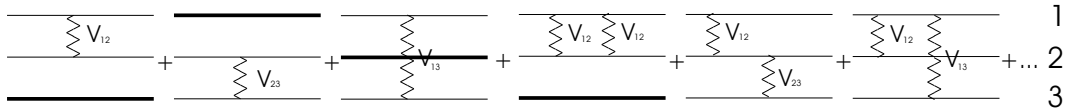


Figure 1.3: Kernel of the three-particle LS equation in graphical representation. Diagrams containing non-interacting particle (presented in bold) lead to singularities in right-hand side of eq. (1.79).

After Faddeev had shown [9] in 1960 that the LS equation does not have a unique solution, he studied the properties of the so called transition operator:

$$T(z) = V + VG(z)V. \quad (1.80)$$

This operator is a formal analogue of the two-particle T-operator, however it is not related to a scattering cross section as directly as in two-body case. One can easily see that operator $T(z)$ satisfies LS equation:

$$T(z) = V + VG_0(z)T(z). \quad (1.81)$$

Transition operator is less singular than resolvent $G(z)$, but integral eq. (1.81) suffers from the same disadvantage as the standard LS equation for the resolvent since they have the same kernels. To eliminate this defect, Faddeev decomposed the total operator $T(z)$ in three:

$$T(z) = T^{(1)}(z) + T^{(2)}(z) + T^{(3)}(z),$$

where

$$T^{(k)}(z) = V_{ij} + V_{ij}G_0(z)T(z), \quad (1.82)$$

with (ijk) being any combination obtained by cyclic permutations of indexes (123) . By moving $T^{(k)}(z)$ term from right hand side to the left one obtain:

$$[1 - V_{ij}G_0](z)T^{(k)}(z) = V_{ij} + V_{ij}G_0(z)[T^{(i)}(z) + T^{(j)}(z)]. \quad (1.83)$$

One can take advantage of the LS equation for pair transition operators

$$T_{ij}(z) = V_{ij} + V_{ij}G_0(z)T_{ij}(z), \quad (1.84)$$

to obtain three equations:

$$T^{(k)}(z) = T_{ij}(z) + T_{ij}(z)G_0(z)[T^{(i)}(z) + T^{(j)}(z)] \quad ijk = 123, 231, 312 \quad (1.85)$$

It is now clear that, owing to the absence of the diagonal term $T^{(k)}(z)$ in the right-hand side of eq. (1.85), the iterated series of the equation will not contain any disconnected diagram terms and, therefore, (this is a necessary but not a sufficient condition, as shows up for Efimov effect [7]) the set of equations (1.85) has a unique solution. In the same manner, one can split the three-particle wave function Ψ , in so called Faddeev components $\psi^{(k)}$, $\Psi = \psi^{(1)} + \psi^{(2)} + \psi^{(3)}$. Faddeev equations for these components are obtained from the equations for the components of the Green functions $G^{(k)}(z)$:

$$G^{(k)}(z) = G_{ij}(z) - G_0(z) + G_0(z)T_{ij}(z)[G^{(i)}(z) + G^{(j)}(z)] \quad (1.86)$$

and using the alternative Green function definition

$$\left| \psi^{(k)} \right\rangle = \lim_{\varepsilon \rightarrow 0} G^{(k)}(E + i\varepsilon) |\Phi\rangle, \quad (1.87)$$

where Φ is the asymptotic function.

For bound state problem one is left with a set of homogenous equations:

$$\left| \psi^{(k)} \right\rangle = G_0(z)T_{ij}(z) [\left| \psi^{(i)} \right\rangle + \left| \psi^{(j)} \right\rangle], \quad (1.88)$$

while in a case of particle 1 scattering on a bound state of particles 2 and 3 one should have:

$$\begin{aligned} \left| \phi^{(1)} \right\rangle &= \Phi_1 + G_0(z)T_{23}(z) [\left| \psi^{(2)} \right\rangle + \left| \psi^{(3)} \right\rangle], \\ \left| \psi^{(2)} \right\rangle &= G_0(z)T_{31}(z) [\left| \psi^{(3)} \right\rangle + \left| \psi^{(1)} \right\rangle], \\ \left| \psi^{(3)} \right\rangle &= G_0(z)T_{12}(z) [\left| \psi^{(1)} \right\rangle + \left| \psi^{(2)} \right\rangle]. \end{aligned} \quad (1.89)$$

By sorting out the free Green's function and transition operator T in favor of a free Hamiltonian operator and pair interactions V_{ij} , one is left with a set of Faddeev equations, in a form useful for solving the problem in coordinate space:

$$\begin{aligned} (E - H_0 - V_{23}) \left| \psi^{(1)} \right\rangle &= V_{23} [\left| \psi^{(2)} \right\rangle + \left| \psi^{(3)} \right\rangle], \\ (E - H_0 - V_{31}) \left| \psi^{(2)} \right\rangle &= V_{31} [\left| \psi^{(3)} \right\rangle + \left| \psi^{(1)} \right\rangle], \\ (E - H_0 - V_{12}) \left| \psi^{(3)} \right\rangle &= V_{12} [\left| \psi^{(1)} \right\rangle + \left| \psi^{(2)} \right\rangle]. \end{aligned} \quad (1.90)$$

1.2.3 Faddeev-Yakubovsky equations

Faddeev's pioneering work of reformulating the LS equations for three-body systems to have mathematically correct solution with a compact kernel was followed by Yakubovsky. In [15] he presented the systematic generalization of Faddeev equations for any number of particles. Here, I will present a simple derivation of Yakubovsky equations with a special emphasis on the four-body problem (to be dealt later in this thesis). We will follow ideas of S.P. Merkuriev and S.L. Yakovlev [25, 26].

In the first place one should note that the rearrangement of the four-particle equations involving only the three-body Faddeev components is insufficient. For four-body systems, in addition to the disconnected diagrams (see Fig. 1.3) which were giving singularities and were successfully eliminated by using Faddeev's decomposition, there arise new disconnected diagrams giving δ -functions in momentum space (see Fig. 1.4).

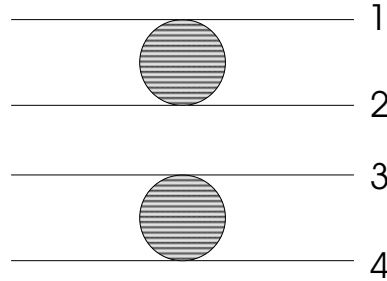


Figure 1.4: Disconnected diagram of four-particle system: interaction differs from zero only in (12) and (34) pair subsystems. These subsystems move independently, while the terms describing the relative motion of these subsystems give singular contributions in LS equation, which are not taken in account by Faddeev decomposition.

We proceed by employing concepts of partitions and chain of partitions introduced in subsection 1.2.1. To derive Yakubovsky four-body equations, one can start by introducing Faddeev-like components of the wave function:

$$\begin{aligned} |\psi_\alpha\rangle &= -G_0(E)V_\alpha|\Psi\rangle \Rightarrow |\Psi\rangle = \sum_\alpha |\psi_\alpha\rangle, \\ |\psi_\alpha\rangle &= -G_\alpha V_\alpha \sum_{\beta \neq \alpha} |\psi_\beta\rangle. \end{aligned} \quad (1.91)$$

As was discussed, these equations still contain singular terms and are not Fredholm equations [27]. With the aid of the chain (a, α) one introduces components for each function:

$$|\psi_{\alpha,a}\rangle = -G_\alpha V_\alpha \sum_{(\beta \neq \alpha) \subset a} |\psi_\beta\rangle. \quad (1.92)$$

Mathematically, it can be proved [15], that the following summation rule holds:

$$\sum_{\alpha \subset a} \sum_{(\beta \neq \alpha) \subset a} = \sum_{\beta \neq \alpha}. \quad (1.93)$$

When applying this rule to both sides of eq. (1.91) we obtain the relation

$$|\psi_\alpha\rangle = \sum_a |\psi_{\alpha,a}\rangle. \quad (1.94)$$

Substituting it into eq. (1.92) and by shifting the resolvent to the left-hand side of equation, one immediately gets differential Yakubovsky equation:

$$(H_0 - E + V_\alpha) |\psi_{\alpha,a}\rangle = -V_\alpha \sum_{(\beta \neq \alpha) \subset a} \sum_b |\psi_{\beta,b}\rangle. \quad (1.95)$$

In a four-particle case one distinguishes two types of components $|\psi_{\alpha,a}\rangle$, (see Fig. 1.2), - K and H. Asymptote of component $K_{ij,k}^l$ (where $(ijkl)$ denotes one of the possible permutations of (1234)) takes into account interaction in pair (ij) of the group (ijk) , while particle l is supposed to propagate freely. Asymptote of component $H_{ij,kl}$ absorbs the interaction in pair (ij) , while in conjunction of component $H_{kl,ij}$, it describes the free relative movement of pairs (ij) and (kl) .

One can remark that K diagram is not affected when interchanging indexes (ij) , except that the sign of vector \vec{x} is reversed. Therefore one can restrict components $K_{ij,k}^l$ to those with $i < j$. For H configurations, one can interchange indexes in pairs (ij) and (kl) , staying within the same diagram. Therefore we restrict H components to those having $i < j$ and $k < l$. Consequently one has only 12 different components $K_{i < j,k}^l$ and 6 different components $H_{i < j,k < l}$.

Faddeev-like component $|\psi_\alpha\rangle$, derived for particle pair interaction $\alpha = (12)$ eq. (1.91) in terms of components H and K , reads as:

$$|\psi_{12}\rangle = K_{12,3}^4 + K_{12,4}^3 + H_{12,34}. \quad (1.96)$$

Wave function of a four-body system is a sum of these Faddeev type components $|\psi_\alpha\rangle$ as given in eq. (1.91). There are 6 components $|\psi_\alpha\rangle$, since one can count 6 different interacting pairs. According to eq. (1.96), every $|\psi_\alpha\rangle$ is expressed by one H and two K components and therefore 4-body wave function is the sum of 18 functions (12 of type K and 6 of type H):

$$\begin{aligned} |\Psi\rangle &= |\psi_{12}\rangle + |\psi_{13}\rangle + |\psi_{14}\rangle + |\psi_{23}\rangle + |\psi_{24}\rangle + |\psi_{34}\rangle \\ &= K_{12,3}^4 + K_{12,4}^3 + H_{12,34} + K_{13,2}^4 + K_{13,4}^2 + H_{13,24} + K_{14,2}^3 + K_{14,3}^2 + H_{14,23} \\ &\quad + K_{23,1}^4 + K_{23,4}^1 + H_{23,14} + K_{24,1}^3 + K_{24,3}^1 + H_{24,13} + K_{34,2}^1 + K_{34,1}^2 + H_{34,12}. \end{aligned} \quad (1.97)$$

Consequently one has a system of 18 coupled differential equations (1.95). Each component of type K (or H) appears once in the left hand side and is coupled with the other components in the right hand side. I will write down only three of these equations⁵ containing each of the 18 terms present in wave functions decomposition eq. (1.97).

$$\begin{aligned} (H_0 - E + V_{12}) |K_{12,3}^4\rangle &= -V_{12} [|K_{23,1}^4\rangle + |K_{23,4}^1\rangle + |H_{23,14}\rangle + |K_{13,2}^4\rangle + |K_{13,4}^2\rangle + |H_{13,24}\rangle] \\ (H_0 - E + V_{12}) |K_{12,4}^3\rangle &= -V_{12} [|K_{24,1}^3\rangle + |K_{24,1}^1\rangle + |H_{24,13}\rangle + |K_{14,2}^3\rangle + |K_{14,3}^2\rangle + |H_{14,23}\rangle] \\ (H_0 - E + V_{12}) |H_{12,34}\rangle &= -V_{12} [|K_{34,1}^2\rangle + |K_{34,2}^1\rangle + |H_{34,12}\rangle]. \end{aligned} \quad (1.98)$$

⁵Other equations are identical, just indexes denoting components K and H should be permuted.

1.2.4 Identity of particles

The uncertainty principle in Quantum mechanics declares the impossibility to define simultaneously the position and the momentum of a particle. Thus, we cannot follow its trajectory (still particles position is exactly known at a given instant, its coordinates have no definite values even at an infinitely close subsequent instant). Hence, by localizing and numbering the identical particles composing some system, we make no progress towards identifying them at subsequent instants. We may say that in quantum mechanics, identical particles entirely loose their individuality and thus lead to their indistinguishability (*principle of indistinguishability of similar particles*). Let us consider some composite system containing two identical particles i and j . The states of the system obtained from each other by merely interchanging these two particles must be completely equivalent physically. This means that, as a result of this interchange, the wave function of the system can change only by an unimportant phase factor. Let $\psi(\xi_1, \dots, \xi_i, \dots, \xi_j, \dots)$ be the wave function of the system, ξ_i denoting the full set of the co-ordinates of i -th particle. Then we have

$$P_{ij}P_{ij}\psi(\xi_1, \dots, \xi_i, \dots, \xi_j, \dots) = P_{ij}\varepsilon\psi(\xi_1, \dots, \xi_j, \dots, \xi_i, \dots) = \varepsilon^2\psi(\xi_1, \dots, \xi_i, \dots, \xi_j, \dots). \quad (1.99)$$

Thus it follows what the only possible values for ε are ± 1 , and the wave function is either *symmetric* or *antisymmetric*.

Particles described with antisymmetric wave functions are said to obey *Fermi-Dirac statistics* and are called *fermions*, while those described by symmetric functions are called *bosons* and obey *Bose-Einstiens statistics*. Furthermore, relativistic quantum mechanics shows that the statistics obeyed by the particles is uniquely related to their spin: particles with half-integer spin are fermions, and those with integer spin are bosons.

Thus, any action of complicated permutation operator of identical particles will satisfy relation:

$$\hat{\phi}|\Psi\rangle = \varepsilon^p |\Psi\rangle, \quad (1.100)$$

where p is the number of the 2-particle permutations needed to restore the previous configuration. The *principle of indistinguishability of similar particles* can be directly implemented to simplify few-body Faddeev (Faddeev-Yakubovski) equations. It is straightforward that some rearrangement channels become indistinguishable if we have a pair of identical particles and, therefore, the number of equations in systems (1.90 or 1.98) can be reduced.

Let us show it in detail. The fact that the Hamiltonian \hat{H} of the system is symmetric in respect to the exchange of any two particles of the same kind means, mathematically, that \hat{H} commutes with all the permutation operators $\hat{\phi}$. Evidently, the same applies for the free Green's function G_0 and the total potential V_{tot} . Furthermore, since the inverse of the single 2-particle permutation coincides with itself, we have: $P_{ij}\hat{H}P_{ij} = \hat{H}$, $P_{ij}G_0P_{ij} = G_0$, $P_{ij}V_{tot}P_{ij} = V_{tot}$. Conversely, one can easily verify that $P_{ij}V_{ik} = V_{jk}P_{ij}$ and therefore $P_{ij}V_{ik}P_{ij} = V_{jk}$; $P_{ij}V_{ij}P_{ij} = V_{ij}$.

Reduction of Faddeev equations for the system with identical particles

As was discussed in section 1.2.2, by using Faddeev decomposition the wave function of a three-particle system is decomposed into a sum of three functions, so-called components:

$$\Psi(\vec{x}, \vec{y}) = \psi^{(1)}(\vec{x}_1, \vec{y}_1) + \psi^{(2)}(\vec{x}_2, \vec{y}_2) + \psi^{(3)}(\vec{x}_3, \vec{y}_3). \quad (1.101)$$

Clearly, for a system of three-identical particles the components $\psi^{(i)}(\vec{r}_1, \vec{r}_2, \vec{r}_3)$ ($i = 1, 2, 3$) are identical. It is useful to define the symmetry operators, which describe transitions between them:

$$P^+ = P_{12}P_{23}. \quad (1.102)$$

This operator makes rise the state index by one:

$$\begin{aligned} \psi^{(2)}(\vec{x}_2, \vec{y}_2) &= P^+ \psi^{(1)}(\vec{x}_1, \vec{y}_1); \\ \psi^{(3)}(\vec{x}_3, \vec{y}_3) &= P^+ \psi^{(2)}(\vec{x}_2, \vec{y}_2); \\ \psi^{(1)}(\vec{x}_3, \vec{y}_3) &= P^+ \psi^{(3)}(\vec{x}_2, \vec{y}_2), \end{aligned} \quad (1.103)$$

whereas its inverse

$$P^- = (P^+)^{-1} = P_{23}P_{12}, \quad (1.104)$$

reduces the component index by one:

$$\begin{aligned} \psi^{(3)}(\vec{x}_3, \vec{y}_3) &= P^- \psi^{(1)}(\vec{x}_1, \vec{y}_1); \\ \psi^{(1)}(\vec{x}_1, \vec{y}_1) &= P^- \psi^{(2)}(\vec{x}_2, \vec{y}_2); \\ \psi^{(2)}(\vec{x}_2, \vec{y}_2) &= P^- \psi^{(3)}(\vec{x}_3, \vec{y}_3). \end{aligned} \quad (1.105)$$

Using these symmetry properties, one can see that the three Faddeev equations (1.90) become identical. Therefore a complete solution of the problem can be obtained after solving only one of them:

$$(E - H_0 - V) |\psi\rangle = V [P^- + P^+] |\psi\rangle \quad (1.106)$$

For a system of four identical particles these two operators are not sufficient, since they do not affect the fourth particle. Therefore, in addition to three-body permutation operators P^- and P^+ , one must introduce two additional ones:

$$\begin{aligned} Q &= \varepsilon P_{34}, \\ \tilde{P} &= P_{13}P_{24} = P_{24}P_{13}. \end{aligned} \quad (1.107)$$

Let us explore the action of these operators on the Yakubovski amplitudes. For example operator P^- :

$$\begin{aligned} P^- |K_{12,3}^4\rangle &= P^- G_{12} V_{12} G_0 (V_{23} + V_{13}) |\Psi\rangle \\ &= P^- G_{12} P^+ P^- V_{12} P^+ P^- G_0 P^+ P^- (V_{23} + V_{13}) P^+ P^- |\Psi\rangle. \end{aligned} \quad (1.108)$$

It is easy to show that:

$$\begin{aligned} P^- |\Psi\rangle &= \varepsilon^2 |\Psi\rangle = |\Psi\rangle \quad P^- G_0 P^+ = G_0 \\ P^- G_{12} P^+ &= P_{23} P_{12} G_{12} P_{12} P_{23} = P_{23} G_{12} P_{23} = G_{13} \\ P^- (V_{23} + V_{13}) P^+ &= P_{23} P_{12} (V_{23} + V_{13}) P_{12} P_{23} = P_{23} (V_{13} + V_{23}) P_{23} = (V_{12} + V_{23}). \end{aligned} \quad (1.109)$$

By projecting these relations into eq. (1.108), one finally obtains:

$$P^- |K_{12,3}^4\rangle = G_{13}V_{13}G_0(V_{12} + V_{23})|\Psi\rangle = |K_{13,2}^4\rangle \quad (1.110)$$

Continuously applying permutation operators (1.102), (1.104) and (1.107), as was shown in the example above, we can reconstruct all the 18 FY components from any given pair of K and H. The necessary relations are summarized below:

$$\begin{aligned} |K_{23,1}^4\rangle &= P^+ & |K_{12,3}^4\rangle &= P^+QP^+|K_{12,3}^4\rangle \\ |K_{13,2}^4\rangle &= P^- & |K_{12,3}^4\rangle &= P^-QP^+|K_{12,3}^4\rangle \\ |K_{12,4}^3\rangle &= Q & |K_{12,3}^4\rangle &= QP^- & |K_{12,3}^4\rangle \\ |K_{23,4}^1\rangle &= P^+Q & |K_{12,3}^4\rangle &= P^+QP^-|K_{12,3}^4\rangle \\ |K_{13,4}^2\rangle &= P^-Q & |K_{34,1}^2\rangle &= P^-QP^-|K_{12,3}^4\rangle \\ |K_{24,1}^3\rangle &= QP^+ & |K_{12,3}^4\rangle &= P^+Q \end{aligned} \quad (1.111)$$

$$\begin{aligned} |H_{34,12}\rangle &= \tilde{P} & |H_{12,34}\rangle &= P^+\tilde{P}|H_{12,34}\rangle \\ |H_{23,14}\rangle &= P^+|H_{12,34}\rangle & |H_{24,13}\rangle &= P^-\tilde{P}|H_{12,34}\rangle \\ |H_{13,24}\rangle &= P^-|H_{12,34}\rangle \end{aligned} \quad (1.112)$$

It follows, that for a four-identical particle system one should know only two FY components: namely one component K and one H. All the other 16 can be reconstructed from those two by using relations (1.111-1.112). Consequently, in the set (1.98) there are only two nontrivial equations, which, by using definitions of permutation operators, can be written:

$$\begin{aligned} (E - \hat{H}_0 - \hat{V})|K\rangle &= \hat{V}(P^+ + P^-)[(1 + Q)|K\rangle + |H\rangle] \\ (E - \hat{H}_0 - \hat{V})|H\rangle &= \hat{V}[(P^-QP^- + P^+QP^+)|K\rangle + \tilde{P}|H_{12,34}\rangle]. \end{aligned} \quad (1.113)$$

By remarking that $P^-QP^- = \tilde{P}$ and $P^+QP^+ = \tilde{P}Q$, the second equation can be rewritten in the form:

$$(E - \hat{H}_0 - \hat{V})|H\rangle = \hat{V}\tilde{P}[(1 + Q)|K\rangle + |H\rangle]. \quad (1.114)$$

This equation is more convenient for subsequent application of permutation operators. Concerning the system's wave function, collecting all the operators from tables (1.111-1.112) and inserting into eq. (1.97), one gets:

$$|\Psi\rangle = [1 + (1 + P^+ + P^-)]Q(1 + P^+ + P^-)|K\rangle + (1 + P^+ + P^-)(1 + \tilde{P})|H\rangle. \quad (1.115)$$

1.2.5 Partial wave decomposition

Once the center of mass motion for a system of N particles is separated, one still has differential equations with $3(N-1)$ configuration space variables to solve. The dimension of the problem can

be further reduced by remarking that for an isolated system the total angular momentum \mathcal{J} and its z-component \mathcal{J}_z are conserved. Thus, it is sensible to choose a representation whose vectors are eigenstates of \mathcal{J} and \mathcal{J}_z . In this way, the number of degrees of freedom are further reduced to $3(N-1)-2$.

In general, particles are not completely described by their spatial distributions. They can possess intrinsic angular momenta (spins), or slightly differ by being member of some finite family of particles (they are distinguished within this family by the isospin quantum number). Therefore, in addition to space coordinates, each particle i should be provided with the spin $(s, s_z)_i$ and isospin $(t, t_z)_i$ coordinates. The total space of states for a multiparticle system is represented as a tensor product of three spaces - configuration, spin and isospin:

$$L_{tot}^N = |\mathcal{R}^{3N}\rangle \otimes |\mathcal{S}^{3N}\rangle \otimes |\mathcal{T}^{3N}\rangle. \quad (1.116)$$

For a system of the particles with spin, the conserved quantity is the total angular momentum $\vec{\mathcal{J}} = \vec{\mathcal{L}} + \vec{\mathcal{S}}$, the sum of the total orbital angular momentum $\vec{\mathcal{L}}$ and the total spin $\vec{\mathcal{S}}$. In most of nuclear systems, with a very high accuracy, the total isospin $\vec{\mathcal{T}}$ is conserved as well. In angular momentum representation, one associates the angular momentum variable to each branch of the multiparticle tree (or each Jacobi coordinate axis x, y, z, \dots) l_x, l_y, l_z, \dots :

$$\hat{l}_x = \hat{p}_x \times \hat{x}; \quad \hat{l}_y = \hat{p}_y \times \hat{y}; \quad \hat{l}_z = \hat{p}_z \times \hat{z}; \quad \dots \quad (1.117)$$

In addition, spins of each particle couples with orbital angular momentum through intermediate sums by giving total angular momentum $\vec{\mathcal{J}}$. Independently, isospins of the particles couple to form the total isospin of the system.

One can use state vectors, which are characterized by the angular momentum, rather than by the angular variables of configuration space. The projection of momentum basis to configuration space is realized by multiharmonic spherical functions [28, 29]:

$$\mathcal{Y}_{l_x l_y l_z}^{\mathcal{LM}}(\hat{x}, \hat{y}, \hat{z}) = \sum_{m_x+m_y+m_z=M} \langle l_x m_x, l_y m_y, l_z m_z | \mathcal{LM} \rangle Y_{l_x}^{m_x}(\hat{x}) Y_{l_y}^{m_y}(\hat{y}) Y_{l_z}^{m_z}(\hat{z}) \quad (1.118)$$

In addition, basis functions $\mathcal{Y}_{l_x l_y l_z}^{\mathcal{LM}}(\hat{x}, \hat{y}, \hat{z})$ are labelled by the internal quantum numbers of the system:

- l_x is the angular momenta of the particle pair (12);
- l_y is the angular momenta of the third particle relative to the center of mass of the pair (12) for three-body as well as for four-body $K_{12,3}^4$ configurations, whereas it describes angular momentum of the particle pair (34) in four-body $H_{12,34}$ configurations;
- l_z is introduced only in four-body problem. It describes the angular momentum of the fourth particle with respect to the center of mass of (123) particle cluster for $K_{12,3}^4$ configurations. On the other hand it describes the relative angular momenta of the two two-body fragments (12) and (34) in $H_{12,34}$ configurations.

Three-body coupling schemes

There are two convenient schemes to realize the angular momentum $|\mathcal{L}S_J\rangle$ basis sets, according to the way one chooses to couple spins and momenta of the different subsystems:

1. In the so called $\mathcal{L}S$ coupling scheme, one first couples all the angular momenta and spins separately. Then, the total orbital momenta and spin are coupled to the total angular momenta. Notations for the three-body $\mathcal{L}S$ coupling basis are as follows:

$$|\mathcal{L}S_J\rangle_{(ij)k} = \left| \left\{ [l_x l_y]_{\mathcal{L}} \left[(s_i s_j)_{\sigma_x} s_k \right]_S \right\}_{\mathcal{J}} \right\rangle \quad (1.119)$$

In this case, Faddeev components are decomposed into a sum of so-called partial amplitudes $F_n^{(k)}(x, y)$, which are functions of only radial variables x and y and represent eigenstates in the angular momenta-isospin basis:

$$\left| \psi^{(k)} \right\rangle = \sum_{n=l_x, l_y, L, \sigma_x, S, t_x} \frac{F_n^{(k)}(x, y)}{xy} \left\langle n, \hat{x}, \hat{y} \left| \left\{ [l_x l_y]_{\mathcal{L}} \left[(s_i s_j)_{\sigma_x} s_k \right]_S \right\}_{\mathcal{J}} \right\rangle \right| \left[(t_i t_j)_{t_x} t_k \right]_{\mathcal{T}} \rangle \quad (1.120)$$

2. Alternatively, in the $\mathcal{J}\mathcal{J}_z$ coupling scheme the total angular momentum of each branch in the configuration tree is first obtained. Then the momenta of each branch are coupled to the total angular momentum of the system. The three-body $\mathcal{J}\mathcal{J}_z$ coupling scheme reads:

$$|\mathcal{J}\mathcal{J}_z\mathcal{J}\rangle_{(ij)k} = \left| \left\{ \left[l_x (s_i s_j)_{\sigma_x} \right]_{j_x} [l_y s_k]_{j_y} \right\}_{\mathcal{J}} \right\rangle. \quad (1.121)$$

Decomposition of Faddeev components in partial wave basis is as follows:

$$\left| \psi^{(k)} \right\rangle = \sum_{n=l_x, \sigma_x, j_x, l_y, j_y, t_x} \frac{F_n^{(k)}(x, y)}{xy} \left\langle n, \hat{x}, \hat{y} \left| \left\{ \left[l_x (s_i s_j)_{\sigma_x} \right]_{j_x} [l_y s_k]_{j_y} \right\}_{\mathcal{J}} \right\rangle \right| \left[(t_i t_j)_{t_x} t_k \right]_{\mathcal{T}} \rangle. \quad (1.122)$$

$\mathcal{L}S$ coupling scheme is more suited when orbital angular momenta \mathcal{L} or/and total spin S are conserved. It is the case for non-identical particle systems with no spin dependent interactions, where one can easily separate the spin part. $\mathcal{J}\mathcal{J}_z$ coupling scheme is advantageous in treating nuclear systems, where orbital angular momentum and spins are no longer conserved separately, but are coupled by the interaction. An other advantage of $\mathcal{J}\mathcal{J}_z$ coupling is that the total basis is created as a sum of jj_z coupling schemes of its subsystems, therefore enabling us to extract(impose) easily 2-body wave functions from (to) the 3-body components.

For a four-body system I will work out only a $\mathcal{J}\mathcal{J}_z$ coupling scheme, since it is advantageous when dealing with nuclear force; this scheme will be used in all practical 4-body calculations. There

are two different $\mathcal{J}\mathcal{J}_z$ coupling schemes depending on which type of partition we are dealing with: K or H . They are as follows:

$$\left\{ \begin{array}{l} |T_{ij,k}^l\rangle = \left| \left[\left\{ (t_i t_j)_{t_x} t_k \right\}_{T_3} t_l \right]_{\mathcal{T}} \right\rangle \\ |J_{ij,k}^l\rangle = \left| \left[\left\{ \left[l_x (s_i s_j)_{\sigma_x} \right]_{j_x} [l_y s_k]_{j_y} \right\}_{j_{xy}} [l_z s_l]_{j_z} \right]_{\mathcal{J}} \right\rangle \\ \text{with} \\ \langle \hat{x} \hat{y} \hat{z} [l_{ij,k}] | J_{ij,k}^l \rangle = \mathcal{Y}_{\mathcal{J}}(\hat{x}, \hat{y}, \hat{z}) \\ = \mathcal{Y}_{\left[\left\{ [l_x (s_i s_j)_{\sigma_x}]_{j_x} [l_y s_k]_{j_y} \right\}_{j_{xy}} [l_z s_l]_{j_z} \right]_{\mathcal{J}}}(\hat{x}, \hat{y}, \hat{z}) \end{array} \right. \quad (1.123)$$

$$\left\{ \begin{array}{l} |T_{ij,kl}\rangle = \left| \left[(t_i t_j)_{t_x} (t_k t_l)_{t_y} \right]_{\mathcal{T}} \right\rangle \\ |J_{ij,kl}\rangle = \left| \left[\left\{ \left[l_x (s_i s_j)_{\sigma_x} \right]_{j_x} \left[l_y (s_k s_l)_{\sigma_y} \right]_{j_y} \right\}_{j_{xy}} l_z \right]_{\mathcal{J}} \right\rangle \\ \text{with} \\ \langle \hat{x} \hat{y} \hat{z} [ij,kl] | J_{ij,kl} \rangle = \mathcal{Y}_{\mathcal{J}}(\hat{x}, \hat{y}, \hat{z}) \\ = \mathcal{Y}_{\left[\left\{ [l_x (s_i s_j)_{\sigma_x}]_{j_x} [l_y (s_k s_l)_{\sigma_y}]_{j_y} \right\}_{j_{xy}} l_z \right]_{\mathcal{J}}}(\hat{x}, \hat{y}, \hat{z}) \end{array} \right. \quad (1.123)$$

To each four-body Faddeev-Yakubovski component – $|K_{ij,k}^l\rangle$ or $|H_{ij,kl}\rangle$ – is therefore associated the natural basis – $|\alpha xyz [l_{ij,k}] \rangle$ or $|\alpha xyz [ij,kl] \rangle$ – and in this basis each component can be decomposed into a sum of regularized functions

$$\begin{aligned} \langle \vec{x} \vec{y} \vec{z} [l_{ij,k}] | K_{ij,k}^l \rangle &= \sum_{\alpha} \frac{\alpha K_{ij,k}^l(x,y,z)}{xyz} \mathcal{Y}_{\alpha[l_{ij,k}]}(\hat{x}, \hat{y}, \hat{z}) \\ \langle \vec{x} \vec{y} \vec{z} [ij,kl] | H_{ij,kl} \rangle &= \sum_{\alpha} \frac{\alpha H_{ij,kl}(x,y,z)}{xyz} \mathcal{Y}_{\alpha[ij,kl]}(\hat{x}, \hat{y}, \hat{z}) \end{aligned} \quad (1.124)$$

Reverse relations are obtained by using the fact that basis functions $\mathcal{Y}_{\alpha[ij,kl]}$ are orthogonal:

$$\begin{aligned} \frac{\alpha K_{ij,k}^l(x,y,z)}{xyz} &= \langle \alpha xyz [l_{ij,k}] | K_{ij,k}^l \rangle \\ \frac{\alpha H_{ij,kl}(x,y,z)}{xyz} &= \langle \alpha xyz [l_{ij,k}] | H_{ij,kl} \rangle \end{aligned} \quad (1.125)$$

Projection of Faddeev equations

We will use the expressions of partial wave decomposed Faddeev components eq. (1.120) (or eq. (1.122)) to project the Faddeev equations into the angular momentum basis:

$$\left\{ \begin{array}{l} \langle n_1 x_1 y_1 | E - \hat{H}_0 - V_{23} | \psi^{(1)} \rangle = \langle n_1 x_1 y_1 | V_{23} (\psi^{(2)} + \psi^{(3)}) \rangle \\ \langle n_2 x_2 y_2 | E - \hat{H}_0 - V_{31} | \psi^{(2)} \rangle = \langle n_2 x_2 y_2 | V_{31} (\psi^{(3)} + \psi^{(1)}) \rangle \\ \langle n_3 x_3 y_3 | E - \hat{H}_0 - V_{12} | \psi^{(3)} \rangle = \langle n_3 x_3 y_3 | V_{12} (\psi^{(1)} + \psi^{(2)}) \rangle \end{array} \right. \quad (1.126)$$

Here \hat{H}_0 is the kinetic energy operator of the system, which in angular momentum basis takes the form:

$$\begin{aligned}\hat{H}_0 &= -\Delta^{(\alpha)}(x, y) \\ &= \frac{\hbar^2}{m_\alpha} \left[-\partial_{x_\alpha}^2 + \frac{l_x(l_x+1)}{x_\alpha^2} - \partial_{y_\alpha}^2 + \frac{l_y(l_y+1)}{y_\alpha^2} \right].\end{aligned}\quad (1.127)$$

If the interaction between the particles is local, then the interaction matrix V , written in its proper Jacobi co-ordinate basis, is diagonal in variables x, y , and furthermore independent of y . In angular momentum basis it takes the matrix form:

$$\hat{V}_{n'x'y',nxy} = V_{n',n}(x) \cdot \delta(x - x') \cdot \delta(y - y'), \quad (1.128)$$

In a general case the interaction matrix $V_{n',n}(x)$ is not diagonal in angular momentum basis. For instance, nuclear interaction has tensor terms, which couples different orbital momenta states. The corresponding interaction matrix can be written as:

$$V_{n',n}(x) = \delta_{j'_x, j_x} \delta_{s'_x, s_x} V_{(l'_x s'_x)_{j'_x}, (l_x s_x)_{j_x}}(x). \quad (1.129)$$

Using the preceding notations, Faddeev equations reads:

$$\left\{ \begin{array}{l} \sum_{\tilde{n}_1} \left[(E + \Delta^{(n_1)}(x_1, y_1)) \delta_{\tilde{n}_1, n_1} - V_{n_1, \tilde{n}_1}^{(23)}(x_1) \right] F_{\tilde{n}_1}^{(1)}(x_1, y_1) = \\ \sum_{\tilde{n}_1} V_{n_1, \tilde{n}_1}^{(23)}(x_1) \left[\sum_{n_2} \langle \tilde{n}_1 x_1 y_1 | \frac{x_1 y_1}{x_2 y_2} F_{n_2}^{(2)}(x_2, y_2) | n_2 x_2 y_2 \rangle + \sum_{n_3} \langle \tilde{n}_1 x_1 y_1 | \frac{x_1 y_1}{x_3 y_3} F_{n_3}^{(3)}(x_3, y_3) | n_3 x_3 y_3 \rangle \right] \\ \sum_{\tilde{n}_2} \left[(E + \Delta^{(n_2)}(x_2, y_2)) \delta_{\tilde{n}_2, n_2} - V_{n_2, \tilde{n}_2}^{(31)}(x_2) \right] F_{\tilde{n}_2}^{(2)}(x_2, y_2) = \\ \sum_{\tilde{n}_2} V_{n_2, \tilde{n}_2}^{(31)}(x_2) \left[\sum_{n_1} \langle \tilde{n}_2 x_2 y_2 | \frac{x_2 y_2}{x_1 y_1} F_{n_1}^{(1)}(x_1, y_1) | n_1 x_1 y_1 \rangle + \sum_{n_3} \langle \tilde{n}_2 x_2 y_2 | \frac{x_2 y_2}{x_3 y_3} F_{n_3}^{(3)}(x_3, y_3) | n_3 x_3 y_3 \rangle \right] \\ \sum_{\tilde{n}_3} \left[(E + \Delta^{(n_3)}(x_3, y_3)) \delta_{\tilde{n}_3, n_3} - V_{n_3, \tilde{n}_3}^{(12)}(x_3) \right] F_{\tilde{n}_3}^{(3)}(x_3, y_3) = \\ \sum_{\tilde{n}_3} V_{n_3, \tilde{n}_3}^{(12)}(x_3) \left[\sum_{n_1} \langle \tilde{n}_3 x_3 y_3 | \frac{x_3 y_3}{x_1 y_1} F_{n_1}^{(1)}(x_1, y_1) | n_1 x_1 y_1 \rangle + \sum_{n_2} \langle \tilde{n}_3 x_3 y_3 | \frac{x_3 y_3}{x_2 y_2} F_{n_2}^{(2)}(x_2, y_2) | n_2 x_2 y_2 \rangle \right] \end{array} \right. \quad (1.130)$$

The coupling terms in the right hand side of equations are obtained using the so called 3-body integral transition operators $\hat{h}_{n_i, n_j}(x_i, y_i, u_i)$, with $u_i = \hat{x}_i \cdot \hat{y}_i$:

$$\langle n_i x_i y_i | \frac{x_i y_i}{x_j y_j} F_{n_j}^{(j)}(x_j, y_j) | n_j x_j y_j \rangle = \int_{-1}^1 \hat{h}_{n_i, n_j}(x_i, y_i, u_i) \frac{x_i y_i}{x_j y_j} F_{n_j}^{(j)}(x_j, y_j) du \quad (1.131)$$

The explicit form of operators \hat{h} is derived in Appendix C. With the later expression we obtain an infinite set of two-dimensional coupled integro-differential equations in the form

$$\sum_{\tilde{n}_i} \left[(E + \Delta^{(n_i)}(x_i, y_i)) \delta_{\tilde{n}_i, n_i} - V_{n_i, \tilde{n}_i}^{(jk)}(x_i) \right] F_{\tilde{n}_i}^{(i)}(x_i, y_i) = \\ \sum_{\tilde{n}_i} V_{n_i, \tilde{n}_i}^{(jk)}(x_i) \left[\int_{-1}^1 \hat{h}_{\tilde{n}_i, n_j}(x_i, y_i, u_i) \frac{x_i y_i}{x_j y_j} F_{n_j}^{(j)}(x_j, y_j) du + \int_{-1}^1 \hat{h}_{\tilde{n}_i, n_k}(x_i, y_i, u_i) \frac{x_i y_i}{x_k y_k} F_{n_k}^{(k)}(x_k, y_k) du \right] \quad (1.132)$$

with $i = 1, 2, 3$ and where n_i indicates the set of quantum numbers for a given partial wave. In general, this set is infinite. In practice one can reduce it to a finite number of partial components by considering only the most relevant ones. Usually one restricts to partial waves with the smallest angular momentum values, hence having the most smooth angular dependence.

Projection of Faddeev-Yakubovski equations

In a similar way as for Faddeev equations, we will project into angular momentum basis Faddeev-Yakubovski equations (1.113) describing systems of four identical particles. Using expression (1.123) one obtains:

$$\begin{cases} \langle \alpha xyz [K] | \left(E - \hat{H}_0 - V \right) | K \rangle = \langle \alpha xyz [K] | V [(P^+ + P^-) \lceil (1 + Q) | K \rangle + | H \rangle] \\ \langle \alpha xyz [H] | \left(E - \hat{H}_0 - V \right) | H \rangle = \langle \alpha xyz [H] | V [\tilde{P} \lceil (1 + Q) | K \rangle + | H_{12,34} \rangle] \end{cases}$$

The kinetic energy operator is similar to the three-body one, but now it is simply three-dimensional:

$$\begin{aligned} \hat{H}_0 &= -\Delta^{(\alpha)}(x, y) \\ &= \frac{\hbar^2}{m} \left[-\partial_x^2 + \frac{l_x(l_x + 1)}{x^2} - \partial_y^2 + \frac{l_y(l_y + 1)}{y^2} - \partial_z^2 + \frac{l_z(l_z + 1)}{z^2} \right] \end{aligned}$$

The coupling terms appearing in the right hand side of equations turn to be double and single integral operators. Their explicit expressions are developed in Appendix D. Interchanging particles 1 and 2 does not change any of the distances x, y, z ; only vector projections onto x -axis change sign. One can easily show that

$$P_{12} |\alpha xyz [K]\rangle = (-1)^{l_x + s_x + t_x} |\alpha xyz [K]\rangle = \varepsilon |\alpha xyz [K]\rangle$$

and

$$P_{12} |\alpha xyz [H]\rangle = \varepsilon |\alpha xyz [H]\rangle .$$

In representation of angular momentum basis it results in reversing the x axis projections of system's momentum, spin and isospin. This gives a factor $(-1)^{l_x + s_x + t_x}$.

Using this simple property, one can easily show that:

$$\begin{aligned} \langle \alpha xyz [K] | P^+ | K \rangle &= \langle \alpha xyz [K] | P_{12} P^+ P_{12} | K \rangle = \langle \alpha xyz [K] | P_{12} P_{12} P_{23} P_{12} | K \rangle \\ &= \langle \alpha xyz [K] | P_{23} P_{12} | K \rangle = \langle \alpha xyz [K] | P^- | K \rangle \end{aligned}$$

and in the similar way:

$$\langle \alpha xyz [H] | P^+ | H \rangle = \langle \alpha xyz [H] | P^- | H \rangle$$

Using the latter expressions, as well as the notations of integral operators indicated in Appendix D, one finally obtains:

$$\begin{aligned} \sum_{\tilde{\alpha}} \left[(E + \Delta^{(\alpha)}(xyz)) \delta_{\alpha, \tilde{\alpha}} - V_{\alpha, \tilde{\alpha}}(x) \right] K_{\tilde{\alpha}}(x, y, z) &= \sum_{\tilde{\alpha}} V_{\alpha, \tilde{\alpha}}(x) \left[\int_{-1}^1 du \sum_{\alpha'} h_{\tilde{\alpha}, \alpha'}(x, y, z, u) \cdot K_{\alpha'}(x', y', z') \right. \\ &\quad + \int_{-1}^1 du \int_{-1}^1 dv \sum_{\alpha''} g_{\tilde{\alpha}, \alpha''}(x, y, z, u, v) K_{\alpha''}(x'', y'', z'') \\ &\quad \left. + \int_{-1}^1 du \int_{-1}^1 dv \sum_{\alpha'} f_{\tilde{\alpha}, \alpha'''}(x, y, z, u, v) \cdot H_{\alpha'''}(x''', y''', z''') \right] \\ \sum_{\tilde{\alpha}} \left[(E + \Delta^{(\alpha)}(xyz)) \delta_{\tilde{\alpha}, \alpha} - V_{\alpha, \tilde{\alpha}}(x) \right] H_{\tilde{\alpha}}(x, y, z) &= \sum_{\tilde{\alpha}} V_{\alpha, \tilde{\alpha}}(x) \left[\int_{-1}^1 du \sum_{\alpha'} j_{\tilde{\alpha}, \alpha'}(x, y, z, u) \cdot K_{\alpha'}(x', y', z') \right. \\ &\quad \left. + \sum_{\alpha''} k_{\tilde{\alpha}, \alpha''} H_{\alpha''}(x'', y'', z'') \right] \end{aligned} \quad (1.133)$$



1.3 Numerical Realization

1.3.1 Piecewise spline method

Once differential equations are established, one has to employ numerical methods to solve them. It turns out that spline decomposition, a method widely used in civil engineering applications, is a very effective tool to solve systems of differential equations. In few-body physics, it was first introduced by Payne [30] to solve the Faddeev equations in configuration space. The spline method mathematical foundations were laid by Boor and Swartz [31, 32]. They showed that a basis of piecewise polynomial functions of degree less than $m+k$ with $m-1$ continuous derivatives can be used to approximate the solution of m -th order differential equation with an error of $O(h^{m+k})$, where h is size of subintervals. One should require that the differential equation is only exactly satisfied at k Gauss quadrature points of the subintervals. The method consists of:

1. Subdividing the domain into a number of subintervals (a grid).
2. Expanding a wave function in a spline basis (we used Hermite polynomials) on the grid.
3. Requiring the equation to be satisfied on a set of well-chosen points (collocation points).

This procedure leads to a finite-dimensional algebraic problem, which is solved using linear algebra techniques.

Let us closer discuss the matter. Suppose we want to solve one-dimensional differential equation described by the linear operator \hat{L} , which is defined on the finite size domain $\mathfrak{R} \in [r_{\min}, r_{\max}]$:

$$\hat{L} * F(r) = 0, \quad (1.134)$$

with a solution F satisfying some boundary conditions at $r = r_{\min}$ and r_{\max} . To solve this system we divide \mathfrak{R} in subintervals $r_0 < r_1 < r_2 < \dots < r_N$ (for some finite grid $r_0 = r_{\min}$, $r_N = r_{\max}$). We search the solution F in the form:

$$F(r) = \sum_{j=0}^{k(N+1)-1} C_j S_j(r), \quad (1.135)$$

where S_j are Hermite piecewise polynomials of k -th order⁶ and where C_j is a set of unknown coefficients to determine. Due to its linearity, operator \hat{L} of eq. (1.134) acts only on known piecewise functions S_j , and its action can be determined at any r inside the domain \mathfrak{R} . In this way eq. (1.134) becomes:

$$\sum_{j=0}^{k(N+1)-1} C_j [\hat{L} * S_j(r)] = 0 \quad (1.136)$$

⁶their expressions for $k = 2$ (cubic splines) and 3 (quintic splines) are given in Appendix E

We demand that this system of equations is satisfied on a number of well-chosen points (collocation points, k for each subinterval)⁷. Consequently we obtain kN equations for $k(N+1)$ unknown coefficients C_j . We can as well implement k different boundary conditions to have a number of linear equations equal to the number of unknowns:

$$\sum_{j=0}^{k(N+1)-1} C_j \left[\hat{L} * S_j(\tilde{r}_i) \right] = 0 \quad i = 1, 2, \dots, k(N+1), \quad (1.137)$$

where \tilde{r}_i signifies i -th collocation point.

It is not very difficult to generalize this method for systems of differential equations depending on more variables. In this way, the unknown function should be expanded on multidimensional basis of Hermite polynomials

$$F(x, y, z, \dots) = \sum_{j_x=0}^{k(N_x+1)-1} S_{j_x}^x(x) \sum_{j_y=0}^{k(N_y+1)-1} S_{j_y}^y(y) \sum_{j_z=0}^{k(N_z+1)-1} S_{j_z}^z(z) \left[\sum \dots \right] C_{j_x, j_y, j_z, \dots} \quad (1.138)$$

The system of coupled differential equations is validated on a set of collocation points of a multidimensional mesh, i.e. at points \vec{r}_i , where i represents a set (i_x, i_y, i_z, \dots) of collocation point indexes at the mesh subdomains. Index i runs through all the possible combinations of the set (i_x, i_y, i_z, \dots) . Each subset index i_w , varies from 1 to $k(N_w + 1)$, and describes \vec{r}_i projection on axis w and gives the collocation point w_{i_w} .

Resulting systems of linear equations

As was discussed in previous section, spline interpolation can be employed to transform a system of differential equations into a finite-dimensional linear algebra problem. For bound states, one obtains a matrix generalized eigenvalue equation, which reads:

$$Ac = EBc. \quad (1.139)$$

For scattering states, since the value of scattering energy is fixed, one is left with a linear system of equations:

$$Ac = b \quad (1.140)$$

The unknown vector c represents the set of spline interpolant coefficients C_i . Homogeneous term b is a vector of spline coefficients imposed by the boundary conditions. Square matrices A, B are obtained by performing the product $\left[\hat{L} * S_j(\tilde{r}_i) \right]$ in eq. (1.137).

Resulting linear systems are of very large size. More precisely, the number of equations is:

$$N = N_a \prod_{i=1}^n k_i(N_i + 1),$$

⁷Knowing the properties of Gauss integral quadrature, it becomes rather obvious [32], that if the exact solution can be extrapolated in any subinterval by polynomials of order $m = 2k - 1$, then the numerically obtained one would be exact if differential equations are satisfied on only k Gauss quadrature points of this subinterval.

where n is the dimension of the configuration space, N_i and k_i are respectively the number of points and the number of spline associated with each point of a given dimension, N_a is the number of coupled integro-differential equations. To obtain a converged solution for the 4-body problem with realistic nuclear potentials one needs $N_a = N_{aH} + N_{aK} \sim (500 - 1000)$ and at least $k_i(N_i + 1) = 30$ for each dimension x, y, z . So, the total number of equations is $N \sim 10^7$ and the resulting matrices have $\sim 10^{14}$ elements. Such dimensions make impossible a direct application of matrix inversion methods, since it would require memory of $\sim 10^9$ MB just for matrices to be stored. This by far exceeds capacities of the largest hard disk installations.

However, one can observe that due to finite size of spline interpolants, obtained matrices are rather sparse. One can employ the iterative methods, which do not need storage space for square matrices to be explicitly provided. These methods, relying only on matrix-vector multiplication operations, turn to be very efficient in treating large linear systems.

Structure of the matrix

In previous section we discussed how to transform a system of differential equations into a system of linear equations by using the spline interpolation functions. It resulted into equivalent linear algebra equations (1.139-1.140). It is useful to have the explicit expressions for matrices A and B .

By analyzing the system of differential equations (1.133), it is convenient to express each term in separate matrix. We make use of the following definitions:

- $[B]$ will stand for matrix appearing with total energy E , as in eq. (1.139)
- $[\Delta]$ gathers the terms implemented by the kinetic energy operator,
- $[V]$ represents the matrix given by potential energy terms in left hand side of equation,
- $[H], [G], [F], [J], [K]$ are the matrices induced by the coupling terms in the right hand sides of Faddeev (FY) equations.

Here and below I will provide explicit expressions for the 4-body problem, with spline interpolation being done in 3-dimensional configuration space. 3-Body equations are imbibed in 4-body ones, and can be extracted from 4-body K components by removing z-coordinate depending terms.

Matrix $[B]$ Although the total energy appears in equation (1.133) as diagonal term (its value being simple scale factor) in variables α, x, y, z , spline interpolation matrix $[B]$ associated with it (or standing behind energy value E) is not diagonal in our approach. In fact, for a given collocation point, several polynomials of interpolation are non-zero (to be precise 2^*k for each coordinate). Using eq. (1.138) one easily finds:

$$[B]_{n,n'} = \delta_{\alpha,\alpha'} S_{j'_x}^x(x_{j_x}) S_{j'_y}^y(y_{j_y}) S_{j'_z}^z(z_{j_z}). \quad (1.141)$$

Indexes n and n' stand for a bijection of sub-indexes (α, j_x, j_y, j_z) and $(\alpha', j'_x, j'_y, j'_z)$ consequently. It is worth noticing that elements of the matrix $[B]$ are independent of α .

Matrix $[V]$ The case of matrix $[V]$ is similar to that of matrix $[B]$. Its elements can be expressed as a product:

$$[V]_{n,n'} = V_{\alpha,\alpha'}(x_{j_x}) \cdot S_{j'_x}^x(x_{j_x}) S_{j'_y}^y(y_{j_y}) S_{j'_z}^z(z_{j_z}) \quad (1.142)$$

It is useful to express this matrix as a product of $[B]$ with pure potential matrix \tilde{V} , which in case of local interactions, is diagonal in variables x, y, z and independent of both y and z :

$$\left[\tilde{V} \right]_{n,\tilde{n}} = V_{\alpha,\tilde{\alpha}}(x_{j_x}) \delta_{j_x, \tilde{j}_x} \delta_{j_y, \tilde{j}_y} \delta_{j_z, \tilde{j}_z}. \quad (1.143)$$

Therefore

$$[V]_{n,n'} = \sum_{\tilde{n}} \left[\tilde{V} \right]_{n,\tilde{n}} [B]_{\tilde{n},n'}. \quad (1.144)$$

Matrix $[\Delta]$ Obtaining elements of this matrix is pure triviality. One simply has to apply kinetic energy operator eq. (1.127) on spline interpolant function basis:

$$\begin{aligned} [\Delta]_{n,n'} &= \frac{\hbar^2}{m} \delta_{\alpha,\alpha'} \left[S_{j'_x}^{x''}(x_{j_x}) S_{j'_y}^y(y_{j_y}) S_{j'_z}^z(z_{j_z}) - \frac{l_x(l_x+1)}{x_{j_x}^2} S_{j'_x}^x(x_{j_x}) S_{j'_y}^y(y_{j_y}) S_{j'_z}^z(z_{j_z}) \right. \\ &\quad + S_{j'_x}^x(x_{j_x}) S_{j'_y}^{y''}(y_{j_y}) S_{j'_z}^z(z_{j_z}) - \frac{l_y(l_y+1)}{y_{j_y}^2} S_{j'_x}^x(x_{j_x}) S_{j'_y}^y(y_{j_y}) S_{j'_z}^z(z_{j_z}) \\ &\quad \left. + S_{j'_x}^x(x_{j_x}) S_{j'_y}^y(y_{j_y}) S_{j'_z}^{z''}(z_{j_z}) - \frac{l_z(l_z+1)}{z_{j_z}^2} S_{j'_x}^x(x_{j_x}) S_{j'_y}^y(y_{j_y}) S_{j'_z}^z(z_{j_z}) \right], \end{aligned} \quad (1.145)$$

S'' designates here the second order derivatives.

Integral operators Let us discuss the general case of integral operators. By using Gauss integration rule one can evaluate integral

$$\int_a^b f(u) du \approx \sum_{i=1}^{N_u} f(u_i) w_i, \quad (1.146)$$

where u_i are Gauss distribution points in interval $[a, b]$, and w_i their relative weights. The former formula is exact for functions $f(u)$ which are polynomials of order not exceeding $2 * N_u - 1$. Therefore, for rather smooth functions it provides a very good approximation even if having only few terms in the sum⁸. Applying this Gauss rule, one obtains the following expressions for integral operators:

$$[H]_{n,n'} = \sum_{\tilde{\alpha}, \alpha'} V_{\alpha, \tilde{\alpha}}(x_{j_x}) \cdot \sum_{i_u=1}^{N_u} h_{\tilde{\alpha}, \alpha'}(x_{j_x}, y_{j_y}, z_{j_z}, u_{i_u}) \cdot S_{j'_x}^x(x_{j_x}^h) S_{j'_y}^y(y_{j_y}^h) S_{j'_z}^z(z_{j_z}^h) \quad (1.147)$$

⁸In practice, results are well converged for relatively low $N_u \sim 8$. Even for the most precision demanding calculations there is no need of taking more than 16 Gauss points per variable.

When dealing with local interactions, one can separate pure potential matrix $[\tilde{V}]$, and express integral operators as a product of two matrices:

$$[H]_{n,n'} = \sum_{\tilde{n}} [\tilde{V}]_{n,\tilde{n}} [\tilde{H}]_{\tilde{n},n'} \quad (1.148)$$

and

$$[\tilde{H}]_{\tilde{n},n'} = \sum_{i_u=1}^{N_u} h_{\tilde{\alpha},\alpha'}(x_{j_x}, y_{j_y}, z_{j_z}, u_{i_u}) \cdot S_{j'_x}^x(x_{\tilde{\alpha},\alpha'}^h) S_{j'_y}^y(y_{\tilde{\alpha},\alpha'}^h) S_{j'_z}^z(z_{\tilde{\alpha},\alpha'}^h). \quad (1.149)$$

This separation is useful in numerical applications: it provides extra flexibility to the code requiring less storage memory.

Other integral operators are analogous to this one. Here, I will develop expressions only for the elements of double integral requiring matrix $[G]$ and no integral requiring matrix $[K]$. Expression for elements of matrix $[F]$ are identical to those of $[G]$, since they are double-integral operators. Expression for $[J]$ -matrix are identical to $[H]$ – *matrix* both being single-integral operators.

$$\begin{aligned} [G]_{n,n'} &= \sum_{\tilde{n}} [\tilde{V}]_{n,\tilde{n}} [\tilde{G}]_{\tilde{n},n'} \\ [K]_{n,n'} &= \sum_{\tilde{n}} [\tilde{V}]_{n,\tilde{n}} [\tilde{K}]_{\tilde{n},n'} \end{aligned} \quad (1.150)$$

$$\begin{aligned} [\tilde{G}]_{\tilde{n},n'} &= \sum_{i_u=1}^{N_u} \sum_{i_v=1}^{N_v} g_{\tilde{\alpha},\alpha'}(x_{j_x}, y_{j_y}, z_{j_z}, u_{i_u}, v_{i_v}) \cdot S_{j'_x}^x(x_{\tilde{\alpha},\alpha'}^g) S_{j'_y}^y(y_{\tilde{\alpha},\alpha'}^g) S_{j'_z}^z(z_{\tilde{\alpha},\alpha'}^g) \\ [\tilde{K}]_{\tilde{n},n'} &= f_{\tilde{\alpha},\alpha'} \cdot S_{j'_x}^x(x_{\tilde{\alpha},\alpha'}^k) S_{j'_y}^y(y_{\tilde{\alpha},\alpha'}^k) S_{j'_z}^z(z_{\tilde{\alpha},\alpha'}^k) \end{aligned} \quad (1.151)$$

Bound states

To obtain eigenvalue equation (1.139), one has just to collect terms in matrix $[A]$:

$$\begin{aligned} [A] &= ([V] - [\Delta] + [W]) \\ &\text{with } [W] \text{ signifying sum of all integral terms} \\ [W] &= [F] + [G] + [H] + [J] + [K] \end{aligned} \quad (1.152)$$

Scattering states

The scattering wave function is not vanishing. Therefore, even for extreme values of the grid it will not fall to zero. One needs to implement additional term due to boundary conditions. With no loss of generalization, one can easily fix the value of the open channels amplitudes at z_m , to be:

$$F_\alpha(x, y, z_M) = f_\alpha(x, y) S_{k_z N_z + 1}(z_M), \quad (1.153)$$

where functions $f_\alpha(x, y)$ represent partial wave components of the residual bound state(s) wave function. For amplitudes K, f_α describes the bound state of particles (123), whereas for amplitudes H it designates the composite state of two separated bound pairs (12) and (34).

The function $f_\alpha(x, y)$ can be projected into spline basis:

$$f_\alpha(x, y) = \sum_{j_x=0}^{k(N_x+1)-1} S_{j_x}^x(x) \sum_{j_y=0}^{k(N_y+1)-1} S_{j_y}^y(y) \cdot C_{\alpha, j_x, j_y} \quad (1.154)$$

Imposing certain value for extreme points of the grid will result in the appearing of the inhomogeneous term, which in eq. (1.137) is denoted by vector b . This vector is a result of the operator \hat{L} eq. (1.134) acting on the irregular wave function term F eq. (1.153), and is given by:

$$\begin{aligned} b_n = & \sum_{\alpha', j'_x, j'_y} C_{\alpha', j'_x, j'_y} \left[(E - V_{\alpha, \alpha'}(x_{j_x})) \cdot S_{j'_x}^x(x_{j_x}) S_{j'_y}^y(y_{j_y}) S_{2N_z+1}(z_M) \right. \\ & - \frac{\hbar^2}{m} \delta_{\alpha, \alpha'} \left(\begin{array}{l} S_{j'_x}^{xx''}(x_{j_x}) S_{j'_y}^y(y_{j_y}) S_{k_z N_z + 1}^z(z_{j_z}) - \frac{l_x(l_x+1)}{x_{j_x}^2} S_{j'_x}^x(x_{j_x}) S_{j'_y}^y(y_{j_y}) S_{k_z N_z + 1}^z(z_{j_z}) \\ + S_{j'_x}^x(x_{j_x}) S_{j'_y}^{yy''}(y_{j_y}) S_{k_z N_z + 1}^z(z_{j_z}) - \frac{l_y(l_y+1)}{y_{j_y}^2} S_{j'_x}^x(x_{j_x}) S_{j'_y}^y(y_{j_y}) S_{k_z N_z + 1}^z(z_{j_z}) \\ + S_{j'_x}^x(x_{j_x}) S_{j'_y}^y(y_{j_y}) S_{k_z N_z + 1}^{zz''}(z_{j_z}) - \frac{l_z(l_z+1)}{z_{j_z}^2} S_{j'_x}^x(x_{j_x}) S_{j'_y}^y(y_{j_y}) S_{k_z N_z + 1}^z(z_{j_z}) \end{array} \right) \\ & + V_{\alpha, \alpha'}(x_{j_x}) \cdot \left[f_{\tilde{\alpha}, \alpha'} \cdot S_{j'_x}^x(x_{\alpha, \alpha'}^h) S_{j'_y}^y(y_{\alpha, \alpha'}^h) S_{k_z N_z + 1}^z(z_{\alpha, \alpha'}^h) \right. \\ & + \sum_{i_u=1}^{N_u} h_{\tilde{\alpha}, \alpha'}(x_{j_x}, y_{j_y}, z_{j_z}, u_{i_u}) \cdot S_{j'_x}^x(x_{\alpha, \alpha'}^h) S_{j'_y}^y(y_{\alpha, \alpha'}^h) S_{j'_z}^z(z_{\alpha, \alpha'}^h) \\ & + \sum_{i_u=1}^{N_u} J_{\tilde{\alpha}, \alpha'}(x_{j_x}, y_{j_y}, z_{j_z}, u_{i_u}) \cdot S_{j'_x}^x(x_{\alpha, \alpha'}^j) S_{j'_y}^y(y_{\alpha, \alpha'}^j) S_{j'_z}^z(z_{\alpha, \alpha'}^j) \\ & + \sum_{i_u=1}^{N_u} \sum_{i_v=1}^{N_v} g_{\tilde{\alpha}, \alpha'}(x_{j_x}, y_{j_y}, z_{j_z}, u_{i_u}, v_{i_v}) \cdot S_{j'_x}^x(x_{\alpha, \alpha'}^g) S_{j'_y}^y(y_{\alpha, \alpha'}^g) S_{j'_z}^z(z_{\alpha, \alpha'}^g) \\ & \left. + \sum_{i_u=1}^{N_u} \sum_{i_v=1}^{N_v} k_{\tilde{\alpha}, \alpha'}(x_{j_x}, y_{j_y}, z_{j_z}, u_{i_u}, v_{i_v}) \cdot S_{j'_x}^x(x_{\alpha, \alpha'}^k) S_{j'_y}^y(y_{\alpha, \alpha'}^k) S_{j'_z}^z(z_{\alpha, \alpha'}^k) \right] \end{aligned} \quad (1.155)$$

It remains to collect all these terms in scattering matrix $[A]$ of eq. (1.137). This matrix differs from the bound state one by the fact that energy terms, represented by the product $E[B]$, are absorbed in it:

$$[A] = ([V] - E[B] - [\Delta] + [W]) \quad (1.156)$$

1.3.2 Numerical methods of linear algebra problems

Bound state problem

Spline expansion for bound states have resulted in linear algebra eigenvalue equations (1.139). However, the obtained linear problem is usually of very large size, which makes application of direct matrix inversion methods impossible. I will stretch here out a few methods, which enable

to extract physical eigenvalues from large size eigenvalue-eigenvector problem by avoiding explicit matrix inversion.

Inverse iteration method Eigenvalue problem, eq. (1.139), can be rewritten in the form:

$$\left(E_0 - [B]^{-1} [A] \right) \psi = (E_0 - E) \psi \quad (1.157)$$

with E_0 being some starting guess value for a searched bound state energy.

By arbitrarily choosing some starting vector x_0 and using the fact that any vector can be decomposed in basis of matrix $B^{-1}A$ eigenvectors, we write

$$x_k = \sum_i C_i^{(k)} \psi_i, \quad (1.158)$$

where $C_i^{(k)}$ are some expansion coefficients.

We define the following recursive sequence:

$$\left(E_0 - [B]^{-1} [A] \right) x_n = x_{n-1}. \quad (1.159)$$

One can easily remark that:

$$x_n = \sum_i C_i^{(n)} \psi_i = \sum_i \frac{1}{(E_0 - E_i)} C_i^{(n-1)} \psi_i = \sum_i \frac{1}{(E_0 - E_i)^n} C_i^{(0)} \psi_i. \quad (1.160)$$

Therefore, if E_0 is close to some eigenvalue E_i , x will converge to the corresponding eigenvector ψ_i . Therefore

$$\lim_{n \rightarrow \infty} \frac{\langle x_n | x_{n-1} \rangle}{\langle x_n | x_n \rangle} = \lim_{n \rightarrow \infty} \frac{\langle x_{n-1} | x_{n-1} \rangle}{\langle x_n | x_{n-1} \rangle} = E_0 - E_i. \quad (1.161)$$

It turns to be that by properly choosing starting energy E_0 and continuously resolving eq. (1.159), independently of guess vector x_0 , we will converge to the closest eigenvalue to E_0 . In other words, eigenvalue-eigenvector problem is reduced to consequent resolution of linear equations of the (1.159) form.

Power (Malfiet-Tjon) method There is another technique to solve physical eigenvalue problem, popularized by Malfiet and Tjon in [33]. It is based on the observation that the absolute largest eigenvalue λ_{\max} for an eigensystem of type:

$$K\psi = \lambda\psi \quad (1.162)$$

is easy to find. The most obvious way is due to the so called Power method. By starting with some $x_0 = \sum_i C_i^{(0)} \psi_i$ we can see that:

$$x_n = K^n x_0 = \sum_i \lambda_i^n C_i^{(0)} \psi_i \quad (1.163)$$

and

$$\lim_{n \rightarrow \infty} \frac{x_n}{x_{n-1}} = \lambda_{\max} \quad \lim_{n \rightarrow \infty} \frac{x_n}{\langle x_n | x_n \rangle} = \psi(\lambda_{\max}) \quad (1.164)$$

Therefore x_n tends towards the eigenstate corresponding to eigenvalue λ_{\max} .

Let us write the eigenvalue equation in a matrix form:

$$([V] - [\Delta] + [W]) \psi = EB\psi. \quad (1.165)$$

By introducing some guess eigenenergy E_0 we can reformulate the upper equation in the form:

$$(E_0 [B] - [V] + [\Delta])^{-1} [W] \psi = \lambda(E_0) \psi. \quad (1.166)$$

So, if E_0 is exactly the ground state energy E_{GS} of eq. (1.166), then $\lambda(E_{GS}) = 1$, whereas if it is some other eigenvalue E_i of eq. (1.165) one will have $\lambda(E_i) < 1$. Furthermore, it can be easily shown that if we have purely attractive potential $0 < \lambda(E_i) \leq 1$. Therefore λ corresponding to the ground state with E_{GS} is the absolute largest eigenvalue. For guess energies $E_0 < E_{GS}$, after solving eq. (1.166), one has $\lambda < 1$, while if $E_0 > E_{GS}$ one gets $\lambda(E_0) > 1$.

If the potential has also a repulsive part, negative eigenvalues λ will also occur and it may become smaller than -1. Then eq. (1.166) will converge towards this spurious eigenvalue. A simple algorithm to overcome this problem was proposed in [34, 35]. Firstly, one should evaluate this parasite eigenvalue $\lambda_{\max} < -1$ and then modify eq. (1.166):

$$\left((E_0 [B] - [V] + [\Delta])^{-1} V - \lambda_{\max} \right) \psi = \lambda'(E_0) \psi. \quad (1.167)$$

Therefore λ_{\max} is mapped onto $\lambda' \approx 0$, whereas the physical eigenvalue, corresponding to E_{GS} , becomes $\lambda' = 1 - \lambda_{\max}$.

Discussion In previous subsection, two different methods were presented to solve physical bound state problem. These methods are based on iterative techniques and both employ similar matrix vector product operations. This enables us to use special properties of these matrices (sparsity, tensor structure) and to avoid their explicit storage. One should mention that these two methods require performing vector multiplication operations with inversed matrices: interpolation matrix $[B]^{-1}$ and inverse of kinetic energy operator $(E_0 [B] - [V] + [\Delta])^{-1}$. However, these matrices turn to have simple tensor structure in Euclidean coordinates and their inverse can be easily performed. This will be discussed in the next section.

The principal technical difference of these two methods is that inverse iteration method requires to perform successively solutions of linear system of equations. And, even though linear system is solved using iterative techniques, more operations are always needed to obtain a converged solution than using the power method. The advantage of inverse iteration method lies in its ability to treat the excited state problem on the same foot as the ground state. Malfiet-Tjon technique for excited states becomes then complicated for it requires finding eigenfunctions of all lower lying states and afterwards, at each step, orthogonalize the solution in this eigenfunction basis.

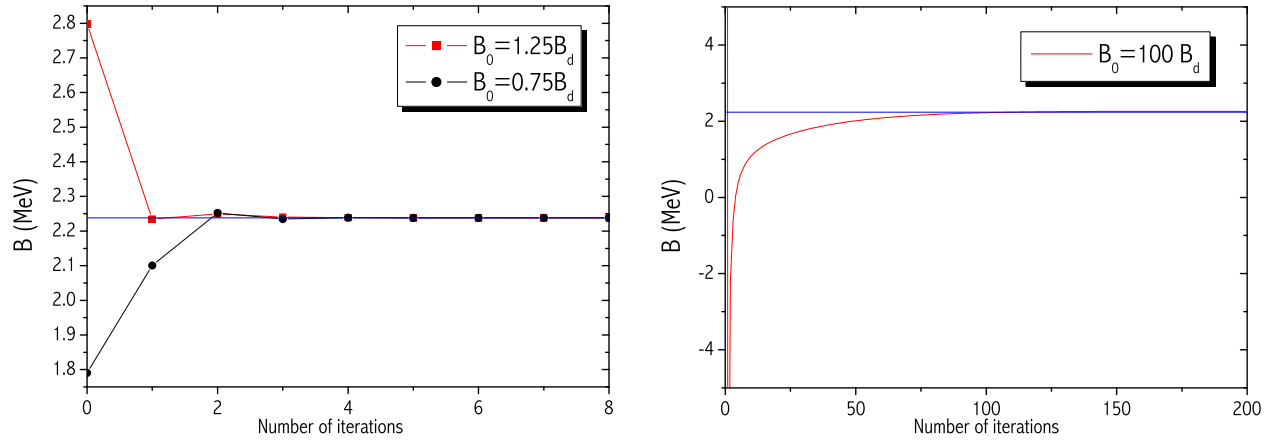


Figure 1.5: Convergence of inverse iteration method in calculating deuterium's ground state binding energy. The guess energies were taken close to eigenvalue $B_0 = 2.2245$ MeV. The same calculations, just guess value for deuterium binding energy, was chosen to be 100 times larger.

One should remark that inverse iteration method is very sensitive on guess energy value and if the guess is not close enough to the searched eigenvalue, it converges very slowly (see Fig. 1.5). For Malfiet-Tjon method, the dependence of $\lambda(E)$ is almost logarithmic (see Fig. 1.6) and therefore very effective codes can be written in order to find ground state energy E_g , for which $\lambda(E_g) = 1$. Usually, one needs no more than 5-10 iterations to get converged value when Malfiet-Tjon method is in use. However, this method fails when the interaction potential has a very repulsive core (as Aziz potential [36]), or some very large eigenvalues (harmonic oscillator⁹). In this case the physical state with negative eigenvalue is hidden by the existence of many non-physical eigenvalues which are extremely large and positive. To impose the physical negative eigenvalue to be the largest in the spectrum, one should find with very high precision the largest positive one, which numerically is not always possible. On the other hand, after the eigenvalue remapping, one obtains negative eigenvalue $\lambda(E)$ being very close to each other and hardly distinguishable.

Solution of linear systems using iterative methods

As mentioned before, due to our need of solving linear systems of extremely large sizes, direct methods can not be put in practice. They require explicit place to store and perform operations with the matrices. Recently a number of efficient iterative methods were developed to handle large sparse linear systems [37, 38]. In general, these methods do not require the storage of matrix; they rather rely on successive application of arithmetic matrix vector operations.

Most of the existing iterative techniques for solving large linear systems utilize, in one or another

⁹Nevertheless, in the case of harmonic oscillator potential, one can single out problem of spurious infinitely large eigenvalues. The growth of potential can be switched off at some large r , where searched bound state wave function is already negligibly small and does't affect bound state energy.

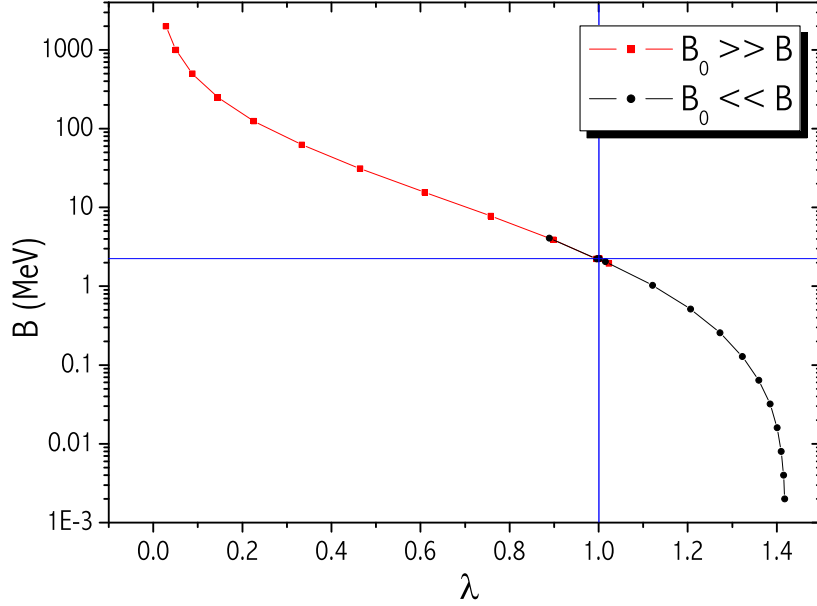


Figure 1.6: Dependence of projected value function $\lambda(B_g)$ on given guess value B in deuterium binding energy calculations.

way, a projection process. Consider the linear system:

$$Ax = b, \quad (1.168)$$

where A is $n \times n$ matrix. The idea of projection technique is to extract an approximation to the solution of a linear system from a subspace of a \mathcal{R}^n (linear map of matrix A). If \mathcal{K} is this subspace of candidate approximates, or search subspace, and m is its dimension, then m constraints should be imposed to be able to extract such an approximation. A typical way of describing these constraints is to impose m independent orthogonality conditions. Specifically, the residual vector $b - Ax$ is constrained to be orthogonal to m linearly independent vectors. This defines another subspace \mathcal{L} of dimension m which is called the subspace of constraints or left subspace. This simple framework is common to many different mathematical methods and is known as the Petrov-Galerkin conditions.

$$b - Ax_m \perp \mathcal{L}_m \quad (1.169)$$

Let $V = [v_1, v_2, \dots, v_m]$, be a $n \times m$ matrix, whose column-vectors form a basis of \mathcal{K}_m , and similarly let $W = [w_1, w_2, \dots, w_m]$ be the matrix representing basis of \mathcal{L}_m . If the approximate solution is written as:

$$x = x_0 + Vy \quad (1.170)$$

and the initial residual vector is $r_0 = b - Ax_0$, then the orthogonality condition leads immediately to the following system of equations for the vector y :

$$W^\dagger AVy = W^\dagger r_0 \quad (1.171)$$

If the assumption is made that the matrix $W^\dagger AV$ is nonsingular, the following expression for the approximate solution \tilde{x} results:

$$\tilde{x} = x_0 + V \left(W^\dagger AV \right)^{-1} W^\dagger r_0 \quad (1.172)$$

In many algorithms the matrix $(W^\dagger AV)$ does not have to be formed since it is available as a by-product of the algorithm. The practical choice of subspace \mathcal{K} is so called Krylov subspace:

$$\mathcal{K}_m(A, r_0) = \text{span} \{ r_0, Ar_0, A^2r_0, \dots, A^{m-1}r_0 \}. \quad (1.173)$$

In this way one constructs the basis for approximate solution by just multiplying some guess vector with the linear system's matrix A . Different versions of Krylovs methods arise from different choices of subspace \mathcal{L}_m . The most straightforward way is the so called orthogonal projection technique, for which \mathcal{L} is the same as \mathcal{K} . We will use a slightly modified definition where $\mathcal{L} = A\mathcal{K}$. Then Arnoldi's procedure can be applied to build an orthogonal basis of the Krylov subspace \mathcal{K}_m . In exact arithmetic, one variant of the algorithm due to Y. Saad [39] is as follows:

Algorithm 1 Arnoldi

1. Choose a vector v_1 of norm 1.
2. For $j=1$ to m Do
 - Compute $h_{ij} = (Av_j, v_i)$ $i = 1, 2, \dots, j$
 - Compute $w_j = Av_j - \sum_{i=1}^j h_{ij}v_i$
 - $h_{j+1,j} = \|w_j\|_2$. If $h_{j+1,j} = 0$ Stop.
 - $v_{j+1} = w_j/h_{j+1,j}$
3. End Do.

By taking as a starting vector $v_1 = r_0 / \|r_0\|_2$ and relaying on Arnoldi procedure, one obtains the so called GMRES algorithm. At each step of Arnoldi's procedure, Heisenberg type matrix $\bar{H}_{m+1,m}$, constituting of elements h_{ij} is supplied by an additional column. Matrix $H = W^\dagger AV$ contains m first lines of matrix \bar{H}_m , and thus the approximate solution after m iterative steps is the one for which the residual norm

$$\begin{aligned} J(y) &= \|b - Ax\|_2 = \|b - A(x_0 + V_m y)\|_2 = \|r_0 - AV_m y\|_2 \\ &= \|V_{m+1} (\|r_0\|_2 e_1 - \bar{H}_m y)\|_2 = \|\|r_0\|_2 e_1 - \bar{H}_m y\|_2 \end{aligned} \quad (1.174)$$

is the smallest. In other words:

$$y = \arg \left(\min_y \|\|r_0\|_2 e_1 - \bar{H}_m y\|_2 \right). \quad (1.175)$$

The minimizer y_m is inexpensive to compute since it requires the solution of an $(m+1) \times m$ least-squares problem, where m should be small (of the order $\preccurlyeq 50$) for well convergent iteration procedure. Thus, approximate solution and its residual norm can be obtained after each Arnoldi's

iteration step. The most computer memory demanding task is due to the need of keeping the $(m + 1)$ vectors of matrix V . It requires storage space for $(m + 1) \times n$ real numbers.

These requirements can be moderated. One should remark that it is not necessary to grow m up till $h_{j+1,j}$ is zero. One can restart Arnoldi's procedure after m reaches some maximal value by imposing new $v_1 = r_0 / \|r_0\|_2 = (b - Ax_m) / \|b - Ax_m\|_2$. However, restarted GMRES algorithm is usually less efficient for it converges after more iteration steps than the standard one.

BICGSTAB While GMRES algorithm looks as the most robust iterative method, its deficiency is the need of accumulating the basis vectors of Krylov subspace (or matrix V), which for very large linear systems can be extremely costly. However, there are a few iterative solution schemes which overcome this deficiency and perform operations only with current vectors of subspaces \mathcal{K}_m and \mathcal{L}_m . One of such algorithms is BICGSTAB due to van der Vorst [40]. This algorithm relies on biorthogonal basis for the two subspaces:

$$\mathcal{K}_m(A, r_0) = \text{span} \{v_1, Av_1, A^2v_1, \dots, A^{m-1}v_1\} \quad (1.176)$$

and

$$\mathcal{L}_m(A, r_0) = \text{span} \left\{w_1, A^\dagger w_1, (A^\dagger)^2 w_1, \dots, (A^\dagger)^{m-1} w_1\right\} \quad (1.177)$$

Thus, in principle, this algorithm should require operations of multiplication with matrices A^\dagger . However, it is remarked that vectors generated with A^\dagger do not contribute directly to the solution. Instead, they are used only to obtain the scalars needed in the algorithm. The multiplication of vectors with A^\dagger matrix is bypassed by making some approximations.

Algorithm 2 BICGSTAB

1. Compute $r_0 = b - Ax_0$; choose arbitrary r_0^*

2. $p_0 = r_0$

3. For $j=1,2\dots$, until convergence Do

$$\alpha_j = (r_j, r_0^*) / (Ap_j, r_0^*)$$

$$s_j = r_j - \alpha_j Ap_j$$

$$w_j = (As_j, s_j) / (As_j, As_j)$$

$$x_{j+1} = x_j + \alpha_j p_j + w_j s_j$$

$$\beta_j = \frac{(r_{j+1}, r_0^*)}{(r_j, r_0^*)} \frac{\alpha_j}{w_j}$$

$$p_{j+1} = r_{j+1} + \beta_j(p_j - w_j Ap_j)$$

4. End Do.

Preconditioning Although the methods seen in previous chapter are well founded theoretically, they are all likely to suffer from slow convergence. Typically, convergence is guaranteed only after $m \sim n$ iterative steps of orthogonalization, where n stands for the dimensions of the matrix. Of course, such convergence is not satisfactory since resolution time will grow as n^3 (even faster than for the direct methods).

The remedy for improving robustness and efficiency of iterative methods is *preconditioning*. *Preconditioning* simply means the transformation of the original linear system into another one, which has the same solution, but which is likely to be easier to be solved with an iterative solver. In fact, the reliability of iterative techniques, when dealing with various applications, depends much more on the quality of the preconditioning than on the particular Krylov subspace accelerator in use.

The principal idea of preconditioning is to solve systems

$$\begin{aligned} M^{-1}Ax &= M^{-1}b \quad (\text{left preconditioning}) \\ \text{or} \\ AM^{-1}x &= M^{-1}b \quad (\text{right preconditioning}) \end{aligned} \tag{1.178}$$

which are identical to the initial system $Ax = b$, but preconditioning matrix M^{-1} is such that it makes iterative process converge more rapidly. It is obvious that if $M^{-1} = A^{-1}$, the exact solution will be obtained after the first iteration. Therefore the successful preconditioning matrix should in some way approximate the inverse of matrix A . In fact, if one supposes that $A = M + \Delta M$, where ΔM only slightly modifies the kernel of matrix M , one has:

$$x = A^{-1}b = (M + \Delta M)^{-1}b = M^{-1}(1 - M^{-1}\Delta M + (M^{-1}\Delta M)^2 - \dots)b. \tag{1.179}$$

After each iteration one will span with at least one more term of the Taylor expansion and therefore iterative method should quickly converge, since $M^{-1}\Delta M \ll 1$.

Standard *preconditioners* proposed by pure mathematical algorithms are based on the non-zero structure of the matrix. The simplest *preconditioner* is the inverse of the diagonal of A . One can improve this technique by inverting more lines close to diagonal, as well as forcing to invert the subdiagonals consisting the largest ('most important') elements of the initial matrix. In Fig. 1.7 is shown the efficiency of various matrix structure based *preconditioners* for a system of 100 equations. It follows that non preconditioned GMRES converges only after the number of iterations, which is almost equal to the size of linear system. Using diagonal inverse and more complicated *preconditioners*, the number of iterations tends to reduce. If one looks at Fig. 1.8, where the number of iterations required to obtain solution is plotted against the size of the system, one remarks that the slope has tendency to bend, presenting some exponential saturation behavior. However, if one extrapolates this curve for larger linear systems, at least ~ 466 iterations are required for any size system to be solved. It is too much. Of course, by using more sophisticated *preconditioners* (as inverse of a few subdiagonals) one can expect a better convergence pattern. On the other hand, the use of more complicated preconditioning matrices requires more numerical efforts to create, to store and finally to apply them¹⁰.

¹⁰Creating a preconditioner based on inverse of diagonal and a few subdiagonals of the matrix requires performing LU factorization of the band structure matrix. Thus it needs providing additional memory to store a preconditioner, as well as it takes time to perform this LU factorization.

If one wishes to take into account also some subdiagonals containing the largest elements - one should perform search operations, which are very time consuming tasks.

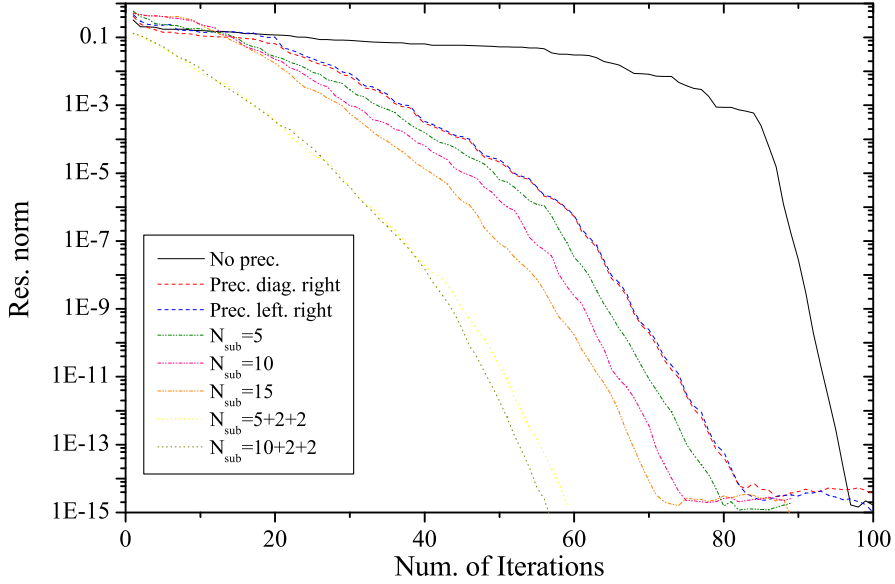


Figure 1.7: Convergence of GMRES algorithm with various matrix non-zero structure based preconditioners. N_{sub} identifies number of subdiagonals inverted to obtain preconditioning matrix. Symbols $5+x+y$ identifies that there are 5 subdiagonals inverted, plus x lower and y upper diagonals containing the largest elements.

One can conclude that such preconditioners based on matrix non-zero structure turns to be not very effective. The reason is that they completely ignore the physical origin of the problem. The non-zero structure of matrix A is not reflecting the physical background of the problem. Thus the preconditioner obtained by pure mathematical speculations is often not a very good approximate of its inverse. In the next section the preconditioner based on physical structure of matrix A would be proposed. It turns to be a very effective one to boost the convergence of the iterative methods.

1.3.3 Tensor inversion

In previous subsection we have seen that for solving bound state problem, one needs to perform vector multiplication operations with inverse matrices $[B]^{-1}$ and $(E_0[B] - [V] + [\Delta])^{-1}$ eq. (1.159) and eq. (1.167). On the other hand, it can be remarked that the matrix $(E_0[B] - [V] + [\Delta])$ contains the great part of operators in the matrix $[A]$ and thus its inverse can serve as a very effective *preconditioning*.

However, one cannot invert them directly since obtained matrices would be full and due to their large size physically unstorables even on computer hard disk.

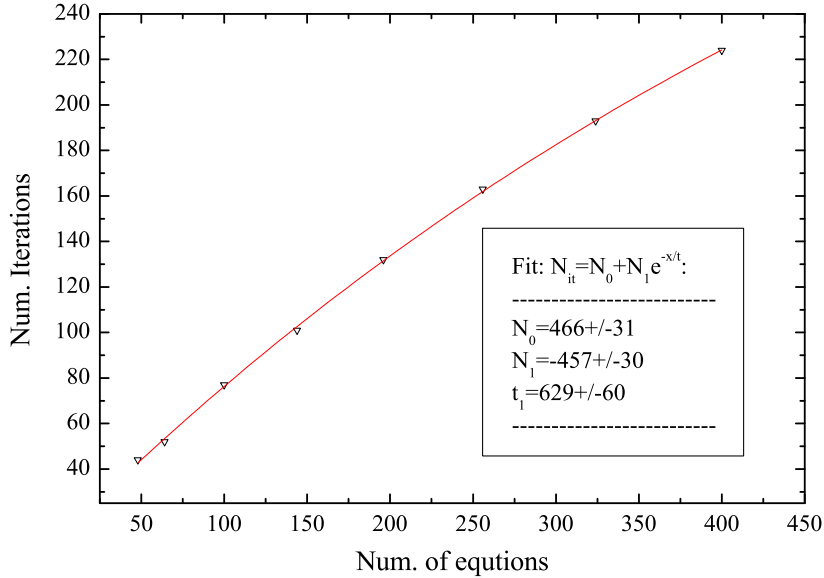


Figure 1.8: Convergence of left preconditioned GMRES algorithm with a diagonal inverse preconditioning matrix; solution is considered to be achieved when residual norm is less than 10^{-12} . Exponential decay function is used to fit the data points, it indicates that for large size systems convergence would be achieved only after more than ~ 466 iterations.

LU Factorization

One rather straightforward way to perform multiplication operations with inverses of the discussed matrices relies on the fact that there are no elements coupling different amplitudes. Thus, these matrices can be written as box diagonal ones, with a number of boxes equal to the number of partial amplitudes (Fig. 1.9). Furthermore, these box matrices, due to the fact that extrapolation splines are piecewise, are rather sparse. By prudently arranging row and column indexes $n = (j_x, j_y, j_z)$, these box matrices have a band structure with rather few upper and lower diagonals. Band matrices can be easily LU factorized [41], i.e. written as a product of lower and upper triangular matrices. For every block one has:

$$[M]_\alpha = [L]_\alpha [U]_\alpha \quad (1.180)$$

Multiplication of vector with the inverse of such matrix can be done after solving the linear system of equations, since:

$$[b']_\alpha = [M]_\alpha^{-1} [b]_\alpha. \quad (1.181)$$

If one wants to obtain $[b']_\alpha$ from $[b]_\alpha$ one has to solve the following sequence of linear systems:

$$\begin{aligned} [b]_\alpha &= [M]_\alpha [b']_\alpha &= [L]_\alpha [U]_\alpha [b']_\alpha \\ [b]_\alpha &= [L]_\alpha [\tilde{b}']_\alpha & [\tilde{b}']_\alpha = [U]_\alpha [b']_\alpha \end{aligned} \quad (1.182)$$

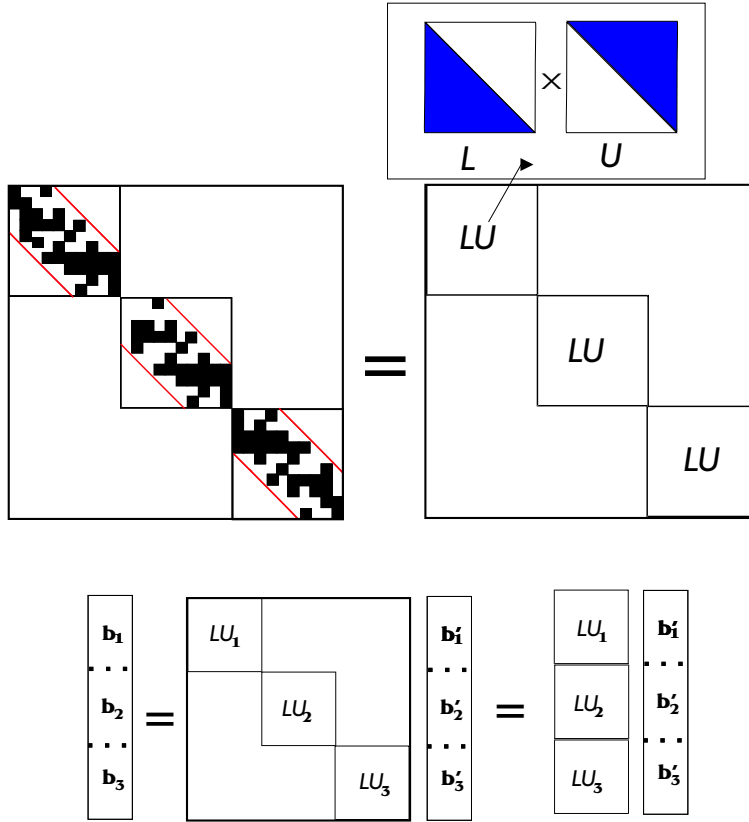


Figure 1.9: The structure of factorization matrix and its LU factorization. Performing of vector's multiplication operation with inverse of this matrix is analogous to resolving linear system of equations, its schematic way presented in lower diagram.

The solution of linear system with triangular matrices is very rapid and needs only $O(n^2)$ floating point operations. However, LU factorization procedure is rather costly, even though it can be performed block by block. Nevertheless the band of matrix ($E_0 [B] - [V] + [\Delta]$) (or $[B]$) is rather compact. However it still continues to grow with the dimension of the problem. This makes LU factorization operations very lengthy, and the method is hardly applicable in solving four-body problem.

Tensor inversion

There exists a more effective method to perform vectors multiplication operations with inverse matrices $[B]$ and $(E_0 [B] - [V] + [\Delta])$. It was first proposed by Payne [30], implemented by Schellingerhout and Bosveld [42] for three-body systems, and reformulated in the four-body case by the same group [43]. This method is based on the fact that former matrices can be expressed as a combination of simpler matrices, such as diagonal ones, or matrices acting only in one of subspaces α, x, y, z . This fact enables to write them as a tensor product of smaller matrices.

Terms in matrix $(E_0 [B] - [V] + [\Delta])$ can be grouped as follows:

$$[\Delta]_{n,n'} = \delta_{\alpha,\alpha'} \cdot \left(\begin{aligned} & \left[\left(E_0 - V_{\alpha,\alpha'}(x_{j_x}) - \frac{\hbar^2}{m} \frac{l_x(l_x+1)}{x_{j_x}^2} \right) S_{j'_x}^x(x_{j_x}) + \frac{\hbar^2}{m} S_{j'_x}^{x''}(x_{j_x}) \right] S_{j'_y}^y(y_{j_y}) S_{j'_z}^z(z_{j_z}) \\ & + S_{j'_x}^x(x_{j_x}) \left[-\frac{\hbar^2}{m} \frac{l_y(l_y+1)}{y_{j_y}^2} S_{j'_y}^y(y_{j_y}) + \frac{\hbar^2}{m} S_{j'_y}^{y''}(y_{j_y}) \right] S_{j'_z}^z(z_{j_z}) \\ & + S_{j'_x}^x(x_{j_x}) S_{j'_y}^y(y_{j_y}) \left[-\frac{\hbar^2}{m} \frac{l_z(l_z+1)}{z_{j_z}^2} S_{j'_z}^z(z_{j_z}) + \frac{\hbar^2}{m} S_{j'_z}^{z''}(z_{j_z}) \right] \end{aligned} \right) \quad (1.183)$$

It is convenient to introduce matrices $[1^\alpha]$, $[\delta_{\alpha_0}^\alpha]$, $[N^X]$, $[N^Y]$, $[N^Z]$, $[D_{\alpha_0}^X]$, $[D^Y]$, $[D^Z]$ with respective sizes N_α , $N_x \times k_x$, $N_y \times k_y$ and $N_z \times k_z$ and defined as:

$$\begin{aligned} [1^\alpha]_{\alpha,\alpha'} &= \delta_{\alpha,\alpha'} && \text{(of dimension } N_\alpha \times N_\alpha) \\ [\delta_{\alpha_0}^\alpha]_{\alpha,\alpha'} &= \delta_{\alpha_0,\alpha} \delta_{\alpha,\alpha'} && \text{(of dimension } N_\alpha \times N_\alpha) \\ [N^X]_{j_x,j'_x} &= S_{j'_x}^x(x_{j_x}) && \text{(of dimension } N_x k_x \times N_x k_x) \\ [N^Y]_{j_y,j'_y} &= S_{j'_y}^y(y_{j_y}) && \text{(of dimension } N_y k_y \times N_y k_y) \\ [N^Z]_{j_z,j'_z} &= S_{j'_z}^z(z_{j_z}) && \text{(of dimension } N_z k_z \times N_z k_z) \\ [D_{\alpha_0}^X]_{j_x,j'_x} &= \left(E_0 - V_{\alpha_0,\alpha'_0}(x_{j_x}) - \frac{\hbar^2}{m} \frac{l_x(l_x+1)}{x_{j_x}^2} \right) S_{j'_x}^x(x_{j_x}) + \frac{\hbar^2}{m} S_{j'_x}^{x''}(x_{j_x}) && \text{(of dimension } N_x k_x \times N_x k_x) \\ [D^Y]_{j_y,j'_y} &= -\frac{\hbar^2}{m} \frac{l_y(l_y+1)}{y_{j_y}^2} S_{j'_y}^y(y_{j_y}) + \frac{\hbar^2}{m} S_{j'_y}^{y''}(y_{j_y}) && \text{(of dimension } N_y k_y \times N_y k_y) \\ [D^Z]_{j_z,j'_z} &= -\frac{\hbar^2}{m} \frac{l_z(l_z+1)}{z_{j_z}^2} S_{j'_z}^z(z_{j_z}) + \frac{\hbar^2}{m} S_{j'_z}^{z''}(z_{j_z}) && \text{(of dimension } N_z k_z \times N_z k_z) \end{aligned}$$

Using these notations, matrix $[B]$, expressed in eq. (1.141), displays its tensor structure:

$$[B] = \begin{bmatrix} [1^\alpha] \\ \otimes \\ [N^X] \\ \otimes \\ [N^Y] \\ \otimes \\ [N^Z] \end{bmatrix} \quad (1.184)$$

The inversion of this matrix is straightforward:

$$[B]^{-1} = \begin{bmatrix} [1^\alpha] \\ \otimes \\ [N^X]^{-1} \\ \otimes \\ [N^Y]^{-1} \\ \otimes \\ [N^Z]^{-1} \end{bmatrix} \quad (1.185)$$

On the other hand, the inversion of matrix $[M] = (E_0 [B] - [V] + [\Delta])$ is less straightforward. In order to invert it, one can decompose this matrix into a sum of the matrices having similar tensor structure:

$$[M] = \left(\sum_{\alpha} \begin{bmatrix} [[\delta_{\alpha}^a]] \\ \otimes \\ [D_{\alpha}^X] \\ \otimes \\ [N^Y] \\ \otimes \\ [N^Z] \end{bmatrix} + \begin{bmatrix} [1^{\alpha}] \\ \otimes \\ [N^X] \\ \otimes \\ [D^Y] \\ \otimes \\ [N^Z] \end{bmatrix} + \begin{bmatrix} [1^{\alpha}] \\ \otimes \\ [N^X] \\ \otimes \\ [N^Y] \\ \otimes \\ [D^Z] \end{bmatrix} \right) \quad (1.186)$$

It is useful to factor out interpolation matrix, or $[B] = [1^{\alpha}] \otimes [N^X] \otimes [N^Y] \otimes [N^Z]$. An important fact is, as we have seen in eq. (1.185), that this matrix is tensor inversible. We obtain:

$$[M] = \left(\sum_{\alpha} \begin{bmatrix} [1^{\alpha}] \\ \otimes \\ [N^X] \\ \otimes \\ [N^Y] \\ \otimes \\ [N^Z] \end{bmatrix} \begin{bmatrix} [\delta_{\alpha}^a] \\ \otimes \\ [N^X]^{-1} [D_{\alpha}^X] \\ \otimes \\ [1^Y] \\ \otimes \\ [1^Z] \end{bmatrix} + \begin{bmatrix} [1^{\alpha}] \\ \otimes \\ [1^X] \\ \otimes \\ [N^Y]^{-1} [D^Y] \\ \otimes \\ [1^Z] \end{bmatrix} + \begin{bmatrix} [1^{\alpha}] \\ \otimes \\ [1^X] \\ \otimes \\ [1^Y] \\ \otimes \\ [N^Z]^{-1} [D^Z] \end{bmatrix} \right). \quad (1.187)$$

Here $[1^X], [1^Y], [1^Z]$ are unity matrices of sizes $N_x k_x, N_y k_y, N_z k_z$.

Direct methods can be applied to diagonalize matrices $[N^X]^{-1} [D_{\alpha}^X]$, $[N^Y]^{-1} [D^Y]$ or $[N^Z]^{-1} [D^Z]$ at relatively low cost, since they are of considerably smaller size than the original system. Furthermore, these matrices can be represented as diagonal matrices affected by *similarity transformation*:

$$\begin{aligned} [N^X]^{-1} [D_{\alpha}^X] &= [U_{\alpha}^X] [d_{\alpha}^X] [U_{\alpha}^X]^{-1} \\ [N^Y]^{-1} [D^Y] &= [U^Y] [d^Y] [U^Y]^{-1} \\ [N^Z]^{-1} [D^Z] &= [U^Z] [d^Z] [U^Z]^{-1} \end{aligned}$$

In this equation, unitary matrices – denoted by $[U]$ – contain the eigenvectors of the original matrix $[N]^{-1} [D]$ while diagonal matrices – denoted by $[d]$ – contain its eigenvalues. Consequently, the matrix $[M]$ can be expressed in the form:

$$[M] = \left(\sum_{\alpha} \begin{bmatrix} [1^{\alpha}] \\ \otimes \\ [N^X] \\ \otimes \\ [N^Y] \\ \otimes \\ [N^Z] \end{bmatrix} \begin{bmatrix} [1^{\alpha}] \\ \otimes \\ [U_{\alpha}^X]^{-1} \\ \otimes \\ [U^Y]^{-1} \\ \otimes \\ [U^Z]^{-1} \end{bmatrix} \left(\sum_{\alpha} \begin{bmatrix} [[\delta_{\alpha}^a]] \\ \otimes \\ [d_{\alpha}^X] \\ \otimes \\ [1^Y] \\ \otimes \\ [1^Z] \end{bmatrix} + \begin{bmatrix} [1^{\alpha}] \\ \otimes \\ [1^X] \\ \otimes \\ [d^Y] \\ \otimes \\ [1^Z] \end{bmatrix} + \begin{bmatrix} [1^{\alpha}] \\ \otimes \\ [1^X] \\ \otimes \\ [1^Y] \\ \otimes \\ [d^Z] \end{bmatrix} \right) \right) \begin{bmatrix} [1^{\alpha}] \\ \otimes \\ [U_{\alpha}^X] \\ \otimes \\ [U^Y] \\ \otimes \\ [U^Z] \end{bmatrix}.$$

The central term, containing sums of tensor products with matrices $[d]$, is purely diagonal and thus is trivial to invert. On the other hand, using the fact that the inverse of a tensor product is the tensor product of their respective inverse [44], one can easily obtain the inverse of $[M]$:

$$[M]^{-1} = \left[\sum_{\alpha} \begin{bmatrix} [1^{\alpha}] \\ \otimes \\ [U_{\alpha}^X]^{-1} \\ \otimes \\ [U^Y]^{-1} \\ \otimes \\ [U^Z]^{-1} \end{bmatrix} \left(\begin{bmatrix} [\delta_{\alpha}^{\alpha}] \\ \otimes \\ [d_{\alpha}^X] \\ \otimes \\ [1^Y] \\ \otimes \\ [1^Z] \end{bmatrix} + \begin{bmatrix} [1^{\alpha}] \\ \otimes \\ [1^X] \\ \otimes \\ [d^Y] \\ \otimes \\ [1^Z] \end{bmatrix} + \begin{bmatrix} [1^{\alpha}] \\ \otimes \\ [1^X] \\ \otimes \\ [1^Y] \\ \otimes \\ [d^Z] \end{bmatrix} \right)^{-1} \begin{bmatrix} [1^{\alpha}] \\ \otimes \\ [U_{\alpha}^X]^{-1} \\ \otimes \\ [U^Y]^{-1} \\ \otimes \\ [U^Z]^{-1} \end{bmatrix} \begin{bmatrix} [1^{\alpha}] \\ \otimes \\ [N^X]^{-1} \\ \otimes \\ [N^Y]^{-1} \\ \otimes \\ [N^Z]^{-1} \end{bmatrix} \right].$$

Analysis

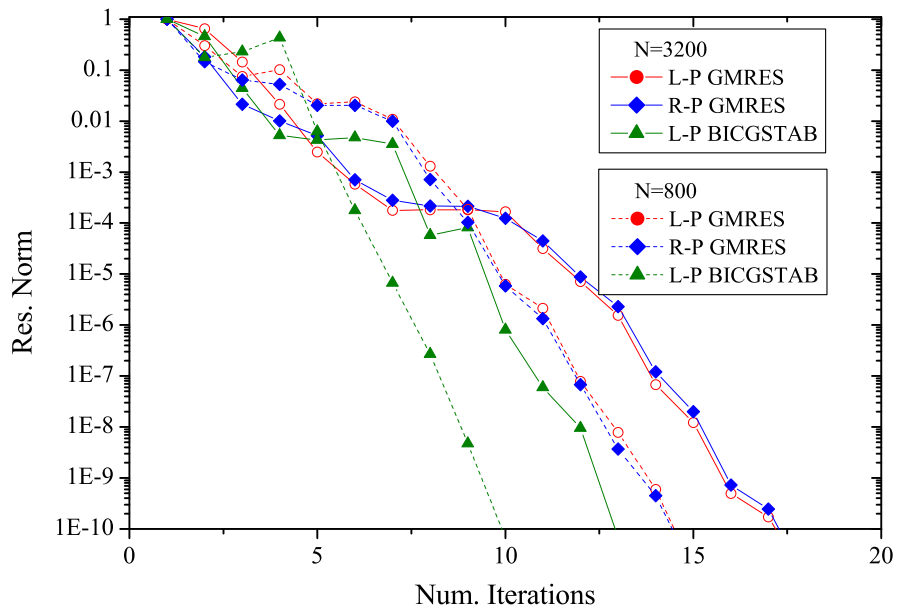


Figure 1.10: Comparison of convergence for right and left preconditioned iterative methods. GMRES and BICGSTAB algorithms were applied for different size linear systems.

As was suggested, the inverse of $(E_0[B] - [V] + [\Delta])$ matrix is found to be the most effective *preconditioning*. It works with equal success in GMRES as well as in BICGSTAB iterative schemes. The number of iteration steps required to obtain a converged solution grows very slowly with the size of the system and stays always reasonable¹². As seen from Fig. 1.10, in most cases left and

¹²The largest number of iterations required to obtain converged solution was ~ 50 for GMRES and ~ 70 for BICGSTAB algorithms. Slow convergence, or its absence, usually indicates ambiguities in physical formulation of the problem.

right preconditioning have almost identical convergence patterns. However, some peculiarities can arise making one of these schemes fail.

It seems that BICGSTAB algorithm needs fewer iterations to converge. One should however keep in mind that each iteration step of BICGSTAB requires two vector-matrix $M^{-1}A$ (or AM^{-1} for right preconditioned) multiplication operations, whereas GMRES requires only one. Thus, in general GMRES scheme turns to be faster. On the other hand BICGSTAB is a more flexible scheme due to its lower orthogonalization vector storage requirements.

To reduce or (and) control the necessary RAM used by GMRES algorithm, one can restart it if some maximal number of iterations (fixed by default) were performed. After that, Arnoldi's orthogonalization procedure is restarted and new Krylov subspace is formed from residual vector, based on the obtained approximate solution. As seen in Fig. 1.11 the number of iteration steps tends to grow if one chooses to restart the algorithm. However, if the maximal size of Krylov's subspace is chosen reasonably, the number of iteration steps grows only a little. In some cases the restarted algorithm can become even faster, since each successful iteration step is heavier than the previous one (new obtained vector should be orthogonalised in respect to the basis formed by all the previous ones). The restart option can accelerate the convergence due to possible stuck down of direct iteration caused by numerical peculiarities. In this case restarted algorithm can converge even after fewer iteration steps.

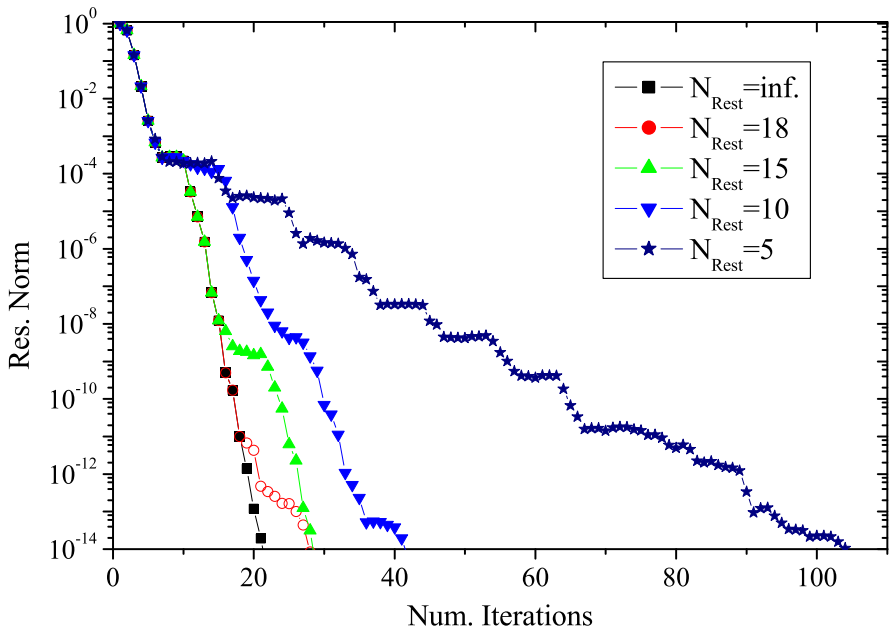


Figure 1.11: Comparison of convergence for restarted GMRES algorithm. One can remark that limiting the size of Krylov subspace (limiting number of iterations in Arnoldi orthogonalization procedure) increases the number of iterations required to obtain converged solution. However, total number of iterations stays reasonable if $N_{\text{rest}} \geq 15$.

Chapter 2

Three-Body Coulomb Scattering

Coulomb interaction is the fundamental ground in the atomic and molecular systems, being the origin of all vital processes in nature. It is the dominant interaction from nano to millimeter shell, therefore the ability to treat Coulomb systems represents a substantial interest for a large community of scientist. In spite of the simplicity of this potential analytical solutions exist only for two interacting charges and are able to account only negligible part of Coulomb systems. Three interacting charges therefore represent the simplest case of this type, which cannot be solved analytically. The straightforward approach should consist of considering the system interacting via some effective potential, however this approach cannot take into account of particle exchange, neither of single particle decomposition effects. Hence, three-charge system constitutes a genuine 3-body problem, including numerous examples of the fundamental importance in physics:

- H_2^+ , H^- being the simplest molecules found in nature
- muonic ($d^+\mu^-t^+$), pionic ($d^+\pi^-t^+$) molecules presenting one of the possible enhancements to solve long-standing catalyzed fusion dilemma.
- scattering of electrons and positrons on H atoms. Representing the simplest experimentally eligible structure to test matter-antimatter symmetry breaking.
- propagation of antiprotons in space, annihilation of the matter and antimatter in antiproton H scattering.

Coulomb systems were studied since the first days of quantum mechanics [?]. From that time much progress has been done in solving bound state problem with explicit results obtained for molecular structures as H_2^+ ([45]-[51]), H^- [52], $d^+\mu^-t^+$ [53, 54] and many others. However, the advances in the scattering problem are weak. Until now, rigorous studies were performed only for the simplest cinematical configurations like $e^- - e^-e^+$ [55], e^- -H and e^+ -H [56], and still only for elastic channels. Considered systems had either all the particles of equal mass, or two charges much lighter than the third one. In this case all the reduced masses of two-particle fragments are of the same order and therefore exhibit comparable dynamics.

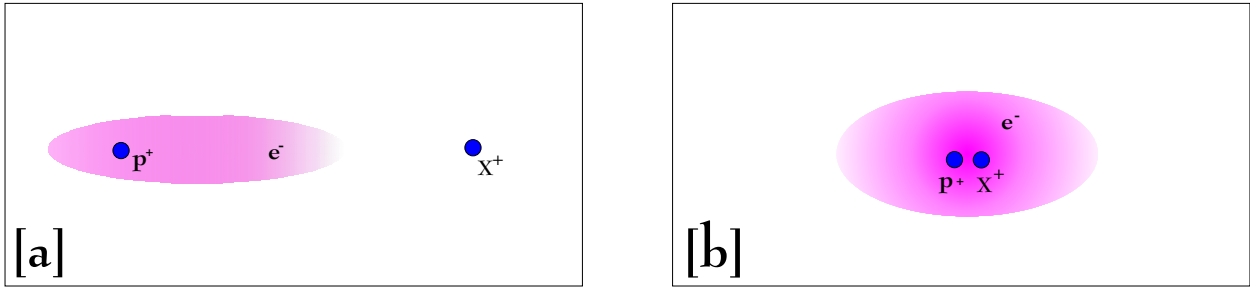


Figure 2.1: Schematic view of Hydrogen atom interacting with a positive projectile particle. In figure [a] projectile is far away, however its static electric field polarizes the atom. Weak attraction appears between the particle and the atom. In figure [b] positive particle penetrates inside the atom by pushing electron cloud outside, projectile feels strong Coulomb repulsion from the same sign charge nucleus.

This section of my thesis is devoted to expand these studies by considering elastic scattering of heavy positively charged particles with masses $m \in [m_e, m_p]$ on atomic hydrogen, since still restricting to the energies below the inelastic thresholds. The principal binding of such systems is due to electron's binding in hydrogen atom, which can have infinite number of bound states. In presence of the third charged particle electron cloud is stretched (see Fig. 2.1) by virtual excitation of electron into excited states, in the way to favor more attraction. Hydrogen atom is deformed and gains dipole moment (polarizes) in the direction of arriving third particle. For the distances when projectile particle is far away its induced dipole moment is proportional to the electric field at the center of the H atom. This dipole moment is furthermore responsible for appearance of a weak attractive force with arriving particle, which behaves as:

$$V_{pol}(r \rightarrow \infty) = -\frac{\alpha_H}{2r^4}, \quad (2.1)$$

α_H being the polarizability of the hydrogen atom. Of course, it is not anymore true when projectile penetrates inside the atom forcing electronic cloud out and interrupting its action as a binding medium. On the other hand, when the projectile gets very close to the nucleus and electronic cloud is all forced outside - it is due to strong repulsion between two charges of the same sign - the effective interaction can be described by the screening potential

$$V(r \rightarrow 0) = \frac{e^{-r}}{r}. \quad (2.2)$$

Consequently, one has some effective potential as presented in Fig. 2.2 with non-trivial behavior at the intermediate distances between cope of validity of the two limiting cases eqs. (2.1-2.2). This potential is very weak having the minimal value only about ~ 0.1 a.u. (2.7 eV), however its attractive part is of long range and if projectile is heavy enough and therefore rather static, as it was shown in [57], this potential can support many nearthreshold bound and resonant states. These states will manifest in the charged particle low energy scattering on H atom. All the facts described above make this system very rich in physical phenomenon and motivate us to study it.

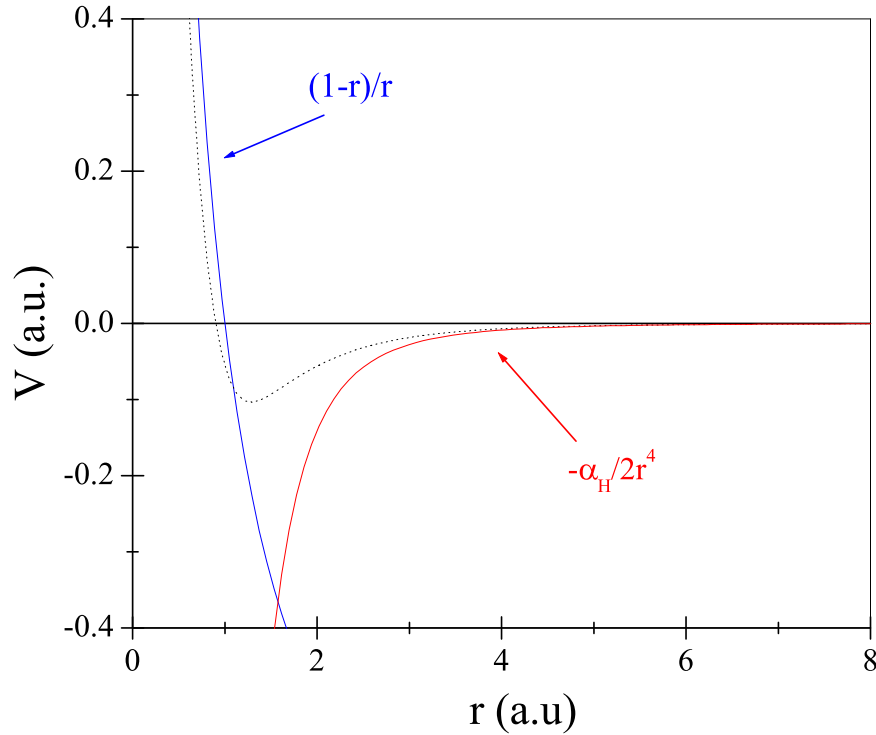


Figure 2.2: Effective polarization potential as a sum of short range repulsion with a nucleus and attractive long range polarization part.

It is worth mentioning that if the projectile is of the opposite charge, the system behavior changes completely. The long range part of the effective potential (polarization part) is not affected, however short range part of this potential becomes attractive. Furthermore, if the projectile is heavier than an electron, its 2-body bound states with proton (nucleus of H atom) lie below those of H atom and represent - when scattering problem is being considered - open rearrangement and eventually annihilation channels. Thus, antiproton-proton system has already 30 S -wave bound states below ground state of H atom. The necessity to take into account all those annihilation channels makes rigorous treatment of such systems very difficult, and until now only approximate solutions were achieved [58, 59, 60].

Many numerical methods are very successful in solving Coulomb few-body bound state problem. The most precise of them are based on variational principle, furthermore relying on the fact that analytical solutions exist for 2-body Coulomb problem. See [50, 61] and references therein.

The Faddeev like equations, that we would like to employ, were for a long time believed to be very useful in nuclear problems, but not in the atomic ones. Due to difficulties I'll describe in the next subsection, nobody even tried to calculate three-body bound states with Coulomb potential. The first essay was done by Cravo and Fonseca [62], by using AGS [163] formalism, to calculate the ground state of Helium atom. However their attempt failed largely, due to inability in representing

the long range Coulomb force by a separable approximation. The first successful calculations were performed by Bosveld and Schellingerhout [42] just one year later.

Remark 3 *We will use electronic atomic units (a.u.) to measure physical quantities throughout this chapter. They are obtained by considering mass of the electron $m_e = 1$ as well as $\hbar = e^2 = 1$. The length unit is the Bohr radius $a_0 = 1 \text{ a.u.} = 0.529 \text{ \AA}$ and the energy unit is the Hartree $1 \text{ Ha} = 1 \text{ a.u.} = 2 \text{ Ry} = 27.2 \text{ eV}$.*

2.1 Merkuriev equations

As introduced in section 1.2.2, it has been proven that Faddeev equations have compact kernels only for fast enough decreasing potentials. If one considers long range potentials, in particular Coulomb potential, kernel of Faddeev equations becomes non-compact and problems formulation is not anymore valid [63]. In configuration space it shows up in two kind of difficulties:

1. Asymptotic motion of the particles is never free. Long range interaction terms continue to couple Faddeev equations even in far asymptote, thus making nontrivial distribution of asymptotic state wave function between the Faddeev components. This non-trivial coupling makes implementation of correct boundary conditions hardly possible.
2. Even more severe difficulties exist above three-body threshold. Faddeev equations above 3-body threshold are not of the Fredholm type. In configuration space, one is confronted with finding asymptotic form of 3-body, Coulomb interacting, breakup wave function, which until now is a non-resolved task. In momentum space, one doesn't need to know asymptotic form of wave function (it is integrated out in equations), however Coulomb singularities make equations not integrable [64].

In this thesis I will not discuss 3-body breakup problem, therefore only the difficulties described in the first point will be confronted. On the other hand, one has to mention that 3-body bound state problem can be tackled even by applying standard Faddeev equations. Uncoupling of Faddeev components is here guaranteed by exponential decay of wave function.

For the systems with Coulomb (V_l^C) plus short-range interaction (V_i), J. Noble formulated modified Faddeev equations [65].

$$(E - H_0 - V_i - \sum_{l=1}^3 V_l^C) |\psi^{(i)}\rangle = V_i [|\psi^{(j)}\rangle + |\psi^{(k)}\rangle] \quad (i, j, k) \in (1, 2, 3) \quad (2.3)$$

One can see that these equations are asymptotically uncoupled. Uncoupling is assured by a rapid vanishing of short range potential terms V_i in the right hand side of the equation. Hence, introducing boundary conditions shouldn't cause big problems. However, the Noble equations have singularities, nevertheless integrable, in the left hand side of equation, due to non-proper long range potential terms at $c_{ij}x_j = s_{ij}y_j$ line, corresponding to the particle configurations when two of them can get close to each other (see Fig. 2.3). If long range interaction is repulsive, one will have

Faddeev components vanishing near this line and since $\phi(x \rightarrow \infty) = 0$ boundary conditions still can be in agreement with these components. On the other hand, if one has attractive Coulomb terms, J. Noble equations become ill behaved. Faddeev components will accumulate around the singular line $c_{ij}x_j = s_{ij}y_j^1$, and therefore the vanishing of Faddeev components is not anymore guaranteed even for $x \rightarrow \infty$. Thus, Faddeev components are not anymore smooth and bound functions. Technically it materializes in two kind of difficulties: first Faddeev components need large grids to implement the boundary conditions, whereas secondly partial wave decomposition is slowly or even non-converging.

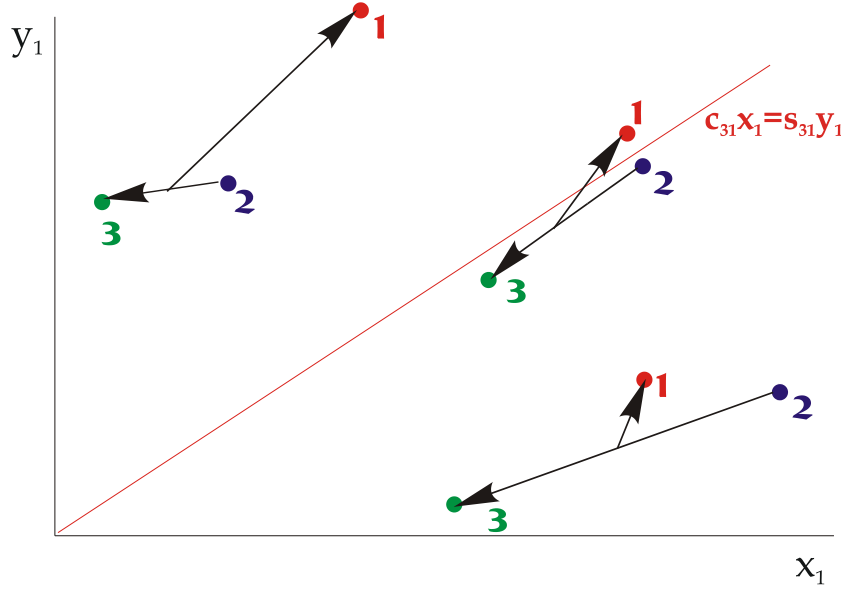


Figure 2.3: Singularities of non-proper potential terms appear when one confronts the situation, in which two particles, coupled by this potential, can get close to each other. These dangerous configurations in Jacobi coordinate space xy are marked by the red-dashed line. Note, that for different mass particles, this line splits into two satisfying equalities: $c_{21}x_1 = s_{21}y_1$ and $c_{31}x_1 = s_{31}y_1$.

In conclusion, one can summarize that when dealing with long range interactions one should have equations satisfying the following conditions:

1. The left hand side of equations should absorb all the contributions of long range potentials at some $y \gg x$, to permit asymptotic uncoupling of the Faddeev components, thus enabling unambiguous implementation of the boundary conditions.
2. On the other hand, potential terms $V_i(x_i)$, for which $x_i \rightarrow 0$, should be kept in the left hand side of their original Faddeev equation, where potential singularities are suppressed by the

¹When one deals with system of non-equal mass particles - for each given $x_i y_i$ ($i = 1, 2, 3$) plane there exist two singular lines. I.e.: If one considers configuration $x_1 y_1$ of Jacobi basis (23) 1 - one obtains singularities for $c_{21}\vec{x}_1 = s_{21}\vec{y}_1$ and $c_{31}\vec{x}_1 = s_{31}\vec{y}_1$, respectively corresponding change of Jacobi basis to (31) 2 and (12) 3.

boundary condition $\psi^{(i)}(x_i = 0, y_i) = 0$. This will avoid appearance of the singular terms near the $x_j = y_j$ line in non-appropriate Faddeev components.

These principal observations motivated Merkuriev [10, 66] to split the Coulomb potential in two parts (short range $V^{(s)}$ and long range $V^{(l)}$), $V^C = V^{(l)} + V^{(s)}$, by means of some arbitrary cut-off function $\chi(x, y)$:

$$V^{(s)}(x, y) = V^C(x)\chi(x, y) \quad V^{(l)}(x, y) = V^C(x)[1 - \chi(x, y)] \quad (2.4)$$

One is then left with a system of equivalent Noble equations:

$$(E - H_0 - V_i^{(s)} - W) |\psi^{(i)}\rangle = V_i^{(s)} [|\psi^{(j)}\rangle + |\psi^{(k)}\rangle] \quad (i, j, k) \in (1, 2, 3) \quad (2.5)$$

in which

$$W = V_i^{(l)} + V_j^{(l)} + V_k^{(l)} \quad (2.6)$$

where right hand side contains only the short range contributions of the proper potential terms. The left hand side of equation is supplied with some effective 3-body potential W_i , containing long range contributions from all potential terms. In order to have a set of equations with an unique solution, the short range potential $V_i^{(s)}(x_i, y_i)$ should be bounded and vanishing fast enough to satisfy the Faddeev condition:

$$V_i^{(s)}(x_i, y_i) = 0 \quad \text{for } x_i > a_0(1 + y_i)^{\nu'}, \quad (2.7)$$

where a_0 is some constant and ν' is the parameter, contained in $(0, \frac{1}{2})$. Additionally, complementary condition should be satisfied (introduced by Merkuriev) to isolate singular potential terms when coupling them in the left hand side of equation with non-proper Faddeev components.

$$V_i^{(s)}(x_i, y_i) = V_i^C(x_i) \quad \text{for } x_i < a_0(1 + y_i)^{\nu} \quad (2.8)$$

and $0 < \nu < \nu'$. To make these two conditions valid, Merkuriev proposed the splitting function χ , which reads

$$\chi(x, y) = \frac{2}{1 + \exp \left[\frac{(x/x_0)^{\mu}}{1+y/y_0} \right]}, \quad (2.9)$$

where $\mu = 1/\nu$ and thus $\mu > 2$. Parameter x_0 evaluates the effective size of the 2-body interactions; it is therefore logic to attribute the size of two body bound state for it. On the other hand parameter y_0 is an evaluate of the size of the so called three body region².

Please note that, no approximations were made by making potential separation in eq. (2.4). Therefore, Faddeev and Merkuriev equations should provide identical solutions (formally they should have the same eigenvalue spectra, as well as the same eigenvectors represented by systems

²Three-body region is the region, where three-particle decomposition of the system is important, here single particle dynamics should be taken into account. In so called, two-body region the system can be described successfully by the residual interaction of two particle cluster, forming a bound pair, and retreating third particle.

total wave function $|\Psi\rangle = |\psi^{(i)}\rangle + |\psi^{(j)}\rangle + |\psi^{(k)}\rangle$. Nevertheless, one has different equations for the Faddeev and Merkuriev components. Hence, total wave functions $|\Psi\rangle$ decomposition into components $|\psi^{(k)}\rangle$ is different.

One can admit that Merkuriev equations, even though their major goal is the scattering states, are advantageous even when dealing with Coulomb bound state problem (see Fig. 2.4). Ground state energy calculations for μ^+H system are presented there by comparing convergence of Faddeev and Merkuriev equations. Convergence was achieved by increasing number of partial waves in bipolar harmonics basis to describe Faddeev (-Merkuriev) components. The two different convergence schemes were employed, when using Faddeev method: in the first one, a number of partial waves in attractive components was chosen to be equal to repulsive ones³, whereas in the second scheme number of partial waves in repulsive component was chosen to be smaller by one than in attractive ones. Such a scheme permitted to trap bound state energy between the two convergence curves. However, convergence of Faddeev equations was rather slow, whereas results with a small number of partial waves couldn't even confirm existence of the bound states.

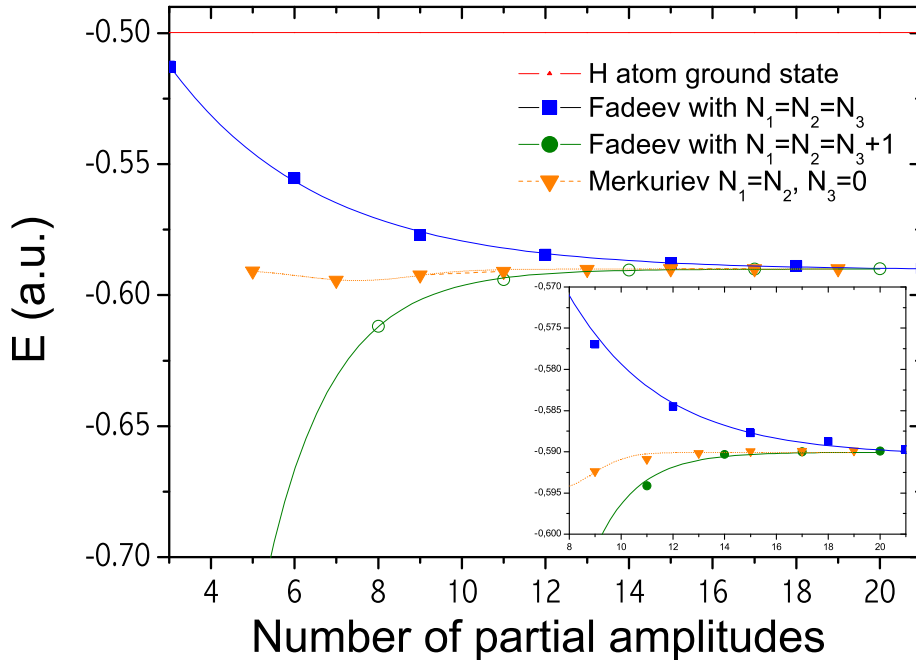


Figure 2.4: Convergence of the μ^+H systems bound state energy calculations. In the smaller plot zoom in converged area is shown. Number of partial amplitudes indicates the sum $N=N_1+N_2+N_3$ of partial waves used in expansion of the Faddeev-Merkuriev components.

³Faddeev components are called attractive if the particles of principal pair in the corresponding configuration tree attracts each other, while repulsive components are those for which principal pairs particles retracts. For the system of two positive and one negative charge, as $\mu^+e^-p^+$ one has two attractive components corresponding to particle trees $(\mu^+e^-)p^+$ and $(p^+e^-)\mu^+$, as well as one repulsive - $(p^+\mu^+)e^-$.

In Merkuriev scheme originally repulsive components become very feeble, and so they can be absorbed in originally attractive components by choosing splitting function $\chi^{rep}(x, y) = 0$ for them. Considering electron as a 3-rd particle, one obtains two component coupled equations.

$$\begin{aligned} (E - H_0 - V_2^{(l)} - V_1 - V_3) |\psi^{(1)}\rangle &= V_1^{(s)} |\psi^{(2)}\rangle \\ (E - H_0 - V_1^{(l)} - V_2 - V_3) |\psi^{(2)}\rangle &= V_2^{(s)} |\psi^{(1)}\rangle \\ |\Psi\rangle &= |\psi^{(1)}\rangle + |\psi^{(2)}\rangle \end{aligned} \quad (2.10)$$

Parameters set of $x_0 = 2$; $y_0 = 2\sqrt{m_x}$, where m_x represent the mass of projectile particle, and $\mu = 2.3$ were found to be a suitable choice for splitting function $\chi^{att}(x, y)$ in two attractive Faddeev-Merkuriev components. Convergence curve in Fig. 2.4 was plotted by choosing equal number of partial waves to approximate these two components.

It can be seen that the exact results for Merkuriev equations are obtained by using rather small partial wave basis. This indicates that by using decomposition of eq. (2.4-2.9), one constrains the components to be the smooth functions, which is not the case when using standard Faddeev equations.

2.2 Bound state calculations

2.2.1 Numerical tests

To test the validity of the numerical code, as well as the efficiency of numerical methods in use, one can consider the well known $e^+e^-e^-$ bound state problem. Very precise results for this system were obtained by variational method [67], as well later reobtained by Faddeev calculations [68], agreeing on binding energy of $E = -0.26200507$ (a.u.). The complexity of this system is due to the very weak binding of the electron to positronium atom (Ps), for which $E_{Ps} = -0.25$ (a.u.). Therefore the wave function decreases very slowly as one of the electrons is separated causing a rather slow convergence with a number of channels, as should be expected for identical mass system.

One of possible improvements relies on factorizing out the positronium's wave function. Faddeev components are searched in form:

$$\psi(\vec{x}, \vec{y}) = e^{-q_{2b} \cdot x} \sum_{\alpha} \frac{F_{\alpha}(x, y)}{xy} \mathcal{Y}_{\alpha}(\hat{x}, \hat{y}), \quad (2.11)$$

where $q_{2b} = \sqrt{-\frac{m_e}{\hbar^2} E_{Ps}}$. This way, one is left with eigenvalue problem for the quantity $E - E_{Ps}$, and therefore is more sensible to the weak binding of the third particle. On the other hand, such factorization numerically gives exact wave function of Positronium atom thus imposing correct 3-Body wave function dependence on variable x , when one of the electrons is far away. To facilitate spline interpolation on variable y one can further factorize

$$\psi(\vec{x}, \vec{y}) = e^{-q_{2b} \cdot x - q_y \cdot y} \sum_{\alpha} \frac{F_{\alpha}(x, y)}{xy} \mathcal{Y}_{\alpha}(\hat{x}, \hat{y}) \quad (2.12)$$

$\max(l_x, l_y)$	<i>Cubic splines</i>		<i>Quintic spl.</i>
	B_{No_fact} (a.u.)	B_{Fact} (a.u.)	B_{No_fact} (a.u.)
1	0.2618468	0.2618462	0.2618454
3	0.2621025	0.2621020	0.2621013
5	0.2620195	0.2620190	0.2620182
7	0.2620080	0.2620075	0.2620067
9	0.26200715	0.26200663	0.26200584
11	0.26200717	0.26200664	0.26200586

Table 2.1: Comparison of convergence in ground state calculations of $e^+e^-e^+$ system. In the first two columns results obtained using Cubic spline interpolation of wave function are presented. In the second column, wave function was additionally factorized as in eq. (2.11). Third column presents results obtained using Quintic spline interpolation without additionally factorizing wave function.

with $q_y = \sqrt{-\frac{m_e}{\hbar^2} (E - E_{Ps})}$, which describes the tail of the wave function in differential equations sensible region, where x is relatively small, while $y \rightarrow \infty$. The precedent eq. (2.12) factorization enables one to impose grid cutoff on variable y at sensibly smaller values. Results obtained for the $(e^+e^-e^-)$ system are collected in Table 2.1. In this study I haven't tried to fight for numerical accuracy and have used rather small and not optimized grids. Density of grid points in calculations using quintic spline interpolants were chosen in proportion of 2/3 to cubic ones to result into the same size linear algebra problem. One can see that the quintic spline interpolation provides slightly more accurate results.

2.2.2 Results for X^+ -H system

Merkuriev equations were employed to calculate a few lowest bound state energies of μ^+ -H, π^+ -H and p^+ -H systems. These systems are difficult to treat using Faddeev-Merkuriev formalism, since they consist of very asymmetric 2-body fragments with very different reduced masses and consequently with different dynamics. It results that important regions of different Faddeev components are non-intersecting and even appear at the shells of different magnitude, therefore one has to use rather dense and asymmetric grids in order to properly describe all these components . Consequently, due to asymmetry, convergence on channels is even slower than in $(e^+e^-e^-)$ case and needs amplitudes containing $(l_x, l_y) \geq 15$. Coupling of such high order amplitudes becomes a lengthy and numerically not very stable task.

The obtained results are summarized in Table 2.2 and plotted in Fig. 2.5. I have tried to reproduce the same results by using some effective 2-body potential, satisfying conditions as provided by eq. (2.1-2.2). Mott-Massey potential V_{MM} [69] was chosen as a driving potential term, used to simulate positron-Hydrogen scattering.

$$V_{MM}(r) = -\frac{\alpha(r)}{2r^4}, \quad (2.13)$$

L^{Π}	v	Systems $B(a.u.)$		
		$\mu^+ - H$	$\pi^+ - H$	$p^+ - H$
0^+	0	0.589721	0.591262	0.597144
	1	0.569195	0.572812	0.587156
	2	0.551350	0.556491	0.577748
	3	0.536042	0.542195	0.568900
	0	0.588470	0.590276	0.596879
	1 ⁻	0.568090	0.571928	0.586912
2^+	0	0.585877	0.5788145	0.596352

Table 2.2: Comparison of binding energies for the lowest $\mathcal{L}^{\Pi} = 0^+, 1^-, 2^+$ energy states in π^+H , μ^+H and p^+H systems

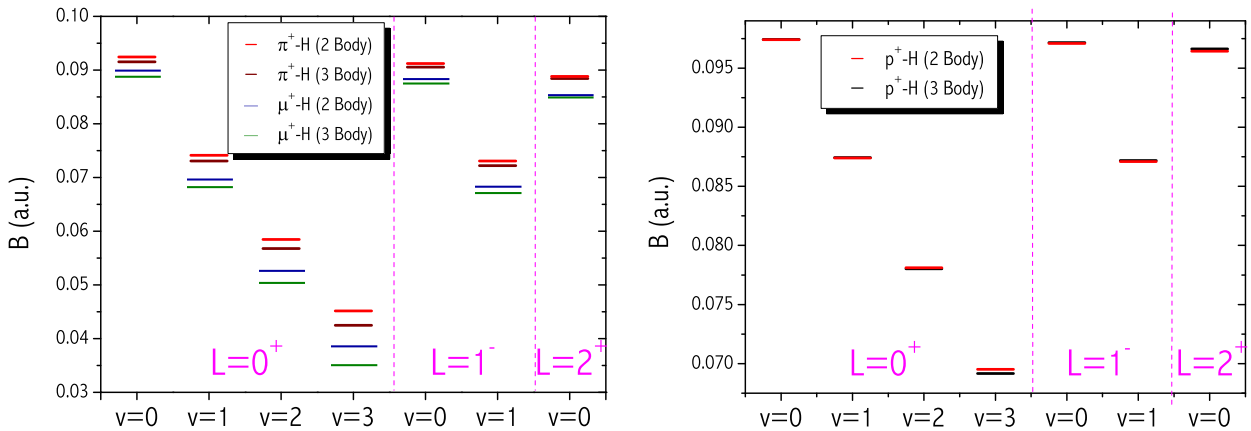


Figure 2.5: Comparison of binding energies obtained using phenomenological 2-body potential with exact 3-body results. 2-body potential eq. (2.15) was adapted to reproduce 2 lowest $H_2^+ 1s\sigma_g$ states.

where $\alpha(r)$ is given by

$$\alpha(r) = \frac{9}{2} - \frac{2}{3} \exp(-2r)(r^5 + \frac{9}{2}r^4 + 9r^3 + \frac{27}{2}r^2 + \frac{27}{2}r + \frac{27}{4}). \quad (2.14)$$

Mott-Massey potential behaves as the hydrogen polarization potential, when $r \rightarrow \infty$, whereas falls to zero as $r \rightarrow 0$. I have added an additional short range potential having repulsive behavior at the origin as required by eq. (2.2), whereas falling to zero as distance with projectile particle increases. This additional potential term read as:

$$V_{ADD}(r) = -\frac{4}{r} \exp(-\frac{r}{R_1}) + \frac{5}{r} \exp(-\frac{r}{R_2}). \quad (2.15)$$

Parameters for this additional potential have been adjusted to reproduce ground and first excited state energies of H_2^+ molecular ion as obtained by exact 3-body calculations. These parameters were found to be: $R_1 = 2.3985$ (a.u.) and $R_2 = 1.6561$ (a.u.). Comparison of two-body and three-body results are presented in Fig. 2.5.

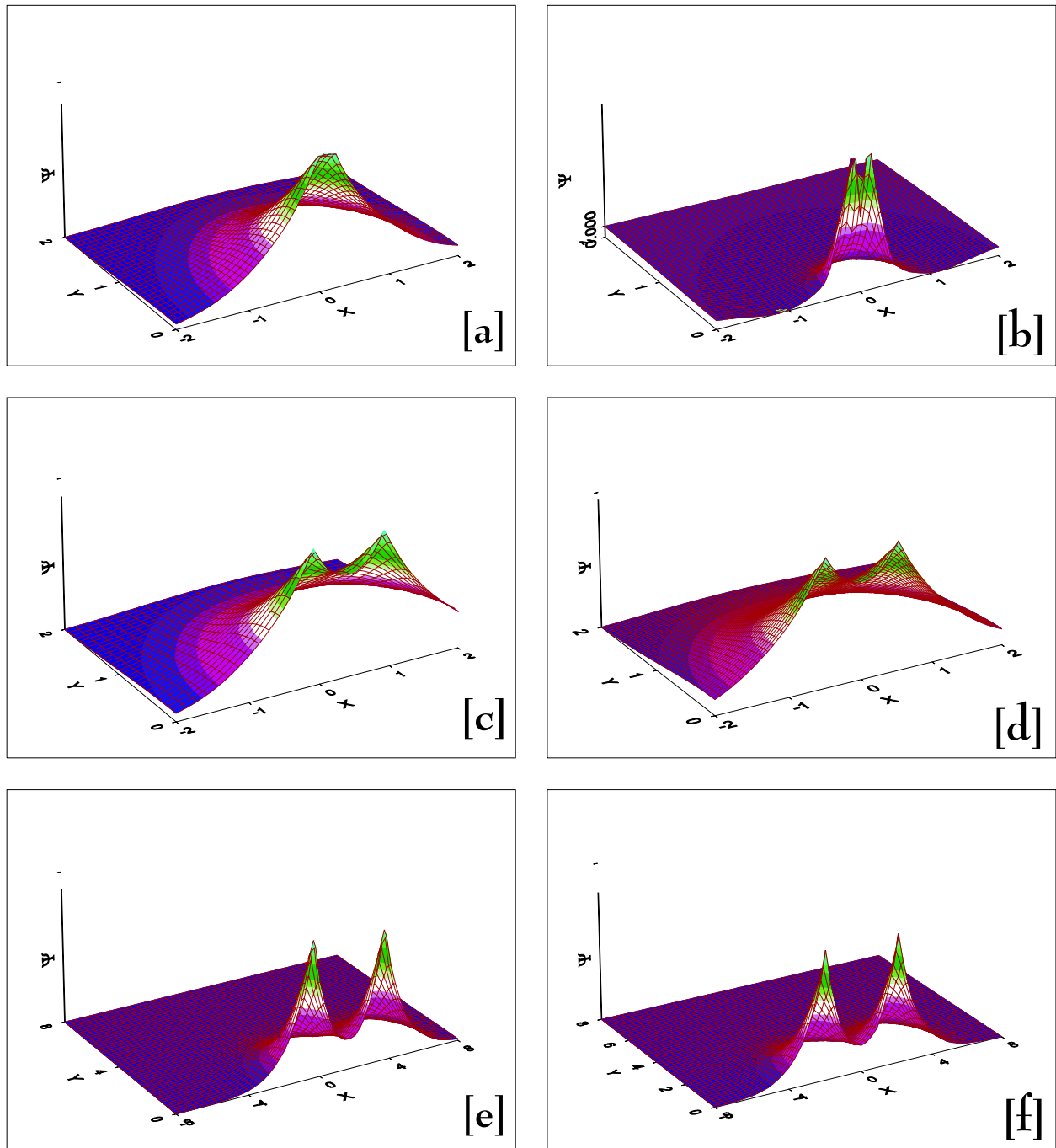


Figure 2.6: Electron distribution densities when distance between two positive charges d is fixed. Figures in the left are plotted for μ^+H system, while figures in the right correspond to p^+H . Figures are made for distances $d = 0.2, 1$ and 4 (a.u.) respectively.

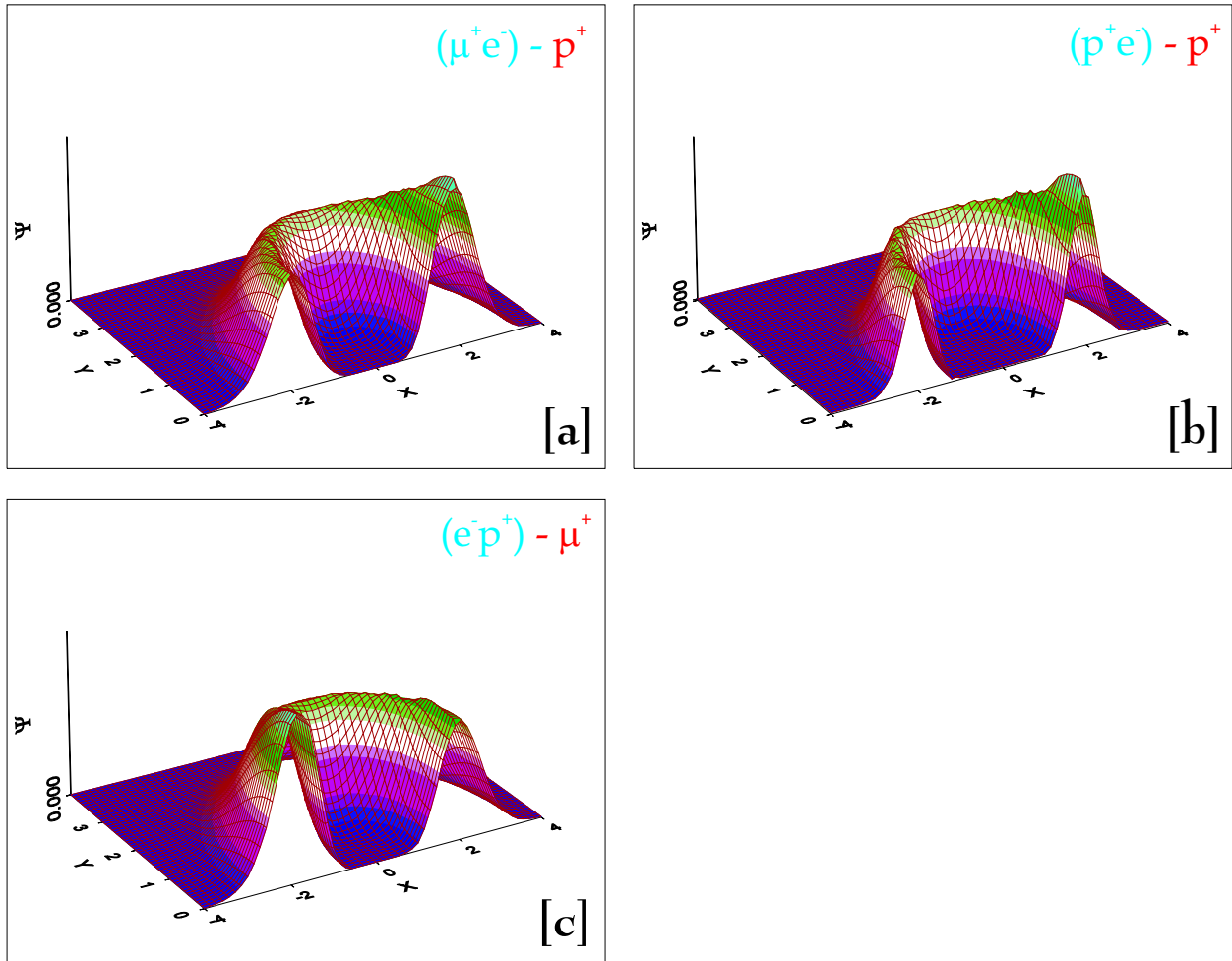


Figure 2.7: Heavy particle distribution in X^+H ground state wave functions, when electron and the third particle are fixed on x axis and separated by 1 (a.u.). Figure [a] presents protons distribution in μ^+H , figure [b] shows proton distribution in H_2^+ ground state, whereas in figure [c] muon distribution in μ^+H is plotted.

Despite the mass variation, from m_p to m_μ , being almost one order of magnitude, one can see that effective two body potential rather successfully predicts energies for the lowest bound states. For the excited states, where wave function becomes more complicated and electrons dynamics less trivial, the difference in results increases. Furthermore, two-body results for μ^+ and π^+ are overestimated. This overestimation is increasing with diminishing projectile mass. It is due to the fact that these systems are less rigid than H_2^+ molecule and furthermore mass asymmetric. Thus electrons dynamics here is relatively more important than in H_2^+ molecule, since electron has small additional momenta due to asymmetry of the system.

Finally, for a better understanding of the dynamics, it is interesting to compare the wave functions of the different systems. These wave functions are multidimensional and therefore not easy to represent. In order to plot them one is obliged to fix some degrees of freedom. In Fig. 2.6 electron distributions for $\mu^+ - H$ and H_2^+ ground states are compared. 3-D representations were made by fixing two positive charges (μ^+ and p^+ , or p^+ and p^+ respectively) on x axis, consequently separated by 0.2, 1 and 4 (a.u.), so that their center of the mass is held at the origin ($x = 0; y = 0$). All these wave functions resemble each other, indicating the similarity of their origin. Nevertheless, one can note, that electron distribution has a sharper peak near the proton than near the μ^+ in $\mu^+ - H$ wave function (see figures [a], [c] and [e]). This is related to the fact that μ^+ is lighter than the p^+ and therefore is easier misbalanced by the quick electron. Furthermore electron distributions are sharper in H_2^+ ground state than in $\mu^+ - H$ (compare figures in the left with their right hand counterparts), simply reflecting the fact that the first system is stronger bound.

Alternatively, in Fig. 2.7 one of positive particles distributions is presented, when the distance between the electron and the other positive particle is fixed to 1 (a.u.). Two fixed charges, as in previous case, are situated on the x axis, whereas their center of the mass is situated at the origin. One can see that a free positive particle rotates around the fixed pair, by having higher density distribution when being screened by the electron. All three plots resembles each other, however one can remark that the muon exhibit stronger oscillations (has wider spread distribution) than the proton.

2.3 Scattering problem

2.3.1 Modified boundary conditions

As stated in section 2.1, in order to solve scattering problem in configuration space, one has to implement equations (2.1) with appropriate boundary conditions. For elastic scattering, when all rearrangement and breakup channels are closed, one supposes that the asymptotic state is due to the free propagation of the projectile particle relatively to the cluster of other two particles, forming a bound pair. Therefore, the asymptotic state can be written as a tensor product of the bound pairs wave function $\varphi(x)$, describing the bound pair, and the scattering wave $f_l(y)$, which on its side is a superposition of incoming and outgoing waves:

$$f_l(y) = \left[\hat{h}_l^-(ky) - s_l(k) \hat{h}_l^+(ky) \right] \quad (2.16)$$

However, when one deals with long range interactions, projectile particle is never free and these boundary conditions, if can be satisfied then only in very far asymptotes, which are hardly attainable numerically. Here, one can distinguish two effects: on one hand the bound pair still feels the presence of retreating projectile and adapts to its created field by 'polarizing', on the other hand retreating particle feels effective interaction of the 'polarized' bound pair. It will be shown that both of these effects can be accounted properly by modifying boundary conditions.

Let us consider three-charge system, in particular scattering of heavy positive charge particle X^+ on Hydrogen atom. If scattered particle is far away, at the distances by a few orders of magnitude larger than electrons orbit in H atom, it will describe the long outer orbit (see Fig. 2.8) with the relatively long period. For the hydrogen atom, having much more compact size, it would look like a static charge. Electrons orbit is much smaller, thus permitting quick electron to adapt to outer particles created field and to follow its slow development. This field is nothing more than static electric field⁴ $\vec{E}_{el}(\vec{y}) = \hat{y}/y^2$, whereas so perturbed hydrogen atom can be described by the Stark effect. As it is well known, since electric field is vector field, therefore non vanishing corrections to the hydrogen atom energies are given by second and higher-order perturbations. Therefore hydrogen atom levels are shifted square proportionally to the strength of the electric field, if weak field is considered. If hydrogen atom is originally in the ground state, its wave function modified by the static electric field, is given by including the second order corrections [70, 71]:

$$\varphi(x, y) = \frac{2}{\sqrt{4\pi}} \left(\frac{1}{a_B} \right)^{\frac{3}{2}} \left[1 + \cos(\hat{x} \cdot \hat{y}) |E_{el}(\vec{y})| (a_B x + \frac{1}{2} x^2) \right] e^{-\frac{x}{a_B}}, \quad (2.17)$$

while the ground state energy is corrected by:

$$\delta E_H = -\frac{9}{4} a_B^3 E_{el}^2 + o(E_{el}^2). \quad (2.18)$$

If one imposes $E_{el}(\vec{y}) = \hat{y}/y^2$, the expression of hydrogen polarization potential will be recovered eq. (2.1), with $\alpha_H = \frac{9}{2} a_B^3 = \frac{9}{2}$ (a.u.).

In terms of the Hamiltonian, these ideas can be translated as follows. We uncouple Hamiltonian, for quick motion of the electron inside Hydrogen atom, dependent on variable \vec{x} for some fixed \vec{y} , where residual motion of scattered particle is described by slow variable \vec{y} . The total state is written as a product of perturbed hydrogens atom state $\varphi(x, y)$ and some function $\chi(y)$, describing recoil propagation:

$$\psi_{(ep)X^+}(x, y) = \varphi(x, y) \chi(y) \quad (2.19)$$

Hamiltonian part of Hydrogen atom cluster absorbs all the potential energy terms, where Hydrogen atoms interaction with a scattered particle (X^+), namely $V = V_{pX^+} + V_{eX^+}$, when $y \gg x$ can be replaced by $\vec{E}_{el}(\vec{y}) \cdot \vec{x}$.

$$\left(H_0^{(pe)} + H_0^{(X^+H)} + V_{pX^+} + V_{eH^+} + V_{pe} - E \right) \psi_{(ep)X^+}(x, y) = (2.20)$$

$$\left(\left[H_0^{(pe)} + \vec{E}_{el}(\vec{y}) \cdot \vec{x} + V_{pe} - E_H - \delta E_H \right] + H_0^{(X^+H)} + \delta E_H - (E - E_H) \right) \psi_{(ep)X^+}(x, y) = (2.21)$$

⁴In this section i express x and y in standard length units, not modified by Jacobi factor.

The approximate solution of the Hamiltonian part contained in parentheses, which becomes very close to exact one for the large values of y , is given by the function eq. (2.17). The rest of Hamiltonian depends only on variable \vec{y} and should be satisfied by function $\chi(y)$, therefore:

$$\left[H_0^{(pe)} + \vec{E}_{el}(\vec{y}) \cdot \vec{x} + V_{pe} - E_H - \delta E_H(y) \right] \varphi(x, y) = 0 \quad (2.22)$$

$$\left(H_0^{(X+H)} + \delta E_H(y) - (E - E_H) \right) \chi(y) = 0 \quad (2.23)$$

The term $(E - E_H)$ is nothing else as kinetic energy of the projectile relatively to the Hydrogen atom in the C.M. frame. The term $\delta E_H(y)$ reflects the origin of the polarization potential. Thus, as was discussed in previous section, scattered particle feels only effective field of hydrogen polarization $\delta E_H(y)$ by not seeing details of the hydrogen atom itself. Propagation of this scattered particle is described by the function $\chi(y)$.

The form eq. (2.17-2.19) can serve as boundary conditions for three-body Faddeev-Merkuriev equations. Implementation of these boundary conditions is done after projecting it into partial wave basis. One can remark that first term in eq. (2.17), not containing $\cos(\hat{x} \cdot \hat{y})$, is projected to Faddeev amplitudes of elastic channel with $\ell_x = 0$ and $\ell_y = L$. Whereas term containing $\cos(\hat{x} \cdot \hat{y})$ is distributed between the elastic channel amplitudes with $\ell_x = 1$ and $\ell_y = L \pm 1$.

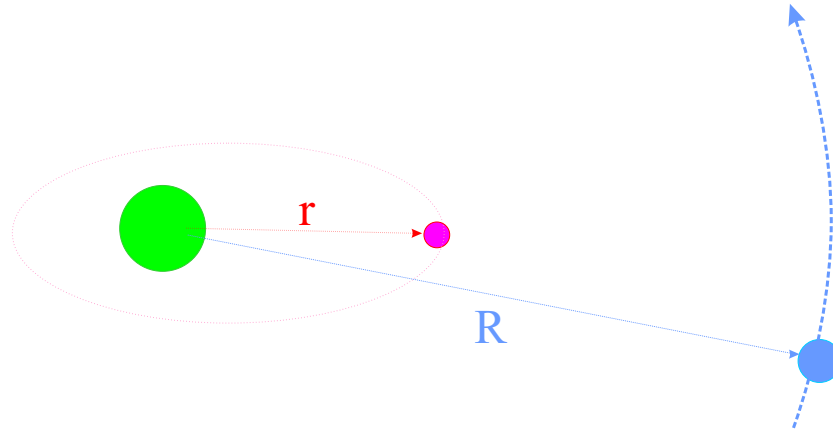


Figure 2.8: Asymptote configuration of hydrogen atom interacting with a positive particle. If distance to this particle is rather large - quick electron moving in small inner orbit is able to adapt to the projectile created field.

Practical implementation

The scattered particle propagation function is the solution of the two-body Schrödinger equation, from eq. (2.23) one has:

$$\left[\frac{\partial^2}{\partial y^2} - \frac{\ell(\ell+1)}{y^2} + k^2 - \frac{2\mu}{\hbar^2} V(y) \right] \chi(y) = 0 \quad (2.24)$$

with $V(y) = \delta E_H(y)$ being hydrogen polarization potential see eq. (2.1). For zero energy scattering ($k = 0$) this equation has an analytical solution

$$\chi(y) = C_1 y \exp\left(-i \frac{\sqrt{\beta}}{y}\right) + C_2 y \exp\left(i \frac{\sqrt{\beta}}{y}\right), \quad \text{with } \beta = \frac{\mu \alpha_H}{\hbar^2}. \quad (2.25)$$

Scattering lengths can be calculated by matching these boundary conditions at some big but finite distance y_{\max} . Whereas, scattering amplitude is found by using its standard definition eq. (1.57):

$$A_0 = \frac{y\chi'(y) - \chi(y)}{\chi'(y)} \Big|_{y \rightarrow \infty} = i \frac{C_1 - C_2}{C_1 + C_2} \sqrt{\beta}$$

On the contrary, for non zero energy scattering analytical solution of eq. (2.24) doesn't exist. However, if for some y_{\max} 3-Body wave function satisfies modified boundary conditions of eq. (2.19), scattering wave function in the outer region $[y_{\max}, \infty)$ can be reproduced by just propagating internal wave functions part by means of differential equation (2.24). Practically it signifies, that three body equations should be solved only in the restrained region $y \in [0, y_{\max}]$; afterwards, once logarithmic derivative of the wave function is found at some finite y_{\max} , external part of wave function is obtained after continuing it by integrating two-body equation (2.24) in the outer region $[y_{\max}, \infty)$ and inserting obtained solution into eq. (2.19).

To test these ideas, we have repeatedly solved the zero energy scattering equations for π^+ -H system by constantly increasing the grid in y direction. Computed π^+ scattering length values were plotted as a function of cut-off in y direction Fig. 2.9. Then by varying values of α_H and A_0 in eq. (2.25) we have fitted calculated $A(y_{\max})$ points (see red curve in Fig. 2.9). This extrapolation provided a hydrogen polarizability value of $\alpha_H = 4.501 \pm 0.017$, which within numerical precision coincides with the theoretical hydrogen atoms polarizability $\frac{9}{2}$, given by the 2-nd order perturbation calculations. Thus, validity of 2-body interaction model of eq. (2.24) for large projectile-Hydrogen atom distances is confirmed. Of course, before introducing cut-off in projectile recoil direction (y_{\max}) one should always make sure that it is sufficiently large to fall in 2-body region, and then that three-body wave function has the corresponding asymptote behavior.

2.3.2 Synthesis of results

Using the ideas developed in the previous section, studies of positive particle scattering on Hydrogen atom have been extended for projectiles with masses $m_{X^+} \in (m_e, 140)$ MeV. Zero energy scattering cross sections (see Fig. 2.11 [a]) as well as scattering lengths in the region of physical interest, $m_{X^+} \in (90, 140)$ MeV, containing μ^+ and π^+ , (see Fig. 2.11 [b]) are presented. Some interesting features of the 3-body Coulomb system can be learned by studying these dependencies.

One should recall remarks pointed out in introduction section of this chapter, that X^+ -H system becomes more static when mass of particle X^+ is increased and therefore number of 3-body bound states should grow. If mass of projectile is such, that it has some $\mathcal{L} = 0$ bound state 'rather near' threshold its wave function will have a node and therefore will result in positive scattering lengths olive curve in Fig. 2.10. Alternatively, wave function of the system without

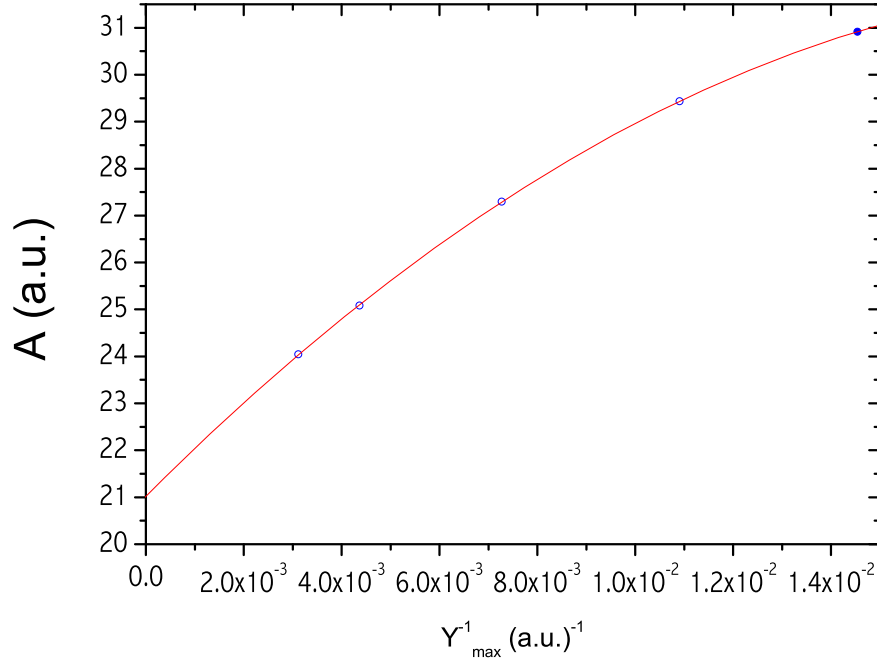


Figure 2.9: Scattering lengths as obtained after solving Faddeev-Merkuriev equations for π^+ -H system and by varying cut-off radius of the grid in y direction. By fitting these results using eq. (2.25) we extrapolated value of hydrogens atom polarizability $\alpha_H = 4.501 \pm 0.017$. Please note, that these calculations were done with slightly smaller PWB, therefore extrapolated scattering length is not very precise.

bound state formed yet cannot have any node and provide negative scattering lengths (blue curve). Conversely if $\mathcal{L} = 0$ bound state is just formed at $E_b = 0$, asymptote of its wave function will be flat (corresponding to exponential decay e^{-ky} , with $k \sim \sqrt{-E_b} = 0$), therefore resulting infinite scattering length, which furthermore has discontinuity passing from $-\infty$ to $+\infty$. Zero energy cross section, being proportional to square of scattering length, therefore tends to infinity for critically bound systems.

v	$m_c(\text{MeV})$	v	$m_c(\text{MeV})$	v	$m_c(\text{MeV})$	v	$m_c(\text{MeV})$
0	1.115	3	21	6	61.5	9	128
1	5.26	4	32	7	81		
2	11.8	5	45.5	8	101		

Table 2.3: Critical masses of positive charge particle X^+ at which X^+ -H states occur.

Thus, each peak (singularity) in Fig. 2.11 indicates the formation of a new S -wave bound state. The critical mass values m_i at which they occur, would enable to generalize the ground state stability triangle [72] to higher excitations.

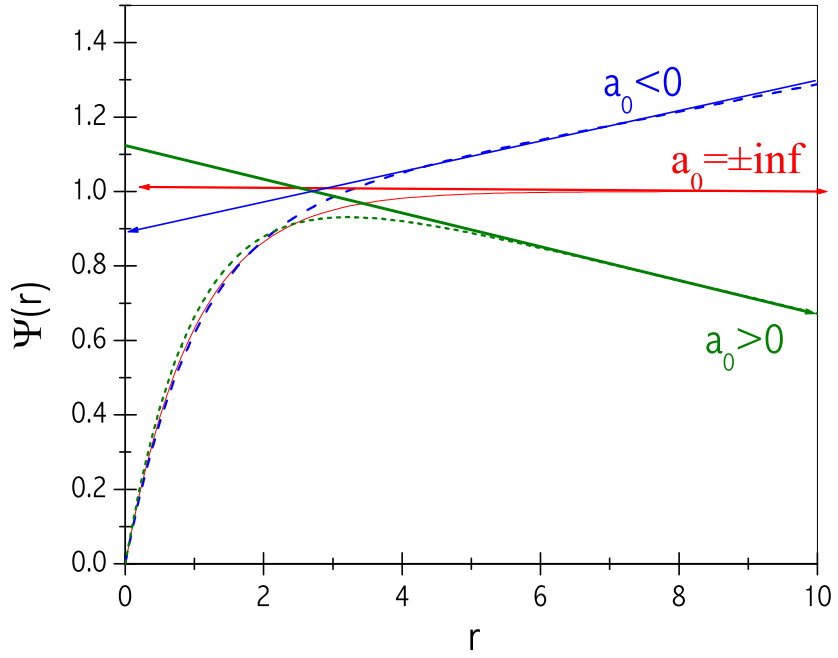


Figure 2.10: Scattering lengths for a $\mathcal{L} = 0$ critically bound projectile-target system.

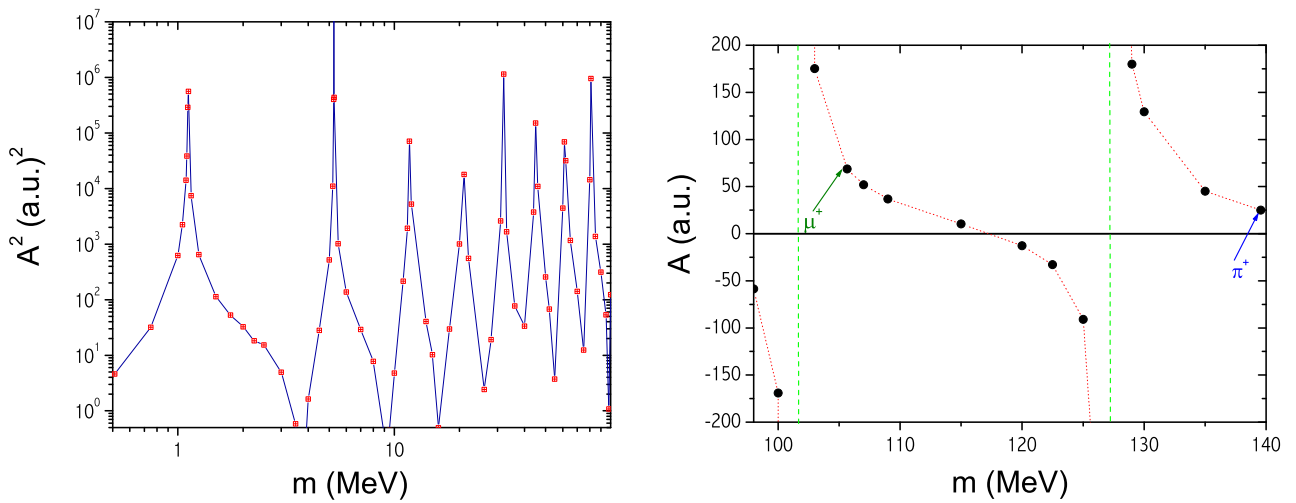


Figure 2.11: Dependence of zero energy $X^+ - H$ scattering cross sections (Figure [a]) on the particles X^+ mass. In Figure [b] similar dependence of scattering lengths is presented in the region of the physical interest $m_{X^+} \in (90, 140)$ MeV, containing μ^+ and π^+ .

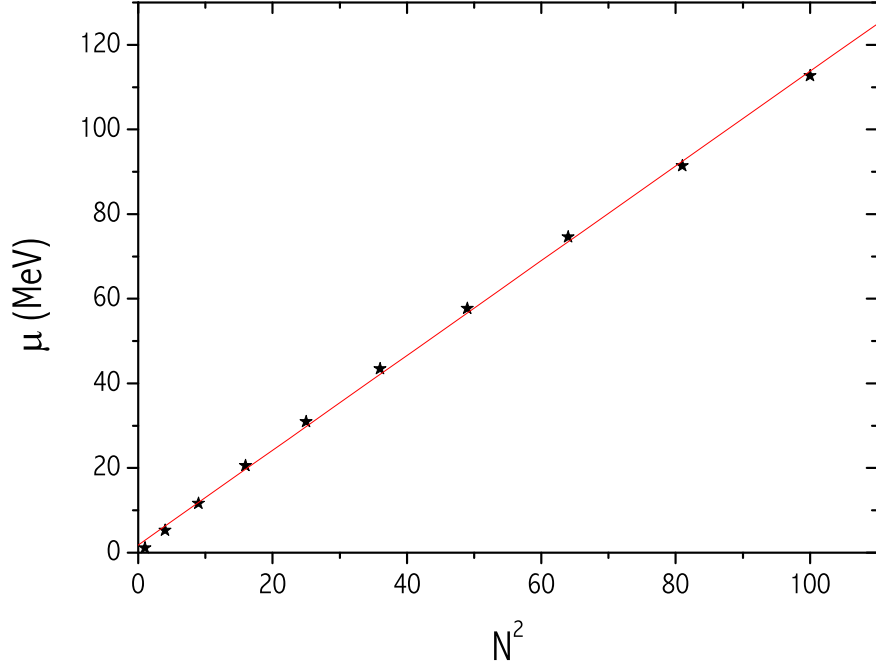


Figure 2.12: Critical mass values of positive charge particle X^+ for which in $X^+ - H$ system $\mathcal{L} = 0$ states appear.

Surprisingly, with rather good precision, number of bound states grows as $\sqrt{\mu}$ with the reduced mass of the system μ (see Fig. 2.12). By prolonging this phenomenological dependency, one can evaluate 21 bound state for H_2^+ molecular ion⁵, which agrees with precise 3-body calculations [46, 50, 51]⁶. Such dependence is very close to well known WKB approximation:

$$\int_a^b \frac{\sqrt{2\mu |E - V(x)|}}{\hbar} dx = (N + \frac{1}{2})\pi,$$

only additional coefficient with N should be moreover 1 than $\frac{1}{2}$. Success of WKB approximation suggests that such a system retains 2-body systems properties and therefore can be rather successfully modelled by effective two body potential.

The critical mass at which $X^+ - H$ system gains the first bound state agrees with the evaluation of [73, 74] $1.1m_e \leq m_1 \leq 2.2m_e$, being however closer to the upper bound and furthermore providing with the exact value $m_1 = 2.182 \cdot m_e = 1.115$ MeV.

Furthermore, we have calculated the scattering lengths for the real physical systems $\mu^+ - H$ and $\pi^+ - H$. They are respectively $a_{\mu^+ H} = 69.1$ (a.u.) and $a_{\pi^+ H} = 24.4$ (a.u.). One can point

⁵Actually, since H_2^+ system consist two identical particles, its wave function should satisfy symmetry relations for the exchange of two protons. In this sense it differs from general three different particle system and therefore it is not fully rigorous to compare.

⁶However we will show later that H_2^+ molecular ion contains one more very loosely bound $\mathcal{L} = 0$ state.

out that these scattering lengths are comparably large, being more than by one order of magnitude larger than Hydrogen atom itself, thus reflecting long range behavior of polarization potential.

By counting number of peaks in the left of scattering cross section curve, one can conclude that $\mu^+ - H$ has 9 $\mathcal{L} = 0$ states below the H atoms ground state, whereas $\pi^+ - H$ has by one bound state more. The information about the total number of those states can be recovered by examining the form of Faddeev components. If one looks at Fig. 2.13, where open elastic channels Faddeev component for μ^+ scattering on H atom at $E = 0$ is presented , one can see that all its nodal structure is situated along the y axis, or in μ^+ separation from H direction. This fact indicates strong vibrational origin of these states. Consequently, the number of bound states is simply equal to the number of nodes along the y axis (in this case $n = 9$). The last node is very broad and only its first half is present in the figure, however it can be seen that asymptote of the wave function will create one more node by diverging linearly with y to $+\infty$.

One should note that the correspondance of number of nodes in Faddeev-Merkuriev components (FMC) to number of systems bound states is by no means a strong proof. Rigorously, only the number of nodes in the systems total wave function can be associated with a number of bound states, whereas the structure of the FMC depends on the parameter choice in potential splitting function (eq.2.9). In general, for a bad parameter set, FMC can have a complicated structure with many parasite bumps, which compensate each other once added to construct systems total wave function. However, we have optimized this parameter set to improve partial wave convergence, therefore making FMC as smooth and regular as possible and, at the same time, minimizing number of nodes in it (note the minimal number should be equal to the number of nodes in systems wave function). On the other hand, since these bound states have a pronounced vibrational structure it is reflected in single FMC as well.

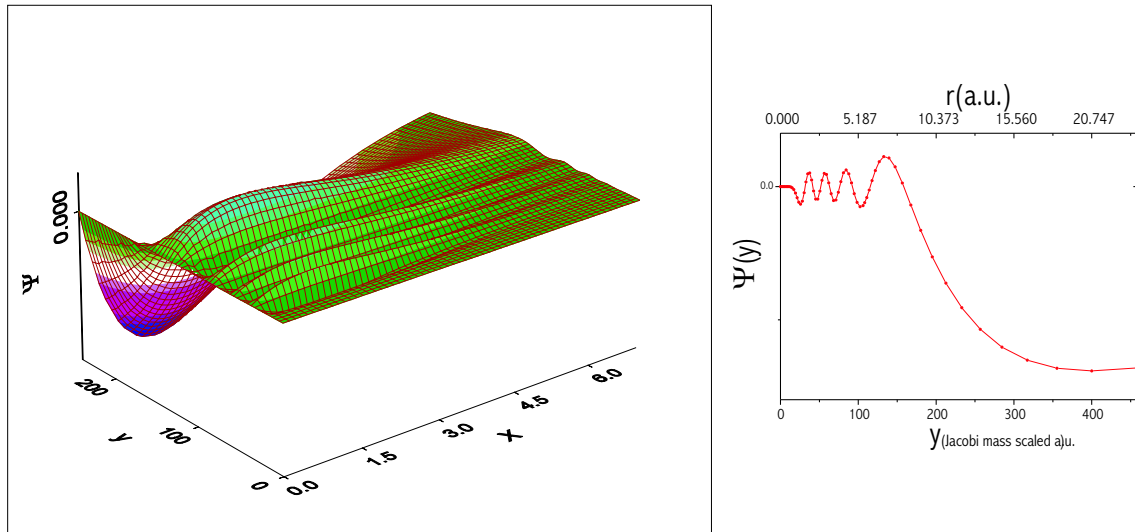


Figure 2.13: Faddeev-Merkuriev component is represented for the zero-energy μ^+ -H scattering. In the second picture a cut along y axis is made. One can count wave function exhibiting up to 9 nods along this axis, therefore indicating presence of 9 vibrational $\mathcal{L} = 0$ bound states.

$\pi^+ - H$ and $\mu^+ - H$ elastic scattering calculations in $\mathcal{L} = 0$ state were extended for non-zero projectile energies up to 2-nd minima. Analogous calculations were also performed for $\mathcal{L} = 1$ states and corresponding results are presented in figures 2.14 [a] and [b].

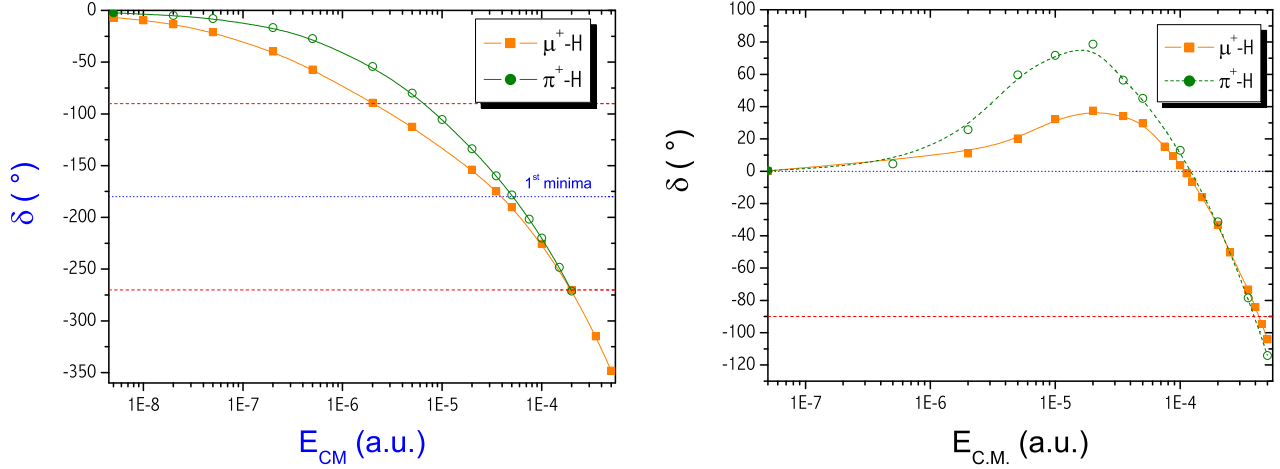


Figure 2.14: Elastic phase shifts in $\pi^+ - H$ and $\mu^+ - H$ scattering. Figure [a] represents total angular momentum $\mathcal{L} = 0$ results, whereas in figure [b] $\mathcal{L} = 1$ phase shifts are plotted.

2.3.3 $p^+ - H$ elastic scattering

The case of proton scattering on atomic Hydrogen is of special interest. Since Hydrogen atom itself contains one proton, the Pauli principle implies that the total wave function of the $p^+ - (p^+e^-)$ system must be antisymmetric in the two proton exchange. This can be realized in two different ways following the proton-proton spin coupling. In case when the two proton spins are antiparallel (spin singlet state, noted σ_g by atomic physicist), the spatial part of the wave function is symmetric in proton exchange, whereas in the case when the two proton spins are parallel (spin triplet state, noted σ_u) it is antisymmetric.

Considering a 2-body approach, in which one of the protons interacts with the Hydrogen atom via an effective potential, these two states give rise to two completely different $p^+ - H$ potentials. The singlet case (σ_g) has a broad attractive well, that supports a great number of bound states (see Fig. 2.15). These states have been calculated since the first days of Quantum Mechanics and are presently known with a very high precision (see e.g. [50, 51] and reference therein). Our 3-body bound state calculations, which have already been presented in Table 2.2, cannot reach such accuracy but are in good agreement for the lower excitations (at the level of 5-6 significant digits). Our calculations provide however the first result for p^+H singlet scattering length $a_s = -29.3$ a.u.. The convergence test for these calculations is presented in Fig. 2.16. We notice that the zero energy Faddeev components have 20 nodes in $p^+ - H$ direction, thus indicating the existence of 20 $\mathcal{L} = 0$ σ_g symmetry energy levels for H_2^+ ion in agreement with the predictions of variational

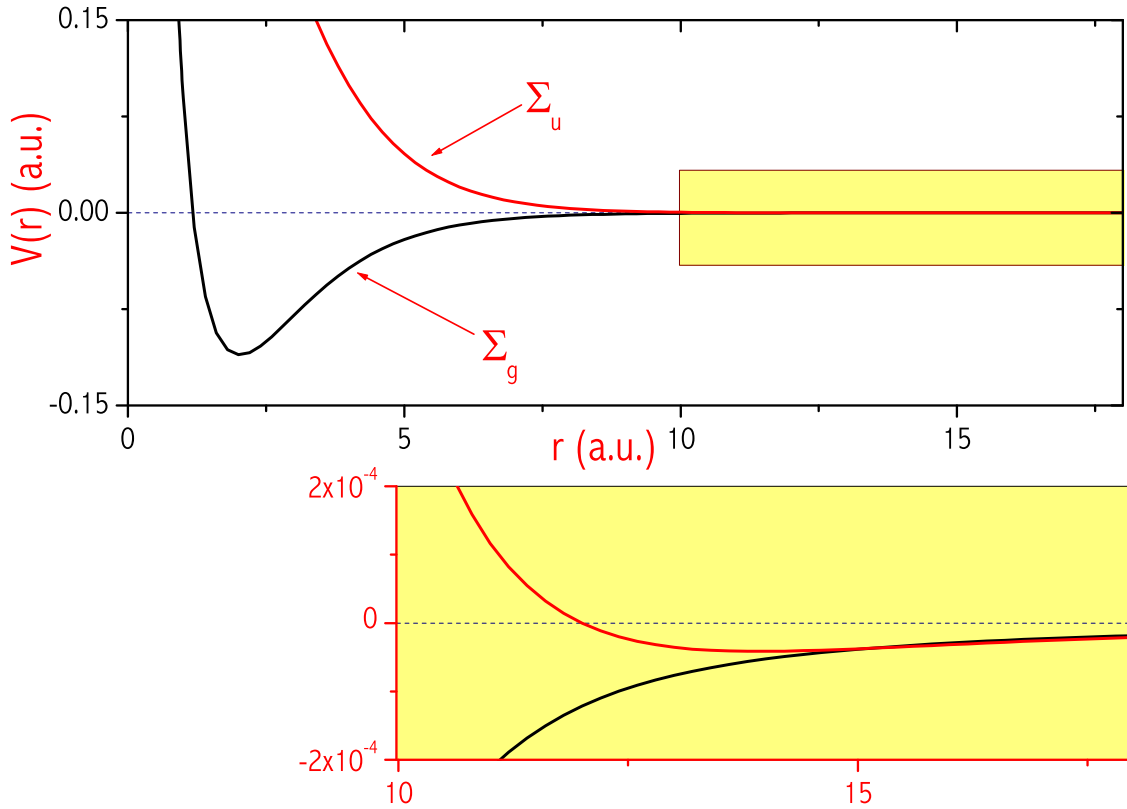


Figure 2.15: Qualitative 2-body H_2^+ effective potentials as a function of internuclear distances for σ_u and σ_g proton exchange symmetries. Effective σ_u potential is basically repulsive due to Pauli principle interdicting protons to approach each other, whereas overbalanced at $r \sim 12$ (a.u.) by attractive polarization potential.

calculations. These states are noted $1s\sigma_g$ in atomic physics.

The necessity to describe wave functions having 20 nodes demands very dense grid in the p^+ -H interdistance. Furthermore, the partial wave convergence is very slow, as it can be seen in Fig.2.16. On one hand, this is due to the complicated structure of the wave function. On the other hand it is caused by the big proton-electron mass difference. One should take into account partial waves with $(\ell_x, \ell_y) \geq 17$ to obtain satisfactory results, what constitutes a numerically very expensive and challenging task.

2p σ_u symmetry states of H_2^+ molecular ion

A completely different situation to σ_g states discussed just above, arises when one considers σ_u symmetry states. These configurations are dominated by the strong Pauli repulsion between two protons, since they should be described by space antisymmetric wave functions. The effective 2-body interaction was successfully modelled by Landau [75] (in the exercise of page 361-362!). This potential has a very simple form

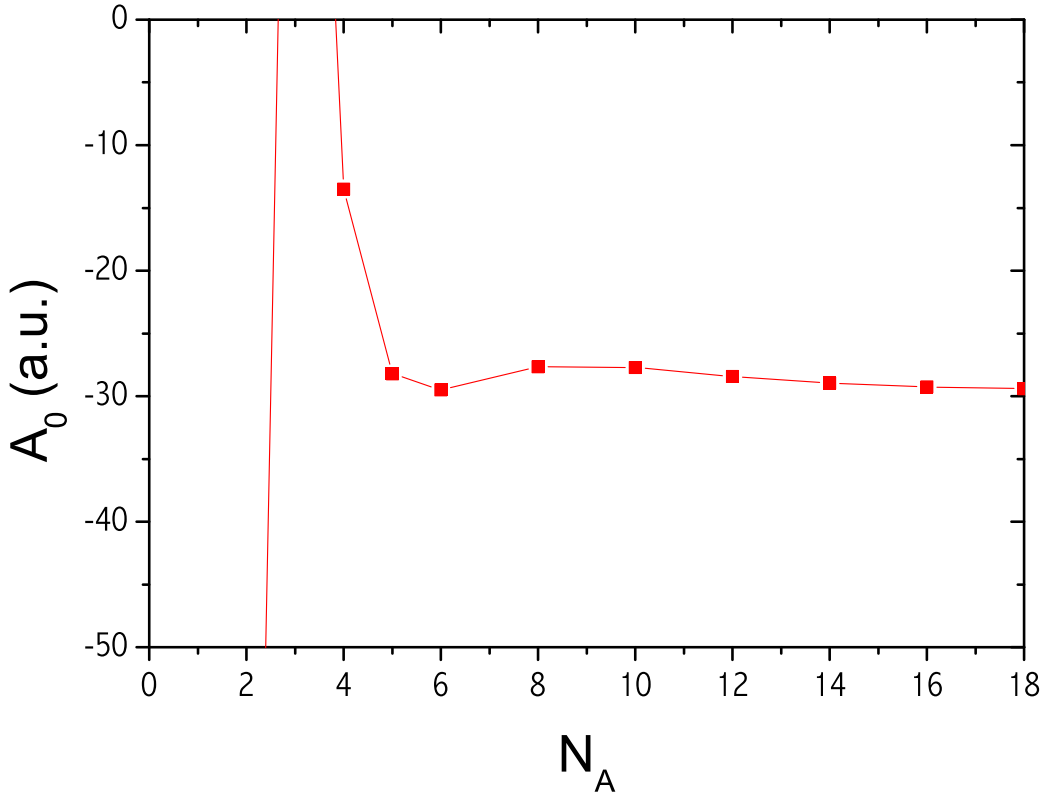


Figure 2.16: Convergence on the number of partial waves in p^+ -H scattering length calculations for proton singlet configurations ($1s\sigma_g$ state). Convergence is very fluctuating, when one has small number of partial waves.

$$V_g(r) = 2r \cdot e^{-(r+1)} - \frac{9}{4r^4}, \quad (2.26)$$

with r representing the distance between two protons. The first term in this potential accounts for Pauli repulsion between the protons, while the second one represents a long-range attraction due to Hydrogen polarizability. Some regularization should be made at short-distance to avoid polarization term becoming infinitely attractive (this regularization does not affect noticeably the results).

Surprisingly, it turns out that the strong Pauli repulsion is still overbalanced at ~ 10 (a.u.) by the attractive polarization forces and therefore the potential has a very weak attractive well of $\sim 10^{-5}$ (a.u.) (see Fig. 2.15). Nevertheless, this shallow potential is able to support a few σ_u symmetry H_2^+ molecular ion bound states, precisely calculated in [46, 47].

One can see in Table 2.4 that Landau potential predicts rather well the binding energies of these states, however slightly underestimating them. This underestimation is caused by the Pauli repulsion term, which in Landau potential is found too strong. This can be shown by constructing Born-Opernhaimer potential [78]. An even better agreement can be obtained by modifying the short range part of Landau potential to give the exact binding of $2p\sigma_u$ ($\mathcal{L} = 0$, $v = 0$) state,

v, \mathcal{L}	3-Body	Landau	Modif. Landau
0,0	$1.56625 \cdot 10^{-5}$	$1.45350 \cdot 10^{-5}$	$1.56625 \cdot 10^{-5}$
0,1	$1.14283 \cdot 10^{-5}$	$1.04144 \cdot 10^{-5}$	$1.13850 \cdot 10^{-5}$
0,2	$0.36829 \cdot 10^{-5}$	$0.29362 \cdot 10^{-5}$	$0.35789 \cdot 10^{-5}$
1,0	-	$3.7126 \cdot 10^{-11}$	$1.2381 \cdot 10^{-9}$

Table 2.4: Comparison of exact 3-body H_2^+ σ_u bound state calculations, values borrowed from [46], with results obtained by simple 2-body Landau potential model.

	Landau	Modif. Landau	3-body
B_{direct}	$3.7126 \cdot 10^{-11}$	$1.2381 \cdot 10^{-9}$	-
B_{Scatt}	$3.7152 \cdot 10^{-11}$	$1.2419 \cdot 10^{-9}$	$1.125 \cdot 10^{-9}$
A_0	3892.3	715.84	750
α	$2.5691 \cdot 10^{-4}$	$1.3970 \cdot 10^{-3}$	$1.330 \cdot 10^{-3}$
β	63.089	49.687	51.82

Table 2.5: Extrapolation of the H_2^+ $2p\sigma_u$ symmetry ($\nu = 1$, $\mathcal{L} = 0$) state binding energy from low energy elastic phase shifts. In case of 2-body Landau potential we were able to perform direct bound state calculations as well.

provided by direct 3-Body calculations⁷, see Table. 2.4. On the other hand, Landau potential suggests the existence of a first excited $\mathcal{L} = 0$ state with extremely small binding energy. One should notice that R.E. Moss [46], in the most complete study of H_2^+ molecular ion spectra, was not able to conclude about the existence of a second $2p\sigma_u$ bound state ($v=1$, $\mathcal{L} = 0$).

The accuracy of our direct 3-body bound state calculations is much smaller than the one obtained by Coulomb problem adapted variational methods [45, 50] and is only sufficient to obtain the $2p\sigma_u$ ground state. Nevertheless, our zero-energy scattering calculations give a large positive value of the triplet scattering length $a_t = 750$ (a.u.). The positive sign of the scattering length and the nodal structure of the Faddeev amplitudes indicate that such a big value is due to the existence of a first excited $\mathcal{L} = 0$ state with extremely small binding energy. In a certain way this confirms the indications of simple 2-body Landau potential model.

One should now wonder whether it is possible to extract the corresponding nearthreshold bound state energy from scattering calculations. In this purpose we will use the ideas of the effective range theory. For potentials having $1/r^4$ asymptotic behavior, it was shown in [20] by L. Rosenberg, T. F. O'Mally and L. Spruch that the effective range expansion has the form

$$k \cot \delta = -\frac{1}{a} + c_1 k + c_2 k^2 \log k + c_3 k^2 + o(k^2) \quad (2.27)$$

However, this formulae is confusing when one considers nearthreshold bound state. Bound state energy $E = \frac{\hbar^2 k^2}{2\mu}$ and $k = ik_0$, should appear as a negative energy pole in this expansion. However the presence of linear, as well as logarithmic terms in k , suggests complex values for this

⁷3-body results were taken from the [46], our 3-body direct calculations are less accurate, giving value E=1.569 · 10^{-5} (a.u.) for ($v = 0, \mathcal{L} = 0$) state.

energy. The later fact was well observed and discussed by the same authors [20]. Usually, when a nearthreshold bound state exist, it is more convenient to make expansion about its energy rather than about $E = 0$. Such procedure will finally lead to the standard effective range expansion

$$k \cot \delta = \alpha + \beta k^2 + o(k^2) \quad (2.28)$$

with $\alpha = -k_0 + \beta k_0^2$. Note that the parameter β can not be anymore straightforwardly related to the effective range of the potential.

One could question the equivalency of these two expansions. The point is that, if a nearthreshold bound state exist, coefficients c_1 and c_2 of eq. (2.27), making the difference between these two expansions, vanishes. Actually, when one makes expansion about $E = 0$, no assumption are made about the magnitude of the scattering length a . On the contrary, in the expansion about nearthreshold bound state a value k_0 is introduced, which scales with the scattering length $k_0 \sim \frac{1}{a}$. It can also be shown that coefficients c_1 and c_2 scale with scattering lengths as well: $c_1 \sim \frac{1}{a^2}$ and $c_2 \sim \frac{1}{a}$. Therefore, these parasite terms in formulae (2.27) are as small as $\frac{1}{a^3}$ and represent higher order corrections in the expansion (2.28), which are here neglected.

The 3-body energy extrapolation procedure from the low energy scattering phase shifts is presented in Fig. 2.18 and the corresponding result is given in Table 2.5. We predict a bound state at $B = (1.125 \pm 0.03) \times 10^{-9}$ (a.u.) below the first dissociation limit ($H(n=1) + p^+$). To our knowledge, this is the weakest bond ever predicted, three times smaller than the ${}^4\text{He}$ atomic dimer [76].

Finally, to erase the last doubts, I have tested this extrapolation procedure by predicting bound state energies of 2-body Landau potential from the scattering observables. In this case direct bound state calculations can be made and therefore two approaches can be compared. In Figs. 2.17 two phase shift calculations with 2-body potentials having $1/r^4$ long range behavior are presented. In the upper plot, results of standard Landau potential are given. Results of bottom plot were obtained by modifying the short range part of Landau potential in order to give the correct 3-body binding energy of the $\mathcal{L} = 0$ ground state, as given in Table 2.4. Both curves in Fig. 2.17 display a linear dependency of $k \cdot ctg\delta$ as a function of k^2 , therefore confirming the validity of expansion (2.28). The binding energies extrapolated from the scattering results are in good agreement with direct calculations, even though we have tested two states with rather different binding energies and scattering length values. Evidently, a better agreement is found for the state which lies closer to the threshold and for which the scattering amplitude is stronger influenced by the nearthreshold bound state.

One can ask an evident question: how can we rely on the the scattering results, while our direct bound state calculations are far below the necessary accuracy. The point is that in scattering calculations the energy is fixed, as well as the asymptotic behavior of the p-H wave function. Thus, the nontrivial part of the 3-Body wave function is restricted. On the contrary, in direct bound state calculations the asymptotic behavior is determined by the separation energy, which is the principal unknown. Since even a magnitude of this value is a priory unknown, one is forced to cover very large regions by the trial functions in order to be able to correctly describe the asymptotic behavior

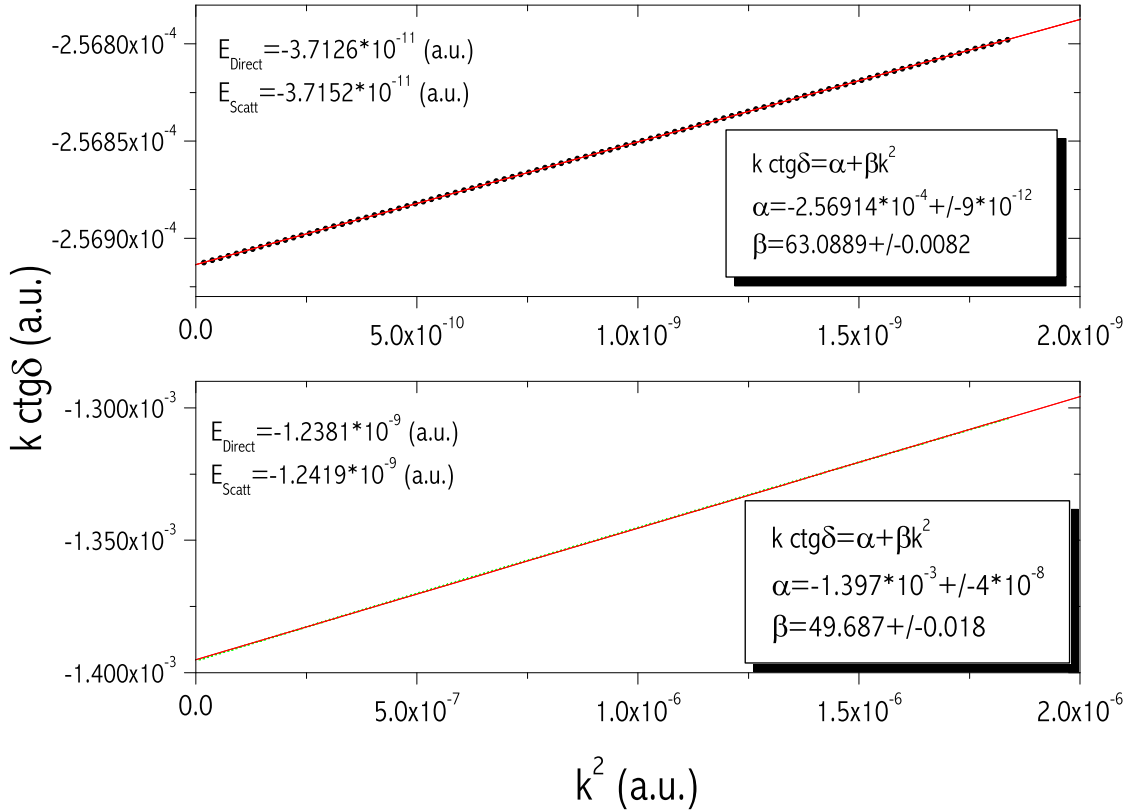


Figure 2.17: Extrapolation of the nearthreshold bound state energy from low energy scattering calculations. In the above figure standard Landau potential was applied, in the bottom figure Landau potential was modified as explained in the body text. In both cases, one has a good agreement between the scattering results and direct bound state energy calculations.

of a bound state. This becomes a cumbersome numerical task. Other difficulty when using direct bound state methods is that they deal with the total 3-body binding energy. Therefore, when looking for states with small separation energies one has to ensure very high numerical accuracy. In scattering calculations the 2-body cluster energy is effectively factorized.

To ensure that obtained results are not due to the numerical deficiency of our methods, we have asked theoreticians of Laboratoire Kastler Brossel to search for this H_2^+ state using a completely different approach. The high accuracy variational method they use [50] is specially adapted to treat the 3-body Coulomb problem. It is able to provide H_2^+ molecular ion $\mathcal{L} = 0$ spectrum with the currently best known precision (15 significant digits). They have recently confirmed our results, providing much more accurate values (see Table 2.6), as well as bound state wave function. In Fig. 2.19 we display the $2p\sigma_u$ ground and first excited state wave functions and compare them with the zero energy p-H scattering wave function. These are full three-body wavefunctions and thus are not easy to plot. However, they take significant values only for rather large internuclear distances (at short distance, the molecular energy curve is very repulsive): consequently, the electronic

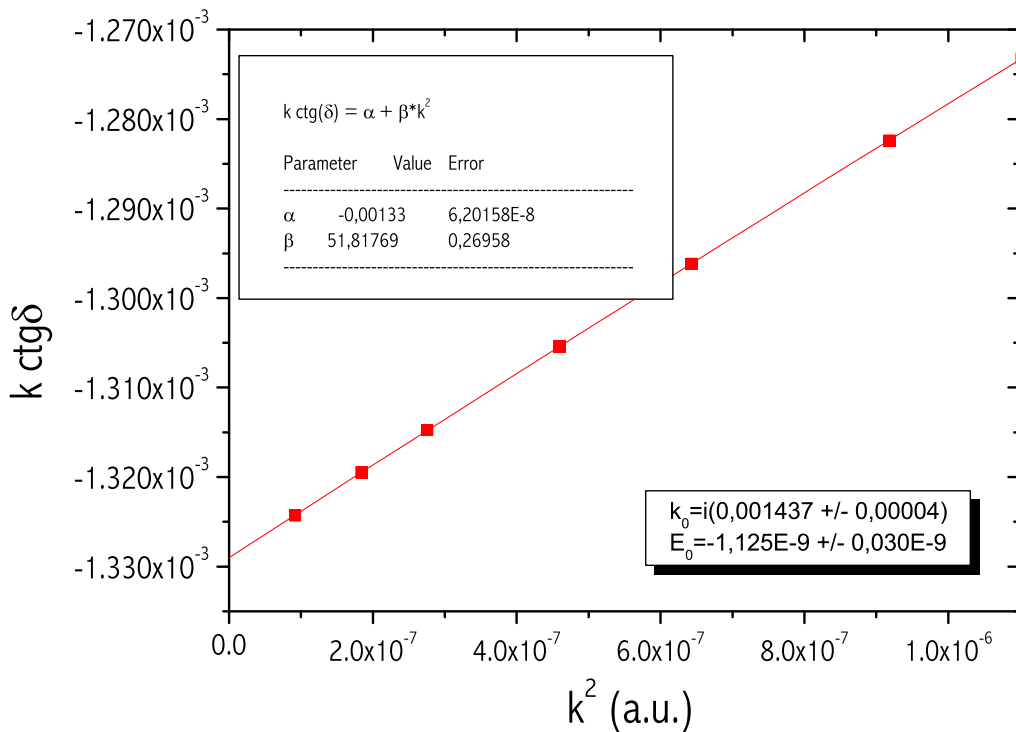


Figure 2.18: Extrapolation of the H_2^+ $2p\sigma_u$ ($\nu = 1$, $\mathcal{L} = 0$) state binding energy from the low energy 3-body scattering calculations of the $p^+\text{H}$ system.

wavefunction is essentially the ground state of the hydrogen atom attached to one of the protons, independently of the internuclear distance. Due to the large size of the excited state, we chose to plot the wavefunction using a logarithmic scale for the internuclear distance r . The ground state is a nodless wavefunction centered around 15 (a.u.), when the excited state extends much further; it has a maximum at $r \sim 100$ (a.u.) and still significant values in the $r \in [1000, 2000]$ (a.u.) range. There is an inflection point at $r \approx 215$ (a.u.). As expected, it is located at the outer turning point of the Born-Oppenheimer (or Landau) potential, where the polarization potential is equal to the binding energy. This gives another indication that calculations are well converged. By comparing zero-energy scattering wave function, one can notice that for small r it is remarkably similar to the wavefunction of the excited state, which is principally due to the small energy difference between the two wavefunctions. At large distances, the zero-energy wave function diverges linearly with r , as is given by eq. (1.56). This linear behavior is already reached before the second node is completed and therefore a wavefunction has a zero at about the scattering length value 750 (a.u.).

Finally, in view of the extremely small binding energy of the predicted state, one should quantify the neglected physical effects that could destroy this state. One should stretch out the fact that we have worked in a non-relativistic frame and that only pure Coulomb interactions were considered. Three following effects can be found:

B_H (a.u.)	B_{pH} (a.u.)	$B_{pH} - B_H$ (a.u.)
0.499727839716466	0.499727840801511	$1.085045 \cdot 10^{-9}$
0.499722416519476	0.499722417601384	$1.081908 \cdot 10^{-9}$

Table 2.6: Values obtained by [77][78] in direct H_2^+ σ_u symmetry ($\nu = 1$, $\mathcal{L} = 0$) state calculations (second line). In the last line values including relativistic and radiative corrections are given. Radiative corrections, being very small for the separation energy $B_{pH} - B_H$, are applied only to B_H .

1. Effects due to relativistic treatment of the electron. Relativistic corrections due to motion of protons will be negligible in comparison. Furthermore, the effects of the nuclear motion on the electron wave function (non-adiabatic effects) are small [79]. Therefore in determining relativistic corrections it is appropriate to treat them as being fixed, point-like charges. One should start by considering Dirac Hamiltonian for the electron in the Coulomb field of two fixed nuclei with an elementary charge +1:

$$H_D(\mathbf{R}) = mc^2 \left[\beta + \alpha \alpha \cdot \mathbf{p} - \alpha^2 \left(\frac{1}{r_1} + \frac{1}{r_2} \right) \right], \quad (2.29)$$

where α is a fine-structure constant, α and β are Dirac matrices. The solution of this Hamiltonian gives relativistic energy of H_2^+ as a function of internuclear separation \mathbf{R} . When relativistic effects are completely neglected, the Schrödinger equation for an electron in the Coulomb field of two fixed nuclei is recovered. Since relativistic effects are small it is attractive to treat them as a perturbation to the solved fixed-nuclei Schrödinger problem. This was achieved in a work of M.H. Howells and A. Kennedy [79]. They have tabulated the corrections for the $2p\sigma_u$ state of H_2^+ as a function of \mathbf{R} , up to $\mathbf{R}_{max}=500$ (a.u.). The extension of this tabulation to $\mathbf{R}_{max}=\infty$ presents no difficulty, since at large distances relativistic corrections $V_{Rel}(\mathbf{R})$ vanishes as $1/\mathbf{R}^4$. Using bound state wave functions calculated by theoreticians of Laboratoire Kastler Brossel [78] $\Psi(\mathbf{R}, \vec{r})$, the evaluation of these corrections is straightforward:

$$\Delta E_{Rel} = \frac{\langle \Psi(\mathbf{R}, \vec{r}) | V_{Rel}(\mathbf{R}) | \Psi(\mathbf{R}, \vec{r}) \rangle}{\langle \Psi(\mathbf{R}, \vec{r}) | \Psi(\mathbf{R}, \vec{r}) \rangle} \quad (2.30)$$

In this way, we have obtained $\Delta E_{Rel} = 3.137 \cdot 10^{-12}$ (a.u.). A very small value unable to destroy, or even to have observable effects on this bound state. The corrected bound state energies are summarized in the last row of Table 2.6.

To check the validity of these calculations we have also calculate the relativistic corrections for the ground $2p\sigma_u$ H_2^+ state. A value $\Delta E_{Rel} = 1.528 \cdot 10^{-9}$ (a.u.) = $3.354 \cdot 10^{-4}$ cm $^{-1}$ was obtained, in agreement with $\Delta E_{Rel} = 3 \cdot 10^{-4}$ cm $^{-1}$ obtained by R.E. Moss [46].

Finally, we display in Fig. 2.20 relative corrections to the binding energy ($\Delta B/B$) for all the $\mathcal{L} = 0$ $1s\sigma_g$ (filled circles, results borrowed from [46]) and $\mathcal{L} = 0$ $2p\sigma_u$ (filled squares, our results) states. In all these states effect of the relativistic corrections is smaller than 0.3% and vary very slowly with the binding energy. Of course at some level, for even much

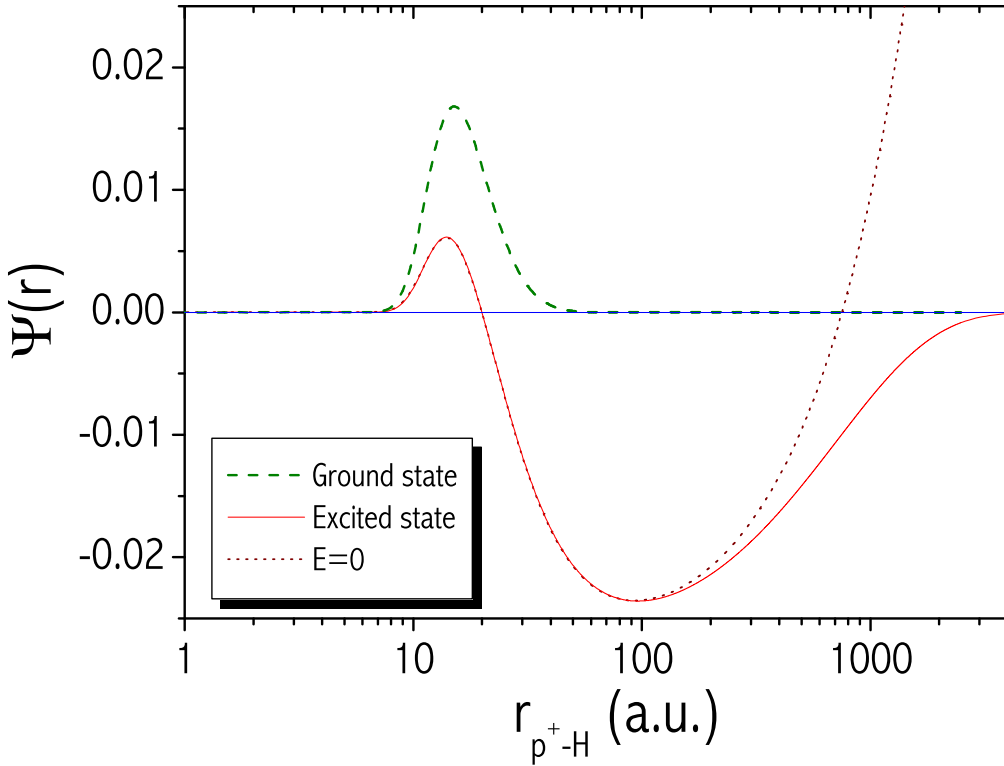


Figure 2.19: Wavefunctions (not normalized) of the ground (dashed line) and excited (solid thick line) of the H_2^+ molecular ion $2p\sigma_u$ ($\mathcal{L} = 0$) states. They are compared with the corresponding $p^+ - H$ zero energy wavefunction (dot line). The existence of an excited level with very small binding energy is predicted by our calculations. Its wavefunction extends very far in the internuclear distance r , with a maximum probability density around 100 (a.u.). It is responsible for a huge scattering length of 750 (a.u.). Note the use of a logarithmic scale on r .

weaker bound states, these corrections become destructive, however it can only happen for the binding energies below 10^{-12} (a.u.).

2. However, Dirac Hamiltonian does not exhaust the complete relativistic treatment of the problem. It misses the effects due to quantification of the electromagnetic field, which are responsible, for instance, for the well known Lamb shift effect in Hydrogen atom. These corrections are known as radiative corrections, being not easy to evaluate. Atomic limit affected by these corrections is modified by $\Delta E_{Rad} = -0.270661 \text{ cm}^{-1} = -1.23322 \cdot 10^{-6}$ (a.u.). Radiative corrections relative to the atomic limit were estimated in work of Kołos et al. [226]. It was shown that they are internuclear distance dependent and rapidly vanishes as the size of the state increases. For the highest $1s\sigma_g$ H_2^+ excited states, with dissociation energies of 10^{-5} (a.u.), they are already smaller than 10^{-10} (a.u.) and are by few orders of magnitude weaker than the relativistic corrections due to the electron motion. Furthermore for the largely extended states these corrections gives even some additional attraction.

3. There is one more effect due to field theory treatment of the interaction: it is known as Casimir-Polder or retardation effect. The classical explanation of this effect relies on the fact that the interaction is spread not instantaneously but with the finite speed of light. In [227] H.B.G Casimir and D. Polder pointed out that if retardation effects are properly taken into account, the long range interaction between two neutral atoms is no longer Van-der Waal's $1/r^6$ law, but approaches a $1/r^7$ law for sufficiently large r [228]. This rather surprising result might suggest that at sufficiently large r , the $1/r^4$ polarization potential, due to the adiabatic approximation, of a proton with a neutral Hydrogen atom could be considerably modified when retardation effects are taken into account. However, in atom-atom case, there are two fluctuating dipole moments (classically there are two rotating dipole moments) and therefore interaction between them strongly depends upon the time it takes to the light to travel from one atom to another. On the contrary, in the case of proton interacting with a neutral Hydrogen atom, the dipole moment, induced by the proton, is not fluctuating. Therefore the retardation effect at extremely small v/c values we are considering, modify the $p - H$ potential by only adding very weak term with $1/r^5$ long range behavior. According to reference [80], the long range polarization potential becomes:

$$V(r) = -\frac{\alpha_d}{2r^4} \left(1 - \frac{11\hbar}{2\pi m_p c r} \right)$$

With $r \sim 100$ (a.u.) and the appearance of the proton mass (m_p) in the denominator, these corrections turn to be negligible.

On the other hand, one should be careful with the spin-orbit and spin-spin interactions. We are indeed interested in triplet states with total two-proton spin $S_{pp} = 1$, so that the total angular momentum can be either $F = 1/2$ or $F = 3/2$ when the electronic spin is taken into account. This hyperfine structure should be very close to the $F = 0 / F = 1$ hyperfine structure of the hydrogen atom. As the latter is much larger than the binding energy we have calculated for the non-relativistic problem, it is likely that the $v = 1, \mathcal{L} = 0, F = 3/2$ level lies above the dissociation limit of the $F = 1/2$ series. The dissociation rate induced by the hyperfine coupling is however most probably very low.

Finally, I would like to stretch that this weakly bound H_2^+ molecular ion state is of fundamental importance. Its interest is not limited by the excitement of a numerical exercise. This state manifests itself in a huge p-H scattering length $a = 750$ (a.u.), which will dominate the low energy scattering cross section of proton by atomic hydrogen. The H_2^+ formation rate will be substantially influenced by this resonant p-H cross section. Since positive charge H_2^+ system can easily catch an electron by exhibiting radiative association, the existence of a resonant p-H scattering cross sections can help to explain the abnormal abundance of H_2 molecules present in the interstellar space [81][82]. This problem is of fundamental astrophysical and geophysical importance and represents up to now an intriguing puzzle.

A direct measurement of the p-H cross section at very low energy seems unlikely. One can however access the low energy p-H continuum in the final state of the H_2^+ photodissociation cross

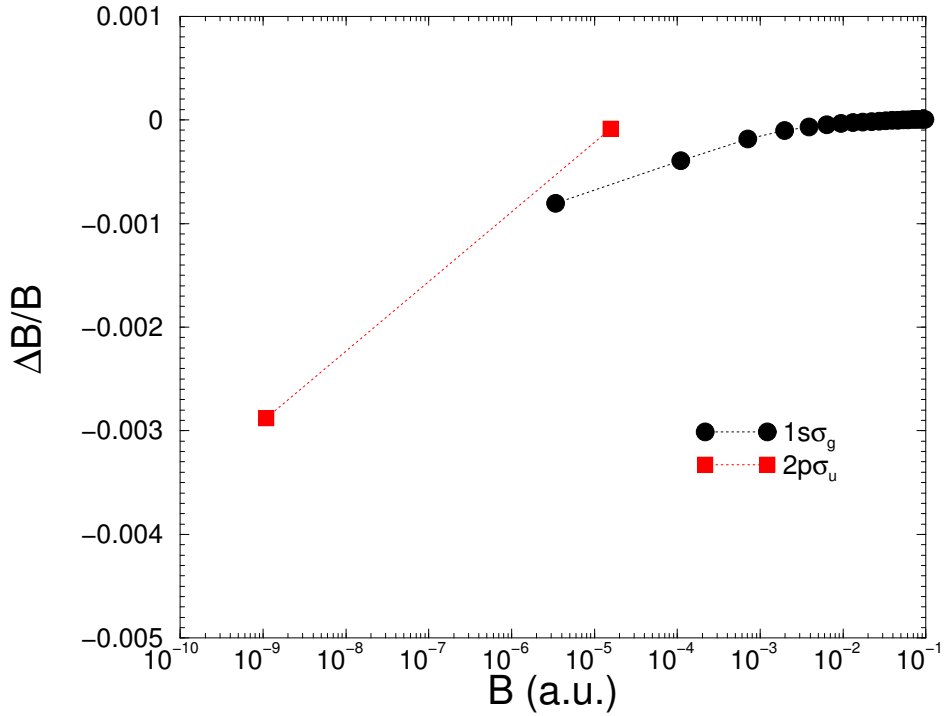


Figure 2.20: Relativistic corrections to the binding energies for $\mathcal{L} = 0$ $1s\sigma_g$ (filled circles) and $\mathcal{L} = 0$ $2p\sigma_u$ (filled squares) states of the H_2^+ molecular ion.

section. The excited vibrational $2p\sigma_u(v = 1, \mathcal{L} = 0)$ level predicted here is radiatively coupled to the $1s\sigma_g(v = 19, \mathcal{L} = 1)$ level. The electric dipole transition between those two levels should be observable in the 6 GHz range using an experiment similar to the one used to detect the $(v = 0, \mathcal{L} = 0) \rightarrow (v = 19, \mathcal{L} = 1)$ transition [83, 84]. An experimental confirmation of our results would be very interesting.

Scattering calculations for σ_u symmetry continuum states were extended to higher energies. The obtained results are presented in Fig. 2.21. They are compared with those provided by the 2-body Landau potential. Scattering cross sections were calculated up to the energies of the second cross sections minima. At even higher energies scattering cross sections continue to oscillate, having few more minima. It seems confusing, since remembering, the well known theorem of Levinson for scattering phase shifts:

$$\delta(k = \infty) - \delta(k = 0) = \pi n,$$

where n -indicates the number of bound states in the system. Thus by translating this theorem to the scattering cross sections, and expecting the smooth behavior of phase shifts on projectile energy, one obtains, that the number of nodes (for $L=0$ states) in the scattering cross section correspond to the number of existent bound states. However it is not a case here and is due to the hard repulsive core of the potential. I.e. for strongly repulsive potentials phase shifts continue to grow up to rather high energies (compatible with a height of repulsive part) and only then start to decrease. If repulsive part of potential is rather wide phase shifts can become few times larger

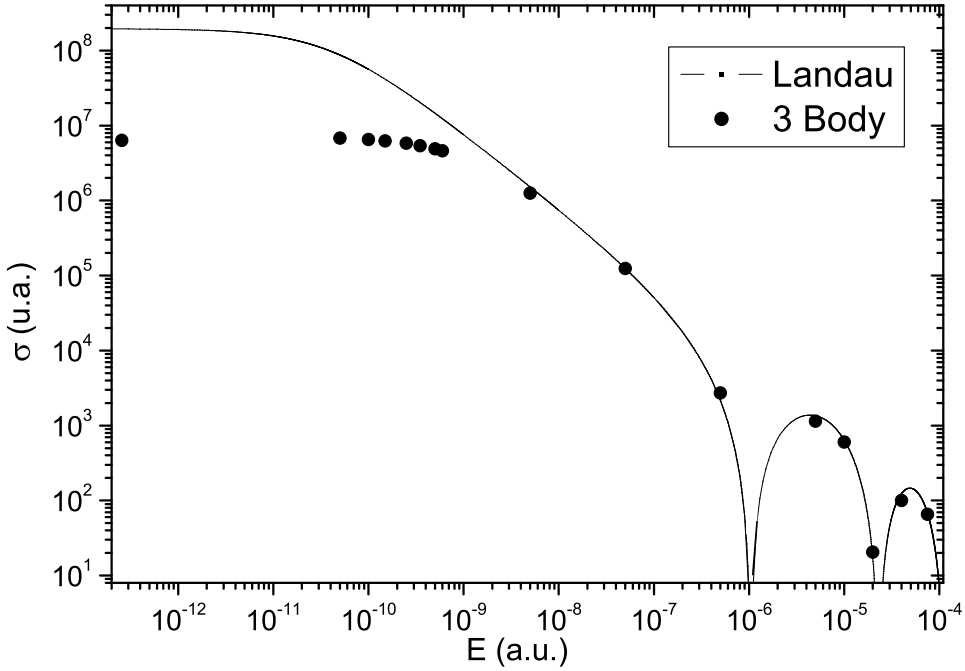


Figure 2.21: p^+ -H elastic scattering cross sections for proton spin triplet (σ_u symmetry states) configurations. 3-body results, obtained by solving Faddeev-Merkuriev equations, are compared with simple Landau potential model. It is worth noticing that Landau potential predictions are rather accurate except for very-low energies, dominated by nearthreshold H_2^+ bound state.

than π before starting to decrease. Therefore total cross section can exhibit several minima, even for repulsive systems without any bound state.

Furthermore, one can observe that apart from the low energies (where scattering is dominated by nearthreshold H_2^+ bound state and therefore is very sensitive to the details of the potential), Landau potential provides very precise results for the elastic cross-sections.

σ_u symmetry resonant states of H_2^+ molecular ion

The pH cross sections were calculated for higher partial waves as well. The principle interest of studying these waves is that they provide the possibility of observing short living resonances. Unfortunately, direct calculations of 3-body resonances are complicated. Using complex plane rotation method [85] one can derive equations similar to the eigenvalue equations of bound state problem, however being in complex algebra. One is then faced to the problem of finding complex eigenvalues of the complex Hamiltonian matrix. However, as it was already noted several times, this matrix is too large to be diagonalized directly. In bound state problem we have avoided direct diagonalization by either searching the largest eigenvalue (Power method), or by being able to provide energy guess value sufficiently close to the searched one (inverse iteration method). For resonant states both these approaches risk to fail: resonances do not correspond to the largest

eigenvalue and furthermore it is not trivial to cover a 2-dimensional plane when trying to provide sufficiently good guess value.

$\mathcal{L} = 3$		$\mathcal{L} = 4$	
E_R (a.u.)	Γ_R (a.u.)	E_R (a.u.)	Γ_R (a.u.)
5.13×10^{-6}	1.61×10^{-6}	1.56×10^{-5}	0.94×10^{-5}

Table 2.7: p^+H resonance energies and widths obtained by using Landau potential.

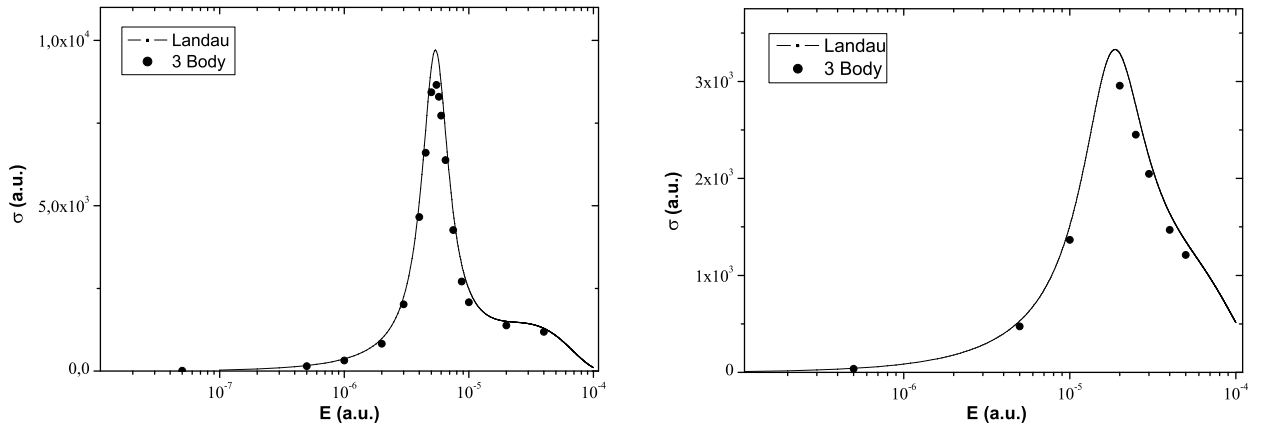


Figure 2.22: Comparison of p^+H scattering cross sections in resonant behavior exhibiting σ_u symmetry states (angular momentum $\mathcal{L} = 3$ results are presented in the figure on the left, whereas figure on the right contains $\mathcal{L} = 4$ results). Points correspond to exact 3-body calculations, whereas line represents 2-body calculations with Landau potential.

However, we have remarked that for non-zero energy scattering, Landau potential provides very good evaluations for 3-body scattering observables. Landau potential results for non-zero angular momentum states should be even more accurate, since these states start contributing in the total cross sections only at higher energies. It does not bring out any difficulty to apply the complex plane rotation method for 2-body Landau potential model. Corresponding matrices are rather small and easy to invert directly.

Two resonances have been found respectively for angular momentum of the system $\mathcal{L} = 3$ and $\mathcal{L} = 4$. Their positions and the widths are given in the Table 2.7. Furthermore we have analyzed the predicted resonance region by calculating elastic scattering phase shifts through Faddeev-Merkuriev equations. Comparison of exact 3-body and Landau potential results is presented in Figure 2.22 [a] and [b]. One can observe an almost perfect agreement. The exact 3-Body resonances still are slightly sharper than those predicted by the effective interaction model.

Finally I present in Fig.2.23 the total scattering cross section for σ_u symmetry states, as obtained with Landau potential. The resonance peaks are clearly visible there. This curve differ from the

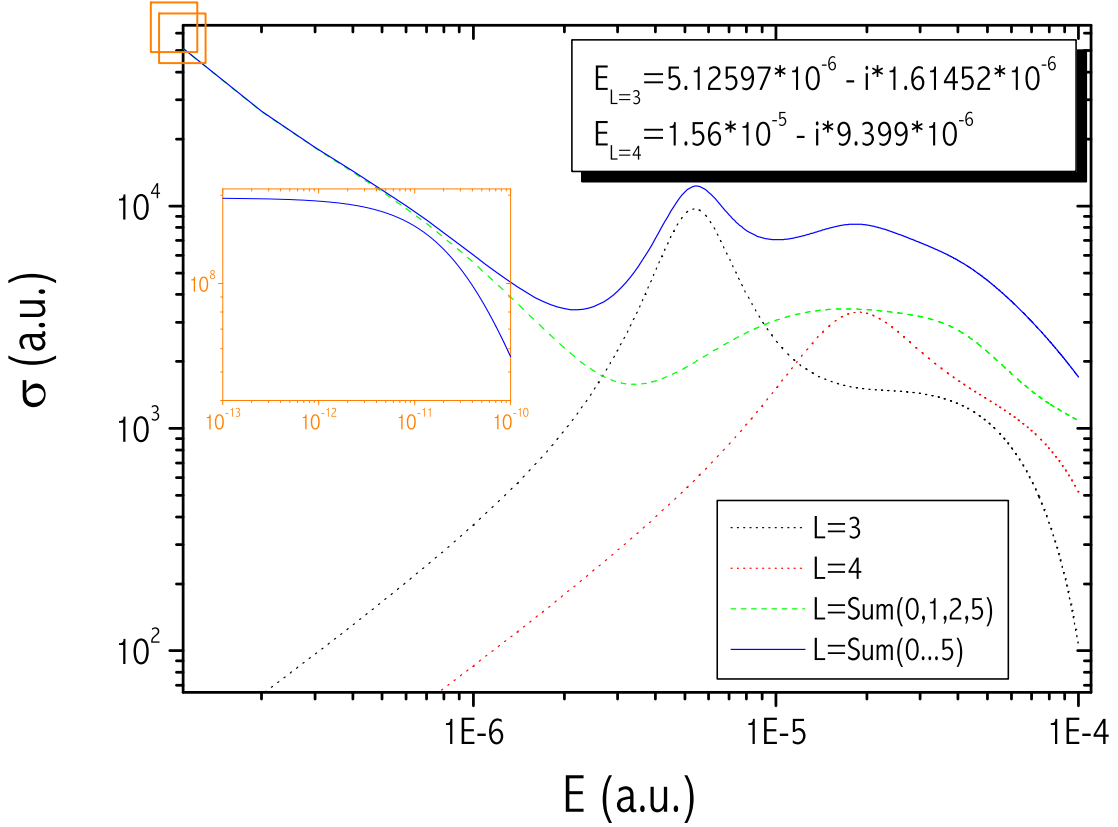


Figure 2.23: Calculated scattering cross sections for the Landau potential. Out of zero-energy region these cross sections coincide with precise 3-Body σ_u symmetry p^+ -H cross sections. Both, $\mathcal{L} = 3$ and $\mathcal{L} = 4$, resonances are visible in total cross sections.

exact results only for very low energies ($E \lesssim 10^{-6}$ a.u.), whereas the resonance region is well reproduced.

One should keep in mind that in experimental setup one usually deals with non-polarized proton beam and non polarized target. Therefore observed p^+ - H scattering cross sections represent an average of two possible proton spin configurations (i.e. one has admixture of σ_u and σ_g states). Nevertheless, the statistical contribution of σ_u states is 3 times larger than the σ_g ones and are therefore dominant. One can thus expect that the above predicted resonant states would be visible even in the total p^+ - H cross sections.

Chapter 3

Clusters of neutrons

3.1 Nucleon-nucleon interaction models

An already long time ago, one succeeded to unveil the mystery of the atomic systems construction. On the contrary, the principal interest in nuclear physics still remains to model the nucleon interaction inside the nucleus. One is not yet able to work out the strong interaction for nuclei constituents: neutrons and protons. Despite the QCD being generally accepted as the underlying theory of the strong interaction, it has not yet been possible to derive the interactions between the hadrons from this fundamental basis. The complexity is due to quark confinement, which makes direct experimental investigation of isolated quarks impossible. Furthermore, the simplest strongly interacting objects which one can investigate experimentally, baryons and mesons, are already rather complex objects. Being non-able to describe rigorously the internal structure of the nucleons, one is constrained to develop less profound and partially phenomenological models, in order to describe the interaction between them.

Many experimental data have been collected in the last 50-60 years, which set up strong constraints on the np and pp interactions. Already at the very beginning of nuclear physics, just after the neutron was discovered by Chadwick [86], Heisenberg suggested that the neutron and the proton can be considered as corresponding states of the same particle [87]: the nucleon. The observations that the strong interaction is very similar for the neutrons and the protons led to the introduction of the concept of isotopic spin [88]. In this formalism the two states are distinguished by their isospin magnetic quantum number. The first modern model of nuclear forces was proposed by Yukawa [89], who assumed that nucleons interact due to the exchange of massive scalar particles (mesons). Within the last, 60 years, the meson-exchange theory of nuclear forces has undergone many developments and improvements. However Yukawa's fundamental idea about meson exchange origin of the nuclear forces is still valid and remains the dominant model for the nuclear interaction.

For further discussion of interaction models one should be familiarized to concepts introduced by Taketani, Nakamura and Sasaki [90]. They suggested that nucleon-nucleon interaction is divided into three regions: a long range part ($r \geq 2 \text{ fm}$), an intermediate region ($1 \text{ fm} \leq r \leq 2 \text{ fm}$) and

a short range or core part $r \leq 1$ fm. Since the nuclear force of Yukawa type due to exchange of particles with the mass m is proportional to

$$V \sim \frac{e^{-mr}}{r}, \quad (3.1)$$

where r denotes the distance between two nucleons, the exchange of the heavier particles are, in general, of shorter range. Therefore, the long range part of the nuclear force is dominated by the exchange of one-pion, while two-pion as well as exchange of heavier mesons become important in the intermediate region. In the core region nucleons are overlapping with each other. So the "classical" meson-exchange picture of the nuclear force is not any more adequate. Furthermore, Taketani and co-workers [91] proposed a phenomenological treatment of the short-range nuclear force, which was commonly agreed as being repulsive. Since, the long-range part of the nuclear interaction due to one-pion exchange became well established. More attention is paid to the intermediate region, by trying to simulate the two-pion and heavier meson exchange contributions. It is not clear whether one can control all these effects. Nevertheless one-boson exchange (OBE) models of the nuclear interaction have been widely accepted. In such models it is assumed that the two- and more-pion exchange can be parameterized in terms of multi-pion resonances.

Relying on the OBE, several 'so-called' realistic potentials were developed to describe the NN interaction. They differ by the operator structure and particle-exchange patterns taken into consideration. All of them are sustained by a fit of more than 15 free parameters and keep as the main purpose, to describe the experimentally available NN scattering data as exactly as possible.

The pioneering model of realistic potentials was constructed by Nijmegen group [92] and is based on the pure one-boson exchange picture. They have also performed a partial-wave analysis (PWA) of all pp and np scattering data [93]. The fit of 15 free parameters permitted *Nijmegen 93* potential to describe NN data with $\chi^2/N_{data} \approx 2$. By introducing some additional free parameters separately in each partial wave, a perfect data description with $\chi^2/N_{data} \approx 1$ was achieved in the Nijmegen I,II potentials [94]. However, the number of free parameters explodes up to about 40. Nijmegen group provides with equivalent momentum and configuration space versions of the potentials. Furthermore there are non-local *Nijm I* and *Nijm 93* potentials, whereas the structure of *Nijm-II* and *Reid-93* potentials is local.

Nijmegen groups work was followed by Paris collaboration [95]. In their potential model, concepts like dispersion relations and field theoretical approaches were introduced to describe the nucleon-nucleon interaction in addition to OBE. In particular, dispersion theory was applied to calculate two-pion exchange contributions in the NN amplitude starting from πN and $\pi\pi$ scattering data. They developed equivalent versions of non-local momentum and configurations space potentials.

One of the most complete works within the meson-exchange models was performed by the Bonn group [96]. They kept the whole Dirac structure of the OBE kernel. Similarly to Nijmegen group, they could describe data set quite well using operator structure of the OBE in *Bonn B* model [97], whereas a perfect fit has only been reached by treating the partial waves independently (*CD-Bonn*

[98]). The last model requires the same amount of about 40 free parameters. Bonn group potentials are defined in momentum space and are strongly non-local.

Realistic potential models of the Argonne group [99, 101] are the most phenomenological. In their potential, only one-pion exchange is explicitly considered, whereas all the remaining contributions were parameterized in a general operator form. Once again, by fitting around 40 adjustable parameters, a quite accurate description of the two-nucleon scattering data with $\chi^2/N_{data} \approx 1.09$ was achieved [100]. Argonne potentials *Av.14* and *Av.18* are local and developed in configuration space.

	3H	3He	4He
Paris[102]	7.46		24.26
Nijm II	7.659	7.008	24.56
Reid. 93	7.636	7.011	
Av.14	7.674	7.053	24.06
Av. 18	7.615	6.917	24.21
CD-Bonn[103][3]	8.013	7.288	26.26
MT I-III	8.535	7.904	29.50
Exp.	8.482	7.718	28.3

Table 3.1: Triton, 3He and α -particle binding energies as predicted by different NN interaction models, compared with experimental values. Results for *CD-Bonn* and *Paris* potentials were borrowed from above indicated references.

All the realistic potentials, mentioned above, currently represent the most successful models to describe the two-nucleon scattering data as well as the deuteron properties in a systematic way. However their success is guaranteed by the large number of fitted parameters, therefore rising doubts on their ability to represent the underlying physical processes. Furthermore, the failure of these OBE models becomes evident when one considers three and more nucleon systems. The simplest three nucleon structure – tritium – is underbound by about 5-10% (see Table 3.1). This seems to be related to the fact that 2-nucleon data, on which all these potential models rely, represent only on-energy-shell physics [24, 104]. Off-energy-shell effects, appearing in reactions with more than two nucleons and in the processes with the external probes, are completely obliterated and seem to be responsible for the difference in tritium binding energies predicted by 2-body phase-equivalent realistic potential models.

It is believed that two additional ingredients – relativistic effects [105] and three-nucleon forces (3NF) – can solve the nucleus underbinding problem. Contribution of 3NF in nuclear Hamiltonians has been considered already 50 years from now [106]. However one should point out that much less is known about their nature compared to the two-body interactions.

At the present time, several models for the three body force are available. Some of them like Fujita-Miyazawa [106] or the Tucson-Melbourne [107] are based on the two-pion exchange with one intermediate Δ excitation. This kind of interaction represents the longest range part of the 3NF. The model proposed by Brazil group [109], pursued with the latest Tucson-Melbourne works

[108], includes in addition $\pi - \rho$ and $\rho - \rho$ exchanges. The Urbana-Argonne group has worked out *Urbana IX (UIX)* 3NF model, which incorporates two-pion exchange graphs completed by a purely phenomenological repulsion [110]. These forces are generally adjusted (typically by fitting values of some required coupling constants and/or cut-off) in conjunction with some two-nucleon force model in order to reproduce the tritium binding energy. However, some low energy 3N scattering observables, as the A_y analyzing power, are not improved in this way [111, 112].

Despite the big success and recognition that OBE models benefited, they face an evident conceptual problem [224, 225]: the charge radius of the proton is $\sqrt{r^2} \approx 0.6$ fm, while the typical size of light mesons is about 0.5 fm. Then the mesons cannot mediate the nuclear force at distances bellow $2 \cdot (0.6 \text{ fm} + 0.5 \text{ fm}) \approx 2.2$ fm. Even if this picture is much simplified and does not account for quantum mechanical effects, it is rather clear that the traditional meson-exchange theory is not adequate to describe the nuclear matter phenomena at distances below 2 fm, when this value is greater than the average distance between the nucleons in the nuclei.

Even disregarding conceptual problems, there are still some uncertainties when determining NN force. Up to 1993, all the potential models supposed the isospin invariance of nuclear interaction. However, two aspects of isospin invariance violation have been noticed:

1. The experimentally well established difference between the np and pp interactions, called charge independence breaking (CIB)
2. The differences in the strong nn and pp interaction, called charge symmetry breaking (CSB). These are less known, due to the impossibility of performing neither direct nn , nor Coulomb-free pp scattering experiments.

The recent indirect measurements of nn [?] scattering lengths provide for 1S_0 state: $a_{nn} = -18.59 \pm 0.40$ fm, whereas the corresponding np value is sensibly different $a_{np} = -23.748 \pm 0.001$ fm. This indicates a sizeable CSB effect. Potential models elaborated after 1993 felt obliged to introduce an isospin breaking, to mimic these experimental findings. However, due to the lack of nn data, one could expect considerable uncertainties in nn potentials.

On the other hand, the difference in the ${}^3\text{He}$ and ${}^3\text{H}$ binding energies predictions, once Coulomb and nucleon mass are corrected, suggests a CSB in the NN force of the order of 2% [117]. Nothing can be said about a CSB in 3NF.

Recent advances in numerical methods permit to calculate the nuclear binding energies up to $A \leq 10$ [4, 5, 6]. Sizeable underbinding of the neutron rich nuclei, obtained by *Av.18* NN interaction model in conjunction with *UIX* three-nucleon force, obliged Urbana-Argonne group to introduce additional isospin dependent terms into their 3NF model. New series of *Illinois* 3NF were developed [4]. These modifications considerably improved the agreement with the experimental results. However, one still confronts increasing difficulty when describing neutron rich nuclei (see Fig. 3.1). These discrepancies can be a consequence of the uncertainties in the nn force.

One should admit that higher nn and pp partial waves are even less controlled. There are no direct experiments on nn scattering and the analysis of low energy pp data is made difficult by

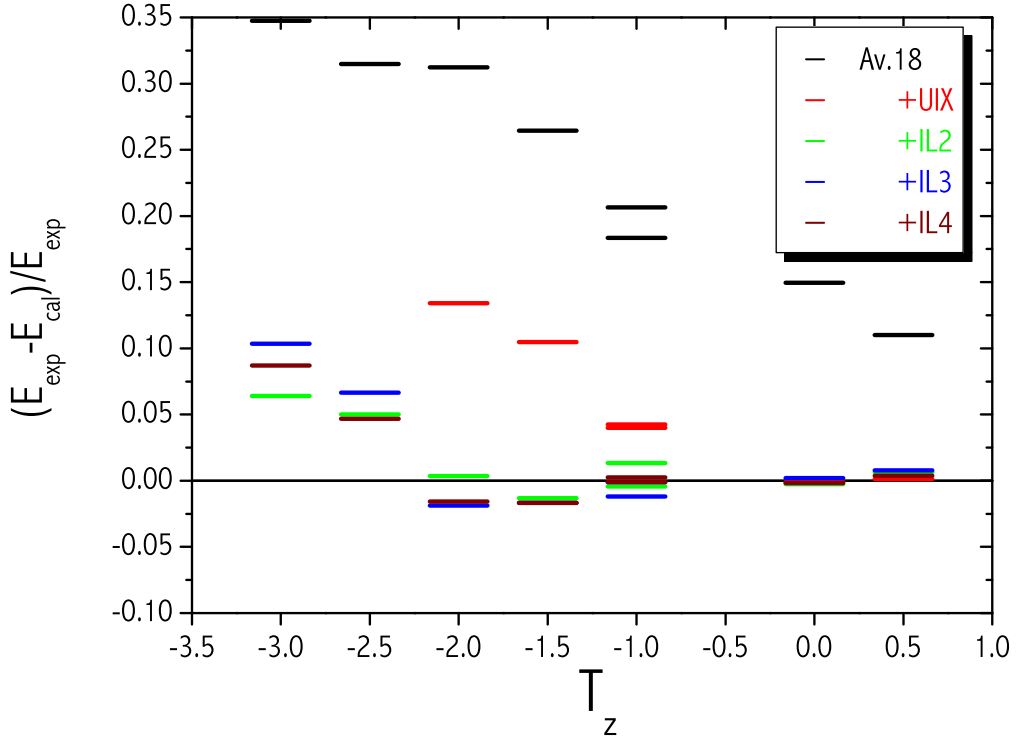


Figure 3.1: Relative discrepancies of binding energy predictions for nuclei of various He isotopes. Data is taken from variational Monte-Carlo calculations of Argonne group [4] [5][6]. Basing on 2N interactions (*Av.18* model) only: one is not able to describe any nucleus beyond $A = 2$, whereas increasing underbinding with growing neutron excess is observed. With aid of *Urbana IX* 3NF one is able to adjust ^3He and ^4He nuclei, however the trend to underbind neutron richer nuclei remains. *Illinois* 3NF was fitted to describe nuclei up to $A = 8$. However the latter model seems to suffer from the same deficiency in describing $A = 9, 10$ nuclei.

the Coulomb effects. The treatment of high energy data, as well as phase shift analysis of higher partial waves, is a piece of art, since in this case the scattering observables result from contribution of very many partial waves.

The discussion of nuclear potential models would not be complete without mentioning the so called 'non-realistic' or 'semi-realistic' potentials. Contrary to realistic ones, these potentials are fully phenomenological. In these models, the physical processes underlying NN interaction were completely ignored. Non-realistic potentials as *ATS3* [118], *Volkov* [119], *MT V*, *MT I-III* [120], were developed to have a simple analytical structure (such as sum of Yukawas or Gaussians). They are usually restricted to a small number of partial waves, that considerably facilitates the calculations. Some of these potentials are averaging interaction over the spins, others like *MT I-III* explicitly distinguishes spin singlet ($\mathfrak{s} = 0$) and spin triplet ($\mathfrak{s} = 1$) states. Furthermore, these potentials lacking spin-orbit and tensor interaction terms conserve separately the total spin

and orbital angular momentum of the system. Consequently, by definition, they are not able to reproduce polarization observables. For the same reason these potentials provide spherically symmetric deuterium wave function, being not able to explain its quadruple momenta. On the other hand, some semi-realistic potentials are very successful in predicting the so-called integrable observables of the system (like binding energies and scattering cross sections) [122, 123, 124]. This is a rather surprising fact, since they contain only a few fitted parameters compared with dozens in their realistic counterparts.

MT I-III is a potential, which form was inspired by the OBE. It contains long-range attractive term corresponding to one massive particle exchange, with the mass slightly smaller than that of the pion. Its short range part is dominated by repulsive term, corresponding to exchange of phenomenological heavy boson, not having any physical analogue. This potential acts only in S -waves and is given as a superposition of two Yukawas, of which coefficients were adjusted in [121]:

$$V(r) = V_r \cdot \frac{\exp(-\mu_r r)}{r} - V_a \cdot \frac{\exp(-\mu_a r)}{r} \quad (3.2)$$

$$\begin{aligned} \text{for the } {}^1S_0 \text{ waves} \quad & V_r = 1438.72 \text{ MeV}\cdot\text{fm} \quad \text{and} \quad V_a = 513.968 \text{ MeV}\cdot\text{fm} \\ \text{for the } {}^3S_1 \text{ waves} \quad & V_r = 1438.72 \text{ MeV}\cdot\text{fm} \quad \text{and} \quad V_a = 626.885 \text{ MeV}\cdot\text{fm} \\ & \mu_a = 1.55 \text{ fm}^{-1} \quad \text{and} \quad \mu_r = 3.11 \text{ fm}^{-1} \end{aligned} \quad (3.3)$$

3.2 On the existence of bound neutron clusters

For a long time, the possible existence of pure neutron nuclei fancied the physicist. One seldom finds a theoretical nuclear physicist who has never considered this question. If confirmed, such nuclei would challenge our understanding of NN interaction, providing invaluable information of the isospin dependence in nuclear forces. This would undoubtedly affect other fields of science, such as astrophysics, by modifying the accepted nucleosynthesis scheme. The possibility of obtaining long-lived neutron nuclei could also have practical applications, since one might then operate with so called "canned neutrons". However, all experimental attempts trying to confirm the existence of the simplest multineutron structures, as 3n or 4n , have failed [125, 126].

A recent experiment performed in GANIL [2] renews the interest in pure neutron systems, claiming their possible existence. GANIL experimentalists mastered the technique of producing and controlling neutron-rich nuclei beams. They have projected a beam of ${}^{14}\text{Be}$ nuclei on lead (Pb) target and have observed neutral recoils in coincidence with Be nuclei (see Fig. 3.2). A few events have been detected exhibiting the characteristic of a multineutron cluster liberated in the ${}^{14}\text{Be}$ reaction, the most promising structure being tetraneutron (a bound state of four neutrons). In this experiment, the detectors were separated from the target by a distance corresponding to recoil runtime of 100 ns or more. Therefore, the recoils of the same breakup event are claimed to be already well separated; this prevents them from being observed by the same detector. As

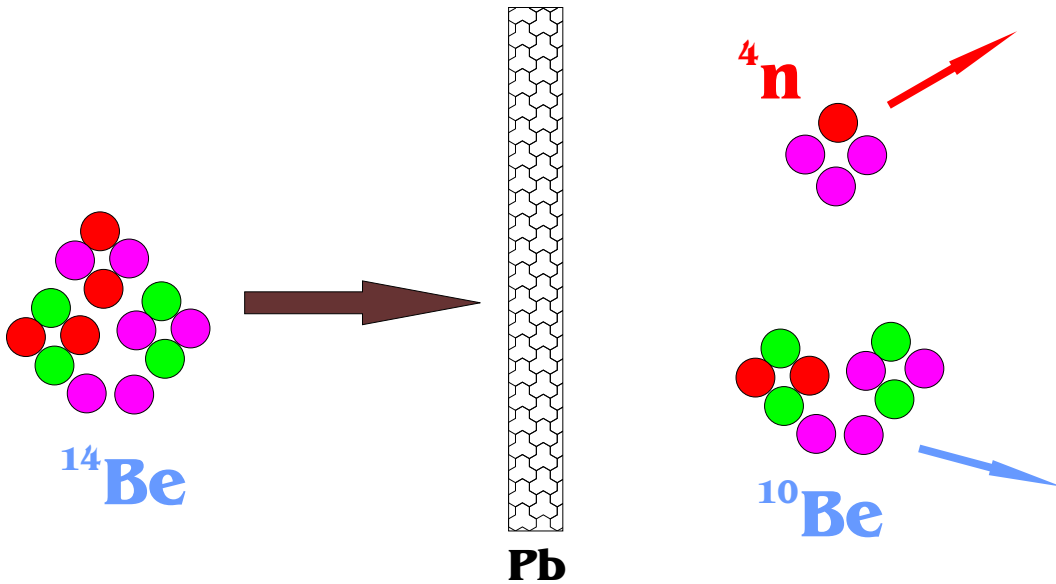
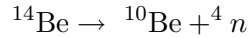


Figure 3.2: The setup of experiment performed by GANIL group [2]. The beam of ^{14}Be nuclei traverse the lead target. Four neutron separation energy is very low in ^{14}Be , thus it is expected that tetraneutron can be formed and released, when ^{14}Be nucleus is scattered by lead (Pb) nuclei of the target. Coincidence of outgoing ^{10}Be nuclei and neutral recoils are observed and analyzed.

indicated in [11] the breakup reaction



represents a privileged channel when searching for a tetraneutron. The ^{10}Be nucleus is strongly bound, whereas the four-neutron separation energy for ^{14}Be is only about 5 MeV. It is known that in an external potential well, neutrons can form drops [127, 4]. Therefore, it is supposed that there is a rather high probability to form tetraneutron like structures inside the ^{14}Be nucleus. During the collision this tetraneutron, being weakly bound to the core nucleus, can be liberated.

In earlier experiments, the tetraneutron was searched by using heavy-ion transfer reactions such as $^7\text{Li}(^{11}\text{B}, {}^{14}\text{O}){}^4n$ [128], $^7\text{Li}(^7\text{Li}, {}^{10}\text{C}){}^4n$ [129] and double exchange reaction ${}^4\text{He}(\pi^-, \pi^+){}^4n$ [130, 131]. However, these reactions should be strongly suppressed by spectroscopic reasons, as well as due to considerably larger decay energies, which leaves little hope for such a fragile structure as tetraneutron to survive. Therefore, a negative outcome in the former experiments could be easily anticipated.

Alternative studies of ${}^3\text{He}(\pi^-, \pi^+)3n$ reaction shows some discrepancies in differential cross sections from what should be expected by a pure phase space description of the final state. The ambitious claims of reference [132], trying to explain the result by the existence of a broad $E = (2 + i * 6)$ MeV three-neutron resonance, were later denied by a more thorough experimental study [133]. The slim indication of a three-nucleon resonance at even larger energies ($E = 20$ MeV) still remains. One can expect that an eventual tetraneutron resonant state would be advantageous due to neutron pairing effect.

3.2.1 What do we know?

It is useful to start by presenting the principle facts at our disposal on pure neutron systems.

- First neutrons are fermions, and therefore their wave functions should be antisymmetric with respect to two neutron exchange. If a two neutron system has relative angular momentum equal to zero (energetically the most favorable state), neutron spins must be antiparallel, which is realized in the 1S_0 state. The experimentally measured negative nn scattering length value in this state indicates that dineutron is not bound.
- The fact that ^6He and ^8He [134]-[137] nuclei are bound, whereas $^7\text{He}(\alpha+^3n)$ is not, testifies that trineutron is, most probably, not bound.
- The stability of ^8He sets an upper limit to the total binding energy of 4n , because decay $^8\text{He} \rightarrow \alpha + ^4n$ does not occur [138]. The most precisely determined mass excess of ^8He [139] yields $B(^4n) \leq 3.1$ MeV. Furthermore, if 4n was bound by more than 1 MeV, the $\alpha + ^4n$ would be the first particle threshold in ^8He . As the breakup of ^8He is dominated by the ^6He channel [140], the tetraneutron, if bound, should be so by less than 1 MeV.
- Thus if bound 4n exists, considering similarity between nn and np interactions, a $\mathcal{T} = 2^1$ state should be found in ^4He at $26 < E < 29$ MeV. Also a $\mathcal{T} = 2$ resonance should occur for $n+^3\text{H}$ scattering at $6 < E_{c.m.} < 9$ MeV. Resonances have been found in $n+^3\text{H}$ (see discussion in the next chapter), but there is no evidence to support a suggestion [141] of $\mathcal{T} = 2$. No low-lying $\mathcal{T} = 2$ ^4He states have been found; systematics give $E(\mathcal{T} = 2) \sim 34$ MeV [142], ≥ 32 MeV [143].

There are numerous theoretical studies on pure neutron systems. However, ideas are not fully settled, principally because of uncertainty when describing the neutron-neutron interaction. There are two principally different ways to tackle the question of bound neutron systems. The first one is the few-body approach, which starts from nn interaction model and checks out the existence of bound neutron systems with increasing complexity. The second one is related to many-body methods: it consists in constructing in-media neutron-neutron potential to conclude about the eventual existence of bound infinite neutron matter. One should remark that a definite answer on the non-existence of infinite neutron matter would impose that the finite size neutron clusters does not exist either. However, the many-body approach suffers from an evident deficiency. It is due to the fact that the nuclear media potentials are density dependent and are determined relying on the nuclear data of well neutron-proton balanced nuclei with steady nuclear densities. In addition, neutron matter, if existent at all, is expected to be unnaturally sparse compared to the stable nuclei. The most neutron asymmetric heavy nuclei have neutron excess of $\eta = (N - Z)/A \sim 0.36$, whereas the stability valley is filled with nuclei having neutron excess of $\eta \sim [0.21 - 0.23]$. Therefore, it is rather clear that the extrapolation of these models to describe neutron matter with $\eta = 1$ is not reliable.

¹ \mathcal{T} is the total isospin quantum number of the system

Most of theoretical few-body calculations on bound pure neutron systems have given negative results. The studies were made by employing various realistic and non-realistic potential models. Varga [144], within the stochastic variational method on a correlated Gaussian basis, has checked for bound tetraneutron with several simple non-realistic NN potentials: *Volkov*, *MT V*, *ATS 3* and *Minnesota*. None of them gave tetraneutron bound. *Volkov* potential is so strong that it binds dineutron, however tetraneutron provided by this potential lies above two dineutron threshold. By using the angular potential functions method with semi-realistic *GPT* and *SSC_B* NN interactions, none of 4n , 6n or 8n systems were found to be bound in [145]. However, the same authors suggested that 0^+ states should be the most favorable. It has been shown in [4], that *Av.18* realistic NN interaction in conjunction with the most recent *Illinois* and *UIX* 3NF models, cannot bind pure neutron systems up to $A = 8$. Furthermore, neutron matter calculations of [127, 146, 147] suggest that even infinite neutron matter can not be bound by the strong interaction.

There were a few theoretical efforts to find 3n and 4n resonances. By using central potential models, no resonances were found neither in 3n nor in 4n [148]. No real tetraneutron resonances was found by Sofianos et al. [149], with *MT I-III* potential model; only some broad subthreshold resonances were discovered. However, realistic interaction models can provide different conclusions. These models contain interactions in \mathcal{P} - and higher partial waves, due to the necessity of antisymmetric wave functions: a crucial point in pure fermion systems.

Glöckle and Witała [150], using realistic potentials, searched for tri-neutron resonances. They claimed that within the current interaction models, trineutron resonances do not exist. However, resonance calculations with realistic potentials drives to some bad numerical instabilities already on the trineutron level. The theoretical research of tetraneutron resonances with realistic potential models is a big challenge and has not been performed yet.

The aim of this study is not to redo or contest the results of mentioned authors, but rather to try to understand the underlaying reasons which prevent pure neutron systems of being bound. Furthermore, we will explore what kind of necessary corrections should be made in the NN interaction to permit the existence of such systems. We will conclude to what extend such modifications can be tolerated within our current understanding of the strong interaction. Unfortunately, at the moment, we are still not able to explore multineutron resonances.

3.3 Borromean effect

The possible existence of bound pure neutron clusters can be formulated in terms of the Boromean² effect in fermionic systems. One can easily check that neutron-neutron interaction supports Bosonic borromean effect. Let us consider for instance a charge dependent (CD) version of *MT I-III* potential (*CD MT I-III*), adjusted to reproduce the experimental value of nn scattering length in ${}^1\mathcal{S}_0$ state. This is achieved by setting the strength of the attractive term in eq. (3.2) equal to $V_a = 509.4$ MeV· fm, i.e. only 1% weaker than in the standard version of this potential. If one

²Borromean effect is well known for the bosons. $N+1$ identical boson system is called borromean when it is bound by pair interactions, nevertheless analogous system of N bosons (or any smaller system) is not.

3n	4n	$({}^3\text{He})_3$	$({}^3\text{He})_4$
0.9423	9.003	not bound	-

Table 3.2: Binding energies for 'fictive trineutron' and tetraneutron, if one permits multineutron system to be described by bosonic wave functions. Results were obtained with *MT I-III* interaction with slightly reduced attractive part, which permits to reproduce experimental 1S_0 nn scattering length.

nn					${}^3\text{He} - {}^3\text{He}$
Nijm II	Reid 93	Av. 14	Av. 18	MT I-III	Aziz
1.0876	1.0872	1.0626	1.0799	1.1011	1.2989

Table 3.3: Enhancement factors needed for nn potentials to bind dineutron in 1S_0 state. These factors are compared to factor needed to bind two He_3 atoms.

permits neutrons to be described by bosonic wave functions: the *CD MT I-III* potential is too weak to bind dineutron, but binds 'bosonic trineutron', whereas 'bosonic tetraneutron' is already bound by more than 9 MeV (see Table 3.2).

However the situation in fermionic systems is completely different, since here Pauli principle results into a strongly repulsive effective interaction. Of course, the requirement for systems wave function to be antisymmetric is important only when particles are close to each other and thus can be overcome if an attractive long range interaction is present. The only long range interaction between two neutrons is due to their spin magnetic momentum coupling. This interaction can be exhibited only when the two neutron spins are parallel and thus the total spin of the system is $s = 1$. However, Pauli principle implies that $\ell + s = 2n$ for two identical fermions, therefore imposing non-zero relative angular momentum and providing an extra kinetic energy. This centrifugal energy is by a few orders stronger than the weak attraction that could be gained by the spin magnetic coupling. Therefore, in order to bind multineutrons, one should completely rely on the strong interaction trying to compensate the Pauli repulsion at short distance.

It is worth noticing that borromean fermion systems exist, governed by short range interactions. One knows that ${}^3\text{He}$ atoms can form liquid drops despite being a fermionic system and despite the striking similarity existent in form of interatomic ${}^3\text{He}-{}^3\text{He}$ and the neutron-neutron potentials (see Fig. 3.3). Recent calculations using Aziz ${}^3\text{He}-{}^3\text{He}$ potential [36], have shown that $({}^3\text{He})_N$ are bound for $N > 35$ [151]. Furthermore, one can see that two neutrons are much closer to be bound, than two ${}^3\text{He}$ atoms. Indeed, the 1S_0 nn potential should be multiplied by an enhancement factor γ of only [1.0626 – 1.1011], depending on interaction model, to bind dineutron. This is to be compared with the value $\gamma = 1.299$ needed in the case of ${}^3\text{He}$ atoms (see Table 3.3). Additionally, as displayed in Table 3.2, bosonic trineutrons and tetraneutrons exist, whereas analogous calculations with Aziz potential give ${}^3\text{He}$ trimers and tetramers unbound. These facts are all in favor of multineutron existence. If these objects turn out to be unbound, one should stretch out the underlying reasons making difference between ${}^3\text{He}$ and neutron multimer structures.

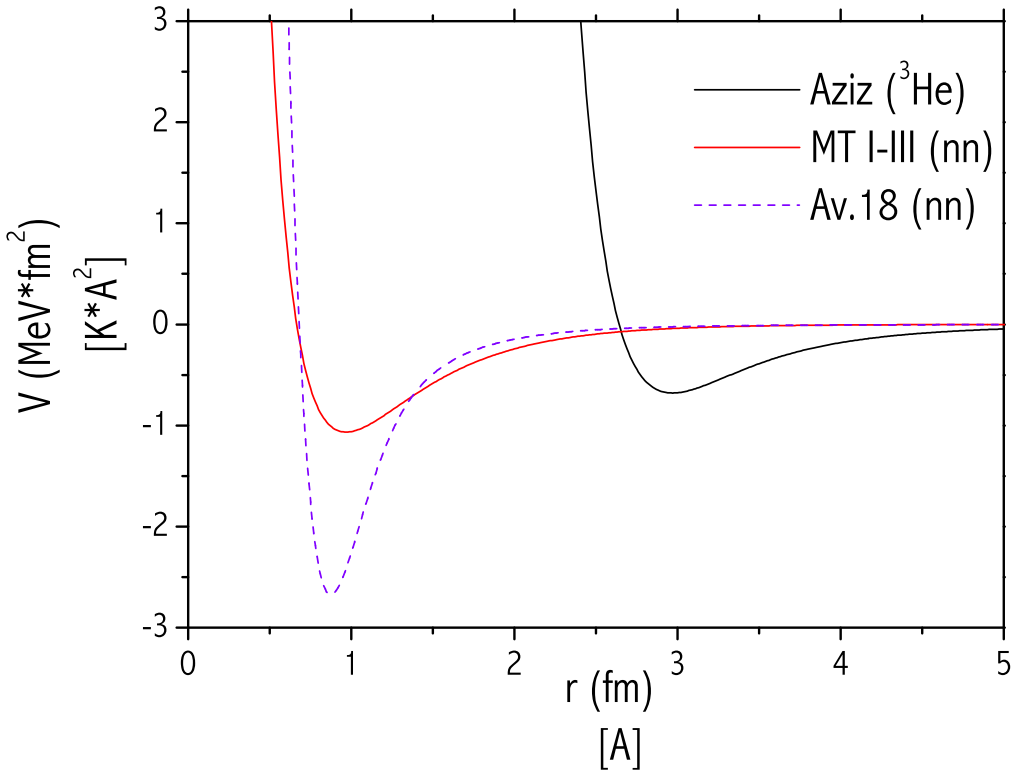


Figure 3.3: Comparison of nn potentials in 1S_0 partial wave. These potentials are compared with Aziz potential between two ${}^3\text{He}$ - ${}^3\text{He}$ atoms (black curve). All the potentials were normalized by multiplying them with a factor $\frac{\hbar^2}{m}$.

One should finally remark the close agreement between the realistic potential models, concerning the nn potential enhancement factor, despite the visible difference in their internal structure (see Fig. 3.3). The smaller value obtained with the *Av.14* potential is due to the fact that this potential is isospin invariant and was fitted to reproduce np scattering length, which is smaller than the nn one. The *CD MT I-III* potential, even adjusted to reproduce nn scattering length, gives slightly larger enhancement factor value. It is determined by the long range part of this potential, which does not have one pion exchange tail. Former facts indicate that the nn 1S_0 partial waves are well controlled by only two ingredients: the experimentally measured nn scattering length and the long range part of the potential, provided by the widely accepted one pion exchange model. Eventual modifications in this partial wave in favor to bind multineutron can be hardly justified.

3.4 Some results

In previous section, we have seen that dineutron is very close of being bound. It would be interesting to know how much one should enhance nn potential to bind even larger neutron structures: trineutron and tetraneutron. In addition, we would like to find out the most favorable quantum states for these systems. This question is far from being obvious. In the stable, well neutron-proton balanced, nuclei, protons and neutrons mingle among themselves by mostly profiting the 1S_0 -wave interaction. Therefore the most favorable states are those for which the nucleus exhibits the highest spatial symmetry. Consequently, the positive parity states with small total angular momentum \mathcal{J} are predominant. In pure neutron systems, due to Pauli principle, many particle pairs must be projected into higher angular momentum states and therefore it is not clear whether or not the positive parity and low angular momentum states remain the most promising.

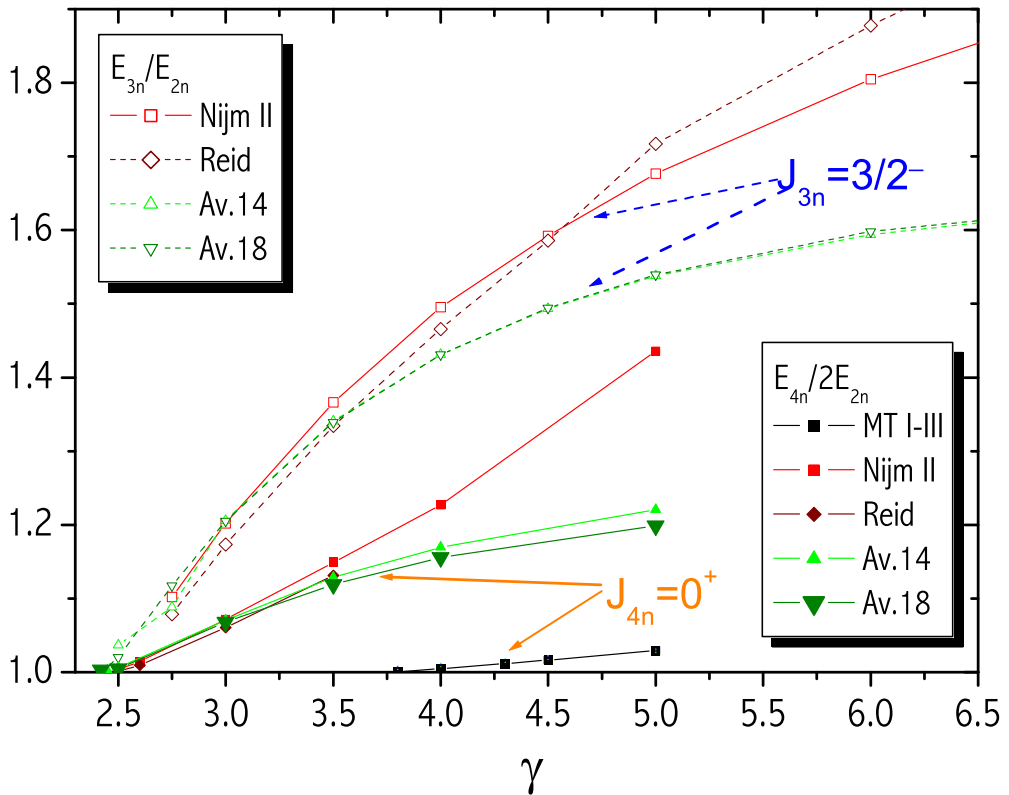


Figure 3.4: Development of relative(compared to dissociation threshold) binding energies of 'fictive trineutron and tetraneutron' with potential enhancement factor. Dependencies for the most favorable states are presented: 0^+ for 4n and $\frac{3}{2}^-$ for 3n .

We have performed calculations using four different realistic nn potential models: *Av.14*, *Av.18*, *Nijm II* and *Reid 93*, as well as the phenomenological *CD MT I-III*. None of these potentials was

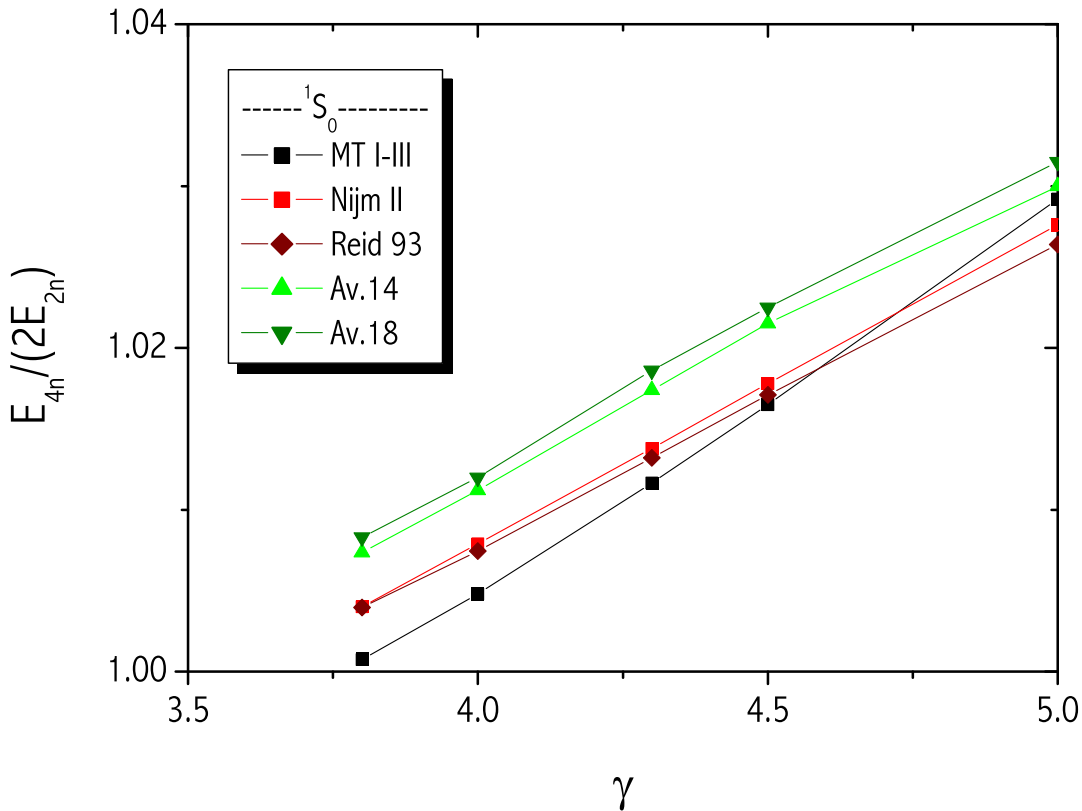


Figure 3.5: Development of relative binding energy of 'fictive tetraneutron' (energy of tetraneutron is divided by double binding energy of dineutron) with enhancement factor. In these calculations restriction was made to interactions in S -waves only. One can see that results of realistic potentials become much closer to those obtained by *MT I-III*, as when interaction in all partial waves is considered (critical enhancement factor grows from ~ 2.4 to ~ 3.6).

able to bind trineutron or tetraneutron for enhancement factors smaller than the required critical values binding dineutron, which are summarized in Table 3.3.

By increasing further the nn enhancement factors we have searched for trineutron states lying below dineutron breakup threshold. Alternatively, 'fictive tetraneutron' should have binding energy twice as large as dineutron one to be 'particle decay stable'. A summary of our results is presented in Fig. 3.4 and Table 3.4. One should first remark that, independently of the potential model we used, 4n system appears almost for the same enhancements as 3n . Nevertheless 4n is slightly more favorable than 3n , although its binding energy stays very close to the two-dineutron threshold. This indicates the dominance of two-dineutron configurations in it.

The most energetically favorable state in 3n system is $\frac{3}{2}^-$. For *CD MT I-III* potential, which conserves separately the orbital angular momentum (\mathcal{L}) and the total spin of the system (S), this state is degenerate with $\frac{1}{2}^-$, both of them being realized with $\mathcal{L} = 1$ and $S = \frac{1}{2}$. The $\frac{1}{2}^+$ and $\frac{3}{2}^+$ states are much less favorable, since here Pauli principle plays a major role by suppressing

		<i>Reid 93</i>	<i>Nijm II</i>	<i>Av.14</i>	<i>Av.18</i>	<i>MT I – III</i>
3n	γ	2.49	2.47	2.41	2.44	4.29
	E_{Th} (MeV)	21.48	21.59	22.66	23.54	45.45
4n	γ	2.44	2.43	2.38	2.38	3.57
	E_{Th} (MeV)	40.36	41.04	43.57	43.50	61.34

Table 3.4: Critical values of enhancement factors for different potential models needed to bind trineutron and tetraneutrons. In addition critical threshold energies are given. Hence, these factors are extremely large, whereas threshold energies are far from that is 'reasonable'.

configuration with $\ell_x = \ell_y = 0$ in the total wave function (the reader is reminded that angular momenta ℓ_x , ℓ_y are associated to 3-body Jacobi variables). Corresponding wave functions are composed of states with $\ell_x + \ell_y \geq 2$ and possess large kinetic energies. The dominance of the $\frac{3}{2}^-$ state compared to $\frac{1}{2}^-$, when realistic interactions intervene, is determined by the presence of attractive tensor force in ${}^3P_2 - {}^3F_2$ channel.

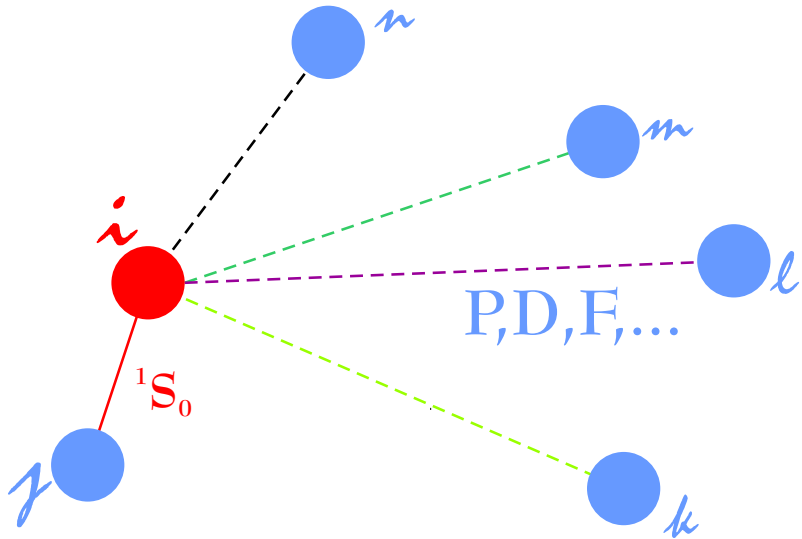


Figure 3.6: The schematic picture of NN interactions in multineutron system. There can exist only one pair interaction in 1S_0 partial wave for a considered neutron (i).

In 4n system, the most favorable state is 0^+ . nn potential is not sufficiently attractive to compensate centrifugal energy, therefore trying to have the smallest possible angular momentum. The major part of potential energy still comes from the nn pairs interacting in 1S_0 waves as well as from dineutron configurations. One should remark that all the realistic models provide very similar results and that a striking difference exists with $CD\ MT\ I-III$ calculations. Realistic potentials need sensibly smaller enhancement factors to bind 4n or 3n than $CD\ MT\ I-III$. This effect can be easily explained. $CD\ MT\ I-III$ potential acts only in S -waves. When higher partial waves are switched off for the realistic potentials, one obtains very similar results to those of $CD\ MT\ I-III$ (see Fig. 3.5). Qualitatively, this can be explained in the shell model language. Let us consider

– see Fig. 3.6 – one particular neutron i . Due to the antisymmetry of the total wave function, this neutron can have only one partner interacting within 1S_0 wave. Other neutrons (relatively to neutron i) should be projected into higher angular momentum states. Therefore, in case of S -wave potentials, other neutrons (k, l, m, \dots) do not contribute in binding neutrons i or j . This fact makes interactions in higher partial waves very important in pure fermionic systems, contrary to bosonic systems, which are dominated by interaction in S -waves. Furthermore, each time one adds a neutron to neutrons i and j , which are originally in 1S_0 state, the average kinetic energy per particle will grow (since one makes system more condense³). If attraction can be gained only in S -waves, no new potential terms with neutrons i and j will be created, thus giving a negative balance. Therefore, uniform fermionic system cannot be bound with only S -wave interactions and with the difermion system being unbound. One can deduct that potential models acting only in S -waves, such like *MT I-III*, exclude the very existence of bound multineutrons.

One should finally remark that the enhancement factors needed to bind multineutron are abnormally high (see Table 3.4). In order to bind tetraneutron, one has to enhance potential with factors as large as ~ 2.4 , compared to the decent $\sim 6\%$ enhancement needed in dineutron. The tetraneutron, forced in such a way, represents rather two weakly bound dineutrons than a qualitatively new four particle structure. Since trineutron and tetraneutron need almost the same enhancement factors to be formed, the same phenomenon should be expected for larger neutron systems. This excludes the eventual multineutron existence in the framework of NN interactions, at least in their present form.

In conclusion, we have seen that nn 1S_0 waves are very important, that they are almost able to bind dineutron on them own and are the principal ingredient in binding multineutrons. Nevertheless multineutron properties are marginally dependent on the particular form this potential can take, once nn scattering length and potential range are fixed. Therefore one should rely on secondary effects to make difference of binding multineutron, when dineutron is not bound. Two different effects can be explored:

- Modified interaction in \mathcal{P} and higher partial waves. These nn waves are much less constrained by the experiment. Their form is determined by analyzing pp scattering data, of which low energy behavior is hidden by Coulomb effects. Whereas one can expect in addition visible CSB (Isospin breaking effects).
- One can try to provide some binding through many nucleon force (three nucleon force (3NF), four nucleon force (4NF),...). These forces are purely phenomenological and cannot be controlled directly by the experiment. Recent many body calculations show that *UIX*, and even more recent *Illinois*, 3NF models rather systematically underbind the rich in neutrons nuclei.

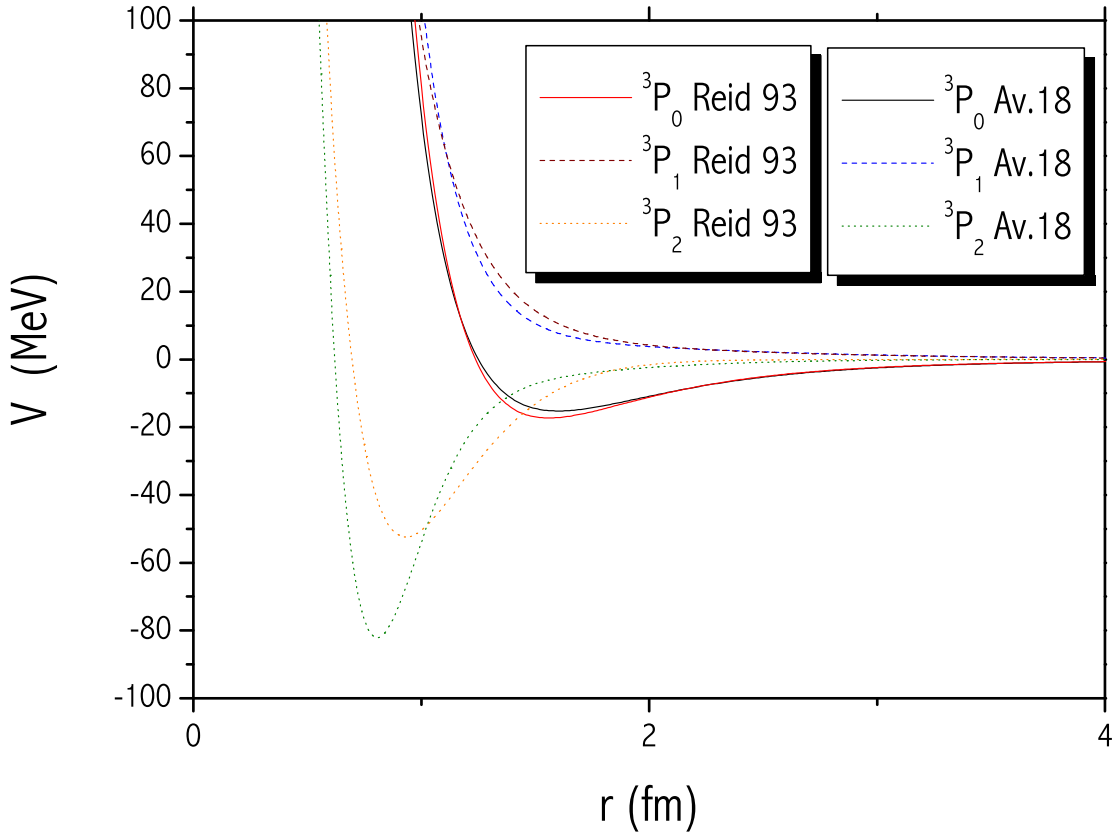


Figure 3.7: Comparison of \mathcal{P} -waves for realistic nn interaction potentials *Reid 93* and *Av.18*.

3.4.1 Importance of \mathcal{P} -waves

The systematics of \mathcal{P} -waves in nuclear systems is a very fragile task. The description of NN scattering data requires a very repulsive $^3\mathcal{P}_1$ wave, whereas tensor force coupled $^3\mathcal{P}_2-^3\mathcal{F}_2$ channel is very attractive (see Fig. 3.7). $^3\mathcal{P}_0$ potential is repulsive at the origin, whereas has some weak attractive well at long internuclear distances. This well does not coincide neither with the attractive part of $^3\mathcal{P}_2-^3\mathcal{F}_2$ channel nor with $^1\mathcal{S}_0$ and it is therefore of minor importance when constructing nuclear systems. All \mathcal{P} -waves added together compensate each other. As a result, they are 'hidden' in the standard nuclei but can provide unexpected effects in asymmetric (exotic) systems due to nontrivial compensations.

We have tried to boost the 3n and 4n binding by modifying only \mathcal{P} -waves. By enhancing all \mathcal{P} -waves with the same enhancement factor, we have not been able to bind any of trineutron or tetraneutron states, without first binding dineutron in $^3\mathcal{P}_2-^3\mathcal{F}_2$ channel. Binding dineutron in \mathcal{P} -waves goes too far beyond the reality of nuclear structure, since one needs enormously large

³Semiclassically, due to Pauli principle, neutron j and i should be provided additional kinetic energy, since they are forced to travel around the added neutron.

	Nijm II	Reid. 93	Av.14	Av.18
$^2n(1^-)$	3.89	4.00	4.29	4.39
$^3n(\frac{3}{2}^-)$	3.61	3.74	3.86	3.98
$^4n(0^+)$	—			3.97
$^4n(2^+)$	3.48			3.78
$^4n(2^-)$				3.93

Table 3.5: Critical enhancement factors for ${}^3\mathcal{P}_2 - {}^3\mathcal{F}_2$ channel needed to bind multineutrons.

enhancement factors in ${}^3\mathcal{P}_2 - {}^3\mathcal{F}_2$ channel (see Table 3.5), making the interaction in these waves considerably stronger than the one in 1S_0 .

The next step consist in trying to enhance only one of \mathcal{P} channels, whereas keeping their natural strengths for the other ones. The ${}^3\mathcal{P}_1$ channel is purely repulsive and the enhancement of this wave could not give any positive effect. The enhancement of ${}^3\mathcal{P}_0$ gave null result as well: dineutron was always bound before any of 3n or 4n states could be formed. By enhancing ${}^3\mathcal{P}_2 - {}^3\mathcal{F}_2$ channel we managed to bind 3n only in $\frac{3}{2}^-$ state, without first binding dineutron. Using enhanced *Av.18* interaction, 4n can be bound in 0^+ , 2^+ and 2^- states, without binding 2n or 3n . The most favorable tetraneutron state becomes 2^+ , whereas 0^+ state is very close to trineutron $j^{\Pi}=\frac{3}{2}^-$ threshold and overshoots it when other potential models are used. All other 4n states lie above trineutron $\frac{3}{2}^-$ threshold. One should remark that all the four realistic NN potential models that we have considered, provide qualitatively identical results.

Please quote that the enhancement factors, for which these states become bound, are extremely large and still very close to those needed to bind two neutrons in ${}^3\mathcal{P}_2 - {}^3\mathcal{F}_2$ channel. No significant reduction is gained for these factors, when passing from trineutron to tetraneutron, thus indicating that even very large neutron systems would require considerably enhanced ${}^3\mathcal{P}_2 - {}^3\mathcal{F}_2$ waves to be bound. Moreover, once multineutron is bound, its binding energy grows very fast with the enhancement factor (see Fig. 3.8). This is due to the non-physical structure of such a system. Multineutron is formed only when sufficiently deep attractive well is created in \mathcal{P} -waves, making them much stronger than the effective centrifugal term and therefore being almost able to bind dineutron on its own. Furthermore, this potential well is realized at internuclear distances smaller than 1 fm. In order to bind multineutron, in the first place all neutrons should be placed very close to each other. Once this is realized, small change in the potential has an enormous effect on the binding energy. In other words, the construction of multineutron goes the very unnatural way: the enhanced potential resist Pauli repulsion at short distances, without trying to overcome it in the periphery. Such a behavior, if one tries to realize multineutron in a similar manner, will lead to condensate the neutron matter beyond the standard nuclear densities. It would undoubtedly affect the other neutron-rich nuclei as 4H or 5He , which will be strongly overbound. For example, with a critical enhancement factor $\gamma = 3.78$ in the ${}^3\mathcal{P}_2 - {}^3\mathcal{F}_2$ waves of *Av.18* potential one obtains an 4H nucleus bound by $B = 46$ MeV⁴ in the $J^{\Pi} = 1^+$ state. Furthermore, such modifications will affect

⁴Experimentally 4H nucleus is not bound, it only has a few resonant states above 3H threshold (E=-8.482 MeV).

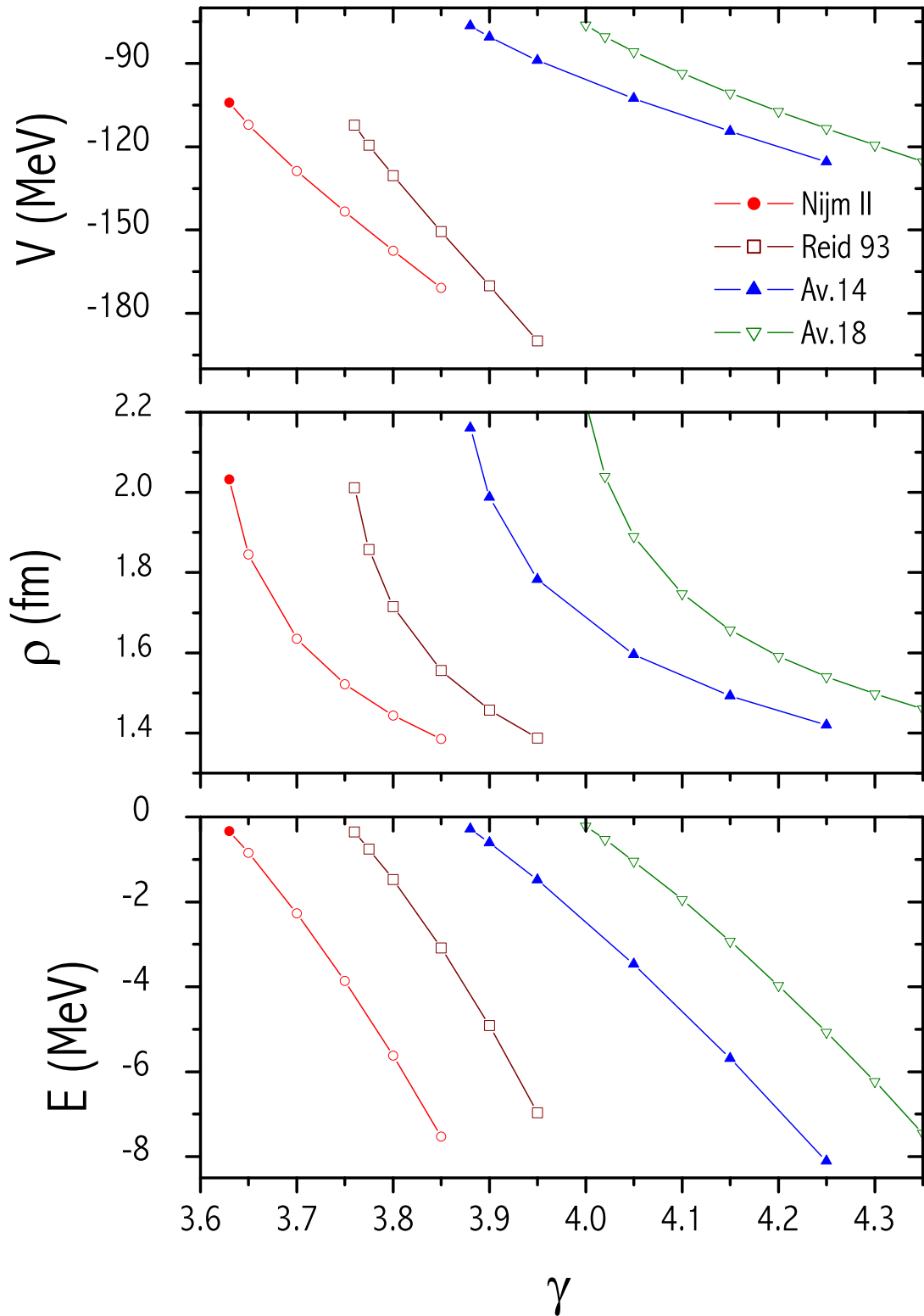


Figure 3.8: Development of binding energy (E), root mean square radius ($\rho = \sqrt{x^2 + y^2}$) and average potential energy (V) for 'fictive trineutron' bound in $j^{\Pi} = \frac{3}{2}^-$ state with enhanced ${}^3\mathcal{P}_2 - {}^3\mathcal{F}_2$ interaction channel by the factor γ .

NN	$B_{^3H}$ (MeV)	$B_{^3He}$ (MeV)
<i>Nijm II</i>	8.545	7.867
<i>Av.18</i>	8.669	7.858
<i>Av.18+UIX</i>	9.765	8.913

Table 3.6: Triton binding energies obtained with critically enhanced NN interaction in ${}^3P_2 - {}^3F_2$ channel to bind tetraneutron.

the nuclear level structure in favor of P -shell nuclei. The former facts clearly show that it is not possible to bind multineutron by modifying \mathcal{P} -waves interaction and without severely disrupting other nuclear properties at the same time.

Rather surprisingly, such dramatic changes in \mathcal{P} -waves do not affect too much the binding energy of tritium and/or 3He (see Table 3.6). Anyway, one should not hold illusions concerning the validity of such modifications: their small effect on tritium binding energy is simply due to the fact that pair configurations in ${}^3P_2 - {}^3F_2$ waves are marginally important. This system requires positive parity configurations, in special the ${}^3S_1 - {}^3D_1$ channel, which request considerably smaller centrifugal energy to be realized.

Nevertheless the possibility of slim modifications in \mathcal{P} -waves should still be explored. Especially, when trying to remove discrepancies in describing the real nuclear systems, such as the $n + {}^3H$ resonance at $E_{cm} = 3$ MeV. Furthermore such modifications can possibly improve the description of neutron-rich nuclei, thus permitting to reduce isospin violation effect in 3NF [4].

3.4.2 Many nucleon force

Finally, one more field of investigation is based on the fact that little is known about the presence and the structure of many nucleon forces (3NF, 4NF). As mentioned above, one needs to modify these forces in favor to supply the additional attraction needed to reproduce the binding energies of neutron-rich nuclei. The 3NF, which is the most explored - namely *UIX*- systematically gives small repulsive effect for multineutron systems and therefore was intentionally neglected in the calculations presented in previous sections.

UIX force consists of two parts. The first one ($O_{ijk}^{2\pi}$) is entirely due to the Δ resonance excitation produced by pion exchange coupling among three nucleons (see diagram [a] in Fig. 3.9). This term is spin-isospin dependent and is very attractive in neutron-proton balanced nuclei, leading to significant overbinding and to the high equilibrium density of nuclear matter. One is thus obliged to add a purely phenomenological repulsive spin-isospin independent potential term (O_{ijk}^R), which is designed to approximate all the other effects contributing in 3NF. *UIX* force reads (its explicit form and discussion of practical implementation are given in Appendix G.2):

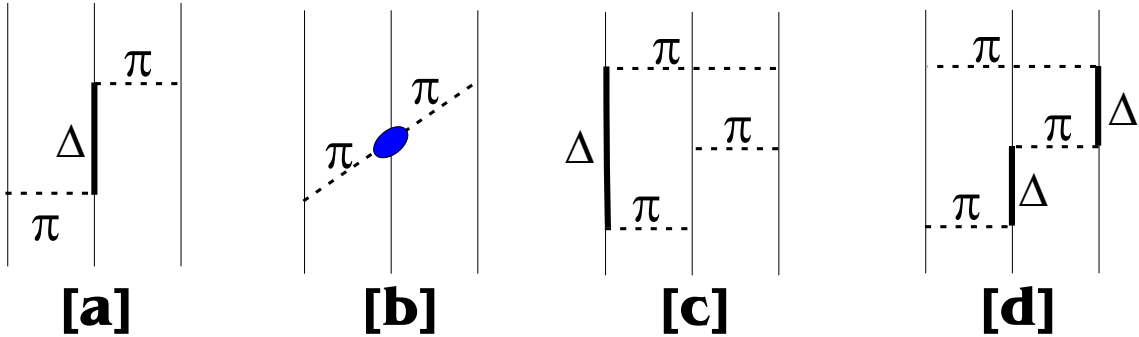


Figure 3.9: Some pion exchange diagrams contributing in 3NF through Δ resonance excitations: a) Fujita-Miyazawa, b) two pion S -wave, c) and d) represent three-pion rings.

$$V_{ijk} = A_{2\pi} \cdot O_{ijk}^{2\pi} + U_0 \cdot O_{ijk}^R \quad (3.4)$$

$$O_{ijk}^{2\pi} = \sum_{cyc} \left(\{X_{ij}, X_{jk}\} \{\tau_i \cdot \tau_j, \tau_j \cdot \tau_k\} + \frac{1}{4} [X_{ij}, X_{jk}] [\tau_i \cdot \tau_j, \tau_j \cdot \tau_k] \right) \quad (3.5)$$

$$O_{ijk}^R = \sum_{cyc} T^2 (m_\pi r_{ij}) T^2 (m_\pi r_{jk}) \quad (3.6)$$

It turns out that in pure neutron systems, due to non-existence of neutral charge Δ resonance, the first (Fujita-Miyazawa) term in eq. (3.4) can contribute only in a second order and therefore becomes very feeble. Therefore, the major contribution in 3NF comes from the repulsive phenomenological isospin independent term O_{ijk}^R . There are however many other diagrams contributing to 3NF, which should have constructive effect in pure neutron systems (ex. [c]-[d] Fig. 3.9) as well as contributions coming from the other meson exchange [223].

j^Π	$\frac{1}{2}^+$	$\frac{3}{2}^+$	$\frac{1}{2}^-$	$\frac{3}{2}^-$	$\frac{5}{2}^-$
$U_C; MeV$	-0.0829	-0.0827	-0.0837	-0.0481	-0.0809
$\langle T \rangle; MeV$	757	768	444	304	1052
$\langle V_{NN} \rangle; MeV$	355	620	497	33	286
$\langle V_{3NF} \rangle; MeV$	-1112	-1387	-941	-337	-1339
$\sqrt{\langle \rho^2 \rangle}; fm$	0.566	0.527	0.743	0.902	0.510

Table 3.7: Characteristic of critically bound trineutrons obtained by changing the strength U_C of phenomenological term of UIX 3NF. Average values of kinetic $\langle T \rangle$, 2NF $\langle V_{NN} \rangle$ and 3NF $\langle V_{3NF} \rangle$ potential energies, as well as root mean square radius $\sqrt{\langle \rho^2 \rangle}$ are given.

We have tried to modify the strength U_0 (its original value is $U_0 = 0.0048 MeV$) of the phenomenological part of 3NF in order to provide the attraction lacking in neutron systems. Since this potential term is repulsive, $U_0 > 0$, one firstly needs in artificial way to make it attractive by changing its sign. This is however still not enough to bind either 3n or 4n . One needs further dramatically reduce this coefficient to make trineutron bound (see 3.7). The effect of changing 3NF

is somehow similar to that of modifying \mathcal{P} -waves and is even more pronounced. Once trineutron is bound, any change in 3NF gives an enormous effect on the binding energy. It appears that trineutron is bound only when the root mean square radius of the system becomes smaller than 1 fm, whereas in tritium it is ~ 1.8 fm. The kinetic energy of such a system is at least twice as large as in the 'fictive trineutron', formed by enhancing \mathcal{P} -waves. Furthermore the attractive contribution in potential energy comes from modified 3NF only: NN forces act even destructively! Tetraneutron calculations with so severely modified 3NF is numerically very unstable and therefore has not been performed. It was nevertheless remarked that in order to make 4n bound these interactions should be almost as much modified as in trineutron case. It is clear that such a structure has no physical meaning. Indeed, if one supposes multineutron existent, it should expected to be a very sparse and weakly bound system in which neutrons are very slow. In addition, and contrary to modifications of \mathcal{P} -waves, such drastic 3NF changes have very large impact on the binding energies of tritium, ^3He or α -particle. Using a critical value $U_C = -0.0481$ MeV of the most favorable trineutron state $j^{\Pi} = \frac{3}{2}^-$, one gets tritium bound by ~ 211 MeV!!! Of course, one can always pledge very strong CIB in 3NF, in order to avoid modifications in the tritium or α -particle. However such dramatic changes in 3NF can not be tolerated neither by the nuclear force underlying theory, neither with respect to binding energies of the other stable neutron-rich nuclei (these nuclei will be found strongly overbound).

The extremely small sensibility of multineutron to 3NF is determined by the fact that these forces are of very short range, whereas to be efficient they need configurations when three neutrons gets very close to each other. Due to the Pauli principle, three neutrons can be put together only when non zero angular momentum pairs are present. Such pairs can be realized in the restrained space only in conjunction with large kinetic energies, much larger than that could be provided by 3NF.

We have therefore tried to increase the range of the 3NF, still staying within that is more or less 'reasonable': being a few times larger than the pion-range. However these modifications could not moderate trineutron results neither. Since the phenomenological (repulsive) term of UIX for neutron systems is much stronger than the attractive one, corresponding to 2π exchange, one cannot bind any neutron system by only modifying the range of the 3NF potentials. By removing repulsive term (setting $U_0 = 0$) one has still to increase the potential range up to $m_\pi = 87$ MeV in order to bind trineutron in $j^{\Pi} = \frac{3}{2}^-$ state. However such trineutron, like in the case of modified strength of 3NF, is very dense, has kinetic energy as large as $\langle T \rangle = 300$ MeV and suffers from repulsive contribution in NN potential $\langle V_{NN} \rangle = 20$ MeV.

By making the phenomenological potential slightly repulsive $U_0 = 10^{-4}$ and by further increasing the potential range to $m_\pi = 74$ MeV we have forced 2NF and 3NF to act constructively. However, even in this way, the obtained trineutron had very large kinetic energy $\langle T \rangle = 200$ MeV and still the principal binding coming from 3NF.

Finally, we have made calculations by introducing hyperradial force, of Yukawa type:

$$V = W \frac{e^{-\rho/\rho_0}}{\rho}, \quad (3.7)$$

where ρ is hyperradius - a quantity invariant in Jacobi coordinate transformations and is expressed as:

$$\rho_{3n} = \sqrt{x^2 + y^2}; \quad \rho_{4n} = \sqrt{x^2 + y^2 + z^2}. \quad (3.8)$$

Such kind of three- and/or four-body force is easy to treat in the numerical calculations. It permits to compare its contribution in conjunction with different NN interaction models. As it was the case for the modified *UIX* model, the most promising states susceptible to this force were found to be $j^\Pi = \frac{3}{2}^-$ for 3n system and $j^\Pi = 0^+$ for 4n . In performing trineutron calculations, we have chosen $\rho_0 = 2$ fm, which roughly corresponds to an exchange particle two times less massive than a pion!! Still, in order to make trineutron bound one needed a potential strength $W > 410$ MeV·fm (see Fig 3.10), i.e. a strength compatible with the attractive part of *MT I-III* potential!!! Different realistic potential model predictions gave similar results, when *MT I-III* required even stronger W values.

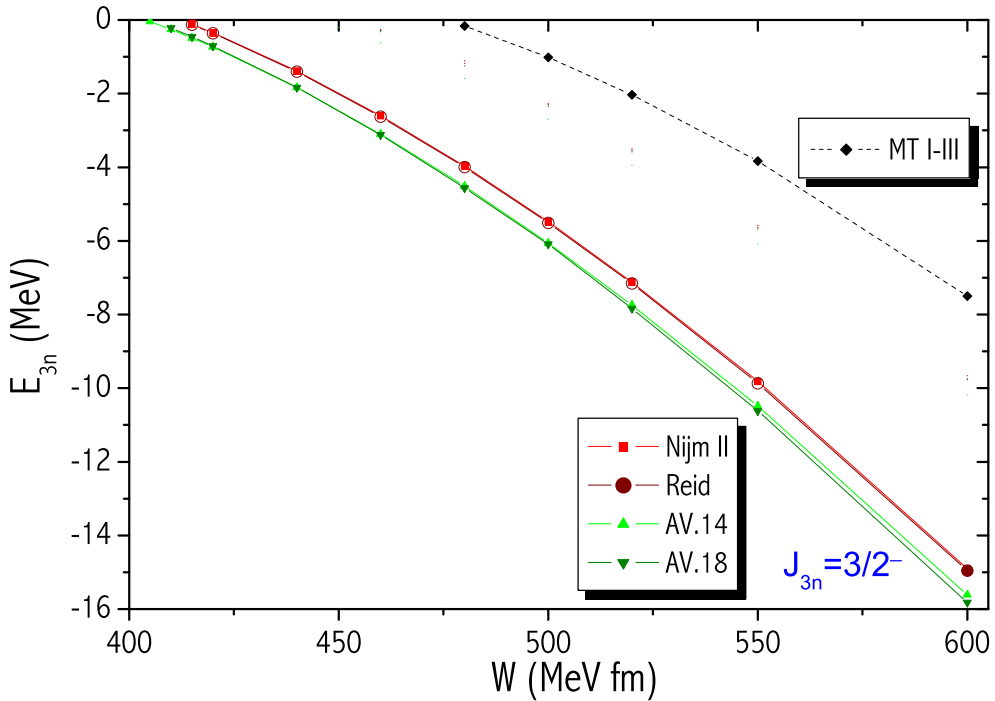


Figure 3.10: Tetraneutron bound using different NN interaction models in conjunction with hyperradial Yukawa type force eq. (3.7), length of which was fixed to $\rho_0 = 2$ fm, whereas its strength W varied.

Tetraneutron case is not any better. In this study, the potential strength value has been fixed to $W = -612.4$ MeV·fm and the evolution of its biding energy as a function of the potential range ρ_0 has been studied. It turns that this range should be increased up to as much as $\rho_0 = 2.32$ fm to make tetraneutron bound (see Fig 3.11). Such a strong force will make α -particle overbound to 78

MeV, whereas in order to compensate the underbinding produced by the realistic NN interaction models, an hyperradial force with $W \simeq 90$ MeV·fm is sufficient (see Fig 3.12).

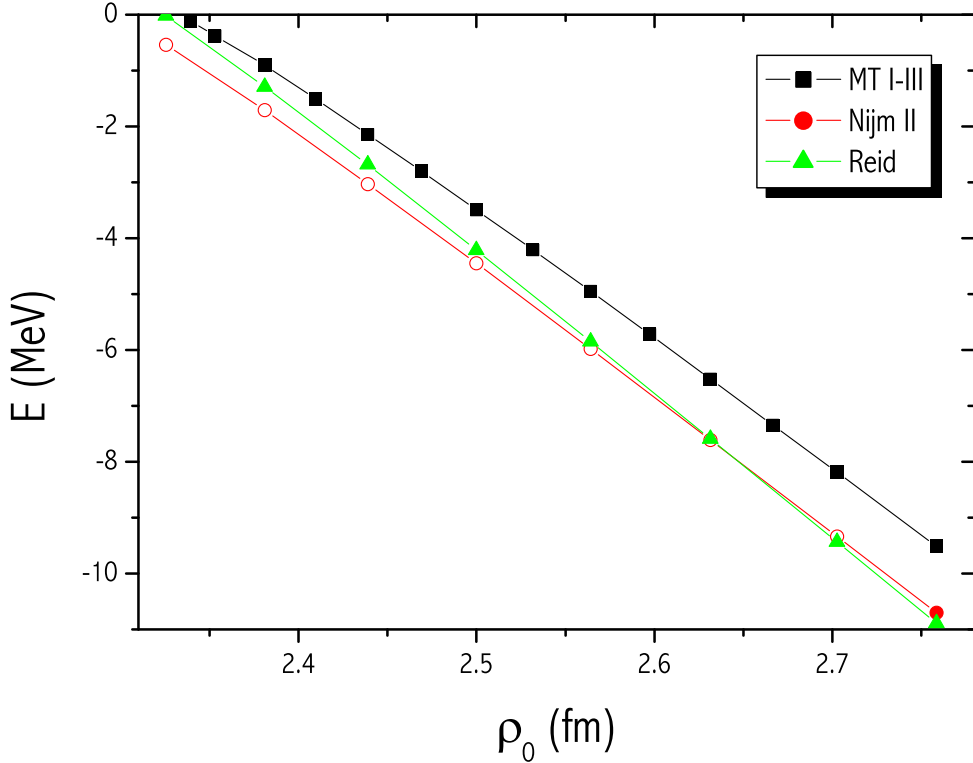


Figure 3.11: Tetraneutron bound using different NN interaction models in conjunction with hyper-radial Yukawa type force eq. (3.7), strength of which was fixed to $W = -612.4$ MeV fm, whereas its length ρ_0 varied.

In that concerns the many body force effects, we conclude that whatever the form they can take, they are not able to ensure the binding of pure neutron systems: their range is too small to act constructively with 2NF for weakly bound, sparse systems. Furthermore in pure neutron systems the many body forces play a minor role and their presence can be eventually neglected. The short range character of these forces makes them fade away, since due to Pauli principle, the probability to find three nucleon close to each other is extremely small .

3.5 Atomic ^3He against the neutrons

In section 3.3 and particularly in Fig. 3.3, we have mentioned that nn interaction is very similar to the one existing between two ^3He atoms. Even a few arguments in favor of the bound multineutron clusters have been presented.

The reasons why multiaatomic ^3He molecules can be bound, whereas multineutrons seems to be

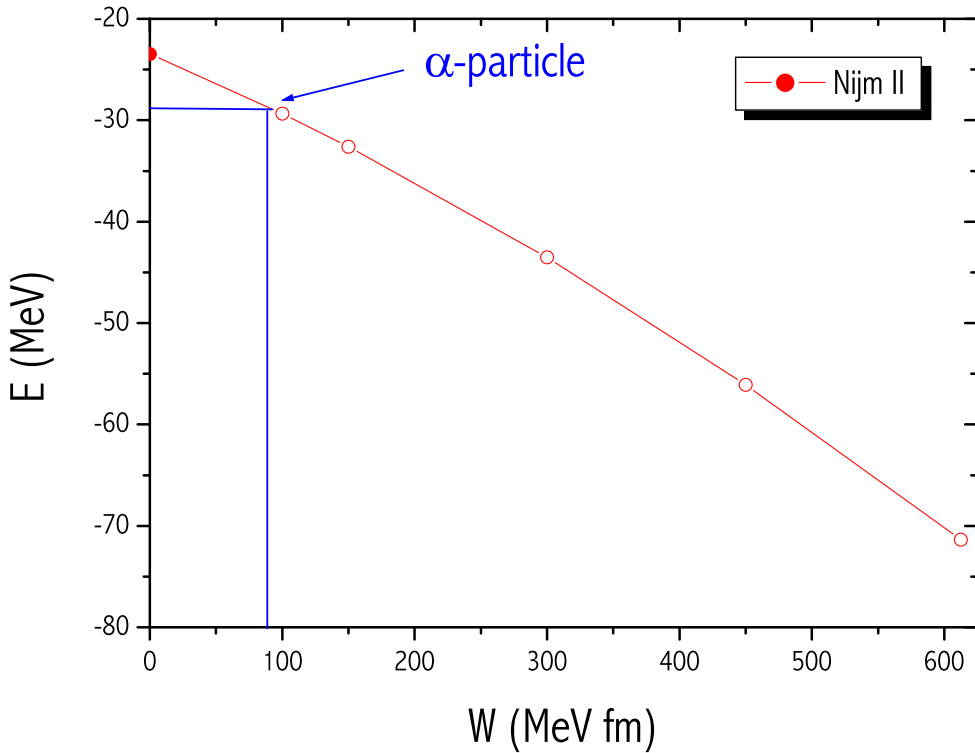


Figure 3.12: α -particle calculations within *Nijm II* NN interaction model in conjunction with Yukawa-type hyperradial force. Dependence of binding energies on the strength W of this force are presented. Real α -particle binding energy, without Coulomb interaction taken into account, should be $\simeq 29$ MeV is marked by the blue lines.

unbound remains unclear. In this chapter we will try to compare the behavior of these two systems and find out their differences.

The complexity of Faddeev-Yakubovski equations, increases very rapidly with the number of constituent particles. Our actual numerical capabilities permit only to study the systems containing up to 4 particles that is far below the number at which bound ${}^3\text{He}$ clusters can be formed. How to compare the relative role of the interactions in two systems, which are both unbound? The first possibility is to enhance the potential. However, as we have seen in sections 3.4 and 3.4.1, in order to form a bound 3-body (4-body) state, the enhancement factors must be very large, considerably modifying the properties of the system.

Furthermore, Aziz potential describing ${}^3\text{He}$ - ${}^3\text{He}$ interaction contains a very strong repulsive core, which makes bound state calculations numerically unstable. A strong enhancement of this potential will further complicate the numerical stability.

In order to circumvent the two mentioned problems we have enhanced the nn and ${}^3\text{He}$ - ${}^3\text{He}$ 1S_0 waves by artificially binding the corresponding dfermion systems. Notice that one needs very

small enhancements for these waves to make dimer bound Table. 3.3, contrary to 3(4)-body case. This allows us to perform dimer-dimer scattering calculations, instead of direct bound state calculations.

The main idea is based on the fact that the scattering length is positive for repulsive systems and diminishes up to $-\infty$ when more attraction is gained. Once the projectile-target interaction is sufficiently strong to form a bound state, the scattering length has a singularity and passes from $-\infty$ to ∞ (see similar discussion in section 1.1.7 and 2.3.3). Therefore, the scattering length sign indicates whether the effective interaction between two multiparticle clusters is attractive or repulsive. On the other hand, by comparing systems with equal number of bound states, the size of the scattering length evaluates the strength of this interaction. Former ideas can be generalized for the scattering of composite systems. In this case, the scattering length will be a measure of the effective interaction between the appropriate scattered clusters.

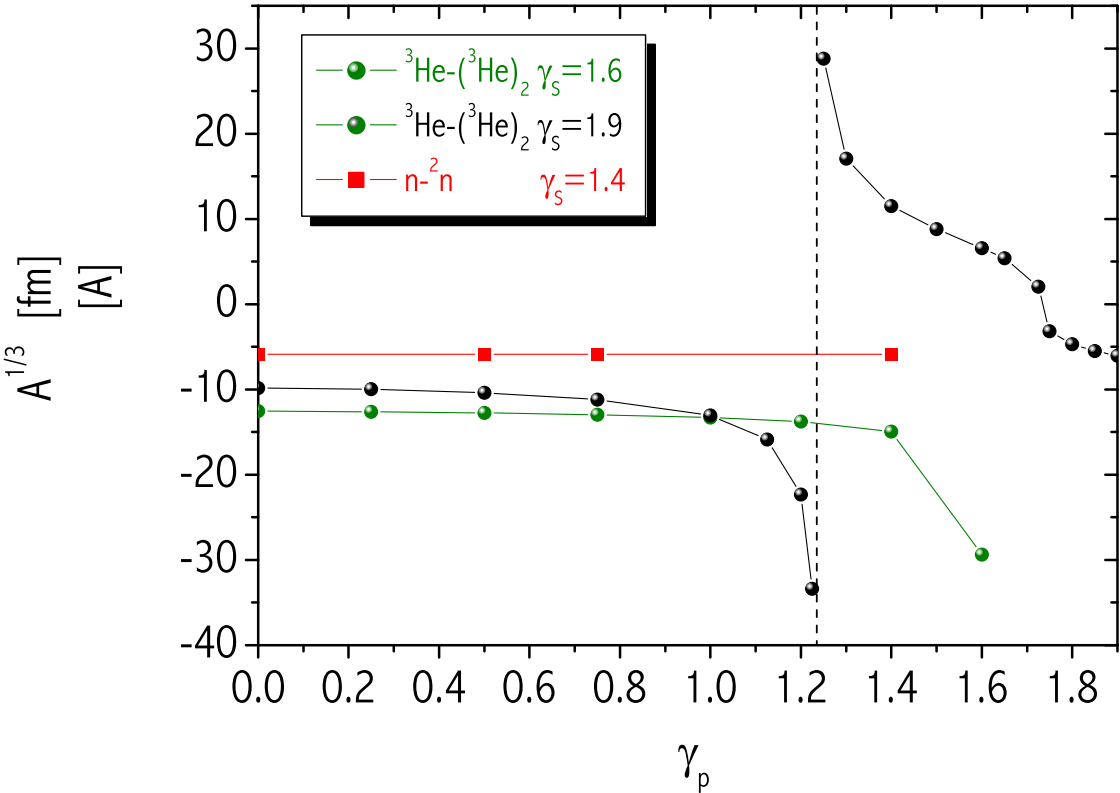


Figure 3.13: Dependence of scattering lengths on interaction in P -waves for $n - (nn)$ and ${}^3\text{He}-({}^3\text{He})_2$ systems. Dineutron was bound with $B = 1.596$ MeV. by enhancing $Av.18$ potentials S -waves with $\gamma_s = 1.4$. Two series of calculations were performed for ${}^3\text{He}-({}^3\text{He})_2$ scattering: ${}^3\text{He}$ dimer was bound by enhancing Aziz potential S -waves with $\gamma_s = 1.6$ and $\gamma_s = 1.9$, which given dimer binding energies $B = 0.1275$ K and 0.4812 K respectively.

The sensitivity of elastic scattering lengths to P -wave interaction in $n - (nn)$ and $(nn) - (nn)$

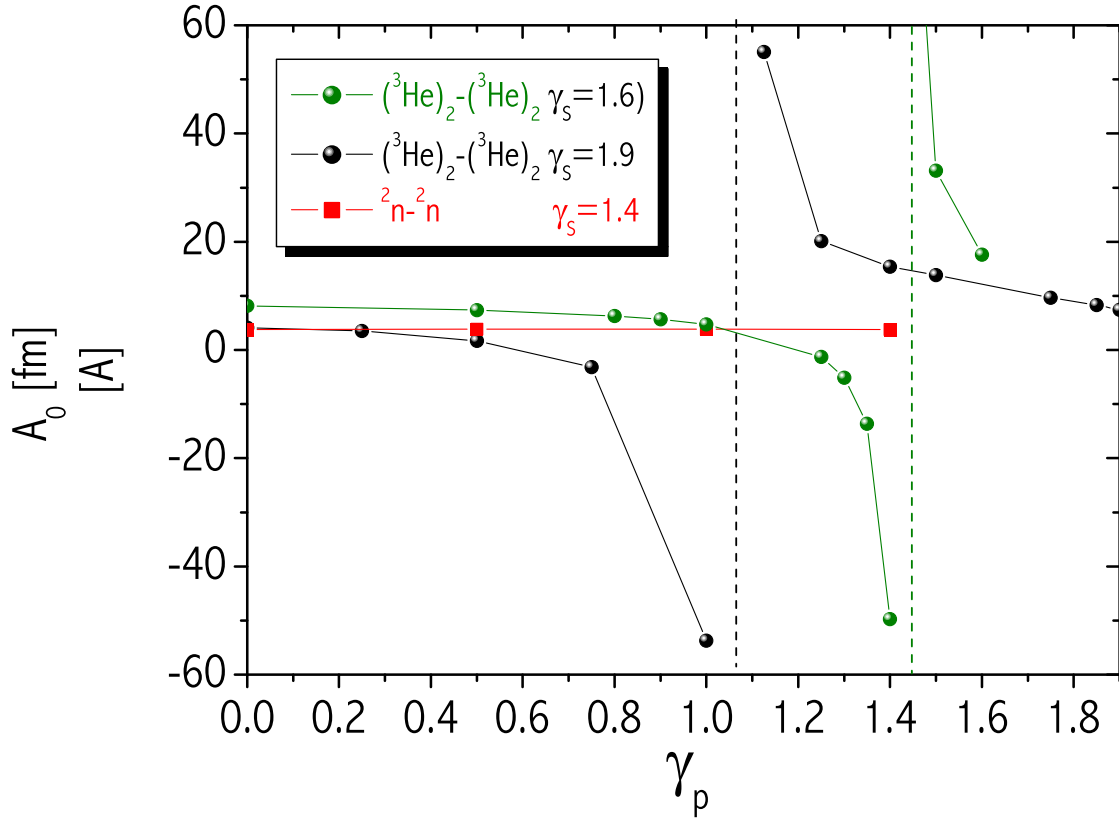


Figure 3.14: The same as in Fig.3.13 just for 4 body scattering in $(XX) - (XX)$ configuration.

systems has been analyzed and compared to the analogous ${}^3\text{He} - (^3\text{He})_2$ and $(^3\text{He})_2 - (^3\text{He})_2$ case. The most promising states to support multifermion clusters, namely $J^\Pi = \frac{3}{2}^-$ for 3-body $X - (XX)$ scattering case and $J^\Pi = 0^+$ for 4-body $(XX) - (XX)$ case, were investigated.

l_x	s_x	j_x	l_y	j_y	J^Π
0	0	0^+	1	$\frac{3}{2}^-$	$\frac{3}{2}^-$

Table 3.8: Partial wave decomposition for the asymptote of the elastic channel in X-(XX) scattering.

In order to realize a $J^\Pi = \frac{3}{2}^-$ 3-body state, the projectile should have an orbital angular momentum $\ell_y = 1$ with respect to the bound (XX) difermion cluster in the asymptotic channel⁵ (see Table 3.8). According to the effective range formulae (1.51), the scattering length a_ℓ has $k^{-(2\ell+1)}$ dimension, that is a cube length unit for scattering with relative orbital momentum $\ell_y = 1$.

⁵Indeed the (XX) cluster is bound in 1S_0 state. Therefore the angular momentum is completely due to the relative motion of the projectile.

l_x	s_x	j_x	l_y	s_y	j_y	l_z	J^Π
0	0	0^+	0	0	0^+	0	0^+

Table 3.9: Partial wave decomposition for the asymptote of the elastic channel in (XX)-(XX) scattering.

Although the interpretation of higher angular momentum scattering lengths has no clear physical meaning, they exhibit a similar singular behavior near the S matrix poles (i.e. those given by bound or resonant states). In order to compare similar quantities in different states, we have transformed $\ell_y = 1$ scattering lengths into length unit by taking its cube root $\sqrt[3]{a_{\ell=1}}$.

In the $(XX) - (XX)$ 4-body scattering, having the most favorable state (i.e. $J^\Pi = 0^+$) in mind, the elastic channel can be realized with a relative angular momentum $\ell_z = 0$ (see Table 3.9). Therefore the corresponding scattering length has the standard length dimension.

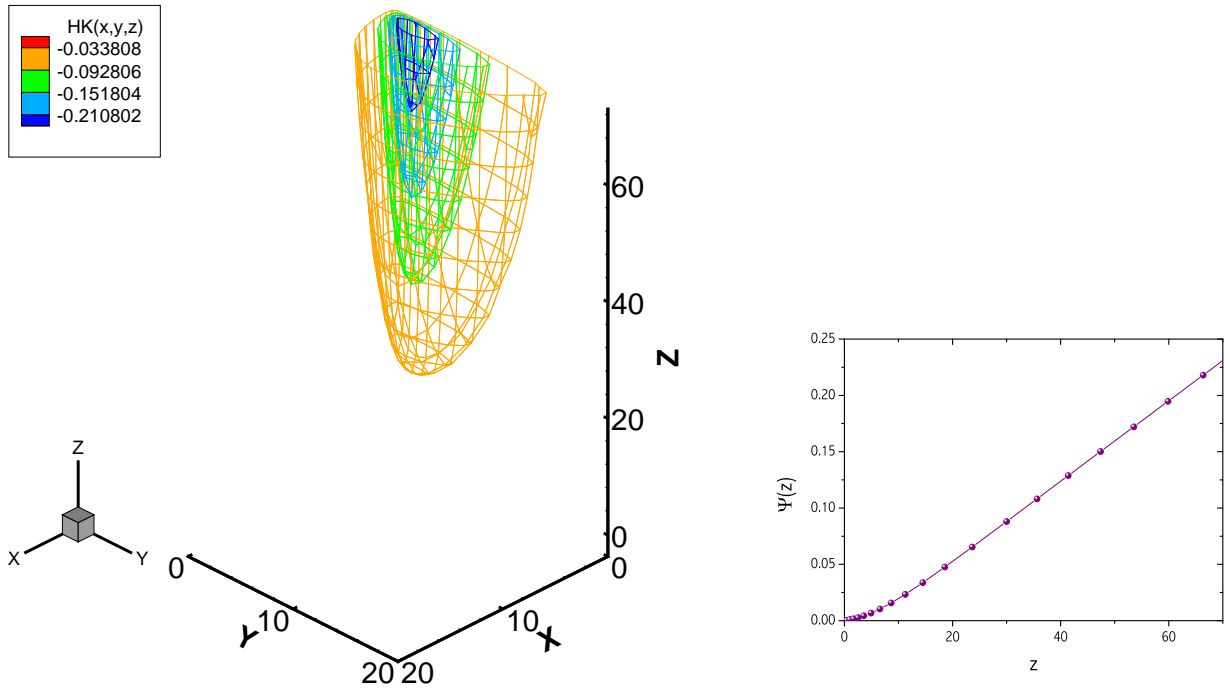


Figure 3.15: 3-dimensional equisurfaces of the Faddeev-Yakubovski amplitude corresponding to ${}^2n - {}^2n$ elastic scattering open channel. Calculations were done with all the *Av.18* potential waves enhanced $\gamma = 1.4$ times. For such enhancement 2n is bound with $B = 1.596$ MeV in 1S_0 state. One can see that these surfaces don't create any close shells, indicating that 4n is not bound. In the right hand side cut of this FY amplitude is plotted with the values x and y being fixed.

Results are presented in Figs. 3.13 and 3.14. One can see that if interaction in \mathcal{P} -waves is

switched off, positive scattering lengths are obtained in both multineutron and ${}^3\text{He}$ cases. This indicates the existence of an effective repulsion between the scattered clusters. As mentioned in section 3.4 in case of S -wave potential, particles try to cluster two by two, while the different 2-body clusters, formed this way, do not interact with each other.

Switching on \mathcal{P} -wave interaction in neutron systems has negligible effect for their scattering lengths as well as for their wave functions (see Fig. 3.15). They do not depend on whether all \mathcal{P} -waves are enhanced or whether one enhance only the attractive ${}^3\mathcal{P}_2 - {}^3\mathcal{F}_2$ channel. These calculations were performed using *Av.18* potential, without 3NF. Note that, as it was a case in the preceding calculations, the introduction of 3NF or the use of other interaction model can not qualitatively modify these results.

The ${}^3\text{He}-{}^3\text{He}$ interaction is assumed to have the same form in all partial waves and to be spin independent. One can not distinguish among the different \mathcal{P} -waves and therefore in our calculations they were scaled by the same factors. Contrary to neutron systems, ${}^3\text{He}$ clusters seems to be very sensitive to the interaction in \mathcal{P} -waves. By enhancing these \mathcal{P} -wave potentials, the scattering length changes considerably in both cases of ${}^3\text{He} - ({}^3\text{He})_2$ and $({}^3\text{He})_2 - ({}^3\text{He})_2$. For some value of the enhancement factor, the scattering length exhibits a singularity, passing from $-\infty$ to ∞ , when the zero energy wave function displays a node in the two cluster separation direction (see Fig. 3.17). This is an indication that the tri- and four- ${}^3\text{He}$ clusters become bound. The critical \mathcal{P} -wave enhancement factors, at which these bound states appear, are reasonable. If one binds $({}^3\text{He})_2$ by enhancing ${}^1\mathcal{S}_0$ waves with $\gamma_s = 1.9$, one can obtain bound ${}^3\text{He}$ tetramers almost without enhancing \mathcal{P} -waves. ${}^3\text{He}$ trimers are less propitious to be bound than tetramers and therefore they need more enhanced interaction. By reducing the ${}^1\mathcal{S}_0$ enhancement factor to $\gamma_s = 1.6$, stronger \mathcal{P} -waves ($\gamma_p > 1.4$) are required to retain ${}^3\text{He}$ tetramer bound. On the other hand ${}^3\text{He}$ trimers are still not bound for ($\gamma_p = 1.6$).

In what precede, we have shown that ${}^3\text{He}$ multimers are much more sensitive to \mathcal{P} -wave interaction than neutrons are. This is due to the fact that attractive potential well in ${}^3\text{He}-{}^3\text{He}$ potential lies at sensibly larger separation distance between the particles than in case of $n - n$ interaction. Centrifugal energy terms in ${}^3\text{He}$ system are thus considerably smaller. Since centrifugal kinetic energy reads

$$T_K = \frac{\hbar^2}{2\mu} \frac{\ell(\ell+1)}{r^2} = \frac{\hbar^2}{m} \frac{\ell(\ell+1)}{r^2}, \quad (3.9)$$

it is useful to compare the rescaled potentials

$$V_{sc}(r) = \frac{m}{\hbar^2} r^2 V(r). \quad (3.10)$$

These potentials represent a measure of systems sensitivity to higher partial waves. For nn interaction, the rescaled potential in any \mathcal{P} partial wave are smaller than 2 ($V_{sc}(r) > -\ell(\ell+1) = -2$) (see Fig. 3.18), therefore indicating that nn \mathcal{P} (and higher order $\mathcal{D}, \mathcal{F}, \dots$) waves are not able to compensate the centrifugal kinetic energy terms. Consequently, one has a very small impact of these waves in binding multineutron systems.

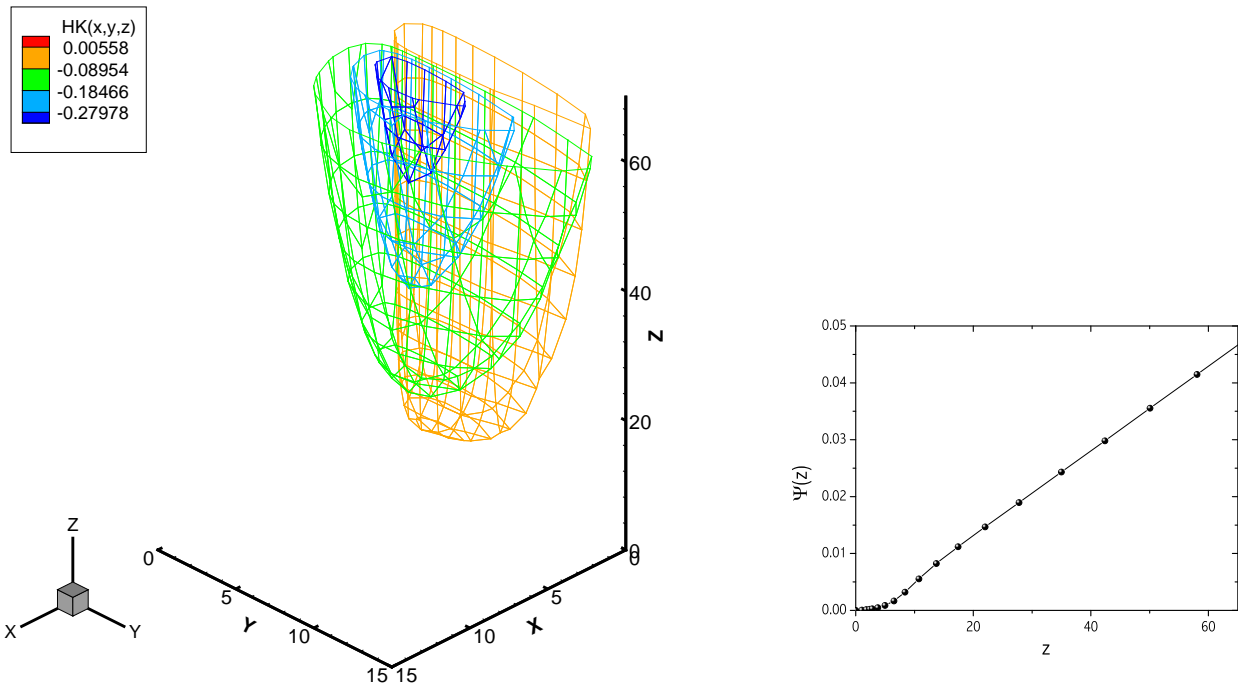


Figure 3.16: 3-dimensional equisurfaces of the Faddeev-Yakubovski amplitude corresponding to $(^3\text{He})_2 - (^3\text{He})_2$ scattering elastic channel. Calculations were done with $\gamma_s = 1.9$ times enhanced S -waves of Aziz potential, for which $(^3\text{He})_2$ is bound at $B = 0.4812$ K. Enhancement of interaction in P -waves was only $\gamma_p = 0.5$. One can see that equisurfaces don't create any close shell, indicating that $(^3\text{He})_4$ is not bound for this parameter set.

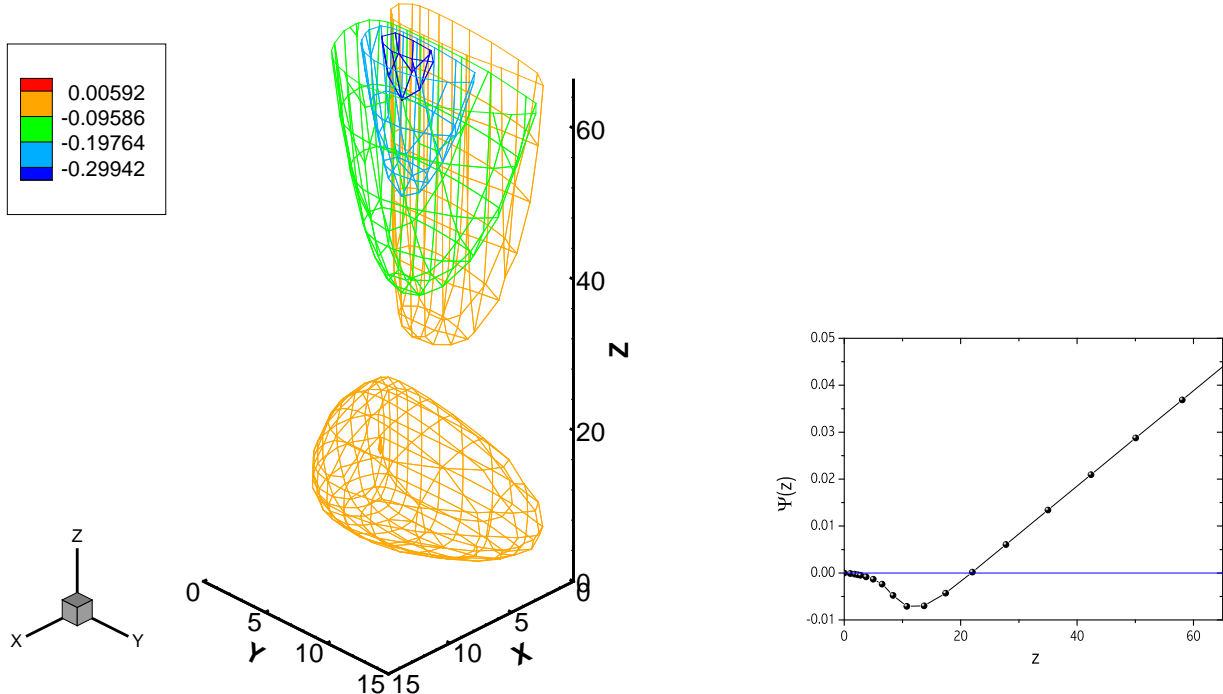


Figure 3.17: Same as in Fig. 3.16 only P -waves here were enhanced with $\gamma_p = 1.4$. One can see closed shell, therefore indicating that $(^3\text{He})_4$ cluster is already bound. Whereas in 2D plot one can see that wave function has a node in the direction of two 2-body cluster separation.

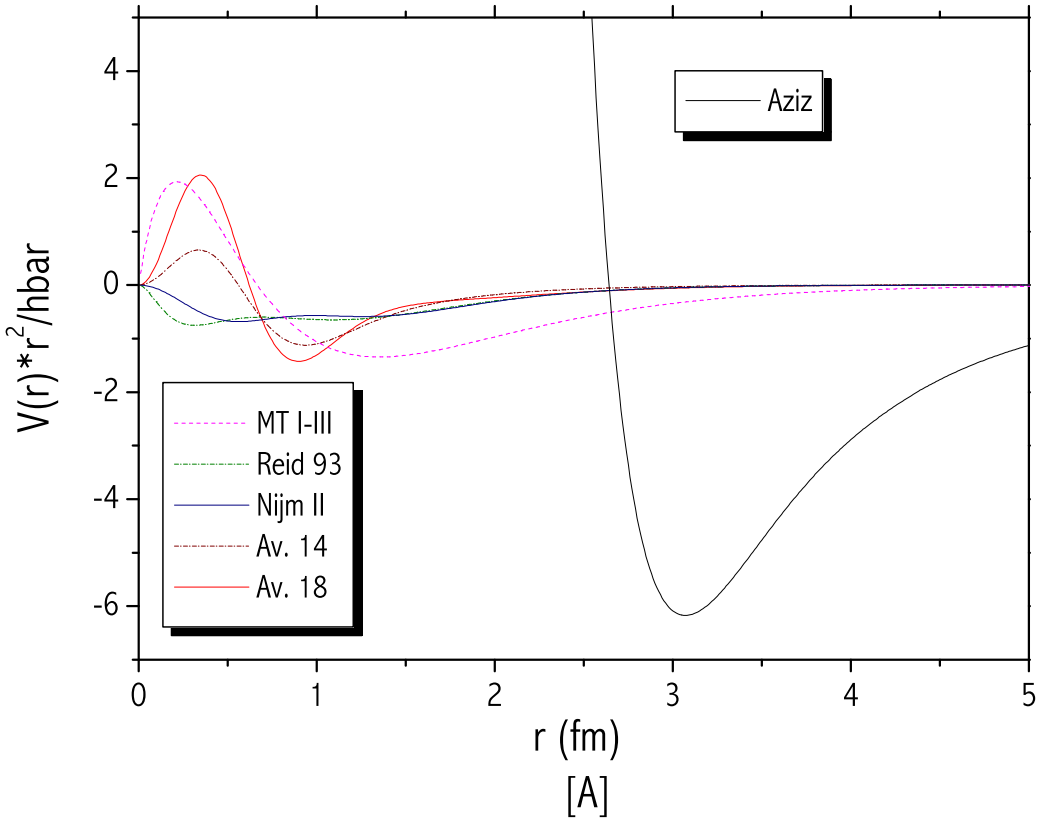


Figure 3.18: Comparison of normalized \mathcal{P} -waves of Aziz potential (describing interaction between ${}^3\text{He}$ atoms) with different model nn ${}^3\mathcal{P}_2$ waves (the most attractive nn \mathcal{P} -waves). In *MT I-III* potential case (having no interaction in \mathcal{P} -waves) renormalized ${}^1\mathcal{S}_0$ waves were plotted.

On the contrary, the ${}^3\text{He} - {}^3\text{He}$ rescaled potential $V_{sc}(r)$ displays a deep minima (smaller than -6). This indicates that the effective potential

$$V_{eff}(r) = V(r) + \frac{\hbar^2}{m} \frac{\ell(\ell+1)}{r^2} \quad (3.11)$$

will have a small attractive well even in \mathcal{D} -waves, making considerable impact in constructing ${}^3\text{He}$ multimers.

In contrary to \mathcal{S} -wave pairwise interaction, where one can have only one interacting partner for each particle, one can create more interacting pairs in \mathcal{P} and \mathcal{D} -waves (6 and 10 respectively). These waves thus play a major role in large fermionic clusters, where the number of nearest neighbors for each particle can be large.

Fermionic systems with predominant \mathcal{S} -waves (like neutrons), even forced to stay together (for instance by confining them in external fields) will try always to split into 2-particle clusters. If the difermion system is not bound, multiparticle cluster will finally break into single particles.

On the contrary, if the effective interaction is attractive even in higher partial waves, multi-fermion condensation will be possible, exhibiting some similarities with the bosonic systems. The number of attractive partial waves, as in solid state physics, determine the signature of the multi-fermion lattice.

Chapter 4

Four nucleon continuum states

4.1 Introduction

The four nucleon continuum is a challenge for the few-body nuclear problem. Its interest lies not only in the natural progression that it represents, towards the systematic description of an increasing complexity nuclear system, but also in the richness of the $A = 4$ nuclear chart itself (see Fig. 4.1). Four nucleon problem, we believe, implies a qualitative jump in respect to the $A = 3$ case.

As mentioned in the previous chapter, one needs to implement 3NF in order to provide the lacking binding energy for the nuclei with $A \geq 3$. These forces are usually adjusted to describe tritium and/or ^3He , eventually α -particle (^4He), binding energies, with no other constraints taken into account. Therefore continuum states could be the supplementary testing ground for these forces.

The $A = 3$ low energy scattering is dominated by the $\mathcal{J}^\Pi = \frac{1}{2}^+$ and $\frac{3}{2}^+$ states, which cannot provide a comprehensive test for 3NF. Indeed, on one hand $\mathcal{J}^\Pi = \frac{1}{2}^+$ has the same quantum numbers as the tritium, without exhibiting any narrow resonances neither in n+d nor in p+d continuum. Therefore success in describing the low energy continuum of the $\mathcal{J}^\Pi = \frac{1}{2}^+$ state is closely correlated with the ability to reproduce the tritium binding energy, a well known effect which manifests by the existence of the 'so called' Philips line [152]. On the other hand, $\mathcal{J}^\Pi = \frac{3}{2}^+$ state can not be constructed without permitting one of the particle pairs to have non-zero angular momentum. The last means that low energy three particle quartet configurations, when they are close to each other, are largely suppressed. Therefore 3NF plays a minor role in $\mathcal{J}^\Pi = \frac{3}{2}^+$ state, whereas all dynamics are dominated by NN interaction only. At higher energies, even though deuterium breakup takes place, 3N scattering observables exhibit smooth behavior (see Fig. 4.2). This means that satisfactory description of 3N problem at low and intermediate energies depends only on a few parameters, which can be found in any existing 3NF.

The strength of the 3NF depends on the underlying NN forces and their main effect is to rescale 3N and 4N bound state energies. Their influence on the 3N continuum, beyond the effect correlated with tritium rescaling, manifests itself only at relatively high energies, above 65 MeV

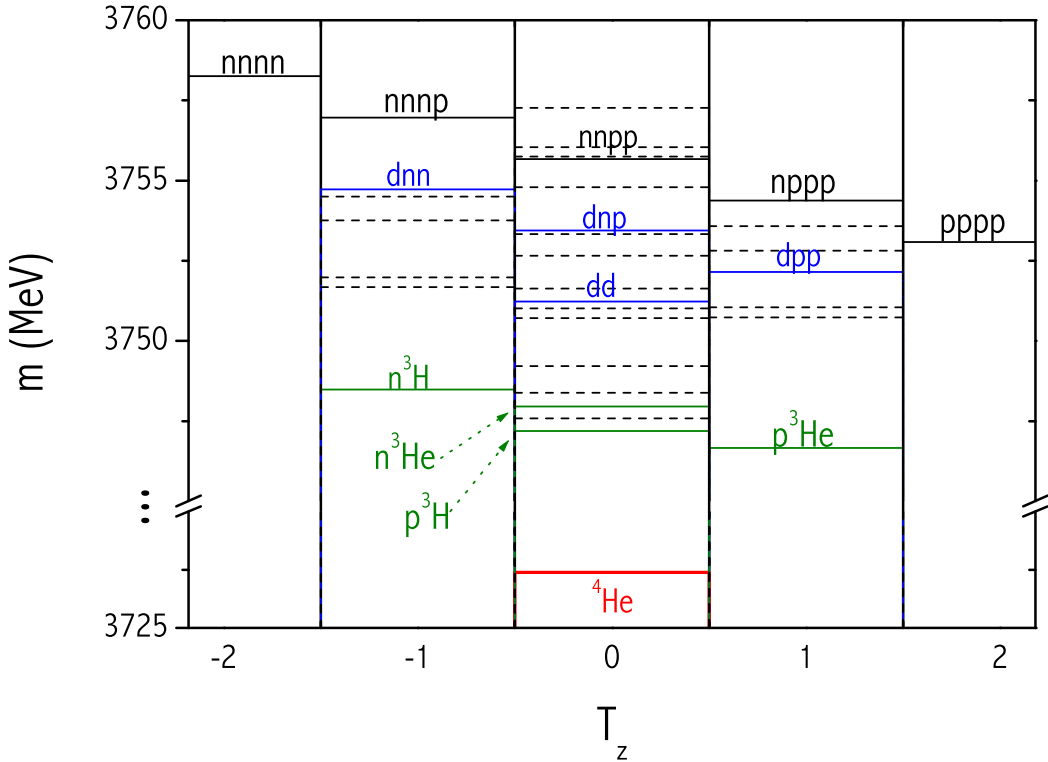


Figure 4.1: Four nucleon energy spectra. Single lines indicate particle thresholds, whereas dashed lines represent particle decay unstable excited states (resonances). These fine structures are manifesting in the scattering experiment, whereas their proper description is a severe test for the nuclear interaction models.

[111, 112, 153].

The only stable 4N bound state is the α -particle. However, α -particles structure is closely correlated to the tritium, effect demonstrated by the existence of a Tjon line [157] (see Fig. 4.3). Therefore being of fundamental interest in testing NN forces, it does not provide qualitatively new features. On the other hand 4N continuum spectrum, unlike in 3N case, exhibits a rich variety of resonances and thresholds. These dynamical structures, being distributed over the large energy region, could show properties different from that of the tritium or α -particle. The naive comparison between the smooth behavior observed in the $n+{}^1H$ and $n+{}^2H$ elastic cross sections and largely non trivial structure manifested in $n+{}^3H$ case illustrates clearly this point (see Fig. 4.2). Therefore it is far from being obvious that the approach followed until now, based on a good description of the 2N observables as well as tritium binding energy, could be successfully extended to 4N continuum. Furthermore 4N spectrum contains many negative parity resonances, which come as the doublet, spin degenerate, states. Precise treatment of these states can provide invaluable information of nuclear force spin dependence, thus permitting us a better understanding of the longstanding A_y problem.

A resonant state spreads over an energy region given by its width and fully displays there the internal dynamics of the 4N system. Its theoretical description provides a severe test in our

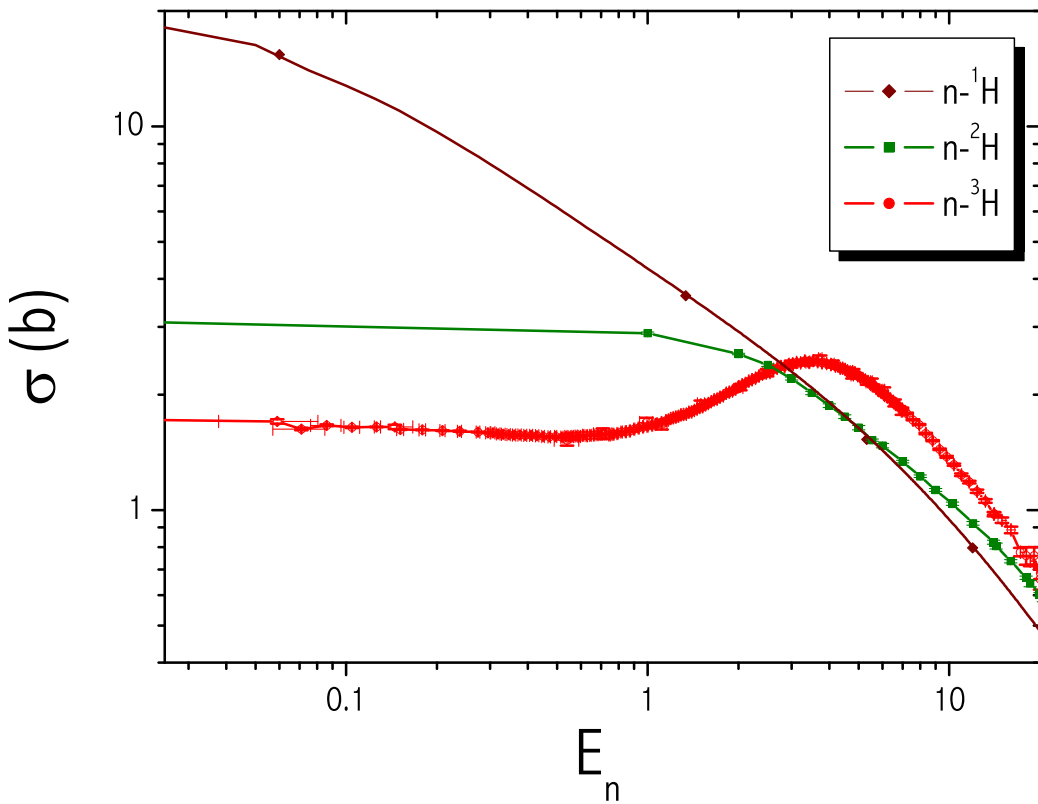


Figure 4.2: Neutron total cross sections for hydrogen (^1H), deuterium (^2H) and tritium (^3H) as given by the experimental data. Naive comparison demonstrates well the qualitative difference of $n+^3\text{H}$ continuum in respect to the $A=2$ and $A=3$ case.

comprehension of the nuclear forces.

There are five different realizations of particle states in four nucleon system and they are enumerated in Fig. 4.1. However, only three of them can be explored experimentally, since one doesn't have pure neutron or proton systems. Furthermore, ^4H ($nnnp$) and ^4Li ($pppn$) are mirror systems for the proton-neutron exchange. Due to similarity of nuclear interaction, these two systems have resembling spectra, which become almost identical once ^4Li data is corrected by removing Coulomb interaction between the protons. The $n+^3\text{H}$ elastic scattering is the simplest 4N reaction and represents a first and incontournable step before a more ambitious program can be undertaken. On one hand, it is almost a pure $\mathcal{T} = 1$ channel, free from the difficulties arising when dealing with Coulomb force. On the other hand, high quality measurement of the total $n+^3\text{H}$ cross sections are available [158]. They show a resonant structure interpreted by the R-matrix analysis of Hale and collaborators [125] as being generated by a family of resonances (see Fig. 4.1).

The next obligatory step should be to describe $n+^3\text{H}$ isospin partners, i.e. $p+^3\text{He}$ continuum states. The comparison of two systems permits us to have a deeper understanding of the CSB in nuclear force. In order to solve $p+^3\text{He}$ problem theoretically one should introduce Coulomb interaction in few-body formalism. This far from trivial issue will be presented in the following section.

	<i>n-d</i>		<i>p-d</i>	
	$\mathcal{J}^{\Pi} = \frac{1}{2}^+$	$\mathcal{J}^{\Pi} = \frac{3}{2}^+$	$\mathcal{J}^{\Pi} = \frac{1}{2}^+$	$\mathcal{J}^{\Pi} = \frac{3}{2}^+$
<i>MT I-III</i>	0.70	6.44	-0.027	13.95
<i>Nijm II</i>	1.24	6.34	1.004	13.46
<i>Reid 93</i>	1.23	6.34	0.989	13.47
<i>Av.14</i>	1.20	6.38	0.920	13.57
<i>Av.18</i>	1.26	6.34	1.42	13.62
<i>Av.18+UIX</i>	0.60	6.34	0.20	13.62
Exp. [154]-[156]	0.65 ± 0.04	6.35 ± 0.02	[1.3 - 4.0]	~ 11.5

Table 4.1: Comparison of calculated $p-d$ and $n-d$ scattering lengths with the experimental data. One can remark very small influence of 3NF on the results.

The $p+{}^3H$ continuum represents the richest and apparently the most complicated 4N system. Even at very low energies one is obliged to separate $p+{}^3H$ and $n+{}^3He$ channels, which are isospin degenerate. Their experimental separation is only 0.764 MeV, principally due to Coulomb repulsion existing between two protons in 3He nucleus [117]. One needs very accurate treatment of Coulomb interaction, as well as a formalism permitting to separate isospin degenerate states. This subject will be discussed in the section 4.3.

4.2 Coulomb interaction

In order to introduce the Coulomb interaction in 4-body Faddeev-Yakubovski equations, we will extend the ideas of Merkuriev. We split Coulomb potential into long and short range parts, similarly as it was done by Merkuriev for 3-body equations [10][66]:

$$V_{Coul}(x) = V_{Coul}^{(short)}(x, y, z) + V_{Coul}^{(long)}(x, y, z), \quad (4.1)$$

where

$$V_{Coul}^{(short)}(x, y, z) = \chi(x, y, z) V_{Coul}(x) \quad (4.2)$$

$$V_{Coul}^{(long)}(x, y, z) = [1 - \chi(x, y, z)] V_{Coul}(x) \quad (4.3)$$

One can rewrite the 4-body Faddeev-Yakubovski equations:

$$(H_0 - E + V_{12} + W) |K_{12,3}^4\rangle = -V_{12}^{(short)} [|K_{13,2}^4\rangle + |K_{23,1}^4\rangle + |K_{13,4}^2\rangle + \quad (4.4)$$

$$|K_{23,4}^1\rangle + |H_{13,24}\rangle + |H_{23,14}\rangle] \quad (4.5)$$

$$(H_0 - E + V_{12} + W) |H_{12,34}\rangle = -V_{12}^{(short)} [|K_{34,1}^2\rangle + |K_{34,2}^1\rangle + |H_{34,12}\rangle] \quad (4.6)$$

with using short notations for potential terms

$$\begin{aligned} W &= V_{13}^{(long)} + V_{14}^{(long)} + V_{23}^{(long)} + V_{24}^{(long)} + V_{34}^{(long)} \\ V_{12}^{(short)} &= \left(V^{(Nucl)} + V_{Coul}^{(short)} \right)_{12} \\ V_{12} &= \left(V^{(Nucl)} + V_{Coul} \right)_{12} \end{aligned} \quad (4.7)$$

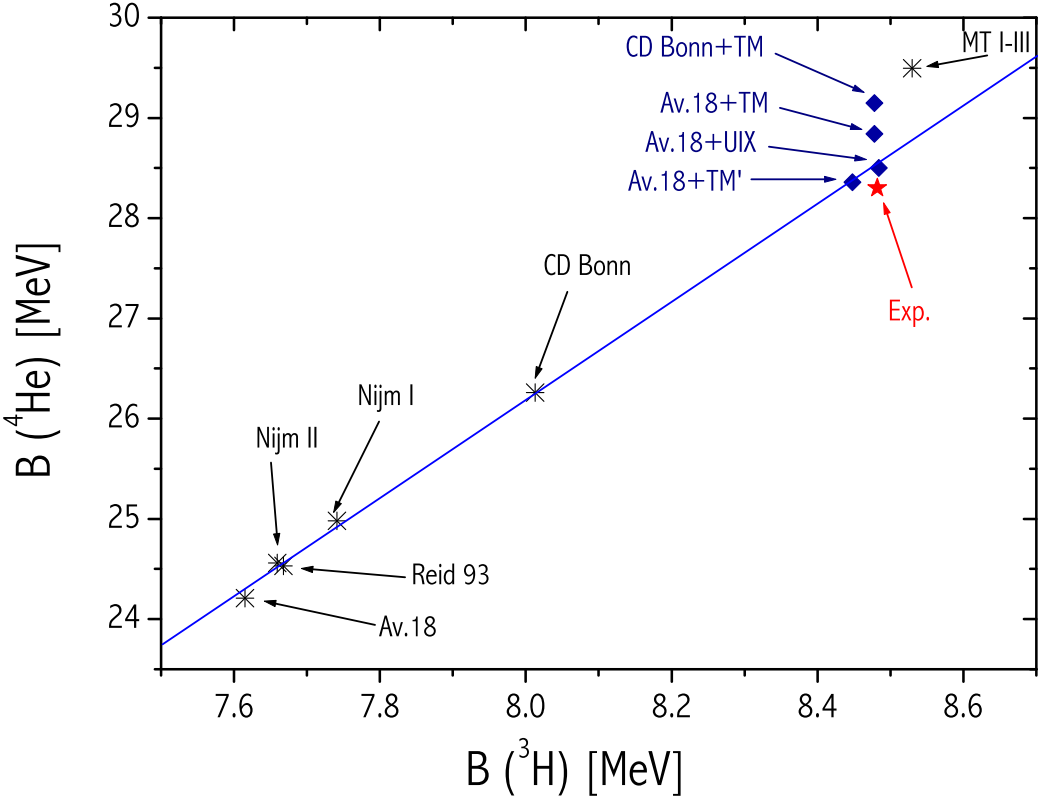


Figure 4.3: Tjon line: α -particle binding energy predictions $B(^4\text{He})$ depend on the prediction of the tritium binding energy $B(^3\text{H})$ for several interaction models. Predictions without 3NF (snowflakes) and with 3NF (diamonds) are shown. The experimental point is marked by a red star. Results for *CD-Bonn*, *Nijm I* as well as *Av.18* in conjunction with Tucson-Melbourne (*TM*) 3NF were borrowed from [103][3].

Actually the choice of splitting function $\chi(x, y, z)$ is arbitrary, moreover one can use different splitting functions for Coulomb terms coupling different particle pairs. To make the calculations of Coulomb integrals as simple as possible, we have used

$$\chi_{i4}(x, y, z) = \chi(x, \sqrt{y^2 + z^2}) \quad i = 1, 2, 3 \quad (4.8)$$

splitting function for Coulomb terms coupling particle pairs (34), (24) and (14). By the contrary, in order to facilitate the reduction of 4-body equations into 3-body Merkuriev equations, similar to those of eq. (2.5), for pair interactions (23) and (13) it is convenient to use standard 3-body definitions as in eq. (2.9):

$$\chi_{i3}(x, y, z) = \chi(x, y) \quad i = 1, 2 \quad (4.9)$$

In this case one should rewrite equations in the following form:

$$(H_0 - E + V_{12}^{(\text{short})} + W) |K_{12,3}^4\rangle = -V_{i3}^{(\text{short})} [|K_{13,2}^4\rangle + |K_{23,1}^4\rangle] \quad (4.10)$$

$$-V_{i4}^{(\text{short})} [|K_{13,4}^2\rangle + |K_{23,4}^1\rangle + |H_{13,24}\rangle + |H_{23,14}\rangle] \quad (4.11)$$

$$(H_0 - E + V_{12}^{(\text{short})} + W) |H_{12,34}\rangle = -V_{i4}^{(\text{short})} [|K_{34,1}^2\rangle + |K_{34,2}^1\rangle + |H_{34,12}\rangle], \quad (4.12)$$

where

$$V_{i4}^{(short)} = \left(V^{(Nucl)} + \chi_{i4}(x, y, z) V_{Coul} \right)_{12} \quad (4.13)$$

$$V_{i3}^{(short)} = \left(V^{(Nucl)} + \chi_{i3}(x, y, z) V_{Coul} \right)_{12} \quad (4.14)$$

The notes on practical implementation of these ideas are presented in Appendices C.2 and D.3.

4.3 Separating ${}^4\text{He}$ channels in the isospin formalism

Since nuclear interaction properties of neutrons and protons are very similar, it is very useful to treat them as a single particle nucleon, introducing 'so called' isospin formalism (see sections 1.2.4-1.2.5). However, the effect of isospin invariance breaking cannot be ignored, especially when one wants to treat Coulomb interactions explicitly. Interaction in pp pairs becomes considerably different from those in nn or np , once the Coulomb interaction is considered. Still matrix elements of Coulomb interactions can be evaluated in the isospin state bases:

$$|\mathcal{T}_{iso}\rangle = \begin{cases} |t_x, T_3, \mathcal{T}, \mathcal{T}_z\rangle & \text{for the configurations of the type K} \\ |t_x, t_y, \mathcal{T}, \mathcal{T}_z\rangle & \text{for the configurations of the type H} \end{cases}. \quad (4.15)$$

Hence these bases are not proper for the particle states. Considered matrix elements are found by introducing the full basis of particle states $|part\rangle = |m_1, m_2, m_3, m_4\rangle$ and using completeness relations:

$$\sum_{part} |part\rangle \langle part| = 1. \quad (4.16)$$

In former relation m_i indicated the z -component of $i - th$ nucleon isospin $t^{(i)}$. This isospin projections of nucleon state can have two possible values $m(n) = -\frac{1}{2}$, $m(p) = \frac{1}{2}$. Then

$$\langle \mathcal{T}'_{iso} | V | \mathcal{T}_{iso} \rangle = \sum_{part, part'} \langle \mathcal{T}'_{iso} | |part'\rangle \langle part'| V | part \rangle \langle part| | \mathcal{T}_{iso} \rangle \quad (4.17)$$

$$= \sum_{part, part'} \delta_{part, part'} \langle \mathcal{T}'_{iso} | |part'\rangle \langle part| V | part \rangle \langle part| | \mathcal{T}_{iso} \rangle \quad (4.18)$$

$$= \sum_{part} \langle \mathcal{T}'_{iso} | |part\rangle \langle part| V | part \rangle \langle part| | \mathcal{T}_{iso} \rangle \quad (4.19)$$

In particle basis, Coulomb interaction terms can be expressed using charge projection operator:

$$\langle part | V_C(r_{ij}) | part \rangle = \left(\frac{1}{2} + m_i \right) \left(\frac{1}{2} + m_j \right) \frac{e^2}{r_{ij}} \quad (4.20)$$

Whereas transitions between particle and isospin states are coupled by the Clebsch-Gordan coefficients. In case of K configuration functions:

$$\langle part | |\mathcal{T}_{iso} \rangle = \langle \mathcal{T}_{iso} | |part \rangle = C_{t_1 m_1 t_2 m_2}^{t_x m_x} C_{t_x m_x t_3 m_3}^{T_3 M_3} C_{T_3 M_3 t_4 m_4}^{\mathcal{T} \mathcal{T}_Z} \quad (4.21)$$

Finally Coulomb interaction terms for a system of interacting nucleons in isospin formalism will have the following form:

$$\begin{aligned} \langle T'_{iso} | V_C(r_{ij}) | \mathcal{T}_{iso} \rangle &= \sum_{m_1+m_2+m_3+m_4=T_Z} C_{t_1 m_1 t_2 m_2}^{t_x m_x} C_{t_x m_x t_3 m_3}^{T_3 M_3} C_{T_3 M_3 t_4 m_4}^{\mathcal{T} \mathcal{T}_Z} \times \\ &\quad \times C_{t_1 m_1 t_2 m_2}^{t'_x m_x} C_{t_x m_x t_3 m_3}^{T'_3 M_3} C_{T'_3 M_3 t_4 m_4}^{\mathcal{T}' \mathcal{T}_Z} \frac{(\frac{1}{2} + m_i)(\frac{1}{2} + m_j)e^2}{r_{ij}} \end{aligned} \quad (4.22)$$

Expressions of matrix elements in H basis are obtained by repeating the same steps as for the K basis. They read:

$$\begin{aligned} \langle \mathcal{T}'_{iso} | V_C(r_{ij}) | \mathcal{T}_{iso} \rangle &= \sum_{m_1+m_2+m_3+m_4=T_Z} C_{t_1 m_1 t_2 m_2}^{t_x m_x} C_{t_3 m_3 t_4 m_4}^{t_y m_y} C_{t_x m_x t_y m_y}^{\mathcal{T} \mathcal{T}_Z} \times \\ &\quad \times C_{t_1 m_1 t_2 m_2}^{t'_x m_x} C_{t_3 m_3 t_4 m_4}^{t'_y m_y} C_{t'_x m_x t'_y m_y}^{\mathcal{T}' \mathcal{T}_Z} \frac{(\frac{1}{2} + m_i)(\frac{1}{2} + m_j)e^2}{r_{ij}} \end{aligned} \quad (4.23)$$

Non-invariant interactions for rotations in the isospin space break the conservation of total isospin quantum number \mathcal{T} . Therefore the 4-body nucleon states are in general the combinations of $\mathcal{T} = 0, 1, 2$ states. Nevertheless the n+ ${}^3\text{H}$ and p+ ${}^3\text{He}$ systems, with a very high accuracy, can be supposed to be $\mathcal{T} = 1$ states. On one hand it is due to the fact that $\mathcal{T} = 0$ states are forbidden, since z component of this quantum number is $\mathcal{T}_z = \pm 1$ and $\mathcal{T} \geq |T_z|$. On the other hand $\mathcal{T} = 2$ states contributes very little, since triton (or ${}^3\text{He}$) are dominated by the $T_3 = \frac{1}{2}$ state (admixture of $T_3 = \frac{3}{2}$ state contributes less than 0.1% in binding energy, this state occupation probability is even smaller [117]).

The non conservation of the isospin becomes evident, when one has to distinguish between n+ ${}^3\text{He}$ and p+ ${}^3\text{H}$ channels in ${}^4\text{He}$ continuum. Both of these channels are proper to K configurations, whereas they couple each other in isospin basis $|t_x, T_3, \mathcal{T}, \mathcal{T}_z\rangle$. To single out these two channels we introduce a new basis:

$$|\mathcal{T}_{M_3}\rangle = |t_x, T_3, M_3, \mathcal{T}_z\rangle \quad (4.24)$$

For the n+ ${}^3\text{He}$ channel $M_3 = \frac{1}{2}$, whereas p+ ${}^3\text{H}$ is represented by the $M_3 = -\frac{1}{2}$. Therefore these two states are separated in the former basis. Transitions between these two bases are effectuated by means of orthogonal transformation matrix A_{ij}

$$|\mathcal{T}_{iso}\rangle_i = \sum_j A_{ij} |\mathcal{T}_{M_3}\rangle_j. \quad (4.25)$$

The elements of this matrix are:

$$\langle t'_x, T'_3, M'_3, \mathcal{T}'_z | |t_x, T_3, \mathcal{T}, \mathcal{T}_z\rangle = \langle t_x, T_3, \mathcal{T}, \mathcal{T}_z | |t'_x, T'_3, M'_3, \mathcal{T}'_z\rangle = \delta_{t_x, t'_x} \delta_{T_3, T'_3} \delta_{\mathcal{T}_z, \mathcal{T}'_z} C_{T'_3 M'_3, t_4 \mathcal{T}_z - M'_3}^{\mathcal{T} \mathcal{T}'_z} \quad (4.26)$$

Observing the last expression – one can remark that it depends only on three parameters T_3, M_3 and \mathcal{T} . Value of \mathcal{T}_z is fixed by the problem, whereas delta term δ_{t_x, t'_x} can be separated. Therefore the matrix A_{ij} can be represented as a tensor product, whose nontrivial part is the matrix coupling the reduced bases $|T'_3, M'_3\rangle$ and $|T_3, \mathcal{T}\rangle$. One has the following possible states in these bases:

$$|T_3, \mathcal{T}\rangle = \begin{cases} |\frac{1}{2}, 0\rangle \\ |\frac{1}{2}, 1\rangle \\ |\frac{3}{2}, 1\rangle \\ |\frac{3}{2}, 2\rangle \end{cases} \quad \text{and} \quad |T'_3, M'_3\rangle = \begin{cases} |\frac{1}{2}, -\frac{1}{2}\rangle \\ |\frac{1}{2}, \frac{1}{2}\rangle \\ |\frac{3}{2}, \frac{1}{2}\rangle \\ |\frac{3}{2}, -\frac{1}{2}\rangle \end{cases} \quad (4.27)$$

In the presented order of states, the coupling matrix reads as

$$|T_3, \mathcal{T}\rangle = \frac{1}{\sqrt{2}} \begin{bmatrix} -1 & 1 & & \\ 1 & 1 & & \\ & & 1 & 1 \\ & & 1 & -1 \end{bmatrix} |T'_3, M'_3\rangle. \quad (4.28)$$

Inverse of this unitary matrix is its own transpose. For a given ordering of states as in eq. (4.27) this transition matrix is identical to its inverse.

4.4 Convergence

The main technical difficulty one encounters when solving four-body problem using Faddeev-Yakubovski (FY) equations is due to the partial wave convergence of the amplitudes. The spin, the isospin and the angular part of these FY amplitudes are developed (see section 1.2.5) into finite size partial wave basis (PWB). In three-body problem, if one limits the number of partial waves describing interaction, one will have a finite number of relevant partial waves contributing in construction of Faddeev amplitudes. Interactions are usually important only in a few lowest partial waves, therefore results tend to converge and a numerically precise solution can be obtained.

In the 4-body case the situation is different. The number of relevant 4-body partial waves is still infinite once two particle interaction terms are truncated. One is obliged to make additional truncations in order to reduce PWB to a finite size. Still, it is expected that partial waves with large angular momentum have small contributions, due to rapidly (as ℓ^2) increasing repulsive centrifugal terms in the Hamiltonian. However the PWB size required to obtain well converged solutions can be extremely large, knowing the number of degrees of freedom they represent [102][103].

Discussion between Grenoble group [161][122] and Fonseca [162] over *Av.14* realistic potentials ability to describe $n+{}^3H$ total cross section at the peak of the resonance (center of mass energy $E_{cm} = 3$ MeV) is apparently PWB convergence related. Grenoble group solving FY equations

performed calculations without making formal approximations, however their PWB was rather poor. Their results indicate that *Av.14* potential underestimates scattering cross section near the resonance peak. Some NN P -waves present in their PWB had very small contributions. Fonseca calculations are based on Alt-Grassberger-Sandhas (AGS) equations [163][164], but rely on only one rank expansion of the T -matrices. His results are in rough agreement with Grenoble group, when NN P -waves are not present. However NN P -waves tend to become much more important in Fonseca's calculations. By introducing them, the scattering cross sections increase enough to describe almost perfectly the experimental data near the resonance peak.

$j_x \leqslant$	N_{amp}	E (MeV)	$\langle T \rangle$ (MeV)	$\sqrt{\langle r^2 \rangle}$ (fm)
1	10	7.196	44.49	1.81
2	18	7.502	46.13	1.78
3	26	7.594	46.63	1.77
4	34	7.606	46.67	1.77
5	42	7.614	46.70	1.77
6	50	7.615	46.71	1.77

Table 4.2: Convergence of the tritium binding energy, r.m.s. radius and kinetic energy calculations. PWB was truncated by choosing the maximal value of angular momentum j_x . N_{amp} indicates number of partial amplitudes present for a given truncation. Calculations were performed using *Av.18* NN interactions model, supposing that neutron and protons have the same mass corresponding to $\frac{\hbar^2}{m} = 41.471$ MeV · fm².

$j_x \leqslant$	N_{amp}	E (MeV)	$\langle T \rangle$ (MeV)	$\sqrt{\langle r^2 \rangle}$ (fm)
1	10	6.499	43.45	1.85
2	18	6.809	45.11	1.82
3	26	6.897	45.60	1.81
4	34	6.907	45.64	1.81
5	42	6.916	45.67	1.81
6	50	6.917	45.68	1.81

Table 4.3: The same as in Table 4.2 only for ${}^3\text{He}$ bound state. Calculations were performed using *Av.18* NN interactions model, supposing that neutrons and protons have the same mass corresponding to $\frac{\hbar^2}{m} = 41.471$ MeV · fm².

To control the convergence in PWB we have performed several tests. First it is necessary to assure the convergence of 3-particle bound states, needed when implementing boundary conditions. Since ${}^3\text{H}$ and ${}^3\text{He}$ are isospin partners, convergence patterns for these two systems are very similar (see Tables 4.2 and 4.3). In tables 4.2 and 4.4 we present convergence of tritium binding energy calculated using respectively *Av.18* and *Av.18+UIX* models. One can see that a good description of the bound states can be achieved with $j_x \leqslant 4$; inclusion of the 3-body force has overall small effect on the convergence.

Test calculations, in order to compare convergence of 4N results with Fonseca, have been

$j_x \leqslant$	N_{amp}	E (MeV)	$\langle T \rangle$ (MeV)	$\sqrt{\langle r^2 \rangle}$ (fm)
1	10	7.863	48.89	1.740
2	18	8.216	50.35	1.707
3	26	8.444	51.24	1.685
4	34	8.445	51.23	1.685
5	42	8.469	51.28	1.684
6	50	8.468	51.28	1.684

Table 4.4: The same as in Table 4.2 only here *Av.18* model has been used in conjunction with *UIX* three nucleon force.

J_3^Π	l_z	j_z^Π	J^Π
$\frac{1}{2}^+$	0	$\frac{1}{2}^+$	0^+
$\frac{1}{2}^+$	0	$\frac{1}{2}^+$	1^+
$\frac{1}{2}^+$	2	$\frac{3}{2}^+$	
$\frac{1}{2}^+$	1	$\frac{1}{2}^-$	0^-
$\frac{1}{2}^+$	1	$\frac{1}{2}^-$	1^-
$\frac{1}{2}^+$	1	$\frac{3}{2}^-$	
$\frac{1}{2}^+$	1	$\frac{3}{2}^-$	2^-
$\frac{1}{2}^+$	3	$\frac{3}{2}^-$	

Table 4.5: The composition of 4N $J^\Pi \leqslant 2^\pm$ elastic $3 + 1$ channels.

performed using *Av.14* potential. This potential has a similar structure to *Av.18*, except of being charge independent. The small charge independence breaking introduced into *Av.18* has an overall small effect in correcting predictions of nuclear observables. In any case these small terms do not affect general structure of the potential and thus cannot influence much the convergence in partial waves.

At very low energies only positive parity states $\mathcal{J}^\Pi = 0^+$ and $\mathcal{J}^\Pi = 1^+$ contribute. Their construction is rather similar, and therefore the convergence patterns are similar as well. In Table 4.6 we present convergence of $n + {}^3H$ scattering lengths in $\mathcal{J}^\Pi = 0^+$ state, whereas analogous phase shift convergence analysis at $E_{cm} = 3$ MeV is presented in Table 4.7. Convergence was achieved by including tritium amplitudes up to $j_x \leqslant 4$. in the open channel, thus permitting to precisely describe elastic channel and situate the tritium threshold. Other amplitudes were limited by truncating interaction terms and maximal angular momenta j_y and j_z . Calculations for positive parity states are rapidly convergent, very precise values can be already obtained by restricting the interaction terms to P -waves and $j_y \leqslant 1, j_z \leqslant 1$. Increasing the scattering energy does not affect much the convergence, as can be seen by comparing results in the tables 4.6 and 4.7.

Similar analysis has been performed for $n + {}^3H$ phase shifts in $\mathcal{J}^\Pi = 0^-$ state at the center of resonance peak $E_{cm} = 3$ MeV (see Table 4.8). This state contains a broad resonance at $E_{0-} = 5.27$ MeV (see Fig. 4.4). However, the scattering cross section near the peak are influenced mostly by the

0 ⁺ state Interaction terms	$j_y, j_z \leq$	
	1	2
S+ ³ D ₁	4.26	4.24
...+ ¹ P ₁	4.27	4.27
...+ ³ P ₀	4.26	4.26
...+ ³ P ₁	4.28	4.28
S+ ³ D ₁ +P+ ³ F ₂	4.28	4.28
S+P+D+ ³ F ₂	4.28	4.28
S+P+D+ ³ G ₃ +F	4.28	4.28

Table 4.6: Convergence of $n + ^3H$ singlet ($J^{\Pi} = 0^+$) scattering lengths. Calculations were performed using *Av.14* NN interaction model. PWB was truncated in NN interaction waves, as well as imposing limits on j_y and j_z . Former truncations were not applied to open channel, which incorporated all the tritium waves up to $j_x \leq 4$. Presented values are in fm .

0 ⁺ state Interaction terms	$j_y, j_z \leq$	
	1	2
S+ ³ D ₁	-69.95	-69.46
...+ ¹ P ₁	-70.32	-70.47
...+ ³ P ₀	-70.11	-70.03
...+ ³ P ₁	-70.60	-70.52
S+ ³ D ₁ +P+ ³ F ₂	-70.40	-70.25
S+P+D+ ³ F ₂	-70.40	-70.09
S+P+D+ ³ G ₃ +F	-70.40	-70.12

Table 4.7: The same as in Table 4.6 only for $n + ^3H$ scattering phase shifts (in degrees) at $E_n = 3.5 MeV$ (3.0 MeV at center of mass). Additional calculations for $j_y \leq 3, j_z \leq 3$ have given $\delta_{n-^3H} = -70.18^\circ$, thus indicating that calculations with $j_y \leq 2, j_z \leq 2$ are very well converged.

0 ⁻ state Interaction terms	$j_y, j_z \leq$		
	1	2	3
S+ ³ D ₁	23.98	22.52	
...+ ¹ P ₁	23.91	22.21	
...+ ³ P ₀	41.28	39.00	
...+ ³ P ₁	27.76	24.33	
S+ ³ D ₁ +P+ ³ F ₂	27.76	24.42	
S+P+D+ ³ F ₂	27.76	24.66	
S+P+D+ ³ G ₃ +F	27.76	24.66	24.59

Table 4.8: Convergence of n+³H scattering phase shifts (in degrees) at $E_n = 3.5\text{ MeV}$ (3.0 MeV at center of mass). Additional calculation for $j_y \leq 3, j_z \leq 3$ almost has not changed the value, thus indicating that calculations with $j_y \leq 2, j_z \leq 2$ are very well converged .

$\mathcal{J}^{\Pi} = 1^-$ and $\mathcal{J}^{\Pi} = 2^-$ resonances. Convergence is worse than in a case of positive parity states. It is partially due to the presence of $l_z = 1$ waves in the open channel rising the importance of larger angular momentum states through the coupling. However, obviously the major reason is due to the importance of interaction in $NN\mathcal{P}$ -waves, as well as the effect of non-trivial compensations of interactions in ³P₀ and ³P₁ waves. Interaction in \mathcal{D} and \mathcal{F} -waves, unless the tensor coupled ³S₁-³D₁ state, does not seem to be important. One should expand PWB to include $j_y \leq 2, j_z \leq 2$ amplitudes in order to obtain up to 0.25% converged results.

The most complicated convergence one encounters is in $\mathcal{J}^{\Pi} = 1^-$, $\mathcal{J}^{\Pi} = 2^-$ states. Both of these states have tensor force coupled open channels (see Table 4.5), furthermore they contain narrow resonances near $E_{cm} = 3\text{ MeV}$. Moreover one of the open channels already has $j_z = 1.5$ contributions. Therefore it is highly unlikely to achieve convergence with $j_z \leq 2$. We have used different convergence scheme, by truncating maximal values of l_z and l_y instead of truncating j_z and j_y as previously. In Table 4.9 we present the convergence for $\mathcal{J}^{\Pi} = 2^-$ state, contributions of the open channel with $l_z = 3$ at $E_{cm} = 3\text{ MeV}$ are only of order 0.1° and in these calculations were neglected. One can remark very strong contributions of tensor force in \mathcal{P} waves (³P₂-³F₂), which was not the case in $\mathcal{J}^{\Pi} = 0^-, 0^+$ and 1^+ states. This fact complicates calculations by making them much more demanding on *PWB* as previously. Unfortunately, our numerical capacities could not allow to go beyond $l_y \leq 2, l_z \leq 2$, without making additional truncations. Nevertheless calculations with more truncated interaction terms suggest that the results with $l_y \leq 2, l_z \leq 2$ are as accurate as $1 - 2^\circ$. Like in other states, interactions in \mathcal{D} and higher partial waves contribute very slightly.

On the end we have compared convergence with Fonseca calculations [165]. Convergence patterns were similar in positive parity states, as well as our results are still in rather good agreement (up to a few percent difference in phase shifts). The major discrepancies are coming from negative parity states. Still, results were much closer without interactions in $NN\mathcal{P}$ -waves. Introduction of \mathcal{P} -waves one by one show qualitatively the similar trends, however \mathcal{P} -wave compensation effect is considerably weaker in Fonseca results.

One should stress that Fonseca calculations rely on separable approximations of the two-body

2^- state	$l_y, l_z \leqslant$	
Interaction terms	1	2
S+ 3D_1	35.3	36.0
...+ 1P_1	35.4	35.9
...+ 3P_0	35.3	36.4
...+ 3P_1	33.2	32.9
S+ 3D_1 +P+ 3F_2	41.3	43.0
S+D+P+ 3F_2	41.5	

Table 4.9: Convergence of $n+^3H$ scattering phase shifts (in degrees) in 2^- state at $E_n = 3.5$ MeV (3.0 MeV at center of mass).

and three-body T-matrices [166]. It has been demonstrated several times [167] that the predictions based on the separable expansions of T-matrices can be rather accurate. However, such a separable approximation is in general a piece of art. There are no objective criteria, whether the approximation is reliable or not and how far in expansion one should go. Is one rank expansion enough to account for strong compensations in the NN \mathcal{P} -waves? This issue should be verified by extending separable expansions to at least the second rank.

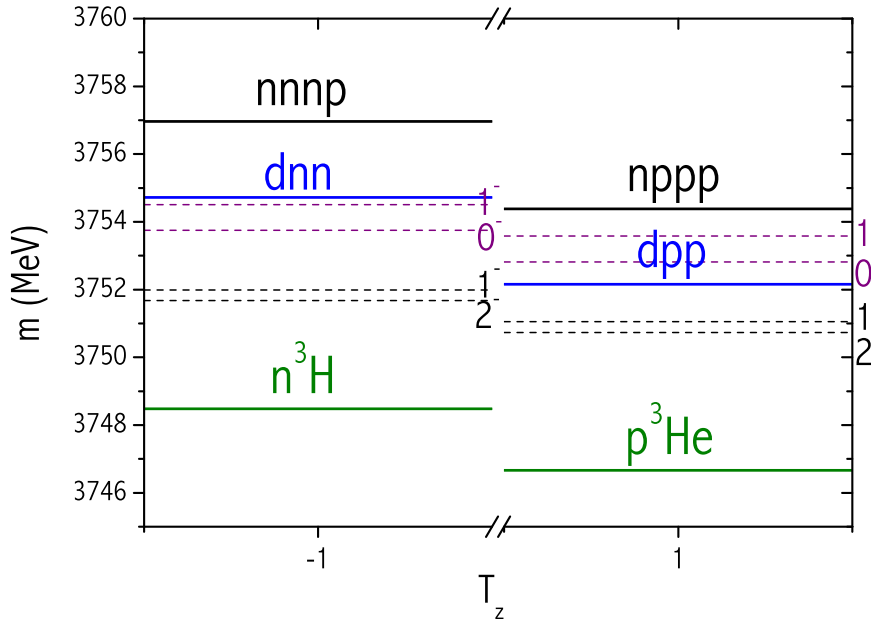


Figure 4.4: Spectra of 4H and 4Li continuum. These two systems are isomers, therefore having similar structure. Comparison of these two systems can be very important in determining CSB in nuclear force. The interesting feature is that Coulomb interaction present in 4Li pushes the broad $J^\pi = 0^-$ and 1^- resonances in-between dpp and 4-particle breakup thresholds.

The previous convergence discussion was based on $n+^3H$ scattering. Analogous convergence

pattern should be expected for its isospin partner p+³He system (note the similar structure of two systems). The slow partial wave convergence is determined by the properties of nuclear potential and the nuclear part of interaction is similar in both cases. The biggest difference in these two systems is due to the presence of Coulomb interactions between protons in p+³He. In the internal region these interactions are weak compared to the nuclear ones, therefore they cannot affect convergence. This has been shown when comparing the convergence of ³H and ³He bound state calculations (see Table 4.2 and 4.3); whereas the open channels asymptotic, where Coulomb interactions are dominant, is described very accurately by using formalism explained in the section 4.2.

4.5 n+³H elastic cross sections

n+³H elastic channel represents the simplest 4N reaction. It is almost pure $\mathcal{T} = 1$ isospin state, free of Coulomb interaction in the final state as well as in the target nucleus. The first calculations of the scattering lengths, using simple interaction models, were already performed in the beginning of the eighties [168][169]. Advances in computation techniques nowadays allow to perform calculations using realistic NN potential models, which have complex structure, as well in conjunction with 3NF. Various model predictions for singlet a_{0^+} and triplet a_{1^+} scattering lengths together with deduced coherent scattering length

$$a_c = \frac{a_{0^+} + 3a_{1^+}}{4} \quad (4.29)$$

and the zero energy cross section

$$\sigma(0) = \pi (a_{0^+}^2 + 3a_{1^+}^2) \quad (4.30)$$

are summarized in Table 4.11. One can remark a very good agreement between the values obtained by different groups, using different numerical methods. Fonseca [170] values were obtained by solving AGS equations, Viviani and collaborators [171][172] used the Correlated Hyperspherical Harmonics Method (CHH), whereas Hoffmans [173] results are based on Resonant Group Method (RGM). The overall agreement in scattering length calculations indicates that theoretical results are well controlled and credible at least for the positive parity states.

Semi-realistic *MT I-III* potential gives slightly too large zero energy cross sections $\sigma(0) = 177$ mb, whereas experiment indicates 170 ± 3 mb [158]. This discrepancy is related to the small overbidding found in tritium and α -particle when using the same potential model.

On the contrary, for the realistic potential models in use, zero energy cross sections become even worse, providing $\approx 12\%$ overestimated values. This failure is not due to a bad choice of realistic NN interaction model. In [122, 174] it has been shown that *Av.14*, *NijmII*, *Reid93* and *Av.18* potentials provide almost identical results, differing only by less than 1%. However, it is remarked, that these 4N scattering lengths are linearly correlated with tritium binding energy, similarly to the well known case of 'Philips line' in n+²H scattering [152]. Underestimation of tritium energy indicates that effective interaction between the nucleons in $A \geq 3$ nuclei is more attractive, as predicted by NN realistic forces alone. On the other hand positive scattering lengths demonstrate

a_0	a_1	a_c	Ref.
3.91 ± 0.12	3.6 ± 0.1	3.68 ± 0.05	[178]
3.70 ± 0.62	3.7 ± 0.21	3.82 ± 0.07	[179]
4.98 ± 0.29	3.13 ± 0.11	3.59 ± 0.02	[180] I
2.10 ± 0.31	4.05 ± 0.09	3.59 ± 0.02	[180] II
4.453 ± 0.1	3.325 ± 0.016	3.607 ± 0.017	[160]

Table 4.10: Experimental values of $n+^3H$ scattering lengths.

$NN + 3NF$	a_{0+}	a_{1+}	a_c	$\sigma(0)$	Ref.
Av.14	4.28	3.81	3.92	194	this work
	4.39	3.89	4.01	203	Fonseca[170]
	4.32	3.80	3.93	195	Viviani[171][172]
Av.18	4.28	3.80	3.92	194	this work
	4.32	3.76	3.90	192	Viviani[171][175]
	4.21(4)	3.65(2)	3.79(3)	181(3)	Hofmann[173][176]
Av.18 + UIX	4.04	3.60	3.71	173	this work
	4.05	3.58	3.71	173	Viviani[175]
	4.00(3)	3.49(1)	3.62(1)	165(2)	Hofmann[173][176]
MTI – III	4.10	3.63	3.75	177	this work
<i>Exp.</i>				170 ± 3	[158]

Table 4.11: Comparison of $n+^3H$ scattering lengths calculated by using different models and obtained by various groups.

that effective $n+^3H$ interaction is repulsive, dominated by Pauli effect between the neutrons. The presence of additional attraction makes smoother this effective potential and that will be reflected in diminished scattering lengths. Therefore adding 3NF, in order to correct tritium binding energy, automatically improves $n+^3H$ zero energy cross section as well.

We have performed calculations using *Av.18* potential model in conjunction with *UIX* 3NF. Partial wave bases, used in these calculations, were selected according to the rules explained in previous section. Such PWB let us have tritium binding energy $E_t = 8.45$ as precise as 30 keV (hence the effect of isospin non-conservation and neutron-proton mass difference gives around 15 keV [117]). The obtained results are compared in the last part of Table 4.11 with other existent calculations. One can quote a very good agreement with Viviani et al. [175] calculations and relatively good agreement with Hofmanns RGM results [176]. The small difference in the last predictions is probably due to the fact that RGM is not very well adapted to work at very low energies. Error bars in former calculations, being induced by the extrapolation used to extract scattering lengths from higher energy results, can be also underestimated.

If the very low energy scattering cross sections are accurately measured and reproduced, situation with scattering lengths looks more precarious (see Table 4.10). The best agreement is found with the results [178]; in fact they contain as a theoretical input ratio a_{1+}/a_{0+} which turns to be

$NN + 3NF$	0^+	1^+	0^-	1^-	2^-	Ref.	
Av.14	-70.2	-62.2	24.7	42.2	21.3	43.0	this work
	-70.3	-64.4	21.2	47.8	26.6	35.4	Grenoble[161] [122]
	-68.4	-63.0	29.7	48.1	23.5	45.8	Fonseca[162] [165]
Av.18	-70.0	-62.3	24.2	41.2	22.3	43.0	this work
	-70.1	-63.9	23.8	~36	~20	~40	Viviani [181]
	-69.5	-61.4	23.5	41.9	22.0	43.6	Hofmann[173][176]
Av.18+UIX	-67.5	-61.3	21.7	41.9	21.5	45.9	this work
	-66.7	-59.1	20.8	41.3	20.9	42.2	Hofmann[173][176]

Table 4.12: Comparison of $n+{}^3H$ scattering phase shifts at $E_n = 3.5 \text{ MeV}$ (3.0 MeV at center of mass) in degrees, calculated by using different interaction models and obtained by various groups. *Values are well converged, however some discrepancies are still present in the 1^- and 2^- states, work to remove these discrepancies is well in progress.*

very close to the one given by the realistic potentials in Table 4.11. The other compatible results are [179]. However, apart from the quite comfortable error bars in a_{0^+} , they have been obtained using a value of $a_c = 3.82 \text{ fm}$, which is in evident disagreement with more recent and precise values of [180]. Finally, as it was pointed out in [175], the experimental value doesn't seem to intersect with the theoretical curve relying $n+{}^3H$ scattering lengths to tritium binding energies.

The usual way to get a_i is by reversing the relations eq. (4.29) and eq. (4.30), respectively giving a_c and $\sigma(0)$. This procedure is numerically quite unstable (see Fig. 4.5). It can be demonstrated in the following way. By fixing the zero energy scattering cross section $\sigma(0)$ one still has a range of permitted values of a_{1^+} and a_{0^+} , which is described by the ellipse slope in $a_{1^+}(a_{0^+})$ plane. Since one has uncertainty in evaluating $\sigma(0)$, the permitted values of scattering lengths will be trapped in-between two ellipse slopes, determined by the minimal and maximal $\sigma(0)$ values (i.e. in-between two red-dotted curves Fig. 4.5). On the other hand, by fixing the coherent scattering length (a_c) - one restricts a_{1^+} and a_{0^+} to values lying on the straight line in $a_{1^+}(a_{0^+})$ plane. Indeed, by assuming an exact value of $a_c = 3.59 \text{ fm}$ (conditioned by the blue dashed line), the small existing error in $\sigma(0)$ leads to two ranges of permitted values $a_{0^+} = [4.7 - 5.2] \text{ fm}$, $a_{1^+} = [3.05 - 3.2] \text{ fm}$ and $a_{0^+} = [2.0 - 2.5] \text{ fm}$, $a_{1^+} = [3.8 - 4.1] \text{ fm}$. In this sense, a more precise measurement of $\sigma(0)$ should be very helpful.

Calculations have been pursued beyond zero energy. Total scattering cross sections can be successfully reproduced up to almost three-body $n+n+d$ breakup threshold (at $E_{cm} \approx 6.2 \text{ MeV}$) with *MT I-III* potential Fig. 4.6. The only small discrepancy is in the $E_{cm} \in [0.04 - 1.5] \text{ MeV}$ region, where experimental data suggest the decrease in the total cross sections, whereas *MT I-III* results remain flat before undertaking the smooth growth towards the resonance peak point. Despite its success, this potential has an evident conceptual problem in neglecting tensor force and thus conserving the angular momentum and the total spin of the system separately. Thus already at its construction the existence of some well known polarization observables (as A_y) is completely ignored. Nevertheless *MT I-III* potential describes surprisingly well the differential cross sections

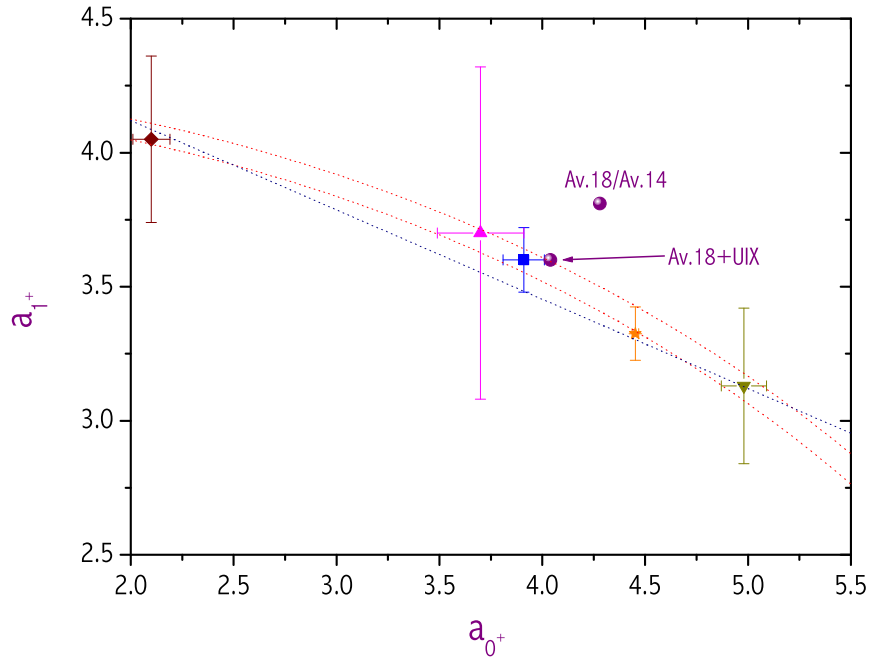


Figure 4.5: Comparison of experimental $n+{}^3H$ singlet (a_{0+}) and triplet (a_{1+}) scattering lengths with theoretically calculated values. Situation with the experimental data is very disturbing: one has direct control of low energy cross sections and coherent scattering lengths in the experiment. Small error bars existent in these measurements cause very big uncertainties in extrapolated singlet/triplet scattering lengths.

Fig. 4.7, being able to reproduce experimental data perfectly within experiment provided error bars. The small underestimation of backward angle differential cross sections at $E_{cm} = 4.5 \text{ MeV}$ can be caused by the impact of \mathcal{F} -waves, not considered in these calculations.

Situation is much more complicated with realistic potential models. As was observed by Grenoble group: although realistic potentials give too large total cross sections at zero energy, they fail to reproduce the experimental results near the resonance peak by underestimating them. Fonseca's claims that $NN \mathcal{P}$ -waves can act constructively and correct the results have not been confirmed by our recent calculations with all the relevant channels added. $NN \mathcal{P}$ -waves increase elastic cross sections in the negative parity states, however seems to have an opposite effect on the positive parity states. Overall gain in the total cross section is rather small.

Although UIX 3NF was able to correct $n+{}^3H$ zero energy cross section, it fails to improve the agreement with experimental data near the resonance peak. On the other hand, one can remark that cross section maxima position is well reproduced by $Av.18+UIX$ model (it was not the case with single NN force). Alternatively to $MT\ I-III$ potential, $Av.18+UIX$ model exhibits a small dip in total cross sections for $E_{cm} \in [0.04 - 1.5] \text{ MeV}$; this dip however is too shallow to follow experimental results. From Fig. 4.8, where influence of \mathcal{S} -waves in total cross sections is presented, it becomes clear that this dip can be reproduced only by further reducing \mathcal{S} -wave cross sections. It is worth noticing that the zero energy scattering lengths are still overestimated by a few percent.

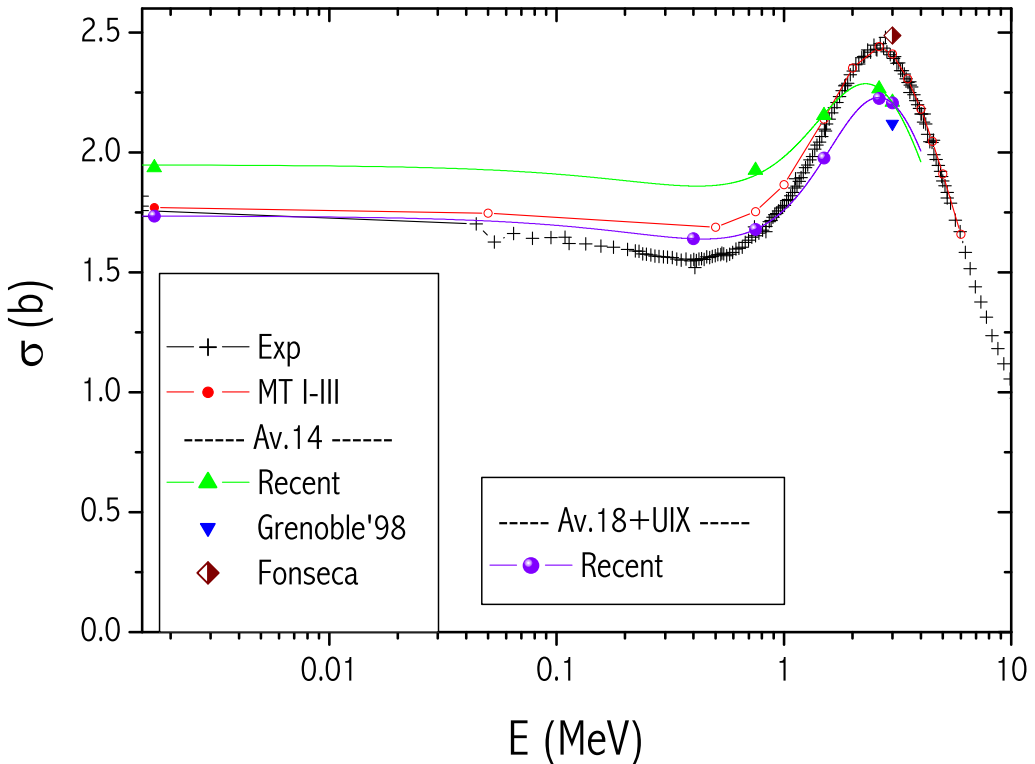


Figure 4.6: Comparison of calculated $n+{}^3H$ total cross sections with experimental data of [158]. Fonseca point is taken from reference [162], Grenoble'98 point is due to Grenoble group calculations of [182][122].

When introducing 3NF, realistic potential predictions for positive parity states become very close to *MT I-III* values. Therefore the principal failure is due to contributions of negative parity states, where series of resonances are present. Comparison of state by state contribution in realistic model cross sections with *MT I-III* results is not easy (see Fig. 4.9). *MT I-III* potential conserves the angular momentum and the spin of the system separately, therefore its 0^- state cross sections are very similar to 2^- state (both being dominated by the $\mathcal{L}=1, \mathcal{S}=1$ state). Thus 0^- state exhibits resonant behavior near the peak, which is not expected by the experimental data. For realistic potential models, this state contributes very little, since the resonance in this state is very broad and situated by a few MeV further in the continuum. One can see that for *Av.18+UIX* model, $\mathcal{J}^\pi = 1^-$ and 2^- cross sections maxima are still shifted to larger energies than in *MT I-III* case, therefore indicating that the resonances are located too far in the continuum. If one manage to locate these resonances properly, their influence for scattering cross sections would be larger and agreement with the experimental data should improve.

The failure of realistic potentials is even more noticeable in the differential cross sections (see Fig. 4.7). Already at the low energies, where the total scattering cross sections are reproduced, *Av.18+UIX* model underestimates backward angle cross sections. At higher energies this tendency becomes even more pronounced. Considering this failure, the description of more sensible polariza-

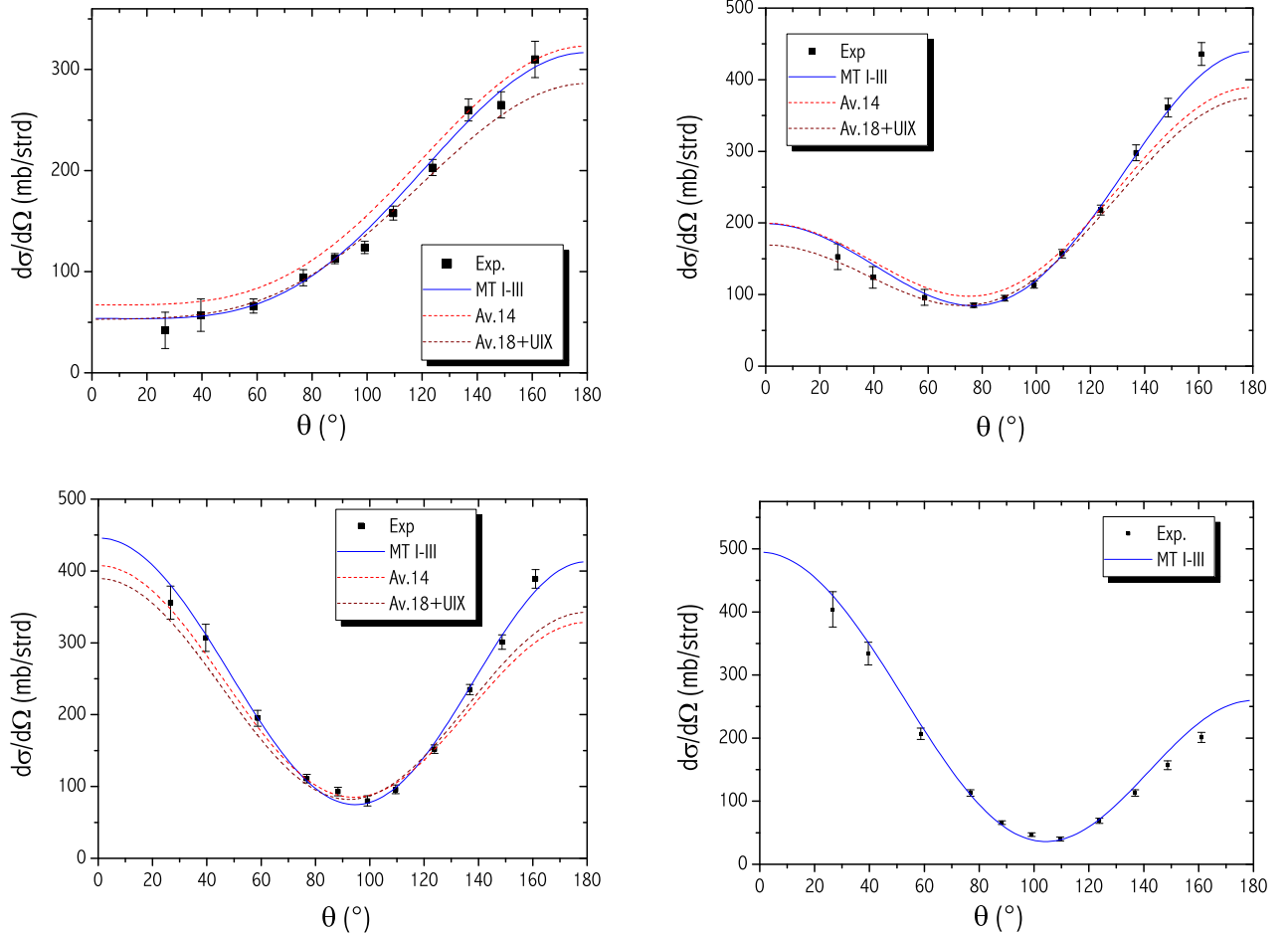


Figure 4.7: Comparison of experimental data [177] and theoretically calculated $n+^3H$ differential cross sections. Figures correspond to center of mass energies: [a] 0.75 MeV , [b] 1.5 MeV , [c] 2.625 MeV and [d] 4.5 MeV . The last figure contains only *MT I-III* model calculations. One can see evident fail of 'so called' realistic potentials. On the other hand, phenomenological *MT I-III* model successfully describes experimental data up to $E_{cm} = 2.625\text{ MeV}$. Small discrepancies appearing for this model at $E_{cm} = 4.5\text{ MeV}$ can be related to the impact of \mathcal{F} -waves, not considered in these calculations.

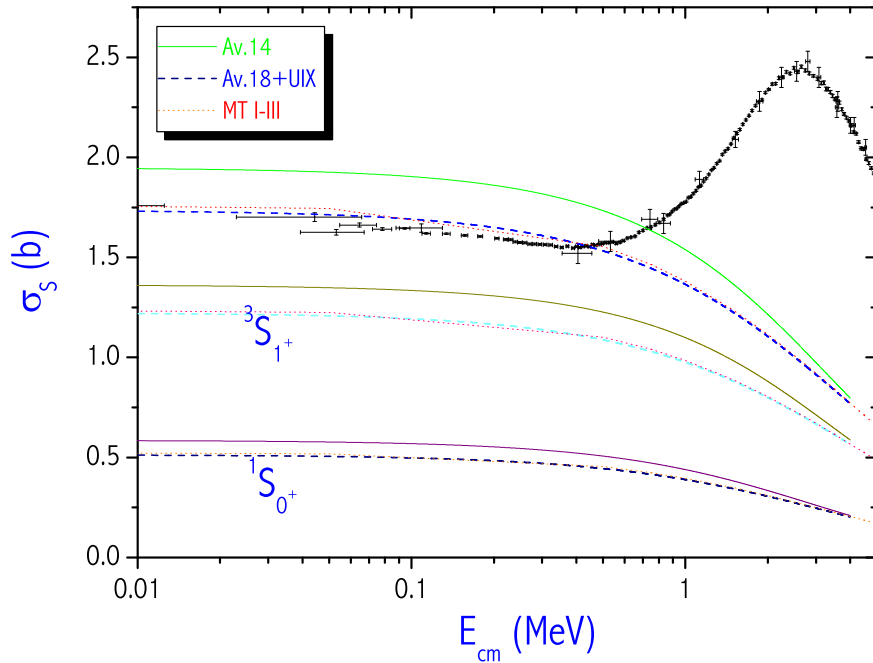


Figure 4.8: Comparison of the positive parity state contributions in $n+{}^3H$ elastic cross sections. By adding 3NF ($Av.18+UIX$) realistic potential predictions become very similar to *MT I-III* results.

tion observables has no sense. These observables are comparably small and much more demanding of accurate nuclear force than the differential cross sections.

Once more, it should be of interest to stress the success of a trivial NN model as *MT I-III* in describing such a non trivial thing as 4N system. This potential acts only in S -waves, has no tensor term, no spin-orbit force, even non-pion tail and the corresponding tritium wave function contains only S -wave Faddeev components. It provides however a very good agreement with the experimental results, specially near the resonance peak and even for differential cross sections, in contrast to its complicated realistic counterparts. Only the zero energy and $E_{cm} \in [0.04 - 1.5] MeV$ dip cross sections are slightly overestimated. In this model the $n+{}^3H$ resonant cross sections has nothing to do with NN P -waves: it is created by the exchange mechanism between incoming and target nucleons. That results into an effective $1 + 3$ potential, which can be successfully generated by only S -wave NN interactions. This furthermore confirms the presence of strong compensation of interaction in higher partial waves. Therefore, nothing is trivial beyond $A = 1$, whereas distinction of the NN interaction from the $N - A$ data is a cumbersome task.

4.6 $p+{}^3He$ low energy scattering

$p+{}^3He$ is an isospin partner of $n+{}^3H$ system, the principal difference of two systems coming from the Coulomb interaction acting between the protons. $p+{}^3He$ scattering presents fundamental interest, since it is the richest composite nuclear system in protons (having proton excess ratio

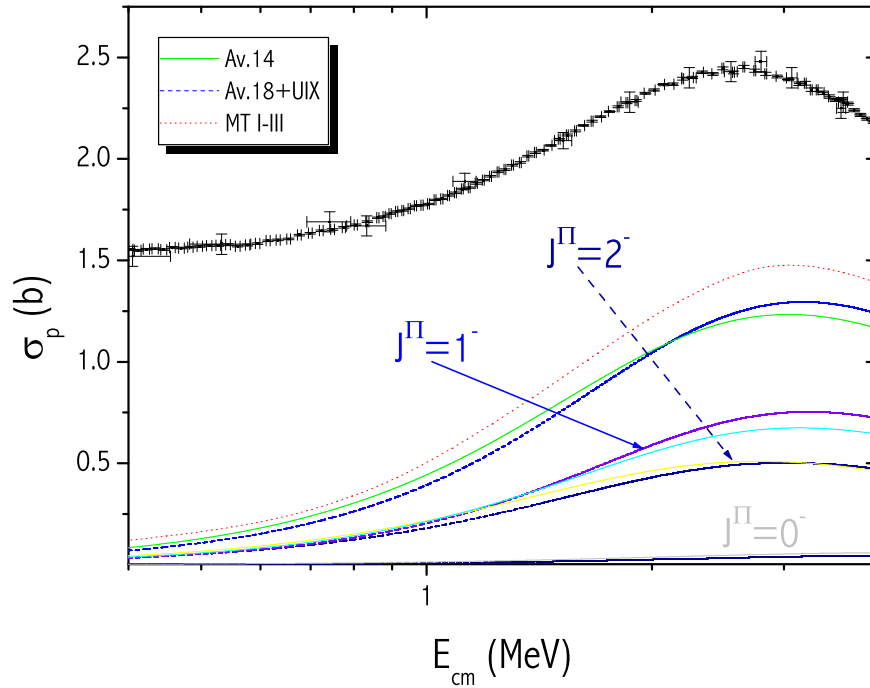


Figure 4.9: Comparison of the negative parity state contributions in $n+{}^3H$ elastic cross sections. For *MT I-III* potential only collective contribution of all these states is plotted.

equal to $\eta_p = 0.5$), displaying such dynamical structures as resonances. There are no nuclei with proton excess ratio so high. Moreover the comparison of $p+{}^3He$ and $n+{}^3H$ scattering spectra is a perfect ground for CSB analysis in nuclear force. Experimentally, this system is more accessible than $n+{}^3H$, since it is easier to produce and to control proton beams, as well as later on detect proton recoils. However experimental data badly suffers from Coulomb effects, which dominates scattering at forward angles as well as at very low energies. Pure Coulomb scattering amplitude

$$f_C = -\frac{\gamma}{2k \sin^2 \frac{\theta}{2}} \exp \left[-i\gamma \ln \left(\sin^2 \frac{\theta}{2} \right) + 2i \arg \Gamma(1 + i\gamma) \right] \quad (4.31)$$

becomes infinite when $\theta \rightarrow 0$, as well when $E \rightarrow 0$. One cannot control the total cross sections, due to Coulomb divergencies in forward angle direction. Analysis of scattering lengths is also very complicated, for it requires non-trivial extrapolation procedure from low energy scattering data. Therefore one has very high uncertainty in very low energy experimental predictions.

Theoretically we calculate scattering lengths by directly performing zero energy calculations. By using analytical zero energy limit expressions of Coulomb wave functions with singularities factorized out, we implement boundary conditions as in eq. (1.60). Therefore we do not encounter extrapolation problem as in experimental data analysis.

Our calculated scattering lengths with *MT I-III* potential falls in-between experimental points. These results, however, are in disagreement with calculations of Yakovlev and Filikhin [183]. In their calculations, restrictions to S -waves were made and further cluster reduction method was

$l_x \leq$	$l_y \leq$	$l_z \leq$	a_{0+}	a_{1+}
0	0	0	11.54	9.551
0	1	1	11.47	9.170
1	1	0	11.56	9.565
1	1	1	11.49	9.200

Table 4.13: Results of scattering lengths for $p - {}^3He$ system calculated using MT I-III potential with truncated PWB. One can see that results are well converged with $(\ell_x, \ell_y, \ell_z) \leq 1$.

NN+3NF	a_{0+}	a_{1+}	Ref.
<i>MT I-III</i>	11.49	9.20	this work
	8.2	7.7	Yakovlev[183]
<i>Av.18</i>	12.7		this work
	12.9	10.0	Viviani [175]
<i>Av.18+UIX</i>	11.3		this work
	11.5	9.13	Viviani [175]
Exp.	10.8 ± 2.6	8.1 ± 0.5	[184]
		10.2 ± 1.5	[185]

Table 4.14: Comparison of the calculated $p + {}^3He$ scattering lengths.

used to solve FY equations. Such a reduction is a crude approximation and, even without taking Coulomb interaction into account, it introduced some discrepancies in the results [186]. Even more doubtful is the evaluation of Coulomb integrals by former authors. These integrals were calculated by making questionable approximations when expanding Coulomb terms in non-proper coordinate bases.

On the contrary, MT I-III scattering lengths are very close to the ones calculated with *Av.18+UIX* model, as should be expected from their agreement in $n + {}^3H$ scattering lengths. CSB breaking is rather small in *Av.18 NN* force, whereas is not present neither in *UIX 3NF* nor in *MT I-III* models. Concerning realistic model calculations of scattering lengths, we are in very good agreement with Viviani et al. results [175], both for *Av.18 NN* alone as well as including *UIX 3NF*. Our values are slightly smaller than Viviani's, similarly as in $n + {}^3H$ case.

Finally, we have expanded calculations to the energies greater than zero. Yet, calculations have been performed by using *MT I-III* model only. Results are accumulated in Table 4.15. We have compared the obtained differential cross sections with the experimental data from [188, 187] in Fig. 4.10 [a]-[e]. This data is reproduced perfectly by *MT I-III* potential, even better than in $n + {}^3H$ case. One can remark the importance off D -waves ($\mathcal{L}=2$ states) in reproducing forward angle differential cross sections for energies above $E_{cm} = 3.0$ MeV. Similar effect was remarked in $n + {}^3H$ differential cross sections, although contribution of D waves was negligible in the total cross sections.

Viviani et al. [175] have calculated these differential cross sections using realistic *Av.18* and

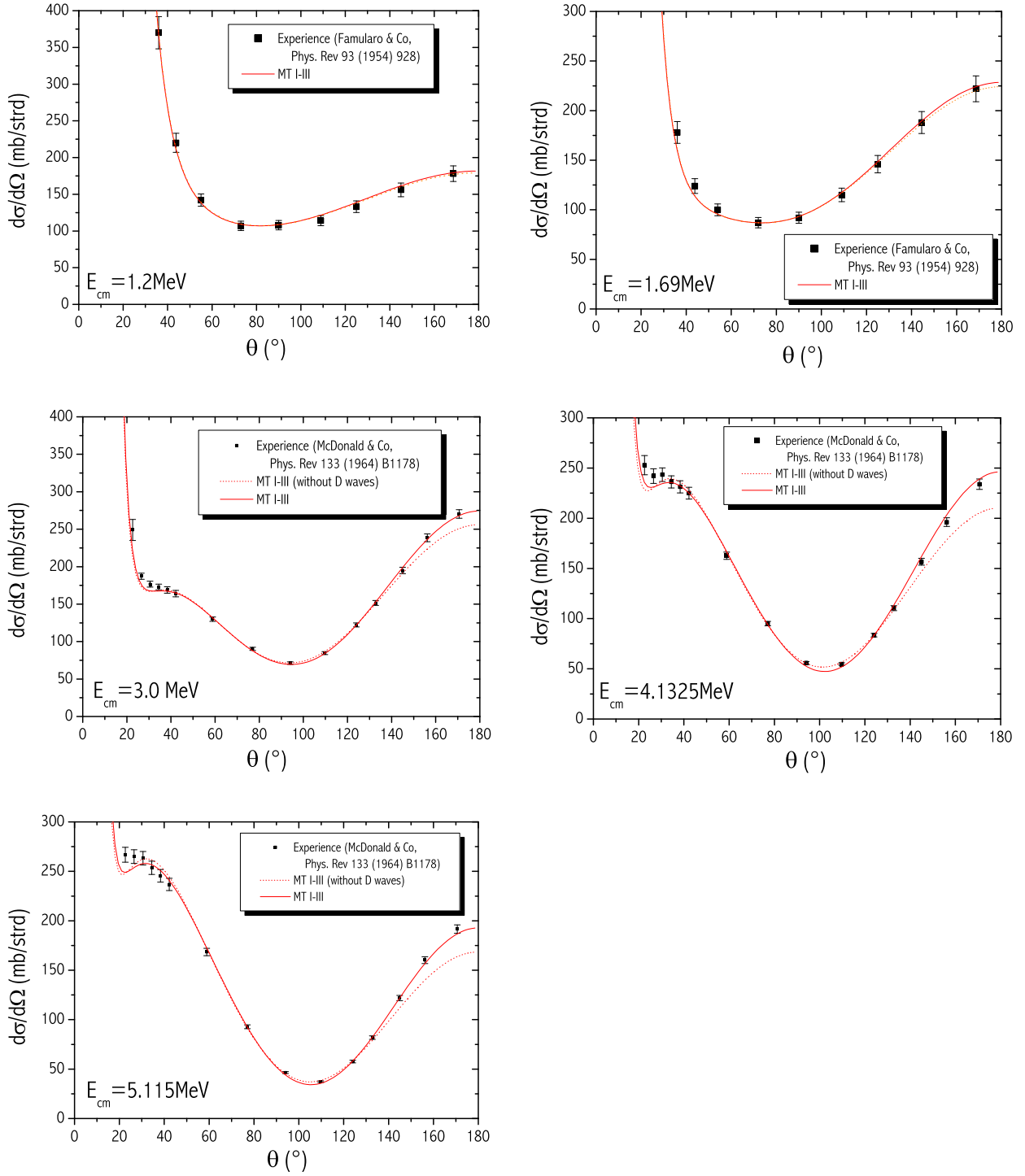


Figure 4.10: Differential cross sections in $p+{}^3He$ elastic scattering calculated using *MT I-III* model. Obtained results are compared with the experimental data from [187] and [188].

E_{cm} (MeV)	$\mathcal{S}=0$			$\mathcal{S}=1$		
	$\mathcal{L}=0$	$\mathcal{L}=1$	$\mathcal{L}=2$	$\mathcal{L}=0$	$\mathcal{L}=1$	$\mathcal{L}=2$
0.05	-0.093			-0.075		
0.1	-0.838			-0.683		
0.2	-3.79	0.188		-3.14	0.166	
0.5	-13.9	1.56		-11.8	1.48	
0.7575	-21.2	3.55		-18.2	3.52	
1.2	-31.3	7.81		-27.1	8.36	
1.69	-40.0	13.1		-34.9	15.1	
3.00	-56.6	24.7	-1.06	-50.2	33.4	-0.58
4.1325	-66.9	30.8	-2.22	-59.7	44.0	-1.5
5.115	-74.0	34.2	-2.10	-66.3	49.6	-1.27

Table 4.15: Phase shifts in degrees calculated for p+ 3 He system using *MT I-III* potential model.

Av.18+UIX models at relatively low energies ($E_{cm}=1.2$ MeV and 1.69 MeV). By comparing their realistic model results with our *MT I-III* calculations, one should remark that *MT I-III* still describes the experimental data in a much better way. *Av.18* potential, without 3NF, provides too large differential cross sections at $E_{cm} = [1.2 - 1.69]$ MeV near the distribution minima centered around $\theta \approx 70 - 80^\circ$. By including 3NF, differential cross section behavior near the minima is corrected, however backward cross sections become underestimated. Note that n+ 3 H differential cross sections suffer from the same effect. Smaller discrepancies in realistic model predictions for p+ 3 He differential cross sections, compared to n+ 3 H results, could be just an artifact of resonance being situated further from the 3 He threshold (see Fig. 4.4). The relative shift of 4 Li spectra is almost 900 keV, therefore energies $E_{cm} = [1.2 - 1.69]$ MeV should correspond to $E_{cm} \lesssim 0.79$ MeV in n+ 3 H. This region, being closely related with successful positioning of 3-body bound state, is rather well described by *Av.18+UIX* model. The real challenge in p+ 3 He continuum states is to describe nearesonance region being situated at $E_{cm} \approx 4$ MeV.

4.7 p+ 3 H scattering at very low energies

4 He continuum presents probably the most complex 4N system, and its spectrum contains numerous resonances Fig. 4.11. Calculations of p+ 3 H scattering are furthermore complicated by the existence of the first $\mathcal{J}^\Pi = 0^+$ excitation of 4 He in its thresholds vicinity. This resonance located at $E_R = 0.4$ MeV above p+ 3 H threshold covers with its width $\Gamma = 0.5$ MeV the almost entire region below n+ 3 He threshold.

It turns out that most of the calculations performed until now find this state below the p+ 3 H threshold, locating it as a second 4 He bound state. The failure of these calculations is due to the exclusion of Coulomb interaction. In this way, p+ 3 H and n+ 3 He thresholds coincide, whereas 4 He resonant state is pushed bellow this degenerate threshold becoming a bound state (see Fig. 4.13). Depending on nuclear interaction model considered, one finds the binding energy of $B_{\alpha^*} =$

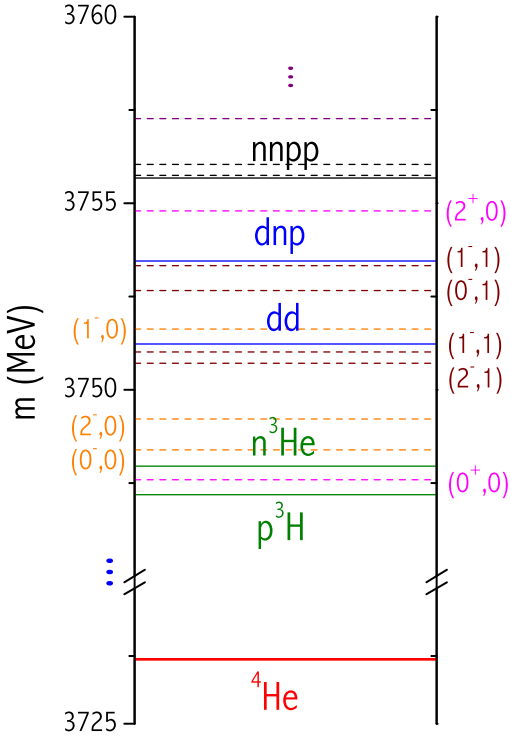


Figure 4.11: Spectra of ${}^4\text{He}$. Single lines represent existing thresholds, whereas dashed lines signify α -particle resonant states. Corresponding values of angular momentum, parity and isospin ($\mathcal{J}^\Pi, \mathcal{T}$) are noted besides.

$[0.25 - 0.4] \text{ MeV}$. Thus, the sign of the strong $\text{p} + {}^3\text{H}$ singlet ($\mathcal{J}^\Pi = 0^+$) scattering length is found positive.

Low energy $\text{p} + {}^3\text{H}$ differential cross sections are dominated by long range Coulomb forces, thus hiding effects due to strong interaction. Non rigorous attempt to describe these cross sections can be performed by using pure strong interaction phase shifts (although they were calculated excluding Coulomb interaction) and then correcting scattering amplitudes by adding analytical expression of Coulomb amplitude. This approach corresponds to scattering, where one supposes that in the internal 4-body region (where all four particles are coupled by the strong interaction) Coulomb interactions are not present. Outside the range of strong interaction, $\text{p} + {}^3\text{H}$ channel is propagated by switching on Coulomb repulsion between receding proton and tritium nucleus. The $\text{p} + {}^3\text{H}$ amplitude reads as

$$f(\theta) = f_c(\theta) + f_s, \quad (4.32)$$

where f_s is the strong amplitude and $f_c(\theta)$ is the pure Coulomb term, the analytical expression of which was given in eq. (1.37). The *MT I-III* model results obtained using this approach are presented in Fig. 4.13 by an orange dashed line. The experimentally observed resonant structure is not reproduced. Instead one has smoothly decreasing differential cross sections. Even at higher energies, when one gets out of the resonance region, the total cross sections are considerably

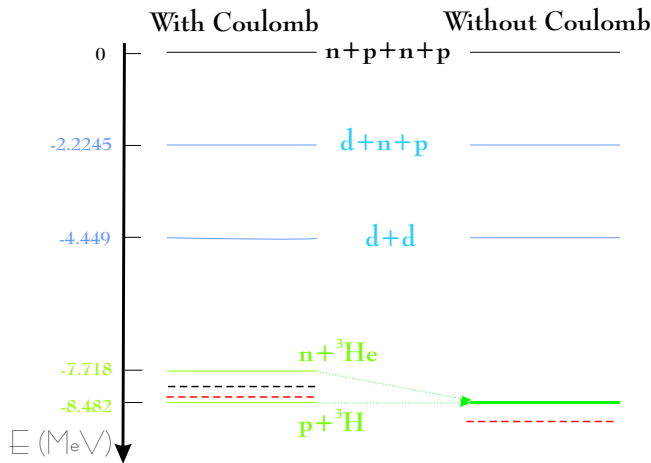


Figure 4.12: Spectra of ${}^4\text{He}$, once with Coulomb interaction considered and once by neglecting it. Red dashed lines indicate the placement of α -particle excited state as obtained by using *MT I-III* model in both cases.

underestimated. In addition, non-existence of $n+{}^3\text{He}$ threshold in this approach further disregards the correct description of the experimental data. Two other resonances ($\mathcal{J}^\Pi = 1^-$ and $\mathcal{J}^\Pi = 2^-$), situated in the vicinity of this threshold, won't be properly placed.

Keeping in mind the very fine structure of thresholds and resonances in ${}^4\text{He}$ continuum, one is obliged to introduce an exact formalism in order to describe this system properly. As was demonstrated, any approximation or inaccuracy made in the theoretical model can lead into misleading conclusions. On the other hand, the complexity of this system makes it the ideal testing ground for NN interaction models.

The major step in the formalism is the inclusion of Coulomb interaction so that to be able to separate $n+{}^3\text{He}$ and $p+{}^3\text{H}$ thresholds. Hence, the standard model of calculating effective Coulomb interactions applied in ${}^3\text{He}$ bound state or $p+d$ scattering calculations is not appropriate here, since one has to separate two Coulomb degenerate channels. This non-trivial issue was discussed in section 4.3.

Scattering length results, obtained after implementing full treatment of Coulomb interaction with *MT I-III* potential are summarized in Table 4.16. One obtains a negative scattering length in 0^+ state, thus indicating that the α -particle excitation is a resonant and not a bound state, as it was erroneously predicted when neglecting Coulomb interactions. However its very large value $a_{0^+} = -63.1$ fm (expected to be $a_0 \approx [-16, -22]$ fm by the experiment) indicates that this resonance is placed too close to $p+{}^3\text{H}$ threshold. Simple evaluations give resonance being placed by only $E_R \approx 70$ keV above this threshold.

The only known calculations of $p+{}^3\text{H}$ scattering lengths with Coulomb separated thresholds and using *MT I-III* potential, were performed by Yakovlev and Filikhin [189], finding $a_{0^+} = -22.6$ fm and $a_{1^+} = 5.2$ fm. We are in strong disagreement with calculations of former authors for a 0^+ state, although their a_{0^+} scattering length fits well the experimental data. By comparing our results, it

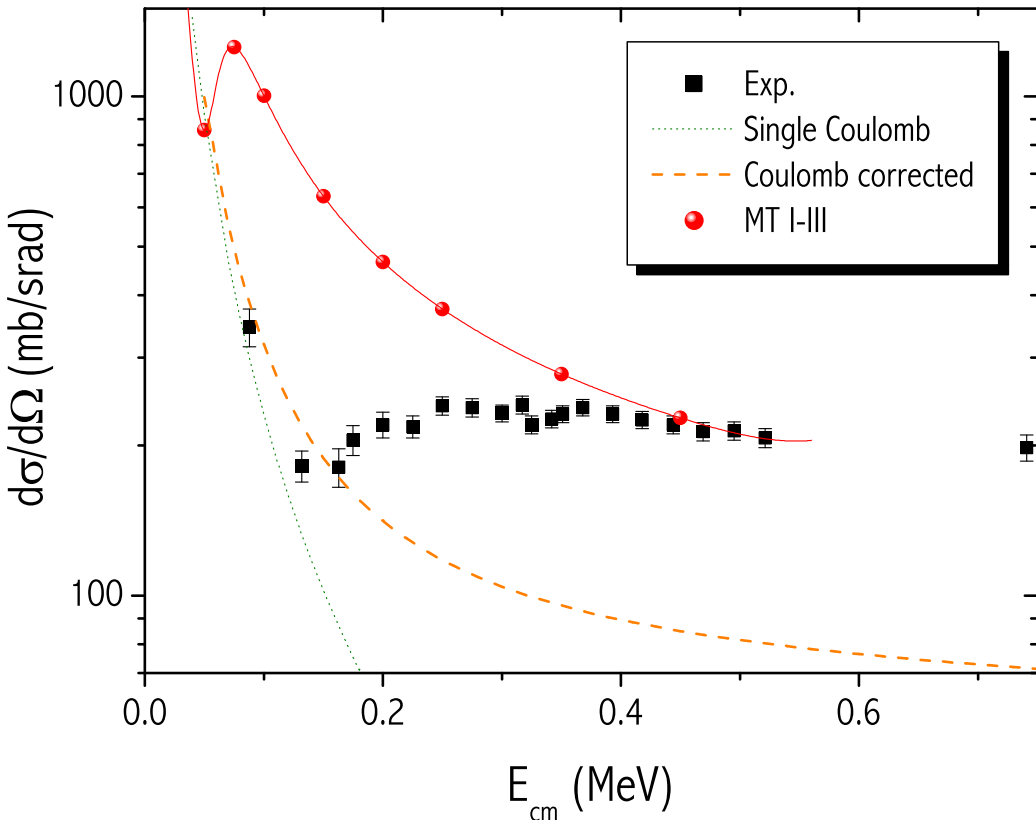


Figure 4.13: $p + {}^3\text{He}$ elastic scattering differential cross sections: experimental results are compared with calculation in which Coulomb interaction was neglected in nuclear region, whereas outside range of nuclear interaction phases were propagated by switching on Coulomb between the scattered clusters (orange-dashed line). Red curve in conjunction with red points disclose our *MT I-III* results, where full Coulomb interaction treatment was considered. Dark green dot line shows cross sections given by single Coulomb interaction taken into account.

can be remarked, like in $p + {}^3\text{He}$ case that [183], Yakovlev and Filikhin find effective interaction of proton with target nucleus being more attractive. This can be due to the approximations that the former authors indulged in calculating Coulomb terms by former authors.

The huge $p + {}^3\text{H}$ singlet scattering length value can be explained by the fact that *MT I-III* potential overbinds α -particle. Note this potential predicts the binding energies much better than any realistic NN interaction model alone (without $3NF$). However relative overbinding of α -particle is considerably stronger than the tritium one. This can be seen from well known Tjon line [157] (see Fig. 4.3), presented in the beginning of this chapter. Predictions of *MT I-III* potential are off this line, placed in overestimated α -particle direction, in spite being very close to the experimental point. Since α -particle is relatively overbound, its excitation is expected to be overbound as well. Experimentally, the ${}^4\text{He}$ resonance is at $E_R \approx 0.4 \text{ MeV}$ (above triton energy), *MT I-III* potential (overestimating it) will push it closer to tritium threshold. Therefore by $\approx 0.33 \text{ MeV}$ overestimated α -particle excitation is compatible with $\approx 0.7 \text{ MeV}$ overestimation found in

its ground state.

	$\mathcal{J}^{\Pi} = 0^+$	$\mathcal{J}^{\Pi} = 1^+$
<i>MT I-III</i>	-63.1	5.50
<i>Av.14*</i>	-11.7	6.04
<i>Av.18+UIX*</i>	-12.1	5.39
<i>Av.14</i>	-13.9	5.77
<i>Av.18+UIX</i>	-16.5	5.39

Table 4.16: Comparison of $p+{}^3H$ scattering lengths in fm for *MT I-III*, *Av.14* and *Av.18+UIX* interaction models. *Av.14** and *Av.18+UIX** lengths correspond to the calculations with the smaller PWB, whereas *Av.14* and *Av.18+UIX* results are the most complete.

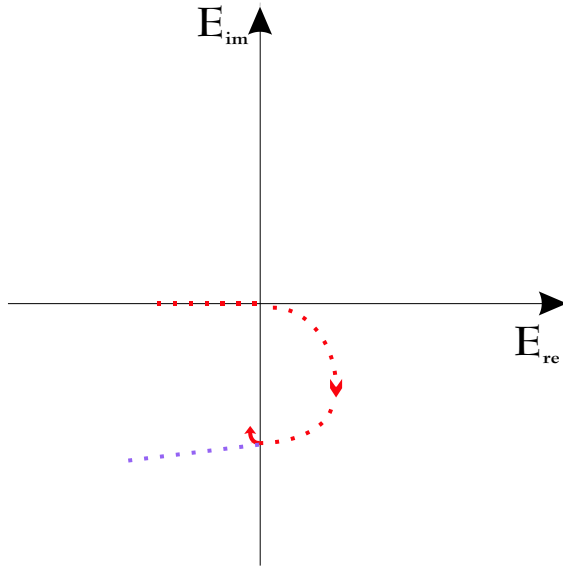


Figure 4.14: Trajectory of S-matrix pole in the complex energy plane.

Calculations were extended to higher energies still staying in within threshold region. Obtained results were compared with experimental results for differential cross sections at $\theta = 120^\circ$ in Fig.4.13. One can clearly see that the α -particle resonance predicted by *MT I-III* potential is situated not only too close to the threshold but has very small width as well. It is not surprising, if one recalls the trajectory of the singularity in complex energy plane [190] (see Fig. 4.14). For sufficiently attractive interaction, this singularity is on the negative part of the real energy axis (representing a bound state). By reducing the attraction in the potential this singularity will move towards zero, still remaining on the axis. At the zero energy it will move to complex energy plane, thus becoming a resonant state with positive energy E_{Re} and width $\Gamma = E_{Im}$. Since this trajectory is smooth, one should expect smaller widths for resonances situated closer to the thresholds.

Finally one can see that out of the resonance region theoretical scattering cross sections approach the experimental values, which was not the case in Coulomb interaction neglecting model.

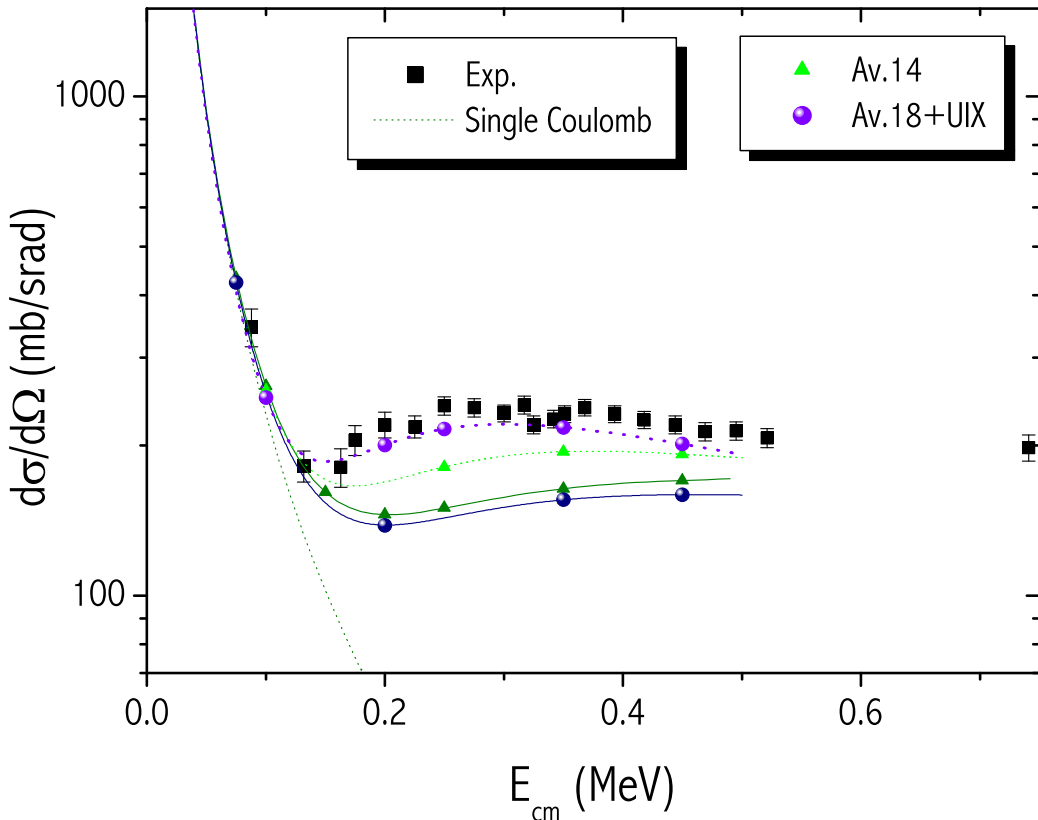


Figure 4.15: $p+{}^3He$ elastic scattering differential cross sections: experimental results are compared with our calculation using *Av.14* and *Av.18+UIX* interaction models, with complete treatment of Coulomb interactions. Dotted curves in conjunction with data points indicate our the most complete PWB calculations, whereas single line results were obtained without partial waves containing $l_z = 2$. Dark green dotted line shows cross sections given by single Coulomb interaction present.

Therefore near $n+{}^3He$ threshold behavior is expected to be well reproduced and this represents a very positive result. This work is expected to be accomplished in the nearest future.

Calculations using realistic interaction models were performed as well. However due to the necessity to calculate time-demanding Coulomb integrals, we were limited to rather small partial wave basis. Expansion of PWB was additionally limited by the fact that in order to distinguish $n+{}^3He$ and $p+{}^3H$ we had to incorporate all the isospin ($T=0,1,2$) states, roughly doubling its size. The first essay was done with the PWB as in previous case containing open channel triton (3He) amplitudes up to $j_x \leq 4$, however other amplitudes were limited to $l_y \leq 2$ and $l_z \leq 1$ and interaction terms up to \mathcal{P} -waves. Results with this limited PWB using *Av.14* model as well as *Av.18* in conjunction with *UIX 3NF* are presented in Table 4.16- 4.17 and Fig. 4.15. Additional calculated values by considering *Av.18 NN* model, without 3NF interaction, have given results coinciding with those of *Av.14* by more than two significant digits. The 0^+ state scattering lengths are negative, therefore indicating that resonance is well situated in-between thresholds. They are smaller than expected by the experiment showing that the resonance is located too far from $p+{}^3H$

	MT I-III		Av.14		Av.18+UIX	
	$\mathcal{J}^\Pi = 0^+$	$\mathcal{J}^\Pi = 1^+$	$\mathcal{J}^\Pi = 0^+$	$\mathcal{J}^\Pi = 1^+$	$\mathcal{J}^\Pi = 0^+$	$\mathcal{J}^\Pi = 1^+$
0.01	0.123	-9.88×10^{-3}	2.46×10^{-2}	-1.03×10^{-2}	2.92×10^{-2}	-9.21×10^{-3}
0.02	1.833	-0.1213	0.3169	-0.1263	0.379	-0.1136
0.05	35.14	-1.107	3.343	-1.153	4.074	-1.056
0.075	84.78	-2.228	7.425	-2.319	9.174	-2.151
0.1	-76.13	-3.400	12.23	-3.536	15.25	-3.310
0.25	-67.59	-9.760	41.27	-10.14	49.60	-9.690
0.45	-69.91	-16.20	65.19	-16.71	71.20	-15.94

Table 4.17: Comparison of p+ ${}^3\text{H}$ scattering nuclear phaseshifts in degrees for *MT I-III*, *Av.14* and *Av.18+UIX* interaction models. *Av.14* and *Av.18+UIX* phaseshifts correspond the calculations with the most complete PWB used.

threshold. On an other hand the scattering observables in 1^+ state, not exhibiting resonance, were compatible to *MT I-III* predictions. With this PWB, 3NF had an overall small, however positive, effect in correcting results.

As was observed in [103, 3] α -particle bound state calculations are very PWB demanding. The sensible state in p+ ${}^3\text{H}$ scattering calculations: $\mathcal{J} = 0^+$ is the α -particle state. Therefore non-surprisingly slow convergence remains. Quoting that α -particle is very sensible to the presence of FY amplitudes with $l_z = 2$ we have added the most contributing $l_z = 2$ amplitudes into our PWB (these amplitudes principally contained NN tensor force terms in ${}^3\mathcal{S}_1$ - ${}^3\mathcal{D}_1$ waves). With this PWB, results are considerably improved (see last two lines of Table 4.16). Furthermore, 3NF started to contribute considerably in correcting results as much as did it the PWB expansion in the calculations with NN forces alone. Singlet scattering length, obtained using *Av.18+UIX* model is very close to the value expected by the experimental data analysis.

In Fig. 4.15 we present differential cross sections calculated at higher energies. The *Av.18+UIX* model describes the experimental data very well. NN interaction model alone places resonance too far from p+ ${}^3\text{H}$ threshold, therefore underestimating cross sections at the resonance, and failing to reproduce its shape. All the calculated curves tend to join the experimental data points near the n+ ${}^3\text{He}$ threshold, therefore indicating success in locating and describing it. Similar calculations were preformed by Hoffman using RGM method [191]. Their *Av.18* curve resembles the one we obtained with *Av.14* potential (note the similarity of *Av.14* and *Av.18* potential predictions for scattering lengths). However once 3NF is included, results of former author starts considerably overestimate the experimental data by visibly placing the resonance too close to p+ ${}^3\text{H}$ threshold (similarly as we had in case of *MT I-III* potential). The problems can be due to the fact that former calculations were also limited in PWB and to peculiarities related with the RGM applicability to describe low energy scattering.

In conclusion, one should admit that p+ ${}^3\text{H}$ results are very promising. PWB has still to be further expanded to guarantee the better converged results. Nevertheless it was demonstrated that *Av.18+UIX* model is able to describe low energy behavior of p+ ${}^3\text{H}$ scattering, as well as to place

fine structure resonance in-between the thresholds.

Curiously realistic potential model seems to do well in describing such accuracy requiring system as $p+^3H$ when it fails in visibly less complicated $n+^3H$ case. On the contrary, semi-realistic *MT I-III* model describes well $n+^3H$ and $p+^3He$ systems, whereas fails in $p+^3H$. A possible explanation could be inaccuracy of realistic NN force models, when describing isospin breaking effects. Note, that $n+^3H$ has a very large neutron excess ratio, being equal 0.5. The only nucleus having such large ratio is 8He . As was discussed in previous chapter and demonstrated in figure 4.1, *Av.18+UIX* model badly suffers in describing neutron rich nuclei as well as when moving away from the stability valley. These observations forced Illinois group [4] to make isospin dependent modifications in 3NF. Are these modifications sufficient, or they manifest a kind of Sisyphus effect when constructing so called realistic nuclear interaction models. First, one has fitted NN force to describe $2N$ observables. However, it became soon evident that these forces begin to suffer already for $A \geq 3$. 3NF was introduced to correct 3 and 4-body bound states, but it fails for 4N continuum as well as for neutron rich nuclei with $A \geq 5$. Recently a big advance was achieved by adapting 3NF to describe nuclear energies up to $A = 8$, however results for nuclei with $A \geq 9$ remain controversial. Are all these discrepancies related to the numerical accuracy only?

4N continuum calculations are very useful here, they represent a comprehensive test of nuclear interaction models. Whereas from a practical point of view – although these calculations are cumbersome and computer time demanding – the required calculation time is by one order less important than the one needed in calculating binding energies of the nuclei with $A \geq 8$.

Conclusion

This thesis concentrates on non-relativistic quantum mechanical " Few-body problem ". The major goal of " Few-body" formalism is to obtain mathematically correct and computationally tractable equations describing exactly processes in a few particle systems (number of particles $N > 2$), for any assumed interaction between them. To obtain Quantum mechanical solutions standard formalism of the Schrödinger equation is not enough, it suffers from several formal and/or practical anomalies, since one is not able to describe the richness of available processes in systems with $N > 2$ by means of a single equation. The mathematically rigorous equations for three particle systems, constrained by short-range pair interactions, were formulated by Faddeev [9]. Ideas of Faddeev, were later generalized by Yakubovski [15] to describe systems with any number of particles. Long range interactions, in particularly Coulomb, presents special difficulties in the scattering theory. The formalism of Faddeev-Yakubovski equations becomes not appropriate. Nevertheless, below the particle break-up threshold, one can still incorporate Coulomb interaction into Faddeev equations in Merkuriev proposed way [10]. In this thesis four particle Faddeev-Yakubovski equations have also been modified to enable treatment of Coulomb interactions. The few-body formalism is very general and therefore can be applied in several fields of theoretical physics. This fact is reflected in the manuscript, where original results were obtained for atomic-molecular as well as for nuclear systems.

In a framework of molecular physics I have studied heavy positive charge particle scattering on the Hydrogen atoms. It is the first time when scattering lengths for $\mu^+ - H$, $\pi^+ - H$ and $p^+ - H$ systems were rigorously calculated. Proton scattering on hydrogen atom presents a special interest as well from the theoretical as from the experimental point of view. The large scattering length found for proton spin triplet configuration, indicates an existence of the first excited H_2^+ ions $\mathcal{L} = 0$ $2p\sigma_u$ symmetry state. By using modified effective range theory we were able to extract its binding energy from our low energy scattering results. This is the weakest bound ever predicted. Effect of the most important relativistic and QED corrections have been estimated. These corrections have been found to be too weak to destroy the state.

Inspired by the recent experiment at GANIL [2, 11], which once again raised doubts on possible existence of bound few neutron systems, I have tried to answer whether such the systems (trineutron, tetraneutron) are compatible with what we know of strong interaction and what necessary corrections should be made to permit such an existence. Sensibility of (n=2, 3, 4) neutron systems to modifications in nucleon-nucleon (NN) force, as well as effects of 3-4 nucleon forces were

examined. This study has shown that such structures can be formed only at the price of very strong violations in nuclear force. Such violations can hardly be tolerated from the point of view of nuclear interaction underlying theory, as well as being in strong disagreement with other observed nuclear properties (like nuclear matter density or the energy chart of stable nuclei). Therefore possible existence of bound 2n , 3n or 4n systems is excluded, existence of even larger multineutron structures seems very doubtful.

Neutron systems have been compared to other fermion system having resembling interaction, however eventually forming bound multifermion clusters (namely with clusters of He_3 molecules). It has been shown that the principal difference in two systems is due to interaction in \mathcal{P} and higher partial waves, which in contrary to bosonic systems, plays a major role in multifermion systems. These interactions, due to presence of angular momentum, come together with centrifugal energy terms. Nuclear potential is weak compared with an effective centrifugal energy at the same range, therefore making interaction in \mathcal{P} and higher partial waves fade away.

Elastic scattering at low energies have been studied in four nucleon systems. For the first time all the 3 (experimentally accessible) 4N system, namely $p+{}^3\text{H}$, $n+{}^3\text{H}$ and $p+{}^3\text{He}$ were examined in a complete and rigorous way. Calculations were performed by using non-realistic (MT I-III) as well as several local realistic potential models.

Non-realistic MT I-III potential is very successful in predicting total as well as differential cross sections in $n+{}^3\text{H}$ and $p+{}^3\text{He}$ systems. However it fails in describing $p+{}^3\text{H}$ scattering below $n+{}^3\text{He}$ threshold, where α -particle excitation is present.

Despite of the complexity of the realistic potentials and the considerable number of partial amplitudes appearing in the calculations, it has been shown that these potentials are not able to reproduce the scattering cross sections in $n+{}^3\text{H}$ system, especially failing near the resonance at $E_{cm} = 3 \text{ MeV}$. Inclusion of three-nucleon force, in exception of very low energies, does not improve agreement with the experimental data. In contrary these potential models seems to be efficient in describing visibly more complex $p+{}^3\text{H}$ system.

These results suggest three possible hypotheses:

- either description of nuclear systems requires three-nucleon force having strong isospin symmetry breaking.
- NN \mathcal{P} waves are not well described, isospin symmetry breaking is not well taken into account.
- finally, description of nuclear systems, due to finite size of nucleons, could require qualitatively different force, in particular one having strong non-locality.

Conclusion et perspectives en français

Ce travail de thèse contient une série de **résultats théoriques obtenus dans la description des systèmes quantiques à petit nombre de corps (Few-Body)**. Le formalisme utilisé est celui des **équations de Fadeev-Yakubovsky**, qui ont été résolues dans l'espace de configuration. Ces équations constituent une formulation mathématiquement rigoureuse, physiquement transparente et numériquement accessible de la **Mécanique Quantique non relativiste**, indispensable dès que le nombre de particules mises en jeu est $N > 2$.

Les **résultats nouveaux** que nous avons obtenus au cours de ce travail concernent le **formalisme** lui-même ainsi que les **méthodes numériques** utilisées et contiennent des **prédictions dans le domaine de la physique atomique et nucléaire**.

A titre de conclusion et pour les perspectives nous voudrions signaler les points suivants:

1. **Les développements formels** obtenus concernent tous le traitement des **forces de longue portée**, soit dans des systèmes purement Coulombiens, soit dans des systèmes en interaction forte mais dont l'inclusion de l'interaction coulombienne dans les paires p-p s'avère indispensable. Dans le cas N=3 nous avons considéré des systèmes chargés ainsi que les **potentiels de polarization** qui en résultent. L'obtention des observables de diffusion nécessite en effet des méthodes appropriées qui ont été mises au point tout au long de ce travail. Dans le cas N=4, nous avons développé le formalisme permettant d'inclure le potentiel de Coulomb dans des systèmes nucléaires en interaction forte.
2. Nous avons mis au point des méthodes numériques puissantes permettant d'inclure les forces à trois et quatre corps par passages en coordonnées hyperradielles. Ces forces jouent un rôle important en physique nucléaire mais leur traitement numérique est très lourd.
3. Dans le domaine de la **physique atomique**, nous présentons des résultats originaux dans la **diffusion d'une particule lourde chargée positivement (X^+) sur des atomes d'Hydrogène**.

Nous avons obtenu en particulier des **prédictions sur les longueurs de diffusion et les sections efficaces pour les cas d'intérêt physique $X = \mu^+, \pi^+, p^+$** . Un grand nombre

de **résonances dans des ondes partielles élevées** ont été également prédites dans ces différents systèmes.

La cas de la **diffusion $p - H$ présente un intérêt spécial**. Nous **prédisons une longueur de diffusion $p - H$** dans l'état triplet de spin proton-proton – $1p_g$, en notation de physique moléculaire – d'une valeur $a_t = 750$ u.a.. Elle traduit l'existence d'un **état excité de l'ion moléculaire H_2^+ très près du seuil**, lié par une énergie de liaison extrêmement faible $B \sim 10^{-9}$. L'existence de cet état conditionne toute la diffusion $p - H$ à très basse énergie avec des sections efficaces de taille nanoscopique.

Outre son caractère exotique, l'existence de cet état pourrait avoir un rôle clé dans la formation de l'hydrogène moléculaire interstellaire, en accélérant le processus intermédiaire de formation $p + H_2 \rightarrow H_2^+ + h\nu$.

Ces résultats pourraient s'étendre sans difficulté, d'une part en considérant des **masses incidentes plus lourdes que le proton** (e.g. système $d - H$) et d'autre part en prenant des **projectiles négativement chargés**. Ce dernier cas implique des seuils inélastiques ouverts même à énergie nulle, e.g. $X^- + H \rightarrow e^- + (p^+, X^-)$, et l'on y devine une **physique potentiellement très riche et encore inexplorée**. En particulier dans la physique des antiprotons ($X = \bar{p}$) avec formation d'un très grand nombre d'états du protonium ($p - \bar{p}$) dans la voie finale.

4. **Notre étude sur les petits clusters de neutrons a été motivée par l'annonce faite au GANIL d'une possible mise en évidence de systèmes liés à trois ou quatre neutrons.** Il s'agit toutefois d'un problème classique dans la communauté Few-Body – autant du point de vue expérimental que théorique – que l'on reconsidère chaque fois que des progrès substantiels ont été accomplis soit dans les interactions, soit dans les techniques de calcul.

Nous avons **examiné les différentes pistes pouvant mener à une éventuelle liaison pour des systèmes avec N=3 et 4**, compte tenu de notre connaissance actuelle des forces neutron-neutron, et surtout de leurs incertitudes. Nous avons ainsi évalué *(i) le changement nécessaire à l'interaction $n-n$ dans l'onde 1S_0 (la seule sous contrôle expérimental direct), (ii) l'intensité des forces à trois et quatre corps, et (iii) l'attraction dans l'onde P nécessaire pour obtenir des systèmes faiblement liés*.

Nous avons conclu à son impossibilité.

Concernant les systèmes plus grands, la situation est moins claire et ne peut pas être strictement infirmée par notre, relativement modeste, technologie actuelle. Nos résultats montrent toutefois son **caractère fortement improbable**.

L'étude a été menée en parallèle avec un système de fermions qui présente des remarquables analogies avec les neutrons: **les atomes d'Helium 3**. On sait ce dernier système lié à partir de N=35 atomes. Or nous avons montré que dans le cas N=2, la liaison des atomes

d'Helium est nettement défavorisé par rapports à celle des neutrons et que ceci reste vrai si l'on "bosonize" le problème, i.e. si l'on ne tient pas compte du principe de Pauli et qu'on laisse jouer tout leur rôle aux interactions.

Nous pensons avoir éclairci la différence qu'existe entre ces deux systèmes de fermions et qui peut aboutir à la formation, dans un cas mais pas dans l'autre, de matière infinie liée. Cette différence se trouve en dernier ressort dans le rayon du coeur dur des interactions respectives. Il diffère par un facteur trois (dans des unités caractéristiques). De ce fait, la barrière centrifuge est un ordre de grandeur moins efficace dans la région où se trouve le puits attractif et les ondes P contribuent de manière importante à la liaison.

5. **Dans l'étude du système à quatre nucléons**, nous avons abordé de façon unifiée les différents processus possibles à basse énergie: n+t, p+³He, p-t.

Nous avons considéré tout d'abord le cas n+t. C'est le cas le plus simple puisqu'il est soumis aux seules interactions fortes, mais dynamiquement très riche car il présente la première résonance hadronique, située seulement à quelques MeV au dessus du seuil. Malgré un nombre très supérieur d'ondes partielles inclu dans les calculs, il semble **y avoir toujours un désaccord avec les données expérimentales aussi bien dans la région "d'onde S" que dans la région du pic de résonance**. Nous avons ainsi mis en évidence **un échec des modèles nucléaires actuels, alors même qu'ils fournissent une description satisfaisante des états liés**. Il est probable que des forces à trois corps plus élaborées incluant une structure en isospin plus riche (e.g. les forces d'Urbana-Illinois) soient nécessaires pour aboutir à un accord satisfaisant.

L'inclusion des forces coulombiennes dans les équations de Faddeev-Yakubovski nous a permis d'obtenir les sections efficaces différentielles de la **réaction p-³He, le système "miroir" de n+t**. Nous avons montré que le modèle MT I-III donne une description très satisfaisante de l'ensemble des observables malgré son extrême simplicité. Des résultats obtenus avec les potentiels réalistes, en incluant les forces à trois corps, sont aussi en assez bon accord avec les calculs existants du groupe de Pisa.

Nous avons ensuite obtenu la **première description théorique du complexe $p + t \rightarrow 4He^* \rightarrow n + ^3He$** . L'inclusion des **forces coulombiennes a permis pour la première fois de placer la première excitation de l'⁴He dans le continuum, entre les seuils p-³H et n-³He**. Nous avons montré que dans ce système, le potentiel semi-réaliste MT I-III, qui était jusqu'à présent le plus performant pour la description des petits noyaux, donne des résultats en désaccord avec l'expérience, en particulier une longueur de diffusion excessivement grande, de l'ordre de -60 fm.

Nous avons présenté la première **prédition pour la longueur de diffusion p+t ($a = -16$ fm) avec des potentiels réalistes** et obtenu une bonne description de la fonction

d'excitation $\sigma(\theta = 120^\circ, E)$ mesurée expérimentalement. **Cet accord nécessite toutefois l'inclusion des forces à trois corps et constitue donc une mise en évidence de leurs effets dans un observable de diffusion à très basse énergie.** L'accord obtenu est un peu surprenant, vue la difficulté que ces mêmes potentiels ont pour la description du système n+t, a priori plus simple.

Ce travail **pourrait être complété par la prise en compte du canal couplé n-³He**, seulement 0.7 MeV au dessus du seuil p-t, ce qui permettra d'obtenir pour la première fois sa longueur de diffusion complexe en incorporant toute la richesse dynamique sous le seuil (p-t, ⁴He*).

Nous voudrions **finalement signaler la puissance du formalisme de Faddeev-Yakubovski** qui a été utilisé dans ce travail et que nous avons, on l'espère, avoir contribué à développer. Si, en ce qui concerne la précision des états liés, ses performances sont bel et bien inférieures à celles des méthodes variationnelles, **c'est le seul formalisme qui présente un degré de souplesse permettant de décrire une grande variété de situations physiques, et ceci quel que soit le type d'interaction.** Nous voudrions souligner à cet égard notre préiction, en utilisant des résultats de diffusion, d'un état lié dont l'énergie extrêmement faible était jusqu'à présent inaccessible par d'autres approches.

Il serait souhaitable de continuer à développer ce formalisme en explorant par exemple le domaine très riche des **résonances** (calcul directe de position et largeurs) ou les **réactions de break-up** avec trois et quatre corps dans la voie finale. Son utilisation **combinée avec la rotation complexe des coordonnées** devrait permettre d'aboutir rapidement à des résultats.

Appendix A

Often used notations and abbreviations

$\sigma_u; \sigma_g$	Designates symmetry state of a diatomic molecule. σ indicates that projection of angular momentum on the axis of two nuclei is equal zero ($\Lambda = 0$). Subscript index marks the parity of the spatial wave function in respect to exchange of two nuclei: u - stands for antisymmetric wave functions, g - for the symmetric ones.
$1s\sigma_g; 2p\sigma_u$	Number and a latin letter in front of notations marks the electronic level in the united atoms limit $r \rightarrow 0$.
3NF	Three nucleon force.
AGS	Alt-Grassberger-Sandhas equations [163].
<i>Av.14</i>	Realistic potential model developped by Argonne group [99].
<i>Av.18</i>	Realistic potential model developped by Argonne group [101].
CD	Charge dependence.
<i>CD MT I-III</i>	Charge dependent Malfiet -Tjon potential, as defined in section 3.3.
CHP	Cubic Hermite interpolants, see Appendix E.
Dineutron	Bound system of two neutrons.
Dimer	Bound state of two identical atoms (molecules).
FY	Faddeev-Yakubovski equations [15], see section 1.2.3.
LS	Lipmann-Schwinger equation [16].
\mathcal{LS}	Angular momentum-spin coupling scheme used in partial wave expansion, see section 1.2.5.
<i>MT I-III</i>	Semirealistic Malfiet -Tjon potential [120][121].
<i>Nijm II</i>	Realistic potential model developped by Nijmegen group [94].
NN	Nucleon-nucleon.
OBE	One boson exchange model.
PWB	Partial wave basis.
QHP	Quintic Hermite interpolants, see Appendix E.
<i>Reid 93</i>	Realistic potential model developped by Nijmegen group [93].

Tetramer	Bound state of four identical atoms (molecules).
Tetraneutron	Bound system of four neutrons.
Trimer	Bound state of three identical atoms (molecules).
Trineutron	Bound system of three neutrons.
<i>UIX</i>	Three nucleon force developed by the Argonne group [110].

Appendix B

Transformation of Jacobi coordinates in arbitrary 4-body systems

In this work Jacobi coordinates were used to describe the motion of the particles. These coordinates are well suited to separate the center of mass motion of the system, as well as of its subsystems, therefore simplifying expressions for kinetic energy operator.

Faddeev-Yakubovski equations are written in terms of so called components. These components are designated to describe different asymptotic configurations of the particles and thus are convenient to write in their proper Jacobi coordinate sets. As it was shown in section 1.2.1, there are two types of Jacobi coordinate sets: one associated with 4-particle partitions of type K and one with type H partitions. They are defined as follows:

$$K_{ij,k}^l \rightarrow \begin{cases} \vec{x}_{ij} &= \sqrt{2\frac{m_i m_j}{m_i + m_j}}(\vec{r}_j - \vec{r}_i) \\ \vec{y}_{ij,k} &= \sqrt{2\frac{m_k(m_i + m_j)}{m_k + m_i + m_j}}(\vec{r}_k - \frac{m_i \vec{r}_i + m_j \vec{r}_j}{m_i + m_j}) \\ \vec{z}_{ijk,l} &= \sqrt{2\frac{m_l(m_i + m_j + m_k)}{m_l + m_k + m_i + m_j}}(\vec{r}_l - \frac{m_i \vec{r}_i + m_j \vec{r}_j + m_k \vec{r}_k}{m_i + m_j + m_k}) \end{cases} \quad (\text{B.1})$$

$$H_{ij,kl} \rightarrow \begin{cases} \vec{x}_{ij} &= \sqrt{2\frac{m_i m_j}{m_i + m_j}}(\vec{r}_j - \vec{r}_i) \\ \vec{y}_{kl} &= \sqrt{2\frac{m_k m_l}{m_k + m_l}}(\vec{r}_l - \vec{r}_k) \\ \vec{z}_{ij,kl} &= \sqrt{2\frac{(m_i + m_j)(m_k + m_l)}{m_i + m_j + m_k + m_l}}(\frac{m_k \vec{r}_k + m_l \vec{r}_l}{m_k + m_l} - \frac{m_i \vec{r}_i + m_j \vec{r}_j}{m_i + m_j}) \end{cases} \quad (\text{B.2})$$

One wishes to establish relations enabling to transform the coordinates between any two Jacobi coordinate sets. In general, such transformation can be written by use of 3-dimensional rotation matrix:

$$\begin{pmatrix} \vec{x}' \\ \vec{y}' \\ \vec{z}' \end{pmatrix} = \begin{bmatrix} a_{11} & a_{12} & a_{13} \\ a_{21} & a_{22} & a_{23} \\ a_{31} & a_{32} & a_{33} \end{bmatrix} \begin{pmatrix} \vec{x} \\ \vec{y} \\ \vec{z} \end{pmatrix}. \quad (\text{B.3})$$

However, since for 4-body system we have as much as 48 different sets of Jacobi coordinates deriving separate expression for each possible coordinate transformation is too burdensome task. Nevertheless one can decompose any complicated coordinate transformation to cyclic application of some notably simpler transformation operations, which keep some of Jacobi coordinates unchanged. Before explicitly writing down equations, I would like to introduce some abbreviate notations of particle mass combinations, to be used in simplifying expressions:

$$\begin{aligned}\mu_{ij} &= \frac{m_i m_j}{m_i + m_j} \\ \eta_{ij} &= \frac{m_i(M - m_i - m_j)}{M - m_i} = \mu_{i(kl)} \\ \gamma_i &= \frac{m_i(M - m_i)}{M} = \mu_{i(jkl)} \\ \lambda_{ij} &= \frac{(m_i + m_j)(M - m_i - m_j)}{M} = \mu_{(ij)(kl)}\end{aligned}\tag{B.4}$$

and the total mass of the system

$$M = \sum_{i=1}^4 m_i \quad (i, j, k, l) \in (1, 2, 3, 4).\tag{B.5}$$

B.1 Transformation between K -type coordinate sets

Transformations between any two $K_{ij,k}^l$ -type coordinate sets can be reduced to subsequent application of transformations, which at the time permute only two neighboring indexes in the set $[(ij)k]l$. Therefore, one has to introduce only four rotation matrices:

1. Rotation matrix R_{ij} enables to permute two first indexes i and j . I.e. this matrix transforms coordinate set $K_{ij,k}^l$ to $K_{ji,k}^l$. Its expression is trivial, since in such transformation only direction of the vector \vec{x} is reversed, whereas other two vectors \vec{y} and \vec{z} are not affected.

$$\begin{pmatrix} \vec{x}' \\ \vec{y}' \\ \vec{z}' \end{pmatrix}_{K_{ji,k}^l} = \begin{pmatrix} -1 & 0 & 0 \\ 0 & 1 & 0 \\ 0 & 0 & 1 \end{pmatrix} \begin{pmatrix} \vec{x} \\ \vec{y} \\ \vec{z} \end{pmatrix}_{K_{ij,k}^l}\tag{B.6}$$

2. Rotation enabling to pass between the coordinate sets with the second and the third particle indexes (j and k) interchanged is the principal coordinate transformation operation used in solving three-body problem. Such transformation relates Jacobi coordinate set $K_{ij,k}^l$ to $K_{ik,j}^l$. Hence, vector \vec{z} is not affected by this, while expressions for this matrix was already provided in eq. (1.76) and eq. (1.76):

$$\begin{pmatrix} \vec{x}' \\ \vec{y}' \\ \vec{z}' \end{pmatrix}_{K_{ik,j}^l} = \begin{pmatrix} \frac{\sqrt{1}}{m_i} & \sqrt{\frac{\mu_{ik}}{\eta_{kl}}} & 0 \\ \sqrt{\frac{\mu_{ij}}{\eta_{jl}}} & -\frac{m_k}{m_k+m_i} \sqrt{\frac{\eta_{jl}}{\eta_{kl}}} & 0 \\ 0 & 0 & 1 \end{pmatrix} \begin{pmatrix} \vec{x} \\ \vec{y} \\ \vec{z} \end{pmatrix}_{K_{ij,k}^l}\tag{B.7}$$

3. Transformations between two K -type coordinate sets are completed by establishing rotation matrix permitting to permute order of the last two indexes in general coordinate set $K_{ij,k}^l$, namely l and k :

$$\begin{pmatrix} \vec{x}' \\ \vec{y}' \\ \vec{z}' \end{pmatrix}_{K_{ij,l}^k} = \begin{pmatrix} 1 & 0 & 0 \\ 0 & \frac{\sqrt{\eta_{kl}\eta_{lk}}}{m_i+m_j} & \sqrt{\frac{\eta_{lk}}{\gamma_l}} \\ 0 & \sqrt{\frac{\eta_{kl}}{\gamma_k}} & -\frac{m_l}{M-m_k} \sqrt{\frac{\gamma_k}{\gamma_l}} \end{pmatrix} \begin{pmatrix} \vec{x} \\ \vec{y} \\ \vec{z} \end{pmatrix}_{K_{ij,k}^l} \quad (\text{B.8})$$

B.2 Transformation between H -type coordinate sets

One can similarly decompose any complicated rotation matrix permitting to pass between any two H -type Jacobi coordinate sets into consequent application of simpler rotation matrixes, which permits to permute only two neighbor indexes at the time.

1. One should remark, that transitions between two H -type coordinate sets, which differ only by the first two (i and j) or the last two (k and l) indexes are very trivial. In this case Yakubovski partition structure is not changed, only direction of single coordinate vectors \vec{x} or \vec{y} is reversed. Respectively, one has two following expressions:

$$\begin{pmatrix} \vec{x}' \\ \vec{y}' \\ \vec{z}' \end{pmatrix}_{H_{ji,kl}} = \begin{pmatrix} -1 & 0 & 0 \\ 0 & 1 & 0 \\ 0 & 0 & 1 \end{pmatrix} \begin{pmatrix} \vec{x} \\ \vec{y} \\ \vec{z} \end{pmatrix}_{H_{ij,kl}} \quad (\text{B.9})$$

$$\begin{pmatrix} \vec{x}' \\ \vec{y}' \\ \vec{z}' \end{pmatrix}_{H_{ij,lk}} = \begin{pmatrix} 1 & 0 & 0 \\ 0 & -1 & 0 \\ 0 & 0 & 1 \end{pmatrix} \begin{pmatrix} \vec{x} \\ \vec{y} \\ \vec{z} \end{pmatrix}_{H_{ij,kl}} \quad (\text{B.10})$$

2. Much more complicated situation arises, when one tries to pass between $H_{ij,kl}$ coordinate sets, which differ by interchange of the indexes in the middle (i.e. k and j). One can see that none of three Jacobi coordinate vectors is conserved. This coordinate transformation matrix is given by

$$\begin{pmatrix} \vec{x}' \\ \vec{y}' \\ \vec{z}' \end{pmatrix}_{H_{ik,jl}} = \begin{pmatrix} \frac{\sqrt{\mu_{ij}\mu_{ik}}}{m_i} & -\frac{\sqrt{\mu_{ik}\mu_{kl}}}{m_k} & \sqrt{\frac{\mu_{ik}}{\lambda_{ij}}} \\ -\frac{\sqrt{\mu_{ij}\mu_{jl}}}{m_j} & \frac{\sqrt{\mu_{jl}\mu_{kl}}}{m_l} & \sqrt{\frac{\mu_{jl}}{\lambda_{ij}}} \\ \sqrt{\frac{\mu_{ij}}{\lambda_{ik}}} & \sqrt{\frac{\mu_{kl}}{\lambda_{ik}}} & \frac{m_im_l-m_jm_k}{M\sqrt{\lambda_{ij}\lambda_{ik}}} \end{pmatrix} \begin{pmatrix} \vec{x} \\ \vec{y} \\ \vec{z} \end{pmatrix}_{H_{ij,kl}} \quad (\text{B.11})$$

B.3 Coordinate transformation between H and K Jacobi bases

Finally, when solving Faddeev-Yakubovki equations situations when one has to switch between Jacobi coordinate representations of K - and H -type are inevitable. Note, one needs to precise two transformation matrices, which furthermore are inverse of each other and enable to pass from (to)

any general coordinate set $K_{ij,l}^k$ to (from) coordinate set $H_{ij,kl}$. These transformation matrices do not affect Jacobi vector \vec{x} , whereas rotation in the plane yz should be performed.

$$\begin{pmatrix} \vec{x}' \\ \vec{y}' \\ \vec{z}' \end{pmatrix}_{H_{ij,kl}} = \begin{pmatrix} 1 & 0 & 0 \\ 0 & -\frac{\sqrt{\mu_{kl}\eta_{kl}}}{m_k} & \sqrt{\frac{\mu_{kl}}{\gamma_l}} \\ 0 & \sqrt{\frac{\eta_{kl}}{\lambda_{ij}}} & \frac{\mu_{kl}}{m_k} \sqrt{\frac{\lambda_{ij}}{\gamma_l}} \end{pmatrix} \begin{pmatrix} \vec{x} \\ \vec{y} \\ \vec{z} \end{pmatrix}_{K_{ij,k}^l} \quad (\text{B.12})$$

and vice versa

$$\begin{pmatrix} \vec{x}' \\ \vec{y}' \\ \vec{z}' \end{pmatrix}_{K_{ij,k}^l} = \begin{pmatrix} 1 & 0 & 0 \\ 0 & -\frac{\sqrt{\mu_{kl}\eta_{kl}}}{m_k} & \sqrt{\frac{\eta_{kl}}{\lambda_{ij}}} \\ 0 & \sqrt{\frac{\mu_{kl}}{\gamma_l}} & \frac{\eta_{kl}}{m_k} \sqrt{\frac{\gamma_l}{\lambda_{ij}}} \end{pmatrix} \begin{pmatrix} \vec{x} \\ \vec{y} \\ \vec{z} \end{pmatrix}_{H_{ij,kl}} \quad (\text{B.13})$$

Appendix C

Three-body operators

C.1 Three-body transformation operator \hat{h}

Using Faddeev formalism we deal with so called Faddeev components, which are described by means of three different Jacobi coordinate sets. For the numerical convenience these components were decomposed into amplitudes (see section 1.2.5) by projecting them into bipolar harmonics basis. Thus one introduces three bipolar harmonic bases, each associated with a given Faddeev component and expressed in the corresponding Jacobi coordinate set.

Thus, one is obliged to define operators, which enable to project Faddeev amplitudes into the amplitude basis of the non-proper Faddeev component. Or, more precisely, to calculate projection of some arbitrary function $\frac{F_{\alpha'}(x',y')}{x'y'} \left[Y_{l_x'}(\hat{x}')Y_{l_y'}(\hat{y}') \right]_{LM}$, defined in the basis of the coordinate set $\alpha'\vec{x}'\vec{y}'$, onto bipolar harmonics basis $\left[Y_{l_x}(\hat{x})Y_{l_y}(\hat{y}) \right]_{LM}$ of the other coordinate set $\alpha\vec{x}\vec{y}$.

As seen in eq. (1.76), transition between different Jacobi coordinate sets can be performed using rotation matrix, which furthermore is unitary:

$$\begin{pmatrix} \vec{x}' \\ \vec{y}' \end{pmatrix} = \begin{pmatrix} c_1 & s_1 \\ s_2 & c_2 \end{pmatrix} \begin{pmatrix} \vec{x} \\ \vec{y} \end{pmatrix} \quad (\text{C.1})$$

One can remark, that scalars $x\ell$, y' can be expressed through only three parameters: x, y and $u = \hat{x} \cdot \hat{y}$. Therefore, the function, depending only on scalar variables $x\ell$, y' , written in the non-proper basis xy , depend only on one angular variable $u = \hat{x} \cdot \hat{y}$ of four possible angular variables (\hat{x} and \hat{y}). The other three angular variables can be integrated out. This property is realized using operator \hat{h} , defined by:

$$\iint d\hat{x}d\hat{y} \left[Y_{l_x}(\hat{x})Y_{l_y}(\hat{y}) \right]_{LM} \frac{xy}{x'y'} F_{\alpha'}(x',y') \left[Y_{l_x'}(\hat{x}')Y_{l_y'}(\hat{y}') \right]_{LM} = \int_{-1}^{+1} \hat{h}_{l_x l_y, l_x' l_y}^{LM}(x,y,u) F_{\alpha'}(x',y') du. \quad (\text{C.2})$$

Derivation of this operator \hat{h} consist of no difficulty [190], it can be written as a convolution of

the geometrical coefficients:

$$\begin{aligned} \hat{h}_{l_x l_y, l'_x l'_y}^{\mathcal{LM}}(x, y, u) &= \sum_{\lambda=0} \frac{\hat{\lambda} \sqrt{\hat{l}_x \hat{l}_y \hat{l}'_x \hat{l}'_y}}{2} P_\lambda(u) \sum_{l_1+l_2=l'_x} \sum_{l_3+l_4=l'_y} \sqrt{\frac{(2l'_x+1)!(2l'_y+1)!}{(2l_1)!(2l_2)!(2l_3)!(2l_4)!}} \\ &\quad \frac{x^{l_1+l_3+1} y^{l_2+l_4+1}}{(x')^{l'_x+1} (y')^{l'_y+1}} c_1^{l_1} c_2^{l_4} s_1^{l_2} s_2^{l_3} \sum_{l_5} \hat{l}_5 \begin{pmatrix} \lambda & l_x & l_5 \\ 0 & 0 & 0 \end{pmatrix} \begin{pmatrix} l_1 & l_3 & l_5 \\ 0 & 0 & 0 \end{pmatrix} \\ &\quad \sum_{l_6} \hat{l}_6 (-)^{l_6+l_x+\mathcal{L}} \begin{pmatrix} \lambda & l_y & l_6 \\ 0 & 0 & 0 \end{pmatrix} \begin{pmatrix} l_2 & l_4 & l_6 \\ 0 & 0 & 0 \end{pmatrix} \left\{ \begin{array}{ccc} l_x & l_y & \mathcal{L} \\ l_6 & l_5 & \lambda \end{array} \right\} \\ &\quad \left\{ \begin{array}{ccc} l_1 & l_3 & l_5 \\ l_2 & l_4 & l_6 \\ l'_x & l'_y & \mathcal{L} \end{array} \right\}. \end{aligned} \quad (\text{C.3})$$

Here $\hat{l} = 2l + 1$ and $P_\lambda(u)$ is polynomial of Lagendre of order λ [18].

Considerable simplifications take place, if angular momentum is equal zero ($\mathcal{L} = 0$). In this particular case bipolar harmonic becomes:

$$[Y_{l_1}(\Omega_1) Y_{l_2}(\Omega_2)]_{00} = \frac{(-)^{l_1} \sqrt{\hat{l}_1}}{4\pi} P_{l_1}(\cos(\widehat{\Omega_1, \Omega_2})), \quad (\text{C.4})$$

whereas expression for the operator \hat{h} is very simple:

$$\hat{h}_{l_x l_y, l'_x l'_y}^{00}(x, y, u) = \delta_{l_x l_y} \delta_{l'_x l'_y} (-)^{l_x+l'_x} \frac{\sqrt{\hat{l}_x \hat{l}'_x} P_{l_x}(u) P_{l'_x}(u')} {2} \frac{xy}{x' y'}. \quad (\text{C.5})$$

Spin (isospin) bases If system posses spins and isospins, expression for projection operator of Faddeev amplitudes should be extended to incorporate these bases as well. Operator \hat{h} merely permits to pass from one representation basis to the other and thus does not affect the physical system as a whole. Therefore collective systems quantum numbers as angular momenta \mathcal{L} , total spin (\mathcal{S}), total isospin (\mathcal{T}) and total angular momenta (\mathcal{J}) are conserved separately by this operator. Therefore, in each of the basis \mathcal{L} , \mathcal{S} and \mathcal{T} transformation operator acts independently and can be written as a simple product of transformation operators in each of these bases.

$$\hat{h}_{\alpha, \alpha'}(x, y, u) = \hat{h}_{\alpha, \alpha'}^{\mathcal{LM}}(x, y, u) \cdot \hat{h}_{\alpha, \alpha'}^{\mathcal{S}} \cdot \hat{h}_{\alpha, \alpha'}^{\mathcal{T}}. \quad (\text{C.6})$$

Expression of these operators are trivial. I will write down only operator permitting to pass from the base with order of particles numbered $(12)3$ to $(31)2$, while all the other transformation operators follow by merely interchanging particle indexes. For spin basis one has:

$$\hat{h}_{\alpha, \alpha'}^{\mathcal{S}} = \left\langle \left[(s_3 s_1)_{\sigma_x} s_2 \right]_{\mathcal{S}} \middle| \left[(s_1 s_2)_{\sigma'_x} s_3 \right]_{\mathcal{S}} \right\rangle = (-)^{\sigma'_x + s_3 - \mathcal{S}} A \left\{ \begin{array}{ccc} s_3 & s_1 & \sigma_x \\ s_2 & \mathcal{S} & \sigma'_x \end{array} \right\} \quad (\text{C.7})$$

One has analogous expression, for transitions between the isospin basis:

$$\hat{h}_{\alpha, \alpha'}^{\mathcal{T}} = \left\langle \left[(t_3 t_1)_{\tau_x} t_2 \right]_{\mathcal{T}} \middle| \left[(t_1 t_2)_{\tau'_x} t_3 \right]_{\mathcal{T}} \right\rangle = (-)^{\tau'_x + t_3 - T} A \left\{ \begin{array}{ccc} t_3 & t_1 & \tau_x \\ t_2 & T & \tau'_x \end{array} \right\} \quad (\text{C.8})$$

Here we have used notation for the modified $6j$ coefficients:

$$A \left\{ \begin{array}{ccc} j_1 & j_2 & j_{12} \\ j_3 & J & j_{23} \end{array} \right\} = (-)^{j_1+j_2+j_3+J} \sqrt{\hat{j}_{12}\hat{j}_{23}} \left\{ \begin{array}{ccc} j_1 & j_2 & j_{12} \\ j_3 & J & j_{23} \end{array} \right\} = \left\langle \left[j_1 (j_2 j_3)_{j_{23}} \right]_J \middle| \left[(j_1 j_2)_{j_{12}} j_3 \right]_J \right\rangle \quad (\text{C.9})$$

C.2 Expectation value operator \hat{W}

When trying to solve scattering problem with long range interaction one needs to artificially uncouple Faddeev components at some finite distance to be able to implement correct boundary conditions (see section 2.1). Therefore, left hand side of Faddeev equation, at some large (but finite) separation of the scattered particle, absorbs full interaction terms. The full three particle potential cannot be simply written as a function of two scalars x and y . It necessarily depends at least on one angular variable, which is the angle between vectors \vec{x} and \vec{y} . Hence, full potential is not diagonal in bipolar harmonic basis and couples the different amplitudes even staying within the same component. One would like to write down the action of general scalar multiplicative operator $F(x, y, u = \hat{x} \cdot \hat{y})$ in bipolar harmonics basis. It is done by using operator $\hat{W}_{l_x l_y, l'_x l'_y}^{\mathcal{LM}}$, which projects action of $F(x, y, u)$ from one general amplitude $(l'_x l'_y)_{\mathcal{LM}}$ to the other ones $(l_x l_y)_{\mathcal{LM}}$, and is defined as:

$$\iint d\hat{x} d\hat{y} [Y_{l_x}(\hat{x}) Y_{l_y}(\hat{y})]_{\mathcal{LM}} F(x, y, u) [Y_{l'_x}(\hat{x}) Y_{l'_y}(\hat{y})]_{\mathcal{LM}} = \int_{-1}^{+1} \hat{W}_{l_x l_y, l'_x l'_y}^{\mathcal{LM}}(x, y, u) F(x, y, u) du. \quad (\text{C.10})$$

Derivation of this operator is similar to that of operator $\hat{h}_{\alpha, \alpha'}^{\mathcal{LM}}(x, y, u)$, after some routine algebra one obtains:

$$\hat{W}_{l_x l_y, l'_x l'_y}^{\mathcal{LM}}(x, y, u) = (-)^{l_x + l'_x - \mathcal{L}} \sqrt{\hat{l}_x \hat{l}_y \hat{l}'_x \hat{l}'_y} \sum_{\lambda=0}^{\hat{\lambda}} \frac{\hat{\lambda}}{2} P_\lambda(u) \left(\begin{array}{ccc} l'_x & l_x & \lambda \\ 0 & 0 & 0 \end{array} \right) \left(\begin{array}{ccc} l'_y & l_y & \lambda \\ 0 & 0 & 0 \end{array} \right) \left\{ \begin{array}{ccc} \lambda & l'_x & l_x \\ \mathcal{L} & l_y & l'_y \end{array} \right\} \quad (\text{C.11})$$

In case of zero angular momentum ($\mathcal{L} = 0$), as in previous section for operator $\hat{h}_{l_x l_y, l'_x l'_y}^{\mathcal{LM}}(x, y, u)$, expression of the operator \hat{W} considerably simplifies:

$$\hat{W}_{l_x l_y, l'_x l'_y}^{00}(x, y, u) = \delta_{l_x l_y} \delta_{l'_x l'_y} (-)^{l_x + l'_x} \frac{\sqrt{\hat{l}_x \hat{l}'_x} P_{l_x}(u) P_{l'_x}(u)}{2}. \quad (\text{C.12})$$

Operator \hat{W} as well can be utilized to evaluate the diagonal terms of Urbana IX three-body force. Therefore, this operator can serve as alternative test to the rotation formalism developed to treat 3-body force (see Appendix G.2).

C.3 Case of the identical particles

Let us suppose particles 2 and 3 to be identical. It follows from the subsection 1.2.4 that component functions in bases 2 and 3, except some phase multiplier, are identical. One has:

$$\begin{aligned}\Psi &= (12) 3 + (23) 1 + (31) 2 \\ &= \varepsilon [(13) 2 + (32) 1 + (21) 3].\end{aligned}\tag{C.13}$$

Here by $(ij) k$ we denote Faddeev components $|\psi_{(ij)k}\rangle$. As discussed in subsection 1.2.5, these components are decomposed into partial wave basis, by means of so called partial amplitudes $F_{\alpha_{(ij)k}}(x, y)$, being projection of Faddeev component $|\psi_{(ij)k}\rangle$ onto partial wave α . By expanding eq. (C.13) in partial waves and regrouping similar terms, one can remark simple symmetry relation for the partial amplitudes:

$$F_{\alpha_{(23)1}} = \varepsilon F_{\alpha_{(32)1}} = \varepsilon (-)^{l_x+t_x+s_x-s_2-s_3-t_2-t_3} F_{\alpha_{(23)1}}\tag{C.14}$$

and

$$F_{\alpha_{(12)3}} = \varepsilon F_{\alpha_{(13)2}} = \varepsilon (-)^{l_x+t_x+s_x-s_1-s_3-t_1-t_3} F_{\alpha_{(31)2}}.\tag{C.15}$$

The first relation imposes certain restrictions to the choice of partial waves in the component $(23) 1$. I.e.

$$\varepsilon = (-)^{l_x+t_x+s_x-s_2-s_3-t_2-t_3} = (-)^{l_x+t_x+s_x}.\tag{C.16}$$

Thus, for the fermionic systems quantity $l_x + t_x + s_x$ should be impair, whereas for bosonic systems it is pair.

Relation (C.15) enables one to reduce number of integro-differential equations to solve, since equations given by decomposition of component $(12) 3$ become identical to those of component $(31) 2$.

Appendix D

Four-body operators

D.1 Four-body basis transformation operators

In this appendix I will develop expressions of the permutation operators, introduced in subsection 1.2.5 and applied in solving four identical particle Faddeev-Yakubovski equations. Before doing this I should like to stress out that matrix elements of these operators are strongly related to partial wave basis transformation operators. Actually, they differ only by the some phase coefficient. This phase appears once one is referring to the identity of the particles, trying to project some wave function into the PWB of its non-proper Faddeev-Yakubovski component (as was done in eq. (C.15)).

D.1.1 Matrix elements of three-body permutation operator $\langle \alpha xyz [K] | P^+ | \alpha' x' y' z' [K] \rangle$

This operator, $\langle \alpha xyz [K] | P^+ | \alpha' x' y' z' [K] \rangle = \langle \alpha xyz [K] | P_{12}P_{23} | \alpha' x' y' z' [K] \rangle$, is identical to three-body rotation operator introduced in previous section. In fact, necessary phase for the transition elements is given by eq. (C.15). However if one deals with the physical states¹ this phase turns to be 1. From eq. (C.14) it follows that the amplitudes of physical states are those for which $\varepsilon = (-)^{l_x+s_x+t_x}$.

By assuming all the 4 particles being identical, thus beyond of all having the same masses as well, rotation matrix given by eq. (B.7) becomes:

$$\begin{pmatrix} \vec{x}' \\ \vec{y}' \\ \vec{z}' \end{pmatrix}_{K_{23,1}^4} = \begin{pmatrix} -\frac{1}{2} & \frac{\sqrt{3}}{2} & 0 \\ -\frac{\sqrt{3}}{2} & -\frac{1}{2} & 0 \\ 0 & 0 & 1 \end{pmatrix} \begin{pmatrix} \vec{x} \\ \vec{y} \\ \vec{z} \end{pmatrix}_{K_{12,3}^4}$$

¹Physical states are the states which have appropriate symmetry of the systems wave function. Hence, waves function of the system of the identical fermions are antisymmetric in exchange of any two particles, whereas in case of bosonic systems wave function is symmetric.

The action of permutation operator P^+ in isospin bases follows immediately, from eq. (C.8):

$$\begin{aligned}\hat{t}_{\alpha,\alpha'} &= \langle T_{K_\alpha} | P^+ | T_{K_{\alpha'}} \rangle = \left\langle \left[\left\{ (t_1 t_2)_{\tau_x} t_3 \right\}_{T_3} t_4 \right]_{\mathcal{T}} \middle| \left[\left\{ (t_2 t_3)_{\tau'_x} t_1 \right\}_{T'_3} t_4 \right]_{\mathcal{T}} \right\rangle = \quad (\text{D.1}) \\ &= (-)^{\tau'_x + t_1 - T'_3} \delta_{T_3, T'_3} A \left\{ \begin{array}{ccc} t_1 & t_2 & \tau_x \\ t_3 & T_3 & \tau'_x \end{array} \right\}\end{aligned}$$

If one works with (\mathcal{LS}) coupling scheme, desired operator can be easily obtained by collecting equations (C.3),(C.7) and (C.8) into eq.(C.6). However in practical 4-body applications we have utilized (\mathcal{JJ}_\ddagger) coupling scheme. Therefore one additional step had to be made to pass from (\mathcal{JJ}_\ddagger) basis to (\mathcal{LS}) basis before expressions of the previous Appendix are applied. Summarizing all this procedures in one equation, one obtains:

$$\langle \alpha xyz [K] | P^+ | \alpha' x' y' z' [K] \rangle = \hat{t}_{\alpha,\alpha'} \int_{-1}^1 h_{\alpha,\alpha'}^{\mathcal{J}}(x, y, u) K_{\alpha'}(x', y', z') du, \quad (\text{D.2})$$

with

$$\begin{aligned}\hat{h}_{\alpha,\alpha'}^{\mathcal{J}}(x, y, z, u) &= \sum_{l_{xy}, \sigma} \delta_{l_z, l'_z} \delta_{j_z, j'_z} \delta_{J_3, J'_3} A \left\{ \begin{array}{ccc} l_x & \sigma_x & j_x \\ l_y & s_3 & j_y \\ l_{xy} & \sigma & J_3 \end{array} \right\} A \left\{ \begin{array}{ccc} l'_x & \sigma'_x & j'_x \\ l'_y & s'_1 & j'_y \\ l'_{xy} & \sigma' & J'_3 \end{array} \right\} \quad (\text{D.3}) \\ &\quad (-)^{\sigma'_x + s_1 - \sigma} A \left\{ \begin{array}{ccc} s_1 & s_2 & \sigma_x \\ s_3 & \sigma & \sigma'_x \end{array} \right\} \frac{xy}{x'y'} \hat{h}_{l_x l_y, l'_x l'_y}^{l_{xy}}(x, y, u).\end{aligned}$$

While symmetry provided coefficients for P^+ matrix elements are shown to be 1, therefore defined expressions are valid for the rotation matrix between the K components as well. However this rotation matrix is twice as large, since once this operator applied it can create non-physical states, which do not satisfy condition (C.16)².

$$\langle (12)3, 4 | \hat{R}_{\alpha,\alpha'} | (23)1, 4 \rangle = \langle (31)2, 4 | \hat{R}_{\alpha,\alpha'} | (12)3, 4 \rangle = \langle (23)1, 4 | \hat{R}_{\alpha,\alpha'} | (31)2, 4 \rangle = \langle K | P^+ | K \rangle \quad (\text{D.4})$$

D.1.2 Permutation matrix $\langle \alpha xyz [K] | Q | \alpha' x' y' z' [K] \rangle = \langle K | \varepsilon P_{34} | K \rangle$ elements

Permutation operator εP_{34} relies the partial wave amplitudes of the base $K_{12,3}^4$ to the base $K_{12,4}^3$ (see eq. 1.111). Transformation of appropriate Jacobi coordinate sets is effected by the rotation matrix eq. (B.8), which for a system of identical particles becomes:

$$\begin{pmatrix} \vec{x}' \\ \vec{y}' \\ \vec{z}' \end{pmatrix}_{K_{12,4}^3} = \begin{pmatrix} 1 & 0 & 0 \\ 0 & \frac{1}{3} & \frac{2\sqrt{2}}{3} \\ 0 & \frac{2\sqrt{2}}{3} & -\frac{1}{3} \end{pmatrix} \begin{pmatrix} \vec{x} \\ \vec{y} \\ \vec{z} \end{pmatrix}_{K_{12,3}^4} \quad (\text{D.5})$$

²Physical FY components $K_{ij,k}^l$ should satisfy condition (C.16) (i.e. having right symmetry relations for exchange of particles i and j), however they are not obliged to have certain symmetry for exchange of any other particle pair. Only the total wave function, being a sum of all these components is (anti)-symmetric in exchange of any two particles. Therefore if we write component $K_{ij,k}^l$ in some other coordinate set, let it be $K_{ik,j}^l$, one will loose validity of condition (C.16), since component of departure does not have defined symmetry for particles i and k .

Permutation matrix we define in a standard way, as

$$\langle \alpha xyz [K] | Q | \alpha' x' y' z' [K] \rangle = \tilde{t}_{\alpha, \alpha'} \int_{-1}^1 \tilde{h}_{\alpha, \alpha'}^{\mathcal{J}}(y, z.u) K_{\alpha'}(x', y', z') du. \quad (\text{D.6})$$

Integration is done only in one angular variable $u = \hat{y} \cdot \hat{z}$, since by permutating particles 3 and 4, vector \vec{x} is unchanged. Therefore rotations are done only in the yz plane. Expressions of the function $\tilde{h}_{\alpha, \alpha'}^{\mathcal{J}}(x, y, z.u)$, as well as corresponding coefficient $\tilde{t}_{\alpha, \alpha'}$ are easy to find:

$$\begin{aligned} \tilde{t}_{\alpha, \alpha'} &= \langle T_{K_\alpha} | P_{34} | T_{K_{\alpha'}} \rangle = \left\langle \left[\left\{ (t_1 t_2)_{\tau_x} t_3 \right\}_{T_3} t_4 \right]_{\mathcal{T}} \middle| \left[\left\{ (t_1 t_2)_{\tau'_x} t_4 \right\}_{T'_3} t_3 \right]_{\mathcal{T}} \right\rangle = \\ &= (-)^{T_3 + T'_3 - \tau'_x - \mathcal{T}} \delta_{\tau_x, \tau'_x} A \left\{ \begin{array}{ccc} t_3 & \tau'_x & T_3 \\ t_4 & \mathcal{T} & T'_3 \end{array} \right\} \end{aligned} \quad (\text{D.7})$$

$$\begin{aligned} \tilde{h}_{\alpha, \alpha'}^{\mathcal{J}}(x, y, z, u) &= \varepsilon \sum_{\sigma, l'_{yz}, J'_2} \delta_{l_x, l'_x} \delta_{\sigma_x, \sigma'_x} \delta_{j_x, j'_x} (-)^{s_3 + s_4 - \sigma} A \left\{ \begin{array}{ccc} j_x & j_y & J_3 \\ j_z & \mathcal{J} & J'_2 \end{array} \right\} A \left\{ \begin{array}{ccc} j'_x & j'_y & J'_3 \\ j'_z & \mathcal{J} & J'_2 \end{array} \right\} \\ &\quad A \left\{ \begin{array}{ccc} l_y & s_3 & j_y \\ l_z & s_4 & j_z \\ l'_{yz} & \sigma & J'_2 \end{array} \right\} A \left\{ \begin{array}{ccc} l'_y & s_4 & j'_y \\ l'_z & s_3 & j'_z \\ l'_{yz} & \sigma & J'_2 \end{array} \right\} \frac{yz}{y'z'} \hat{h}_{l_y l_z, l'_y l'_z}^{l_{yz}}(y, z, u). \end{aligned} \quad (\text{D.8})$$

D.1.3 Permutation operator $\langle \alpha xyz [H] | \tilde{P} | \alpha' x' y' z' [H] \rangle = \langle \alpha xyz [H] | P_{13} P_{24} | \alpha' x' y' z' [H] \rangle$

Operator $P_{13} P_{24}$ when applied on components H (see eq. (1.112) retains the form of the partition tree, simply vectors \vec{x} and \vec{y} are permuted:

$$\begin{pmatrix} \vec{x}' \\ \vec{y}' \\ \vec{z}' \end{pmatrix}_{H_{34,12}} = \begin{pmatrix} 0 & 1 & 0 \\ 1 & 0 & 0 \\ 0 & 0 & -1 \end{pmatrix} \begin{pmatrix} \vec{x} \\ \vec{y} \\ \vec{z} \end{pmatrix}_{H_{12,34}} \quad (\text{D.9})$$

Since rotation matrix is a simple variable permutation its resultant permutation operator is isotropic in space and therefore presents as a simple phase factor.

$$t_{\alpha, \alpha'} = \delta_{\tau_y, \tau'_x} \delta_{\tau_x, \tau'_y} (-)^{\tau_x + \tau_y - \mathcal{T}} \quad (\text{D.10})$$

$$\langle H | P_{13} P_{24} | H \rangle = \sum_{\alpha'} t_{\alpha, \alpha'} \delta_{l_x, l'_y} \delta_{l_y, l'_x} \delta_{l_z, l'_z} \delta_{l_x, l'_x} \delta_{\sigma_x, \sigma'_y} \delta_{\sigma_y, \sigma'_x} \delta_{\sigma_z, \sigma'_z} \delta_{j_x, j'_y} \delta_{j_y, j'_x} \delta_{j_z, j'_z} \delta_{j_{xy}, j'_{xy}} (-)^{j_x + j_y - j_{xy} + l_z} \quad (\text{D.11})$$

D.1.4 Transitions between the bases **K** and **H**

Transition between the PWB sets of *K*-type and *H*-type components, having the same particle indexing order, is effected by the rotation matrix, which in case of identical particle coincides with

its own inverse (see eq. (B.12) and eq. (B.13)):

$$\begin{pmatrix} \vec{x}' \\ \vec{y}' \\ \vec{z}' \end{pmatrix}_{H(K)} = \begin{pmatrix} 1 & 0 & 0 \\ 0 & -\frac{1}{\sqrt{3}} & \sqrt{\frac{2}{3}} \\ 0 & \sqrt{\frac{2}{3}} & \frac{1}{\sqrt{3}} \end{pmatrix} \begin{pmatrix} \vec{x} \\ \vec{y} \\ \vec{z} \end{pmatrix}_{K(H)} \quad (\text{D.12})$$

This rotation matrix conserves \vec{x} value and thus describes rotations only in yz plane. Rotation angle of yz plane we denote by $u = \hat{y} \cdot \hat{z}$. Permutation operator we write in the standard one-dimensional integral form:

$$\langle \alpha xyz [K] | Q | \alpha' x' y' z' [H] \rangle = \tilde{t}_{\alpha, \alpha'} \int_{-1}^1 \tilde{h}_{\alpha, \alpha'}^{\mathcal{J}}(y, z, u) K_{\alpha'}(x', y', z') du. \quad (\text{D.13})$$

Since, rotation matrix is the same for transitions from H to K components as for transitions from K to H , simple relation between corresponding permutation functions $\tilde{h}_{\alpha, \alpha'}(y, z, u)$ exist:

$$h_{\alpha, \alpha'}^{\langle K || H \rangle}(x, y, z, u) = h_{\alpha', \alpha}^{\langle H || K \rangle}(x, y, z, u). \quad (\text{D.14})$$

These permutation operators are easy to calculate, they result in the following expressions:

$$t_{\alpha, \alpha'} = \delta_{\tau_x, \tau'_x} A \left\{ \begin{array}{ccc} \tau'_x & t_3 & T_3 \\ t_4 & \mathcal{T} & \tau'_y \end{array} \right\} \quad (\text{D.15})$$

$$\begin{aligned} h_{\alpha, \alpha'}^{\langle K || H \rangle}(x, y, z, u) &= t_{\alpha, \alpha'} \sum_{l'_{yz}, J'_2} \delta_{l_x, l'_x} \delta_{\sigma_x, \sigma'_x} \delta_{j_x, j'_x} (-)^{j'_y + l'_{yz} - l'_y - J'_2} A \left\{ \begin{array}{ccc} j_x & j_y & J_3 \\ l_z & \mathcal{J} & J'_2 \end{array} \right\} \\ &\quad A \left\{ \begin{array}{ccc} j'_x & j'_y & j'_{xy} \\ l'_z & \mathcal{J} & J'_2 \end{array} \right\} A \left\{ \begin{array}{ccc} l'_z & l'_y & l'_{yz} \\ \sigma'_y & J'_2 & j'_y \end{array} \right\} A \left\{ \begin{array}{ccc} l_y & s_3 & j_y \\ l_z & s_4 & j_z \\ l'_{yz} & \sigma'_y & J'_2 \end{array} \right\} \quad (\text{D.16}) \\ &\quad \frac{xyz}{x'y'z'} \hat{h}_{l_y l_z, l'_y l'_z}^{l_{yz}}(y, z, u). \end{aligned}$$

D.2 Double operators

In general, four operators defined above are sufficient to solve 4-body problem and construct systems wave function. However, one needs their successive application already when solving FY equations. Even if one only wishes to evaluate projection of a single amplitude into other one from different basis by consequent application of a few permutation operators, one should introduce a full function basis in-between those operators. Note the first permutation operator, when applied to a given amplitude, will project it to full amplitude set of the intermediate basis. By limiting (truncating) this basis to the amplitudes selected in the solution one makes approximation and thus cannot blame that obtained results are well converged. Alternative is to define the double operators, which need double integrals, and appear in FY equations.

Systems wave function consist some terms, which can be obtained only after three subsequent plane rotations (has three permutation operator terms). Therefore, in general, they need some triple integrals to be performed. Evaluation of these integrals is very costly numerical task, that's why we always reconstruct the wave function by at least once truncating the basis.

D.2.1 Permutation operator $\langle H| P^- Q P^- |K\rangle = \langle H| P_{13} P_{24} |K\rangle$

This operator can be expressed as $\langle H| \tilde{P} |H\rangle \langle H| |K\rangle$, however due to triviality of operation $\langle H| \tilde{P} |H\rangle$ it can still be obtained by performing a single integral. Expressions for it follows directly by combining expressions of $\langle H| \tilde{P} |H\rangle$ and $\langle H| |K\rangle$ operators:

$$\begin{pmatrix} \vec{x}' \\ \vec{y}' \\ \vec{z}' \end{pmatrix}_{K_{34,1}^2} = \begin{pmatrix} 1 & 0 & 0 \\ 0 & -\frac{1}{\sqrt{3}} & \sqrt{\frac{2}{3}} \\ 0 & \sqrt{\frac{2}{3}} & \frac{1}{\sqrt{3}} \end{pmatrix} \begin{pmatrix} 0 & 1 & 0 \\ 1 & 0 & 0 \\ 0 & 0 & -1 \end{pmatrix} \begin{pmatrix} \vec{x} \\ \vec{y} \\ \vec{z} \end{pmatrix}_{H_{12,34}} = \begin{pmatrix} 0 & 1 & 0 \\ -\frac{1}{\sqrt{3}} & 0 & -\sqrt{\frac{2}{3}} \\ \sqrt{\frac{2}{3}} & 0 & -\frac{1}{\sqrt{3}} \end{pmatrix} \begin{pmatrix} \vec{x} \\ \vec{y} \\ \vec{z} \end{pmatrix}_{H_{12,34}} \quad (\text{D.17})$$

For the isospin part we have:

$$t_{\alpha,\alpha'} = \delta_{\tau'_x,\tau_y} (-)^{\tau_x+\tau_y-\mathcal{T}} A \left\{ \begin{array}{ccc} \tau_x & t_3 & T'_3 \\ t_4 & \mathcal{T} & \tau_y \end{array} \right\} \quad (\text{D.18})$$

and finally:

$$\begin{aligned} h_{\alpha,\alpha'}^{\langle H||K\rangle}(x,y,z,u) &= t_{\alpha,\alpha'} \sum_{l'_{yz}, J'_2} \delta_{l_y, l'_x} \delta_{\sigma_y, \sigma'_x} \delta_{j_y, j'_x} (-)^{2j_x + j_y - j_{xy} - J'_2 + l_x - l'_{yz}} A \left\{ \begin{array}{ccc} j_y & j_x & j_{xy} \\ l_z & \mathcal{J} & J'_2 \end{array} \right\} \\ &\quad A \left\{ \begin{array}{ccc} j'_x & j'_y & J'_3 \\ j'_z & \mathcal{J} & J'_2 \end{array} \right\} A \left\{ \begin{array}{ccc} l_z & l_x & l'_{yz} \\ \sigma_x & J'_2 & j_x \end{array} \right\} A \left\{ \begin{array}{ccc} l'_y & s_1 & j'_y \\ l'_z & s_2 & j'_z \\ l'_{yz} & \sigma_x & J'_2 \end{array} \right\} \quad (\text{D.19}) \\ &\quad \frac{xyz}{x'y'z'} \hat{h}_{l_x l_z, l'_y l'_z}^{l'_{yz}}(x,z,u). \end{aligned}$$

D.2.2 Double operator $\langle \alpha xyz [K] | P^+ Q | \alpha' x' y' z' [K] \rangle = \varepsilon \langle \alpha xyz [K] | P_{12} P_{23} P_{34} | \alpha' x' y' z' [K] \rangle$

This operator projects the partial wave amplitudes of base $K_{12,3}^4$ to the base $K_{23,4}^1$ (see eq. 1.111). To express Jacobi coordinates of $K_{23,4}^1$ set through coordinates of the set $K_{12,3}^4$ one should perform at least two consequent rotations.

First we perform rotation in xy plane and afterwards in the plane y_0z . The vectors \vec{y}_0 is intermediate coordinate vector \vec{y} , obtained after the first rotation. The subsequent rotation operation can be written in the matrix form:

$$\begin{pmatrix} \vec{x}' \\ \vec{y}' \\ \vec{z}' \end{pmatrix}_{K_{23,4}^1} = \begin{pmatrix} 1 & 0 & 0 \\ 0 & \frac{1}{3} & \frac{2\sqrt{2}}{3} \\ 0 & \frac{2\sqrt{2}}{3} & -\frac{1}{3} \end{pmatrix} \begin{pmatrix} \vec{x}' \\ \vec{y}_0 \\ \vec{z} \end{pmatrix}_{K_{23,1}^4} \quad \begin{pmatrix} \vec{x}' \\ \vec{y}_0 \\ \vec{z} \end{pmatrix}_{K_{23,1}^4} = \begin{pmatrix} -\frac{1}{2} & \frac{\sqrt{3}}{2} & 0 \\ -\frac{\sqrt{3}}{2} & -\frac{1}{2} & 0 \\ 0 & 0 & 1 \end{pmatrix} \begin{pmatrix} \vec{x} \\ \vec{y} \\ \vec{z} \end{pmatrix}_{K_{12,3}^4} \quad (\text{D.20})$$

Isospin part of this operator can be easily obtained by collecting terms from eq. (D.1) and eq. (D.7), which correspond respectively action of operators P^+ and Q :

$$\begin{aligned} t_{\alpha,\alpha'} &= \left\langle \left[\left\{ (t_1 t_2)_{\tau_x} t_3 \right\}_{T_3} t_4 \right]_{\mathcal{T}} \middle| \left[\left\{ (t_2 t_3)_{\tau'_x} t_4 \right\}_{T'_3} t_1 \right]_{\mathcal{T}} \right\rangle \quad (\text{D.21}) \\ &= (-)^{t_1 + T'_3 - T} A \left\{ \begin{array}{ccc} t_1 & t_2 & \tau_x \\ t_3 & T_3 & \tau'_x \end{array} \right\} A \left\{ \begin{array}{ccc} t_1 & \tau'_x & T_3 \\ t_4 & T & T'_3 \end{array} \right\}. \end{aligned}$$

By noting $u = \cos(\widehat{\vec{x}}, \widehat{\vec{y}})$, $v = \cos(\widehat{\vec{y}_0}, \widehat{\vec{z}})$ and after applying some routine algebra the following relation is obtained by:

$$\begin{aligned} g_{\alpha,\alpha'}^{(K||K)}(x, y, z, u, v) &= t_{\alpha,\alpha'} \sum_{l_{xy}, l'_{xy}, \sigma, \sigma', l'_{yz}, \lambda, L, S} A \left\{ \begin{array}{ccc} l_x & \sigma_x & j_x \\ l_y & s_3 & j_y \\ l_{xy} & \sigma & J_3 \end{array} \right\} A \left\{ \begin{array}{ccc} l'_x & \sigma'_x & j'_x \\ l'_y & s_4 & j'_y \\ l'_{xy} & \sigma' & J'_3 \end{array} \right\} \\ &\quad A \left\{ \begin{array}{ccc} l_{xy} & \sigma & J_3 \\ l_z & s_4 & j_z \\ L & S & \mathcal{J} \end{array} \right\} A \left\{ \begin{array}{ccc} l'_{xy} & \sigma' & J'_3 \\ l'_z & s_2 & j'_z \\ L & S & \mathcal{J} \end{array} \right\} A \left\{ \begin{array}{ccc} l'_x & l'_y & l'_{xy} \\ l'_z & L & l'_{yz} \end{array} \right\} \quad (\text{D.22}) \\ &\quad A \left\{ \begin{array}{ccc} l'_x & \lambda & l_{xy} \\ l_z & L & l'_{yz} \end{array} \right\} (-)^{s_1 + \sigma' - S} A \left\{ \begin{array}{ccc} s_1 & s_2 & \sigma_x \\ s_3 & \sigma & \sigma'_x \end{array} \right\} A \left\{ \begin{array}{ccc} s_1 & \sigma'_x & \sigma \\ s_4 & S & \sigma' \end{array} \right\} \\ &\quad \frac{xyz}{x'y'z'} \hat{h}_{l_{xy} l_y, l'_x \lambda}^{l_{xy}}(x, y, u) \hat{h}_{\lambda l_z, l'_y l'_z}^{l'_{yz}}(y_0, z, v) \end{aligned}$$

Transition between these two basis is done after calculating a double integral:

$$\langle K_{\alpha xyz} | P^+ Q | K \rangle = \sum_{\alpha'} \int_{-1}^1 du \int_{-1}^1 g_{\alpha,\alpha'}^{(K||K)}(x, y, z, u, v) K_{\alpha'}(x', y', z') dv. \quad (\text{D.23})$$

D.2.3 Double operator $\langle \alpha xyz [K] | P^+ | \alpha' x' y' z' [H] \rangle = \langle \alpha xyz [K] | P_{12} P_{23} | \alpha' x' y' z' [H] \rangle$

It is clear that this operator can be decomposed into two operators, demanding single integration each (i.e. $\langle K | P_{12} P_{23} | K \rangle \langle K | H \rangle$), by introducing full functions basis of K -type components in between those two operators. But, as was mentioned above in order to have more assured convergence one is obliged to perform it directly. Following the same steps and using the same notations as for the previous double integral operator, one obtains:

$$\begin{pmatrix} \vec{x}' \\ \vec{y}' \\ \vec{z}' \end{pmatrix}_{H_{23,14}} = \begin{pmatrix} 1 & 0 & 0 \\ 0 & -\frac{1}{\sqrt{3}} & \sqrt{\frac{2}{3}} \\ 0 & \sqrt{\frac{2}{3}} & \frac{1}{\sqrt{3}} \end{pmatrix} \begin{pmatrix} \vec{x}' \\ \vec{y}_0 \\ \vec{z} \end{pmatrix}_{K_{23,1}^4} \quad \begin{pmatrix} \vec{x}' \\ \vec{y}_0 \\ \vec{z} \end{pmatrix}_{K_{23,1}^4} = \begin{pmatrix} -\frac{1}{2} & \frac{\sqrt{3}}{2} & 0 \\ -\frac{\sqrt{3}}{2} & -\frac{1}{2} & 0 \\ 0 & 0 & 1 \end{pmatrix} \begin{pmatrix} \vec{x} \\ \vec{y} \\ \vec{z} \end{pmatrix}_{K_{12,3}^4} \quad (\text{D.24})$$

$$\begin{aligned} t_{\alpha,\alpha'} &= \left\langle \left[\left\{ (t_1 t_2)_{\tau_x} t_3 \right\}_{T_3} t_4 \right]_{\mathcal{T}} \middle| \left[\left\{ (t_2 t_3)_{\tau'_x} (t_1 t_4)_{\tau'_y} \right\}_{T'_3} \right]_{\mathcal{T}} \right\rangle \quad (\text{D.25}) \\ &= (-)^{t_1 + \tau'_x - T_3} A \left\{ \begin{array}{ccc} t_2 & t_3 & \tau'_x \\ t_1 & T & T_3 \end{array} \right\} A \left\{ \begin{array}{ccc} t_1 & t_2 & \tau_x \\ t_3 & T_3 & \tau'_x \end{array} \right\} \end{aligned}$$

And finally:

$$\begin{aligned}
g_{\alpha,\alpha'}^{\langle K||K \rangle}(x,y,z,u,v) &= t_{\alpha,\alpha'} \sum_{l_{xy}, l'_{xy}, \sigma, l'_{yz}, \lambda, L, S} A \left\{ \begin{array}{ccc} l_x & \sigma_x & j_x \\ l_y & s_3 & j_y \\ l_{xy} & \sigma & J_3 \end{array} \right\} A \left\{ \begin{array}{ccc} l'_x & \sigma'_x & j'_x \\ l'_y & \sigma'_y & j'_y \\ l'_{xy} & S & j'_{xy} \end{array} \right\} \\
&\quad A \left\{ \begin{array}{ccc} l_{xy} & \sigma & J_3 \\ l_z & s_4 & j_z \\ L & S & \mathcal{J} \end{array} \right\} (-)^{J-L-j'_{xy}+l'_{xy}} A \left\{ \begin{array}{ccc} S & l'_{xy} & J'_3 \\ l'_z & \mathcal{J} & L \end{array} \right\} \\
&\quad A \left\{ \begin{array}{ccc} l'_x & l'_y & l'_{xy} \\ l'_z & L & l'_{yz} \end{array} \right\} A \left\{ \begin{array}{ccc} l'_x & \lambda & l_{xy} \\ l_z & L & l'_{yz} \end{array} \right\} \\
&\quad (-)^{s_1+\sigma'_x-\sigma} A \left\{ \begin{array}{ccc} s_2 & s_3 & \sigma'_x \\ s_1 & S & \sigma \end{array} \right\} A \left\{ \begin{array}{ccc} s_1 & s_2 & \sigma_x \\ s_3 & \sigma & \sigma'_x \end{array} \right\} \\
&\quad \frac{xyz}{x'y'z'} \hat{h}_{l_x l_y, l'_x \lambda}^{l_{xy}}(x,y,u) \hat{h}_{\lambda l_z, l'_y l'_z}^{l'_{yz}}(y_0, z, v)
\end{aligned} \tag{D.26}$$

D.3 Four body W operators

In full analogy with \hat{W} operators introduced for 3-body system, one can define operators for 4-body system, which enables one to evaluate potential terms expressed in non-proper Jacobi coordinate sets. These operators enable to shift full long-range interaction terms into the left hand side of Faddeev-Yakubovski equations. Therefore one can afford to uncouple FY components at some finite distance and implement the correct boundary conditions.

Let suppose that we have to calculate impact of potential terms $V^l = F(x', y', z')$ in one of FY components amplitude basis, described by non proper Jacobi coordinate set xyz . Furthermore, suppose that transformation from $\vec{x}, \vec{y}, \vec{z}$ to $\vec{x}', \vec{y}', \vec{z}'$ can be effected by two consequent rotations³:

$$\begin{pmatrix} \vec{x}' \\ \vec{y}' \\ \vec{z}' \end{pmatrix} = \begin{pmatrix} c_2 & s_2 & 0 \\ s_2 & -c_2 & 0 \\ 0 & 0 & 1 \end{pmatrix} \begin{pmatrix} \vec{x} \\ \vec{y}_0 \\ \vec{z}' \end{pmatrix} \quad \begin{pmatrix} \vec{x} \\ \vec{y}_0 \\ \vec{z}' \end{pmatrix} = \begin{pmatrix} 1 & 0 & 0 \\ 0 & c_1 & s_1 \\ 0 & s_1 & -c_1 \end{pmatrix} \begin{pmatrix} \vec{x} \\ \vec{y} \\ \vec{z} \end{pmatrix} \tag{D.27}$$

Our aim is to find such function $\mathbb{Y}_{l_x l_y, l_z, l'_x l'_y l'_z}^{\mathcal{L}\mathcal{M}}$, which enables equality:

$$\begin{aligned}
\iiint d\hat{x} d\hat{y} d\hat{z} \left[\{ Y_{l_x}(\hat{x}) Y_{l_y}(\hat{y}) \}_{l_{xy}} Y_{l_z}(\hat{z}) \right]_{\mathcal{L}\mathcal{M}} F(x', y', z') \left[\{ Y_{l'_x}(\hat{x}) Y_{l'_y}(\hat{y}) \}_{l'_{xy}} Y_{l_z}(\hat{z}) \right]_{\mathcal{L}\mathcal{M}} = \\
\int_{-1}^{+1} \int_{-1}^{+1} \mathbb{Y}_{l_x l_y, l_z, l'_x l'_y l'_z}^{\mathcal{L}\mathcal{M}}(x, y, z, u, v) F(x', y', z') du dv
\end{aligned}$$

³In general, not all the relations between 4-body Jacobi coordinate sets can be established by 2 successive rotations. For some coordinate sets necessary relations can be given only after effecting three successive rotations (ex.: $K_{12,3}^4$ and $K_{24,3}^1$). However, local potential terms depend only on distances between two particles (i.e. only distance x is of interest), whereas other two vectors \vec{y} and \vec{z} are relevant. Therefore to evaluate non-proper potential terms one needs only to reproduce vector \vec{x} , which can always be done by two consequent rotations.

where as previously $u = \cos(\widehat{\hat{x}, \hat{y}_0})$ and $v = \cos(\widehat{\hat{y}, \hat{z}})$. One can verify that this operator $\mathbb{Y}_{l_x l_y, l_z, l'_x l'_y l'_z}^{\mathcal{LM}}$ can be expressed using the following relation:

$$\begin{aligned} \mathbb{Y}_{l_x l_y, l_z, l'_x l'_y l'_z}^{\mathcal{LM}}(x, y, z, u, v) &= \sum_{l'_{yz}, \lambda} (-)^{l'_{xy} + l_x + l_y + L + l_2 + l_3} \frac{\hat{l}_1 \hat{l}_2 \hat{l}_5 \hat{l}_6 (c_1 y)^{l_3} (s_1 z)^{l_4}}{4 y_0^{l_2}} \sqrt{\frac{(2l_2 + 1)! \hat{l}_x \hat{l}'_x \hat{l}_y \hat{l}'_y \hat{l}_z \hat{l}'_z \hat{l}_{xy} \hat{l}'_{xy} \hat{l}_3 \hat{l}_4}{(2l_3 + 1)! (2l_4 + 1)!}} \\ &\quad \left(\begin{array}{ccc} l_1 & l_3 & l_5 \end{array} \right) \left(\begin{array}{ccc} l_1 & l_4 & l_6 \end{array} \right) \left(\begin{array}{ccc} l_x & l'_x & l_2 \end{array} \right) \left(\begin{array}{ccc} l_y & l'_y & l_5 \end{array} \right) \left(\begin{array}{ccc} l_z & l'_z & l_6 \end{array} \right) \\ &\quad \left\{ \begin{array}{ccc} l'_{xy} & l_6 & l_{xy} \\ l_z & L & l'_z \end{array} \right\} \left\{ \begin{array}{ccc} l_2 & l_6 & l_5 \\ l_1 & l_3 & l_4 \end{array} \right\} \left\{ \begin{array}{ccc} l_x & l'_x & l_2 \\ l_y & l'_y & l_5 \\ l_{xy} & l'_{xy} & l_6 \end{array} \right\} P_{l_2}(u) P_{l_1}(v) \end{aligned} \quad (\text{D.28})$$

Four identical particles possess certain trivial symmetry properties, which can be used to reduce number of matrix elements to evaluate:

$$\begin{aligned} \langle K_\alpha | V_{13} | K_{\alpha'} \rangle &= (-)^{l_x + l'_x + t_x + t'_x + \sigma_x + \sigma'_x} \langle K_\alpha | V_{23} | K_{\alpha'} \rangle \\ \langle K_\alpha | V_{14} | K_{\alpha'} \rangle &= (-)^{l_x + l'_x + t_x + t'_x + \sigma_x + \sigma'_x} \langle K_\alpha | V_{24} | K_{\alpha'} \rangle \\ \langle H_\alpha | V_{13} | H_{\alpha'} \rangle &= (-)^{l_x + l'_x + t_x + t'_x + \sigma_x + \sigma'_x} \langle H_\alpha | V_{23} | H_{\alpha'} \rangle \\ &= (-)^{l_y + l'_y + t_y + t'_y + \sigma_y + \sigma'_y} \langle H_\alpha | V_{14} | H_{\alpha'} \rangle \\ \langle H_\alpha | V_{14} | H_{\alpha'} \rangle &= (-)^{l_x + l'_x + t_x + t'_x + \sigma_x + \sigma'_x} \langle H_\alpha | V_{24} | H_{\alpha'} \rangle \end{aligned} \quad (\text{D.29})$$

For the physical states $\varepsilon = (-)^{l_x + t_x + \sigma_x}$, all the phase factors above give 1. Furthermore, Coulomb potential does not depend on spins of the interacting particle pair, and therefore conserves spin quantum numbers, thus for the physical states one has:

$$\begin{aligned} \langle K_\alpha | V_{13} | K_{\alpha'} \rangle &= \langle K_\alpha | V_{23} | K_{\alpha'} \rangle \delta_{\sigma_x, \sigma'_x} \\ \langle K_\alpha | V_{14} | K_{\alpha'} \rangle &= \langle K_\alpha | V_{24} | K_{\alpha'} \rangle \delta_{\sigma_x, \sigma'_x} \\ \langle H_\alpha | V_{13} | H_{\alpha'} \rangle &= \langle H_\alpha | V_{23} | H_{\alpha'} \rangle \delta_{\sigma_x, \sigma'_x} \\ &= \langle H_\alpha | V_{14} | H_{\alpha'} \rangle \delta_{\sigma_y, \sigma'_y} \\ \langle H_\alpha | V_{14} | H_{\alpha'} \rangle &= \langle H_\alpha | V_{24} | H_{\alpha'} \rangle \delta_{\sigma_x, \sigma'_x}, \end{aligned} \quad (\text{D.30})$$

which finally leads to:

$$\begin{aligned} \langle K_\alpha | V_{13} + V_{23} | K_{\alpha'} \rangle &= 2 \langle K_\alpha | V_{13} | K_{\alpha'} \rangle \delta_{\sigma_x, \sigma'_x} \\ \langle K_\alpha | V_{14} + V_{24} | K_{\alpha'} \rangle &= 2 \langle K_\alpha | V_{14} | K_{\alpha'} \rangle \delta_{\sigma_x, \sigma'_x} \\ \langle H_\alpha | V_{13} + V_{23} + V_{14} + V_{24} | H_{\alpha'} \rangle &= 4 \langle H_\alpha | V_{13} | H_{\alpha'} \rangle \delta_{\sigma_x, \sigma'_x} \delta_{\sigma_y, \sigma'_y}. \end{aligned} \quad (\text{D.31})$$

Appendix E

Spline interpolation

This appendix is devoted to describe function interpolation techniques used throughout this thesis. The smooth function can be approximated on a finite domain $x \in [a, b]$ by expanding it in a complete set of basis functions; that is:

$$f(x) = \sum_{n=0}^{k \cdot (N+1)-1} C_n S_n(x), \quad (\text{E.1})$$

where the choice of the basis functions $S_n(x)$ is arbitrary. A basis set with many numerical advantages is the set of spline functions. The spline functions are defined as piecewise polynomials of degree k with a continuous derivative of order m . By dividing interval $[a, b]$ into subintervals, separated by the breakpoints x_0, x_1, \dots, x_N , one associates k splines with each of them. The breakpoints can be distributed so that there are less breakpoints in the region where the function is smooth. This is one of advantages of the splines, since by a careful choice of breakpoints one can reduce the size of spline basis without losing precision in approximation.

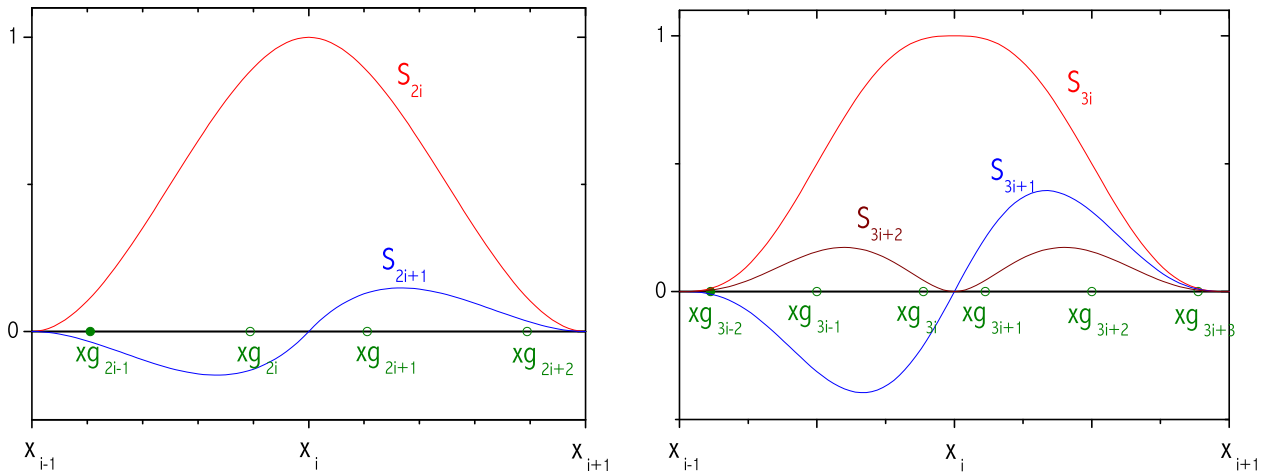


Figure E.1: The form of CHP (figure on the left) and QHP (figure on the right) interpolants.

In order for the m -th derivative to be continuous interpolant polynomial functions should be of degree $m + 1$ or higher. Since we deal with the second-order differential equations, the spline functions should have second order continuous derivatives. The minimal order polynomials satisfying it are cubic ones. Therefore we associate $k = 2$ cubic Hermite polynomials (CHP) with each breakpoint (see Fig. E.1), being defined as:

$$\begin{aligned} \text{for } X_{i-1} \leq x \leq X_i \\ (\text{with } r = \frac{x-X_{i-1}}{X_i-X_{i-1}}) \end{aligned} \quad \begin{cases} S_{2i}(x) = r^2(3 - 2r) \\ S_{2i+1}(x) = -(X_i - X_{i-1})r^2(1 - r) \end{cases} \quad (\text{E.2})$$

$$\begin{aligned} \text{for } X_i \leq x \leq X_{i+1} \\ (\text{with } r = \frac{x-X_i}{X_{i+1}-X_i}) \end{aligned} \quad \begin{cases} S_{2i}(x) = (1 - r)^2(1 + 2r) \\ S_{2i+1}(x) = -(X_{i+1} - X_i)r(1 - r)^2 \end{cases}$$

It turns to be an optimal choice [32]. However, sometimes dealing with more acute wave functions or trying to obtain better precision (especially, when expectation value of kinetic energy is required), it is useful to use quintic Hermite polynomials (QHP), having $k = 3$ polynomials associated with each breakpoint (see Fig. E.1):

$$\begin{aligned} \text{for } X_{i-1} \leq x \leq X_i \\ (\text{with } r = \frac{x-X_{i-1}}{X_i-X_{i-1}}) \end{aligned} \quad \begin{cases} S_{3i}(x) = (1 - r^3)[1 + 3r(1 + 2r)] \\ S_{3i+1}(x) = -(X_i - X_{i-1})(1 - r^3)(1 + 3r) \\ S_{3i+2}(x) = \frac{1}{2}(X_i - X_{i-1})^2r^2(1 - r)^3 \end{cases} \quad (\text{E.3})$$

$$\begin{aligned} \text{for } X_i \leq x \leq X_{i+1} \\ (\text{with } r = \frac{x-X_i}{X_{i+1}-X_i}) \end{aligned} \quad \begin{cases} S_{3i}(x) = r^3[3(1 - r)(3 - 2r) + 1] \\ S_{3i+1}(x) = (X_{i+1} - X_i)r^3(1 - r)(4 - 3r) \\ S_{3i+2}(x) = \frac{1}{2}(X_i - X_{i-1})^2r^3(1 - r)^2 \end{cases} \quad (\text{E.4})$$

Here I will figure out some useful properties of QHP and CHP interpolants. First, one can notice that in each subinterval $i \equiv [x_{i-1}, x_i]$ there are only $2 \cdot k$ non zero splines, therefore one needs to sum only $2 \cdot k$ terms to reconstruct the functions value at any given point:

$$f(x) = \sum_{n=k \cdot (i-1)}^{k \cdot (i+1)-1} C_n S_n(x) \quad x \in [x_{i-1}, x_i] \quad (\text{E.5})$$

This fact turns to be crucial in numerical applications, since it enables one to reduce number of arithmetical operations and furthermore, when applied for solving systems of differential equations, results in linear systems with sparse matrices. Sparse matrices can be compactly stored, therefore considerably reducing requirements of computer memory.

One can remark that it is easy to obtain the interpolated function and its derivative values at the breakpoints, when QHP or CHP interpolants in use:

$$\begin{aligned} f(x_i) &= C_{k \cdot i} & f'(x_i) &= C_{k \cdot i+1} \\ f''(x_i) &= C_{k \cdot i+2} & \text{for QHP interpolants.} \end{aligned} \quad (\text{E.6})$$

These relations facilitates implementation of the boundary conditions. Furthermore, they can serve to interpolate the functions, which values and derivatives are known at the breakpoints:

$$\begin{aligned} f(x) &= \sum_{i=0}^N [f(x_i)S_{2i}(x) + f'(x_i)S_{2i+1}(x)] && \text{for CHP.} \\ f(x) &= \sum_{i=0}^N [f(x_i)S_{3i}(x) + f'(x_i)S_{3i+1}(x) + f''(x_i)S_{3i+2}(x)] && \text{for QHP.} \end{aligned} \quad (\text{E.7})$$

Appendix F

Passing to spherical coordinates

In solving FY equations we have chosen Cartesian Jacobi coordinates x, y, z , since in these coordinates expressions of potential and kinetic energy operators have simple separable form. Separability of these two operators results in major advantage of the Cartesian coordinates, which is separability of elastic scattering wave function into two independent wave functions - one describing plane wave propagation in z direction, whereas other internal wave function of two scattered fragments. However, one can remark that permutation operators described in Appendix D conserve the hyperradius value: $\rho = \sqrt{x^2 + y^2 + z^2}$. Therefore by using spherical coordinates these operators can be represented by significantly smaller matrices, in which dependency on hyperradius is separated. These observations pose an evident question: if one can make use advantages of both coordinate systems in the same resolution code? In order of doing that - one should be able to transform easily the wave function from one coordinate system to the other. Spline interpolation can be effectively applied for it.

Transformation from spherical to Cartesian coordinates is affected using relations:

$$\begin{aligned} x &= \rho \cos \theta \sin \varphi \\ y &= \rho \sin \theta \sin \varphi \\ z &= \rho \cos \varphi \end{aligned} \tag{F.1}$$

Its backtransformation follows

$$\begin{aligned} \rho &= \sqrt{x^2 + y^2 + z^2} \\ u &= \cos \theta = \frac{x}{\sqrt{x^2 + y^2}} \\ v &= \cos \varphi = \frac{z}{\rho} \end{aligned} \tag{F.2}$$

We define two spline bases: one associated with the Cartesian coordinates and the other with the spherical. Spherical variables are contained in $\rho \in [0, \rho_{\max}]$, $u \in [0, 1]$ and $v \in [0, 1]$. One can interpolate any function by developing it in the former two spline bases:

$$\begin{aligned}
f(x, y, z) &= \sum_{i_x=0}^{k_x \cdot (N_x+1)-1} S_{i_x}(x) \sum_{i_y=0}^{k_y \cdot (N_y+1)-1} S_{i_y}(y) \sum_{i_z=0}^{k_z \cdot (N_z+1)-1} S_{i_z}(z) \cdot C_{i_x, i_y, i_z}^{(xyz)} \\
&= \sum_{i_R=0}^{k_R \cdot (N_\rho+1)-1} S_{i_R}(\rho(x, y, z)) \sum_{i_u=0}^{k_u \cdot (N_u+1)-1} S_{i_u}(u(x, y, z)) \sum_{i_v=0}^{k_v \cdot (N_v+1)-1} S_{i_v}(v(x, y, z)) \cdot C_{i_R, i_u, i_v}^{(\rho u v, 4)}
\end{aligned} \tag{F.3}$$

At the Gauss points of the Cartesian spline mesh, using notations of section 1.3.3, function values are obtained employing the following relations:

$$\left[f^{(xyz)} \right]_{j_x, j_y, j_z} = \begin{bmatrix} [N^X] \\ \otimes \\ [N^Y] \\ \otimes \\ [N^Z] \end{bmatrix} \left[C_{i_x, i_y, i_z}^{(xyz)} \right] = \left[M_{(xyz)}^{(\rho u v)} \right]_{j_x, j_y, j_z}^{i_\rho, i_u, i_v} \left[C^{(\rho u v)} \right]_{i_\rho, i_u, i_v} \tag{F.5}$$

where $\left[M_{(xyz)}^{(\rho u v)} \right]_{j_x, j_y, j_z}^{i_\rho, i_u, i_v}$ is a square matrix, permitting to project a function, given its spherical coordinate spline interpolants $\left[C_{i_R, i_u, i_v}^{(\rho u v)} \right]$, to the Gauss points of Cartesian spline mesh. Analogous expression can be written for the Gauss points of the spherical spline mesh:

$$\left[f^{(Ruv)} \right]_{j_R, j_u, j_v} = \begin{bmatrix} [N^\rho] \\ \otimes \\ [N^u] \\ \otimes \\ [N^v] \end{bmatrix} \left[C^{(\rho u v)} \right]_{i_R, i_u, i_v} = \left[M_{(\rho u v)}^{(xyz)} \right]_{j_R, j_u, j_v}^{i_x, i_y, i_z} \left[C^{(xyz)} \right]_{i_x, i_y, i_z} \tag{F.6}$$

Spline interpolation matrices, written in tensor form, can be easily inverted. Therefore, necessary procedure to represent function in spherical coordinate system spline basis $\left[C^{(\rho u v)} \right]_{i_R, i_u, i_v}$, when the values of cartesian grid spline interpolant coefficients are known $\left[C^{(xyz)} \right]_{i_x, i_y, i_z}$, is:

$$\left[C^{(\rho u v)} \right]_{i_R, i_u, i_v} = \begin{bmatrix} [N^\rho]^{-1} \\ \otimes \\ [N^u]^{-1} \\ \otimes \\ [N^v]^{-1} \end{bmatrix} \left[M_{(\rho u v)}^{(xyz)} \right]_{j_R, j_u, j_v}^{i_x, i_y, i_z} \left[C^{(xyz)} \right]_{i_x, i_y, i_z} \tag{F.7}$$

One can establish relation for the inverse process, to determine unknown spline interpolant coefficients of the Cartesian spline basis:

$$\left[C^{(xyz)} \right]_{i_x, i_y, i_z} = \begin{bmatrix} [N^X]^{-1} \\ \otimes \\ [N^Y]^{-1} \\ \otimes \\ [N^Z]^{-1} \end{bmatrix} \left[M_{(xyz)}^{(\rho u v)} \right]_{j_x, j_y, j_z}^{i_R, i_u, i_v} \left[C^{(\rho u v)} \right]_{i_R, i_u, i_v} \tag{F.8}$$

Therefore, one can represent permutation matrices in spherical coordinates, whereas working in Cartesian ones. To evaluate this matrix action - one should transform spline basis to spherical coordinates using eq. (F.7), then multiply with desired permutation matrix and return back to Cartesian coordinates by using eq. (F.8). This procedure, even though looking rather heavy, considerably reduces storage requirements as well as number of arithmetical operations to perform. Note square matrices $\begin{bmatrix} M_{(xyz)}^{(\rho uv)} \end{bmatrix}$ and $\begin{bmatrix} M_{(\rho uv)}^{(xyz)} \end{bmatrix}$ are very sparse, having respectively only $8k_\rho k_u k_v$ and $8k_x k_y k_z$ non-zero elements per line.

Appendix G

Implementing three-body force

G.1 Modified FY equations

Three-body force exhibited between the particles (ijk) can be written as a sum of three terms:

$$V_{ijk} = V_{ij}^{(k)} + V_{jk}^{(i)} + V_{ik}^{(l)}. \quad (\text{G.1})$$

The only restriction in former decomposition is that term $V_{ij}^{(k)}$ is symmetric in exchange of particles (ij) . There is though infinitely many possible ways to perform such a decomposition.

Using these definitions the total potential for the four particle system contains a sum of 6 different pair interaction terms (V_{ij}) and 12 three-body potential terms ($V_{ij}^{(k)}$):

$$V = \sum_{i < j} V_{ij} + \sum_{i < j, k} V_{ij}^{(k)} \quad (\text{G.2})$$

The eq. (1.91) can be rewritten in next evident form:

$$\psi_{ij} = G_0 V_{ij} \Psi + G_0 (V_{ij}^{(k)} + V_{ij}^{(l)}) \Psi. \quad (\text{G.3})$$

By multiplying both sides of this equation by $[1 + G_{ij} V_{ij}]$ and employing the identity:

$$[1 + G_{ij} V_{ij}] G_0 = G_{ij} \quad (\text{G.4})$$

one obtains:

$$\psi_{ij} = G_{ij} V_{ij} [\Psi - \psi_{ij}] + G_{ij} (V_{ij}^{(k)} + V_{ij}^{(l)}) \Psi. \quad (\text{G.5})$$

The function ψ_{ij} can be further decomposed into a sum of subcomponents $K_{ij,k}^l$, $K_{ij,l}^k$ and $H_{ij,kl}$, whereas regrouping terms in the last relation one obtains a set of modified FY equations, which permits treatment of three-body interactions:

$$\begin{cases} K_{ij,k}^l = G_{ij} V_{ij} [\psi_{jk} + \psi_{ik}] + G_{ij} V_{ij}^{(k)} \Psi \\ K_{ij,l}^k = G_{ij} V_{ij} [\psi_{jl} + \psi_{il}] + G_{ij} V_{ij}^{(l)} \Psi \\ H_{ij,kl} = G_{ij} V_{ij} \psi_{kl} \end{cases} \quad (\text{G.6})$$

G.2 Implementing UIX forces

G.2.1 Urbana IX model

The Urbana 3NF model is based on the 2π mechanism with an intermediate Δ excitation proposed in [106]. It is supplemented by a purely phenomenological repulsive short range part. The parameter set of *Urbana IX* 3NF, was recently adjusted [220], when in conjunction of *Av18* NN interaction model, the experimental ^3H binding energy and the nuclear matter density were reproduced.

Usually one express the Urbana interaction in terms of a commutator and anti-commutator part. This reads:

$$\tilde{V}_{12}^{(3)} = A_{2\pi} \left(\{X_{31}, X_{12}\} \{\vec{\tau}_3 \cdot \vec{\tau}_1, \vec{\tau}_1 \cdot \vec{\tau}_2\} + \frac{1}{4} [X_{31}, X_{12}] [\vec{\tau}_3 \cdot \vec{\tau}_1, \vec{\tau}_1 \cdot \vec{\tau}_2] \right) + U_0 T^2(r_{31}) T^2(r_{12}). \quad (\text{G.7})$$

By expanding isospin terms one can rewrite it, as:

$$\tilde{V}_{12}^{(3)} = A_{2\pi} (X_{31} X_{12} I_{23}^- + X_{12} X_{31} I_{23}^+) + U_0 T^2(r_{31}) T^2(r_{12}) \quad (\text{G.8})$$

with

$$\begin{aligned} I_{23}^- &= 2 \left(\vec{\tau}_2 \cdot \vec{\tau}_3 - \frac{i}{4} \vec{\tau}_1 \cdot \vec{\tau}_2 \times \vec{\tau}_3 \right) \\ I_{23}^+ &= 2 \left(\vec{\tau}_2 \cdot \vec{\tau}_3 + \frac{i}{4} \vec{\tau}_1 \cdot \vec{\tau}_2 \times \vec{\tau}_3 \right). \end{aligned} \quad (\text{G.9})$$

The force is explicitly defined as an ensemble of NN interactions, derived from π exchange NN force.

$$X_{ij} = Y(r_{ij}) \vec{\sigma}_i \cdot \vec{\sigma}_j + T(r_{ij}) S_{ij} \quad (\text{G.10})$$

It contains a spin-spin $\vec{\sigma}_i \cdot \vec{\sigma}_j$ and a tensor part

$$S_{ij} = 3 (\vec{\sigma}_i \cdot \vec{r}_{ij}) (\vec{\sigma}_j \cdot \vec{r}_{ij}) - \vec{\sigma}_i \cdot \vec{\sigma}_j \quad (\text{G.11})$$

The radial dependence is provided by

$$\begin{aligned} Y(r) &= \frac{e^{-m_\pi r}}{m_\pi r} \left(1 - e^{-cr^2} \right) \\ T(r) &= \left[1 + \frac{3}{m_\pi r} + \frac{3}{(m_\pi r)^2} \right] \frac{e^{-m_\pi r}}{m_\pi r} \left(1 - e^{-cr^2} \right)^2 \end{aligned} \quad (\text{G.12})$$

Urbana IX model is supplied by 3 adjusted parameters, having following values $A_{2\pi} = -0.0293$ MeV, $U_0 = 0.0048$ MeV and $c = 2.1 \text{ fm}^{-2}$.

G.2.2 Practical implementation

To calculate matrix elements introduced by three-body force we use a trick proposed by W. Glöeckle et al. in [221]. However different three-body force decomposition scheme is employed, which helps us to write equations in more symmetrical form and further simplify the numerical task.

Complete UIX force between particles (123) reads as:

$$\begin{aligned} V_{123} = & A_{2\pi} (X_{31}X_{12}I_{23}^- + X_{12}X_{31}I_{23}^+ + X_{12}X_{23}I_{31}^- + X_{23}X_{12}I_{31}^+ + X_{23}X_{31}I_{12}^- + X_{31}X_{23}I_{12}^+) \\ & + U_0 T^2(r_{31})T^2(r_{12}) + U_0 T^2(r_{12})T^2(r_{23}) + U_0 T^2(r_{23})T^2(r_{31}) \end{aligned} \quad (\text{G.13})$$

Decomposed terms of eq. (G.1) we define as:

$$V_{12}^{(3)} = A_{2\pi} (X_{12}X_{31}I_{23}^+ + X_{12}X_{23}I_{31}^-) + \frac{1}{2}U_0 [T^2(r_{12})T^2(r_{23}) + T^2(r_{31})T^2(r_{12})] \quad (\text{G.14})$$

In FY scheme we are using matrix elements $\langle \alpha xyz [K_{12,3}^4] | V_{12}^{(3)} | \Psi \rangle$ are present. One is left with a task of calculating them:

$$\begin{aligned} \langle \alpha xyz [K_{12,3}^4] | V_{12}^{(3)} | \Psi \rangle = & A_{2\pi} \langle \alpha xyz [K_{12,3}^4] | X_{12}X_{31}I_{23}^+ + X_{12}X_{23}I_{31}^- | \Psi \rangle \\ & + \frac{1}{2}U_0 \langle \alpha xyz [K_{12,3}^4] | T^2(r_{12})T^2(r_{23}) + T^2(r_{31})T^2(r_{12}) | \Psi \rangle \end{aligned} \quad (\text{G.15})$$

Let us precise the necessary steps one should follow in order to evaluate the matrix elements given by the first two potential terms in eq.(G.14). Expressions for the other two potential terms, having only radial dependence, will follow immediately.

$$\begin{aligned} \langle \alpha xyz [K_{12,3}^4] | X_{12}X_{31}I_{23}^+ + X_{12}X_{23}I_{31}^- | \Psi \rangle = & \langle \alpha xyz [K_{12,3}^4] | X_{12} | \alpha' x' y' z' [K_{12,3}^4] \rangle \\ & \times [\langle \alpha' x' y' z' [K_{12,3}^4] | I_{23}^+ | \alpha'' x'' y'' z'' [K_{31,2}^4] \rangle \langle \alpha'' x'' y'' z'' [K_{31,2}^4] | X_{31} | \Psi \rangle \\ & + \langle \alpha' x' y' z' [K_{12,3}^4] | I_{31}^- | \alpha'' x'' y'' z'' [K_{23,1}^4] \rangle \langle \alpha'' x'' y'' z'' [K_{23,1}^4] | X_{23} | \Psi \rangle] \end{aligned} \quad (\text{G.16})$$

Here we have introduced intermediate states noted with bars. We suppose that the basis of the intermediate states is full and integration over its vectors is performed on. The implementation of the intermediate states was made to enable calculation of X_{ij} and T_{ij} potential terms in their proper Jacobi coordinate sets.

First, it is straightforward to prove the identities:

$$\begin{aligned} \langle \alpha' x' y' z' [K_{12,3}^4] | I_{23}^+ | \alpha'' x'' y'' z'' [K_{31,2}^4] \rangle = & \varepsilon_{\alpha'} \varepsilon_{\alpha''} \langle \alpha' x' y' z' [K_{31,2}^4] | I_{23}^- | \alpha'' x'' y'' z'' [K_{12,3}^4] \rangle \\ = & \varepsilon_{\alpha'} \varepsilon_{\alpha''} \langle \alpha' x' y' z' [K_{12,3}^4] | I_{31}^- | \alpha'' x'' y'' z'' [K_{23,1}^4] \rangle \end{aligned} \quad (\text{G.17})$$

and

$$\begin{aligned} \langle \alpha xyz [K_{12,3}^4] | X_{12}X_{31}I_{23}^+ + X_{12}X_{23}I_{31}^- | \Psi \rangle = & [1 + \varepsilon_{\alpha'} \varepsilon_{\alpha''}] \langle \alpha xyz [K_{12,3}^4] | X_{12} | \alpha' x' y' z' [K_{12,3}^4] \rangle \\ & \times \langle \alpha' x' y' z' [K_{12,3}^4] | I_{31}^- | \alpha'' x'' y'' z'' [K_{23,1}^4] \rangle \langle \alpha'' x'' y'' z'' [K_{23,1}^4] | X_{23} | \Psi \rangle \end{aligned}$$

Here $\varepsilon_{\alpha'}$ and $\varepsilon_{\alpha''}$ denotes symmetry factor of the states α' and α'' consequently $(\varepsilon = (-)^{t_x+s_x+l_x})$.

It worths mentioning, that multiplication with operator I_{23}^+ (I_{31}^-) results in loosing antisymmetry properties of FY components. However, since operators X_{ij} are symmetric in exchange of particles (ij) and since the total wave function of the system Ψ is fully antisymmetric, states α'' are antisymmetric. Furthermore states α' are also antisymmetric (physical) in exchange of particles (12), since $X_{12}X_{31}I_{23}^+ + X_{12}X_{23}I_{31}^-$ is symmetric in exchange of particles (12). It means that contributions of symmetric(non-physical) states α' singles out, when one adds contributions of matrix

elements of $X_{12}X_{31}I_{23}^+$ and $X_{12}X_{23}I_{31}^-$. On the other hand contributions of physical states are equal and adds up. Therefore one can restrict to only physical states and replace the phase factor $[1 + \varepsilon_{\alpha'}\varepsilon_{\alpha''}]$ by 2.

Equation for the other two potential terms can be obtained in the similar way:

$$\begin{aligned} \langle \alpha xyz [K_{12,3}^4] | T^2(r_{12})T^2(r_{23})+T^2(r_{31})T^2(r_{12}) | \Psi \rangle &= [1 + \varepsilon_{\alpha'}\varepsilon_{\alpha''}] \langle \alpha xyz [K_{12,3}^4] | T^2(r_{12}) | \alpha' x' y' z' [K_{12,3}^4] \rangle \\ &\times \langle \alpha' x' y' z' [K_{12,3}^4] | \alpha'' x'' y'' z'' [K_{23,1}^4] \rangle \langle \alpha'' x'' y'' z'' [K_{23,1}^4] | T^2(r_{23}) | \Psi \rangle \end{aligned}$$

The same strategy is valid in calculating these matrix elements. One can restrict to only physical intermediate basis functions and calculate the double contribution of one of two terms.

The ability to restrict in calculations to only physical states is a major advantage of modified decomposition of *UIX* 3BF. Original method, proposed by Glöeckle et al. [221], required doubling the basis states by introducing non-physical, spurious, states. Furthermore, we must perform only one Jacobi basis transformation operation, which is the most CPU-time requiring task, whereas in [221] two such operations were used.

G.2.3 Explicit form of matrix elements

In this section we briefly summarize the matrix elements of the NN-like interactions X_{ij} , as well as I^\pm isospin operators. Matrix elements of the operator X_{ij} in its proper Jacobi basis reads as:

$$\begin{aligned} \langle \alpha xyz [K_{12,3}^4] | X_{12} | \alpha' x' y' z' [K_{12,3}^4] \rangle &= \delta(x-x')\delta(y-y')\delta(z-z')\delta_{\sigma_x,\sigma'_x}\delta_{j_x,j'_x}\delta_{l_y,l'_y}\delta_{j_y,j'_y}\delta_{J_3,J'_3}\delta_{l_z,l'_z}\delta_{j_z,j'_z}\delta_{J,J'}\delta_{\tau_x,\tau'_x}\delta_{T_3,T'_3}\delta_{T,T'} \\ &\times [\delta_{l_x,l'_x}(4\sigma_x - 3)Y(x) + \delta_{\sigma_x,1}T(x)S_{l_x,l'_x,j_x}] \end{aligned}$$

with

$$S_{l_x,l'_x,j_x} = \begin{bmatrix} -2\frac{j_x-1}{2j_x+1} & 0 & 6\frac{\sqrt{j_x(j_x+1)}}{2j_x+1} \\ 0 & 2 & 0 \\ 6\frac{\sqrt{j_x(j_x+1)}}{2j_x+1} & 0 & -2\frac{j_x+2}{2j_x+1} \end{bmatrix} \quad \begin{array}{ll} l_x=j_x-1 \\ l_x=j_x \\ l_x=j_x+1 \end{array} \quad \begin{array}{l} l'_x=j_x-1 \\ l'_x=j_x \\ l'_x=j_x+1 \end{array} \quad (G.18)$$

Terms of the isospin operators $I_{\alpha\beta}^\pm$ are easy to calculate, they give following expressions:

$$\begin{aligned}
& \langle ((\tau_1 \tau_2)_t \tau_3)_T | \vec{\tau}_3 \cdot \vec{\tau}_1 | ((\tau_2 \tau_3)_{t'} \tau_1)_{T'} \rangle = \delta_{TT'} (-)^{t+1} 6 \sqrt{\hat{t} \hat{t}'} \left\{ \begin{array}{ccc} \frac{1}{2} & \frac{1}{2} & t' \\ \frac{1}{2} & 1 & \frac{1}{2} \\ t & \frac{1}{2} & T \end{array} \right\} \\
& - \frac{i}{4} \langle ((\tau_1 \tau_2)_t \tau_3)_T | \vec{\tau}_2 \cdot \vec{\tau}_3 \times \vec{\tau}_1 | ((\tau_2 \tau_3)_{t'} \tau_1)_{T'} \rangle \\
& = \delta_{TT'} 6 \sqrt{\hat{t} \hat{t}'} \sum_{\xi} (-)^{2T-\xi+\frac{1}{2}} \left\{ \begin{array}{ccc} \xi & \frac{1}{2} & 1 \\ \frac{1}{2} & \frac{1}{2} & t \end{array} \right\} \left\{ \begin{array}{ccc} T & \frac{1}{2} & t \\ \frac{1}{2} & 1 & \xi \\ t' & \frac{1}{2} & \frac{1}{2} \end{array} \right\}
\end{aligned}$$

This concludes the summary on the three-body force implementation in FY equations. The form of Jacobi basis transformation operators required in expressions have been already provided through eq. (D.4) in Appendix D.

Appendix H

The Scattering amplitude

In the main part of the thesis it was shown how to calculate the total cross sections and the phase-shifts of the scattering process. However one can not measure these quantities by the scattering experiment directly. To obtain the total cross sections one should cover the target by the detectors and integrate number of detected events. Extraction of phaseshifts is even more complicated and one should perform far from trivial analysis in order to extract these quantities from the experimental data. Directly controlled quantities in the experiment are the scattered particle angular distributions, or differential cross sections. In addition if one deals with polarized particle target and beam one is able to measure 'so called' polarization observables. In this appendix I will outline how to relate theoretically calculated phaseshifts to the quantities controlled by the experiment.

First, I would like to outline the formalism, when no Coulomb interaction are present. For an incoming plane wave with momentum p_i along the z axis in the channel i , with the spin state $\xi_{\mathcal{S}\nu}$, the wave function asymptote can be written as:

$$|\psi_{\mathcal{S}\nu}(\vec{r})\rangle \xrightarrow[r \rightarrow \infty]{} e^{ik_i z} \xi_{\mathcal{S}\nu} \beta_i + \sum_{f, s', \nu'} \left(\frac{m_i v_i}{m_f v_f} \right)^{\frac{1}{2}} \xi_{\mathcal{S}'\nu'} \beta_f M_{\mathcal{S}'\nu', \mathcal{S}\nu}^{fi}(\theta, \varphi) \frac{e^{ik_f z}}{r}, \quad (\text{H.1})$$

where β_i and β_f denote the particle channels. We expand the incoming plane wave in partial waves using the spherical Hankel functions [18]:

$$e^{ik_i z} \xi_{\mathcal{S}\nu} = \sum_{\mathcal{L}=0}^{\infty} i^{\mathcal{L}} \frac{\sqrt{4\pi(2\mathcal{L}+1)}}{2} \left\{ \hat{h}_{\mathcal{L}}^{(-)}(k_i r) + \hat{h}_{\mathcal{L}}^{(+)}(k_i r) \right\} Y_{\mathcal{L}0}(\theta, \varphi) \xi_{\mathcal{S}\nu} \quad (\text{H.2})$$

$$= \sum_{\mathcal{L}, \mathcal{J}} \frac{\sqrt{4\pi(2\mathcal{L}+1)}}{2} \left\{ \hat{h}_{\mathcal{L}}^{(-)}(k_i r) + \hat{h}_{\mathcal{L}}^{(+)}(k_i r) \right\} C_{\mathcal{L}0, \mathcal{S}\nu}^{\mathcal{J}\nu} \Phi_{|\mathcal{L}\mathcal{S}\mathcal{J}\nu\rangle} \quad (\text{H.3})$$

Where $\Phi_{|\mathcal{L}\mathcal{S}\mathcal{J}\nu\rangle}$ is eigenfunction of the system in $|\mathcal{L}\mathcal{S}\mathcal{J}\nu\rangle$ basis, which can be projected to corresponding $\mathcal{L}\mathcal{S}$ basis $|\mathcal{L}\nu - \nu'\mathcal{S}\nu'\rangle$ basis:

$$\Phi_{|\mathcal{L}\mathcal{S}\mathcal{J}\nu\rangle} = i^{\mathcal{L}} \sum_{\nu'} C_{\mathcal{L}\nu - \nu', \mathcal{S}\nu'}^{\mathcal{J}\nu} \xi_{\mathcal{S}\nu'} Y_{\mathcal{L}\nu - \nu'}(\theta, \varphi). \quad (\text{H.4})$$

Expressed in the partial waves outside the range of the nuclear potential the wave function

reads:

$$\begin{aligned} |\psi_{S\nu}(\vec{r})\rangle \xrightarrow[r \rightarrow \infty]{} & \sum_{\mathcal{J}\mathcal{L}\mathcal{L}'\mathcal{S}'f} \frac{\sqrt{4\pi(2\mathcal{L}+1)}}{2} C_{\mathcal{L}0,S\nu}^{\mathcal{J}\nu} \left\{ \hat{h}_{\mathcal{L}}^{(-)}(k_ir) \delta_{fi} \delta_{\mathcal{L}\mathcal{L}'} \delta_{SS'} \right. \\ & \left. + \langle f, \mathcal{L}', \mathcal{S}' | S^{\mathcal{J}} | i, \mathcal{L}, \mathcal{S} \rangle \left(\frac{m_i v_i}{m_f v_f} \right)^{\frac{1}{2}} \hat{h}_{\mathcal{L}}^{(+)}(k_ir) \Phi_{|\mathcal{L}'\mathcal{S}'\mathcal{J}\nu\rangle} \beta_f \right\} \end{aligned}$$

One should note that S matrix $\langle f, \mathcal{L}', \mathcal{S}' | S^{\mathcal{J}} | i, \mathcal{L}, \mathcal{S} \rangle$ is diagonal in \mathcal{J} and independent of ν , because of the rotational invariance of the Hamiltonian. The factor $\left(\frac{m_i v_i}{m_f v_f} \right)^{\frac{1}{2}}$ has been inserted in order to obtain unitarity of S matrix. By inserting eq. (H.4) into the last formulae and comparing with eq. (H.1) one gets the final expression for the scattering amplitude:

$$M_{\mathcal{S}'\nu',S\nu}^{fi}(\theta, \varphi) = \sum_{\mathcal{J}\mathcal{L}\mathcal{L}'} \frac{\sqrt{\pi(2\mathcal{L}+1)}}{ik_i} C_{\mathcal{L}0,S\nu}^{\mathcal{J}\nu} C_{\mathcal{L}\nu-\nu',S\nu'}^{\mathcal{J}\nu'} \langle f, \mathcal{L}', \mathcal{S}' | S^{\mathcal{J}} - 1 | i, \mathcal{L}, \mathcal{S} \rangle Y_{\mathcal{L}'\nu-\nu'}(\theta, \varphi). \quad (\text{H.5})$$

Differential cross section one obtains after summing all the scattering cross sections occurring after transitions between different spin states and after dividing by the number of initial spin configurations:

$$\frac{d\sigma}{d\Omega}(\theta, \varphi) = \frac{1}{\hat{s}_1 \hat{s}_2} \text{Tr} [M^\dagger(\theta, \varphi) M(\theta, \varphi)]. \quad (\text{H.6})$$

Here I use notation $\hat{s}_i = 2s_i + 1$ to indicate number of possible spin degenerated states for a given spin quantum number s_i .

Total elastic scattering cross section one obtains after integrating angular parts of the last equation and using the fact that spherical harmonics are orthogonal functions. In the case when both systems orbital angular momentum (\mathcal{L}) and spin (S) are conserved by the interaction, one has:

$$\sigma = \frac{4\pi}{k^2} \frac{1}{\hat{s}_1 \hat{s}_2} \sum_i \hat{\mathcal{L}}_i \hat{S}_i \sin^2 \delta_i \quad (\text{H.7})$$

δ_i - here indicates elastic scattering phase shift in state with \mathcal{L}_i and S_i , whereas the sum runs over all the partial waves i and their subdivisions, in case of degeneracy.

More general formula, when only total angular momenta is conserved is:

$$\sigma = \frac{4\pi}{k^2} \frac{1}{\hat{s}_1 \hat{s}_2} \sum_i \hat{\mathcal{J}}_i \sin^2 \delta_i \quad (\text{H.8})$$

Experimentally determined spin observables, or various polarization parameters, are obtained by taking averages of various target-beam spin projection combinations:

$$A_{ik} = \frac{\text{Tr} [M^\dagger(\theta, \varphi) \mathcal{S}_{1i} M(\theta, \varphi) \mathcal{S}_{2k}]}{\text{Tr} [M^\dagger(\theta, \varphi) M(\theta, \varphi)]} \quad (\text{H.9})$$

These observables are called analyzing powers. Powers with only average taken of one particles spin projection is called vector analyzing power and is indicated by only one index, whereas two particle spin correlation observables are called tensor analyzing powers.

When Coulomb interaction is present the strong scattering amplitude absorbs the Coulomb phase factor as in eq. (1.32). In analogy with scattering of particles without spin eq. (1.34) the full scattering amplitude is the sum of strong and Coulomb amplitude. Keeping in mind that Coulomb interaction conserves spin quantum number one has:

$$M_{S'\nu',S\nu}^{fi}(\theta, \varphi) = f_C \delta_{SS'} \delta_{\nu\nu'} + \sum_{\mathcal{J}\mathcal{L}\mathcal{L}'} \frac{\sqrt{\pi(2\mathcal{L}+1)}}{ik_i} \times \\ C_{\mathcal{L}0,S\nu}^{\mathcal{J}\nu} C_{L\nu-\nu',S\nu'}^{\mathcal{J}\nu} e^{i\sigma_{\mathcal{L}'}} \langle f, \mathcal{L}', S' | S^{\mathcal{J}} - 1 | i, \mathcal{L}, S \rangle e^{i\sigma_{\mathcal{L}}} Y_{\mathcal{L}'\nu-\nu'}(\theta, \varphi)$$

where f_C is the same as in eq. (1.37).

For scattering of two demi-integer spin corps, that is a case of N-N, N-³He or N-³H not all the elements of scattering amplitude matrix (or M -matrix) are independent, and numerous symmetry relations can be established [199],[200]. In practice using M -matrix elements one can define 7 independent quantities called invariant amplitudes, which are expressed as [198]:

$$a = \frac{1}{2} (M_{10,10} + M_{11,11} - M_{1-1,11}) \quad (\text{H.10})$$

$$b = \frac{1}{2} (M_{10,10} + M_{11,11} + M_{1-1,11}) \quad (\text{H.11})$$

$$c = \frac{1}{2} (-M_{00,00} + M_{11,11} + M_{1-1,11}) \quad (\text{H.12})$$

$$d = -\frac{1}{\sqrt{2}\sin\theta} (M_{11,10} + M_{10,11}) \quad (\text{H.13})$$

$$e = \frac{1}{\sqrt{2}} (M_{11,10} - M_{10,11}) \quad (\text{H.14})$$

$$f = -i\sqrt{2}M_{11,00} \quad (\text{H.15})$$

The M-matrix in this formalism can be written as [199], [200]:

$$M(k_f, k_i) = \frac{1}{2} \left\{ (a+b) + (a-b) (\sigma_1 \cdot \hat{n}) (\sigma_2 \cdot \hat{n}) + (c+d) (\sigma_1 \cdot \hat{m}) (\sigma_2 \cdot \hat{m}) \right. \\ \left. + (c-d) (\sigma_1 \cdot \hat{l}) (\sigma_2 \cdot \hat{l}) + e (\sigma_1 + \sigma_2) \cdot \hat{n} + f (\sigma_1 - \sigma_2) \cdot \hat{n} \right\}$$

where $\hat{l}, \hat{m}, \hat{n}$ are defined according to

$$\hat{l} = \frac{\vec{k}_f + \vec{k}_i}{|\vec{k}_f + \vec{k}_i|}, \quad \hat{m} = \frac{\vec{k}_f - \vec{k}_i}{|\vec{k}_f - \vec{k}_i|}, \quad \hat{n} = \frac{\vec{k}_f \times \vec{k}_i}{|\vec{k}_f \times \vec{k}_i|}. \quad (\text{H.16})$$

By σ_1 and σ_2 Pauli operators are denoted acting on the spin wave functions of the projectile and target particles of demi-integer spin. Experimentally controlled elastic scattering observables

are given by:

$$\sigma_0 = \frac{d\sigma}{d\Omega}(\theta, \varphi) = \frac{1}{2} (|a|^2 + |b|^2 + |c|^2 + |d|^2 + |e|^2 + |f|^2) \quad (\text{H.17})$$

$$\sigma_0 A_{y0} = \operatorname{Re}(a^* e + b^* f) \quad (\text{H.18})$$

$$\sigma_0 A_{0y} = \operatorname{Re}(a^* e - b^* f) \quad (\text{H.19})$$

$$\sigma_0 A_{yy} = \frac{1}{2} (|a|^2 - |b|^2 - |c|^2 + |d|^2 + |e|^2 - |f|^2) \quad (\text{H.20})$$

$$\sigma_0 A_{xz} = -\operatorname{Re}(a^* d) \sin \theta + \operatorname{Im}(c^* f) - \operatorname{Im}(d^* e) \cos \theta \quad (\text{H.21})$$

$$\sigma_0 A_{zx} = -\operatorname{Re}(a^* d) \sin \theta - \operatorname{Im}(c^* f) - \operatorname{Im}(d^* e) \cos \theta \quad (\text{H.22})$$

$$\sigma_0 A_{xx} = \operatorname{Re}(a^* d) \cos \theta + \operatorname{Re}(b^* c) - \operatorname{Im}(d^* e) \sin \theta \quad (\text{H.23})$$

$$\sigma_0 A_{zz} = -\operatorname{Re}(a^* d) \cos \theta + \operatorname{Re}(b^* c) + \operatorname{Im}(d^* e) \sin \theta \quad (\text{H.24})$$

Bibliography

- [1] F. M. Gutzwiller: *Chaos in Classical and Quantum Mechanics* (Springer Verlag, 1990) p.36.
- [2] F.M. Marqués et al: Phys. Rev. **C 65** (2002) 044006.
- [3] A. Nogga, H. Kamada, W. Glöckle and B.R. Barrett: Phys. Rev. **C 65** (2002) 044002.
- [4] S.C. Pieper, V.R. Pandharipande, R.B. Wiringa and J. Carlson: Phys. Rev. **C 64** (2001) 014001.
- [5] R.B. Wiringa, S.C. Pieper: Phys. Rev. Lett. **89** (2002) 182501.
- [6] S.C. Pieper, K. Varga, R.B. Wiringa: Phys. Rev. **C 66** (2002) 044310.
- [7] V. Efimov: Phys. Lett. **33 B** (1970) 563; Nucl. Phys. **A 210** (1973) 157.
- [8] L. Thomas: Phys. Rev. **47** (1935) 903.
- [9] L.D. Faddeev: Zh. Eksp. Teor. Fiz. **39**, (1960) (Wiley & Sons Inc., 1972). 1459 [Sov. Phys. JETP **12**, (1961) 1014].
- [10] S.P. Merkuriev: Ann. Phys. (N.Y.) **130** (1980) 395.
- [11] N. Orr: Prog. Theor. Phys. Suppl. **146** (2003) 201.
- [12] J.R. Taylor: *Scattering Theory*.
- [13] Ch. J. Joachain: *Quantum Collision Theory*. (North-Holland Publishing Co., Amsterdam, Oxford 1975).
- [14] R. G. Newton: *Scattering Theory of Waves and Particles*. (Springer-Verlag, Berlin, Heidelberg 1982).
- [15] O.A. Yakubowsky: Sov. J. Nucl. Phys. **5** (1967) 937.
- [16] B.A. Lippmann and J. Schwinger: Phys. Rev. **79** (1950) 469.
- [17] B.A. Lippmann: Phys. Rev. **102** (1956) 264.
- [18] M. Abramowitz and I.A. Stegun (editors): *Handbook of mathematical functions. With formulas, graphs, and mathematical tables* (Dover Publications, New York 1965).

- [19] A. Messiah: *Mécanique Quantique*. (Dunod 1972).
- [20] T.F. O'Malley, L. Spruch and L. Rosenberg: J. Math. Phys. **125** (1961) 491.
- [21] Gy. Bencze, C. Chandler, J.L. Friar, A.G. Gibson and G.L. Payne: Phys. Rev. **C 35** (1987) 1188
- [22] J. Carbonell and K.V. Protasov: Z. Phys. A, Hadrons and Nuclei **355** (1996) 87
- [23] L.D. Faddeev: *Mathematical aspects of the three-body problem in the quantum scattering theory* (Israel Program for Scientific Translations, Jerusalem 1965).
- [24] E. W. Schmid and H. Ziegelmann: *The Quantum Mechanical Three-Body Problem* (Vieweg tracts in pure and applied physics 1974).
- [25] S.P. Merkuriev and S.L. Yakovlev: Teor. Mat. Fiz. **56** (1983) 60 [Theor. Math. Phys. **56** (1984) 673].
- [26] S.P. Merkuriev and S.L. Yakovlev: Yad. Fiz. **39** (1984) 1580 [Sov. J. Nucl. Phys. **39** (1984) 1002].
- [27] V. B. Belyaev: *Lectures on the Theory of Few-Body Systems* (Springer-Verlag, Berlin, Heidelberg 1990).
- [28] A.P. Yutsis, A.A. Bandzaitis: *The Theory of Angular Momentum in Quantum Mechanics* (Mintis, Vilnius, 1965).
- [29] D.A. Varshalovich, A.N. Moskalev and V.K. Khersonskii: *Quantum Theory of Angular Momentum* (World Scientific, 1988).
- [30] G.L. Payne: Lecture notes in Physics **273** (Springer-Verlag, Berlin 1987) 64.
- [31] C. de Boor and B. Swartz: SIAM J. Numer. Anal. **10** (1973) 582.
- [32] C. de Boor: *A Practical Guide to Splines* (Springer-Verlag, Berlin 1978).
- [33] R.A. Malfliet and J.A. Tjon: Nucl. Phys. **A 127** (1969) 161.
- [34] W. Glöckle: Nucl. Phys. A **381** (1982) 343.
- [35] K. Laganke, J.A. Maruhn and S.E. Koonin (editors): *Computational Nuclear Physics 1* (Springer-Verlag, Berlin, Heidelberg 1991) 152.
- [36] R.A. Aziz, M. J. Slaman: J. Chem. Phys **94** (1991) 12:8047.
- [37] Y. Saad: *Numerical Methods for Large Eigenvalue Problems* (Manchester University Press, Series in Algorithms and Architectures for Advanced Scientific Computing, New York 1992.)

- [38] Y. Saad: *Iterative Methods for Sparse Linear Systems* (Society for Industrial & Applied Mathematics, 2nd edd. 2003).
- [39] Y. Saad, M.H. Schultz: SIAM J. Sci. Stat. Comput. **7** (1986) 856.
- [40] H.A. van der Vorst: SIAM J. Sci. Stat. Comput. **12** (1992) 631.
- [41] G.H. Golub and C.F. van Loan: *Matrix computations, volume 3* (The Johns Hopkins University Press, Baltimore 1983).
- [42] N.W. Schellingerhout, L.P. Kok and G.D. Bosveld: Phys. Rev **A 40** (1989) 5568.
- [43] N.W. Schellingerhout, J.J. Schut and L.P. Kok: Phys. Rev **C 46** (1992) 1192.
- [44] F. W. Byron and R. W. Fuller: *Mathematics of Classical and Quantum physics* (Dover Publications, Inc., New York 1992).
- [45] L. Wolniewicz and T. Orlikowski: Molec. Phys. **74** (1991) 103.
- [46] R. E. Moss: Molec. Phys. **80** (1993) 1541.
- [47] J. M. Taylor, Zong-Chao Yan, A. Dalgarno, J. F. Babb: Molec. Phys. **97** (1999) 1.
- [48] A. M. Frolov: Phys. Rev. **A 57** (1998) 2436.
- [49] V. I. Korobov: Phys. Rev. **A 61** (2000) 064503.
- [50] L. Hilico, N. Billy, B. Grémaud and D. Delande: Eur. Phys. J. **D 12** (2000) 449.
- [51] L. Hilico, N. Billy, B. Grémaud and D. Delande: J. Phys. **B 34** (2001) 491.
- [52] C.D. Lin: Adv. At. Mol. Phys. **22** (1986) 77.
- [53] V.V. Gusev et al: Few Body Syst. **9** (1990) 137.
- [54] C. Y. Hu, A.A. Kvitsinsky: Phys. Rev. **A 46** (1992) 7301.
- [55] A. A. Kvitsinsky, J. Carbonell and C. Gignoux: Phys Rev. **A 46** (1992) 1310.
- [56] A. A. Kvitsinsky, J. Carbonell and C. Gignoux: Phys Rev. **A 51** (1995) 2997
- [57] R. Lazauskas: *Rapport de Stage DEA*, ISN-UJF (2000).
- [58] J. Carbonell, F. Ciesielski and C. Gignoux: Few-Body Systems Suppl. **8** (1995) 428.
- [59] A. Voronin and J. Carbonell: Phys. Rev. **A 57** 4335 (1998).
- [60] B.D. Esry and H.R. Sadeghpour: Phys. Rev. **A 67** (2003) 012704.
- [61] J.M. Taylor, Z. Yan, A. Dalgarno and J.F. Babb: Molec. Phys. **97** (1999) 25.

- [62] E. Cravo and A.C. Fonseca: Few-Body Systems **5** (1988) 117.
- [63] A. M. Veselova: Theor. Math. Phys. **3** (1970) 542; **13** (1972) 369.
- [64] E.O. Alt, W. Sandhas and H. Ziegelmann: Nucl. Phys. **A 445** (1985) 429; **A 465** (1987) 755.
- [65] J.V. Noble: Phys. Rev. **161** (1967) 945.
- [66] S.P. Merkuriev: Acta Physica Austriaca, Supplementum **XXIII** (1981) 65.
- [67] A. Yeremin, A.M. Frolov and E.B. Kutukova: Few-Body Systems **4** (1988) 111.
- [68] N. W. Schellingerhout: *Factorizability in the numerical few-body problem* (PhD thesis, Rijksuniversiteit Groningen 1995).
- [69] N.F. Mott and H.S.W. Massey: *The Theory of Atomic Collisions* (Oxford Sc. Pub. 3rd Ed. 1965).
- [70] L. I. Schiff: *Quantum mechanics* (McGraw-Hill, New York, 1968).
- [71] I. Bialynicki-Birula, M. Cieplak and J. Kaminski: *Theory of Quanta* (Oxford University Press, New York, Oxford 1992).
- [72] A. Martin, J.-M. Richard and T.T. Wu: Phys. Rev. **A 46** (1992) 3697.
- [73] M. Rotenberg and J. Stein: Phys. Rev. **182** (1969) 1.
- [74] E.A.G. Armour and D.M. Schrader: Can. J. Phys. **60** (1982) 581.
- [75] L. Landau and E. Lifchitz: *Mécanique Quantique* (Ed. Mir, Moscou 1975).
- [76] F. Luo, G. McBane, G. Kim, C. Giese and W. Gentry: J. Chem. Phys. **98** (1993) 3564.
- [77] J. Carbonell, R. Lazauskas, D. Delande, L. Hilico and S. Kilic: physics/0207007 (2002).
- [78] D. Delande, L. Hilico and S. Kilic: private communications.
- [79] M.H. Howells and R.A. Kennedy: J. Chem. Soc. Faraday Trans **86** (1990) 3495.
- [80] J. Bernabeu and R. Tarrach: Annals of Physics **102** (1976) 323.
- [81] D.R. Bates: MNRAS **111** (1951) 303B.
- [82] D.R. Bates: The Astroph. Journ. **270** (1983) 564.
- [83] A. Carrington, C.A. Leach, R.E. Moss et al.: Chem. Soc. Faraday Trans. **89** (1993) 603.
- [84] A.D.J. Critchley, A.N. Hughes and I.R. McNab: Phys. Rev. Lett. **86** (2001) 0031.
- [85] N. Moiseyev: Phys. Rep. **302** (1998) 211.

- [86] J. Chadwick: Nature **129** (1932) 312.
- [87] W. Heisenberg: Zeits. f. Phys. **77** (1932) 1.
- [88] B. Cassen and E.U. Condon: Phys. Rev. **50** (1936) 846.
- [89] H. Yukawa: Proc. Phys. Math. Soc. (Japan) **17** (1935) 48.
- [90] M. Taketani, S. Nakamura, and M. Sasaki: Prog.Theor. Phys. (Kyoto) **6** (1951) 581.
- [91] M. Taketani, S. Machida and S. Onuma: Prog.Theor. Phys. (Kyoto) **7** (1952) 45.
- [92] M.M. Nagels, T.A. Rijken and J.J. de Swart: Phys. Rev. **D 17** (1978) 768.
- [93] V.G.J. Stoks, R.A.M. Klomp, M.C.M. Rentmeester and J.J. de Swart: Phys. Rev. **C 48** (1993) 792.
- [94] V.G.J. Stoks, R.A.M. Klomp, C.P.F. Terheggen and J.J. de Swart: Phys. Rev. **C 49** (1994) 2950.
- [95] M. Lacombe, B. Loiseau, J.M. Richard, R. Vinh Mau, J. Coté, R. Pirés and R. de Tourreil: Phys Rev **C 21** (1980) 861.
- [96] R. Machleidt, K. Holinde and Ch. Elster: Phys. Rep. **149** (1987) 1.
- [97] R. Machleidt: Adv. Nucl. Phys. **19** (1989) 189.
- [98] R. Machleidt: Phys. Rev. **C 63** (2001) 024001.
- [99] R.B. Wiringa, R.A. Smith and T.L. Ainsworth: Phys. Rev. **C 29** (1984) 4:1207.
- [100] R.B. Wiringa: Nucl. Phys. **A 401** (1983) 86.
- [101] R.B. Wiringa, V.G.J. Stoks, and R. Schiavilla: Phys. Rev. **C 51** (1995) 38.
- [102] W. Glöckle and H. Kamada: Phys. Rev. Lett. **71** (1993) 971.
- [103] A. Nogga: *Nuclear and Hypernuclear three- and four-body bound states* (PhD thesis, Ruhr-Universität, Bochum 2001).
- [104] J.L. Friar: Phys. Rev. **C 60** (1999) 034002.
- [105] F. Gross and A. Stadler: Phys. Rev. Lett **78** (1997) 26.
- [106] J. Fujita and H. Miyazawa: Prog. Theor. Phys. **17** (1957) 360; 366.
- [107] S.A. Coon, M.D. Scadron, P.C. McNamee, B.R. Barrett et al.: Nucl. Phys. **A 317** (1979) 242.
- [108] S.A. Coon and M.T. Peña: Phys. Rev. **C 48** (1993) 1559.
- [109] H.T. Coelho, T.K. Das and M.R. Robiloita: Phys. Rev. **C 28** (1983) 1812.

- [110] B.S. Pudliner, V.R. Pandharipande, J. Carlson and R.B. Wiringa: Phys. Rev. Lett. **74** (1995) 4396.
- [111] W. Glöckle, H. Witala, D. Huber, H. Kamada and J. Golak: Phys. Rep. **274** (1996) 109.
- [112] A. Kievsky, M. Viviani and S. Rosati: Phys. Rev. **C 64** (2001) 024002.
- [113] B. Gabioud et. al.: Phys Rev. Lett. **42** (1979) 1508.
- [114] O. Schori et. al.: Phys Rev. **C 35** (1987) 2252.
- [115] I. Šlaus, Y. Akaishi and H. Tanaka: Phys. Rep. **173** (1989) 259.
- [116] C. R. Howell et. al.: Phys. Lett. **B 444** (1998) 252.
- [117] A. Nogga, A. Kievsky,, H. Kamada, W. Glöckle, L.E. Marcucci, S. Rosati and M. Viviani: Phys. Rev. **C67** (2003) 034004.
- [118] I.R. Afnan and Y.C. Tang: Phys. Rev. **175** (1968) 1337.
- [119] A.B. Volkov: Nucl. Phys. **74** (1965) 33.
- [120] R.A. Malfliet and J.A. Tjon: Nucl. Phys. **A 127** (1969) 161.
- [121] G.L. Payne, J.L. Friar and G.F. Gibson: Phys. Rev. **C 26** (1982) 1385.
- [122] F. Ciesielski: *Systèmes à quatre corps: états liés et états de diffusion par la résolution numérique des équations de Faddeev-Yakubovski* (PhD thesis, Université Joseph Fourier, Grenoble 1997).
- [123] F. Ciesielski, J. Carbonell and C. Gignoux: Nucl. Phys. **A 631** (1998) 653c.
- [124] F. Ciesielski, J. Carbonell and C. Gignoux: Phys. Lett. **B 447** (1999) 199.
- [125] D.R. Tilley, H.R. Weller and G.M. Hale: Nucl. Phys. **A 541** (1992) 1.
- [126] A.A. Oglobin, Y.E. Penionzhkevich: *Treatise on Heavy-Ion Science (vol. 8): Nuclei Far From Stability*, Ed. D. A. Bromley (Plenum Press, New York, 1989) 261.
- [127] B.S. Pudliner, A. Smerzi, J. Carlson, V.R. Pandharipande, S.C. Pieper and D.G. Ravenhall: Phys. Rev. Lett. **76** (1996) 2416.
- [128] A.V. Belozyorov et al: Nucl. Phys. **A 477** (1988) 131.
- [129] D.V. Aleksandrov et al: Yad. Fiz **47** (1988) 3.
- [130] J.E. Ungar et al: Phys. Lett. **B 144** (1984) 131.
- [131] T.P. Gorrige et al.: Phys. Rev. **C 40** (1989) 2390.

- [132] J. Sperinde, D. Frederickson, R. Hinkis, V. Perez-Mendez and B. Smith: Phys. Lett. **32 B** (1970) 185.
- [133] A. Stetz et al.: Nucl. Phys. **A 457** (1986) 669.
- [134] Batusov et al.: Sov. J. Nucl. Phys. **7** (1968) 20.
- [135] Meyerhof and Tombrello: Nucl. Phys. **A 109** (1968) 1.
- [136] Fiarman and Meyerhof: Nucl. Phys. **A 206** (1973) 1.
- [137] Ajzenberg-Selove: Nucl. Phys. **A 490** (1988) 1.
- [138] Goldanski: Phys. Lett. **9** (1964) 184.
- [139] Wapitra, Audi and Hoekstra: Atomic Data and Nuclear Data Tables **39** (1988) 281.
- [140] R.E. Warner et al: Phys. Rev. **C 62** (2000) 024608.
- [141] Argan and Piazzoli: Phys. Lett. **4** (1963) 350.
- [142] Franzini and Radicati: Phys. Lett. **6** (1963) 322.
- [143] Schiffer and Vandenbosch: Phys. Lett. **5** (1963) 292.
- [144] K. Varga and Y. Suzuki: Phys. Rev. **C 52** (1995) 2885.
- [145] A.M. Gorbatov, P.V. Komarov, Yu.N. Krylov, A.V. Brusak, V.L. Skopich, P.Yu. Nikishov and E.A. Kolganova: Sov. J. Nucl. Phys. **50** (1989) 218.
- [146] A. Smerzi, D.G. Ravenhall and V.R. Pandharipande: Phys. Rev. **C 56** (1997) 2549.
- [147] J. Carlson, J. Morales, V.R. Pandharipande and D.G. Ravenhall: arxiv: nucl-th/0302041.
- [148] A.M. Bedalyan, T.I. Belova, N.B. Konyukhova and V.D. Efros: Yad. Fiz. **23** (1985) 1460.
- [149] S.A. Sofianos, S.A. Rakityansky and G.P. Vermaak: Phys. G. Nucl. Part. Phys. **23** (1997) 1619.
- [150] H. Witała, W. Glöckle: nucl-th/9901074.
- [151] R. Guardiola and J. Navarro: Phys. Rev. Lett: **84** (2001) 1144.
- [152] A.C. Philips: Phys. Lett. **28 B** (1969) 378; Rep. Prog. Phys. **40** (1977) 905.
- [153] H. Witała, W. Glöckle, D. Hüber, J. Golak and H. Kamada: Phys. Rev. Lett. **81** (1998) 1183
- [154] W.T.H. van Oers and K.W. Brockman: Jr. Nucl. Phys. 1 **92** (1967) 561.
- [155] J. Arvieux: Nucl. Phys. **A 221** (1974) 253.

- [156] E. Huttel, W. Arnold, H. Baumgart, H. Berg and G. Clausnitzer: Nucl. Phys. **A 406** (1983) 443.
- [157] J.A. Tjon: Phys. Lett. **56 B** (1975) 217.
- [158] T.W. Phillips, B.L. Berman and J.D. Seagrave: Phys. Rev. **C 22** (1980) 384.
- [159] T.W. Phillips, B.L. Berman and J.D. Seagrave Phys. Rev. **C 22** (1980) 2:384.
- [160] G.M. Hale, D.C. Dodder, J.D. Seagrave, B.L. Berman and T.W. Phillips. Phys. Rev. **C 42** (1990) 1:438.
- [161] F. Ciesielski, J. Carbonell and C. Gignoux: Phys. Lett. **B 447** (1999) 199.
- [162] A.C. Fonseca: Phys. Rev. Lett. **83** (1999) 4021.
- [163] E.O. Alt, P. Grassberger, W. Sandhas: Phys. Rev. **C1** (1970) 85
- [164] H. Haberzettl and W. Sandhas: Phys. Rev. **C24** (1981) 359
- [165] A.C. Fonseca: private communications.
- [166] A. C. Fonseca: Phys. Rev. **C 40** (1989) 1390.
- [167] W. Schadow, W. Sandhas, J. Haidenbauer, A. Nogga: Few-Body Systems **28** (2000) 241.
- [168] H. Kröger, W. Sandhas: Phys. Rev. Lett. **40** (1978) 834.
- [169] J.A. Tjon: Nucl. Phys. **A 353** (1981) 47.
- [170] F. Ciesielski, J. Carbonell, C. Gignoux and A.C. Fonseca: Few-Body Syst. **10** (1999) 359.
- [171] M. Viviani: Nucl. Phys. **A 631**. (1998) 111c.
- [172] M. Viviani: Few-Body Systems Suppl. **10** (1999) 363.
- [173] B. Pfitzinger, H.M. Hofmann and G.M. Hale: Phys. Rev. **C 64** (2001) 044003.
- [174] F. Ciesielski, J. Carbonell, C. Gignoux: Nucl. Phys. **A 631**. (1998) 653c.
- [175] M. Viviani, S. Rosati, A. Kievski: Phys. Rev. Lett. **81** (1998) 1580.
- [176] H.M. Hofmann private communications.
- [177] J.D. Seagrave, L. Cranberg and J.E. Simmons: Phys. Rev. **119** (1960) 1981.
- [178] J.D. Seagrave, B.L. Berman, T.W. Phillips: Phys. Lett. **91 B** (1980) 200.
- [179] S. Hammerschmied, H. Rauch, H. Clerc, U. Kishko: Z. Phys **A 302** (1981) 323.
- [180] H. Rauch, D. Tuppinger, H. Wolwitsch, T. Wroblewski: Phys. Lett. **165 B** (1985) 39.

- [181] M. Viviani: private communication.
- [182] F. Ciesielski, J. Carbonell: Phys. Rev. **C 58** (1998) 58.
- [183] I.N. Filikhin and S. Yakovlev: Physics of Atomic Nuclei **Vol. 63 No. 1** (2000) 69; Yad. Fiz. **Vol. 63 No. 1** (2000) 79.
- [184] M.T. Alley and L.D. Knutson: Phys. Rev. **C 48** (1993) 1901.
- [185] P.E. Tegnér and C. Bargholtz: Astrophys. J. **272** (1983) 311.
- [186] I.N. Filikhin and S. Yakovlev: Physics of Atomic Nuclei **Vol. 58 No. 5** (1995) 754.
- [187] McDonald et all: Phys. Rev. **133** (1964) B1178.
- [188] Famularo et all: Phys. Rev. **93** (1954) 928.
- [189] I.N. Filikhin and S. Yakovlev: Physics of Atomic Nuclei **Vol. 63 No. 1** (2000) 55; Yad. Fiz. **Vol. 63 No. 1** (2000) 63.
- [190] W. Glöckle: *The Quantum Mechanical Few-Body Problem*. (Springer-Verlag, Berlin, Heidelberg 1983)
- [191] H.M. Hofmann and G.M. Hale: nucl-th/0211008.
- [192] M. Viviani, A. Kievski and S. Rosati: AIP Conf. Proc. **334** (1995) 844.
- [193] S. Yakovlev, I.N. Filikhin: Few-Body Systems Suppl. **10** (1999) 37.
- [194] H.M. Hofmann and G.M. Hale: Nucl. Phys. **A 613** (1997) 69.
- [195] A.C. Fonseca: Nucl. Phys. **A 631** (1998) 675.
- [196] A.C. Fonseca: Few-Body Systems Suppl. **10** (1999) 367.
- [197] N.W. Schellinghout: Few-Body Syst. Suppl. **7** (1994) 361.
- [198] M.T. Alley, L.D.Knutson: Phys. Rev. **C 48** (1993) 1901.
- [199] P. La France, P. Winternitz: J. de Phys. **41** (1980) 1391.
- [200] J. Bistricky, F. Lehar, P. Winternitz: J. de Phys. **39** (1978) 1.
- [201] J. Carbonell and C. Gignoux: Few-Body Systems, Supplementum **7** (1994) 270.
- [202] J. Carbonell, C. Gignoux, and S.P. Merkuriev: Few-Body Systems, Supplementum **6** (1993) 298.
- [203] C.R. Chen, G.L. Payne, J.L. Friar, and B.F. Gibson: Phys. Rev. **C 31** (1985) 2266.
- [204] C.R. Chen, G.L. Payne, J.L. Friar, and B.F. Gibson: Phys. Rev. **C 33** (1986) 1740.

- [205] C.R. Chen, G.L. Payne, J.L. Friar, and B.F. Gibson: Phys. Rev. **C 39** (1989) 1261.
- [206] J.L. Friar, B.F. Gibson, and G.L. Payne: Phys. Rev. **C 22** (1980) 284.
- [207] J.L. Friar, B.F. Gibson, and G.L. Payne: Phys. Rev. **C 36** (1987) 1140.
- [208] J.L. Friar, B.F. Gibson, and G.L. Payne: Phys. Rev. **C 37** (1988) 2869.
- [209] J.L. Friar, G.L. Payne, V.G.J. Stoks, and J.J. de Swart: Phys. Lett. **B 311** (1993) 4.
- [210] W. Glöckle: Z. Phys. **271** (1974) 31.
- [211] W. Glöckle and G.L. Payne: Phys. Rev. **C 45** (1992) 974.
- [212] H. Kamada and W. Glöckle: Nucl. Phys. **A 548** (1992) 205.
- [213] L.P. Kok and N.W. Schellingerhout: Few-Body Systems **11** (1991) 99.
- [214] Z.C. Kuruoglu and F.S. Levin (1987): Asymptotic boundary conditions for three-body breakup: Probable nonutility of the standard approach, Phys. Rev. **C 36** 49.
- [215] A. Laverne and C. Gignoux: Nucl. Phys. **A 203** (1973) 597.
- [216] R.A. Malfliet and J.A. Tjon : (1972), Three-nucleon ground state properties for realistic local and non-local nucleon{nucleon interactions, in Few particle problems in the nuclear interaction. Proceedings of the International Conference on Few Particle Problems in the Nuclear Interaction (Los Angeles, August 28{September 1, 1972), edited by I. Slaus, S.A. Moszkowski, R.P. Haddock, and W.T.H. van Oers (North-Holland Publishing Company, Amsterdam), pp. 441.
- [217] S.P. Merkuriev, C. Gignoux and A. Laverne: Three-body scattering in configuration space, Ann. Phys. (N.Y.) **99** (1976) 30.
- [218] V.V. Kostrykin, A.A. Kvitsinskii and S.P. Merkuriev: Few-Body Systems **6** (1989) 97.
- [219] Yu.A. Kuperin, S.P. Merkuriev, and A.A. Kvitsinskii: Elastic scattering and disintegration of the pd system, Yad. Fiz. **37** (1983) 1440 [Sov. J. Nucl. Phys. 37 (1983) 857].
- [220] B.S. Pudliner et al: Phys. Rev. **C56** (1997) 1720.
- [221] D. Hüber, H. Witała, A. Nogga, W. Glöckle and H. Kamada: Few-Body Syst **22** (1997) 107
- [222] H. Witała et al: Phys. Rev. Lett. **81** (1998) 1183.
- [223] P. Grangé, A. Lejeune, M. Martzolff, J.-F. Mathiot: Phys. Rev. **C40** (1989) 1040
- [224] R.F. Lebed: nucl-th/9809093.
- [225] E. Epelbaum: *The Nucleon-Nucleon Interaction in a Chiral Effective Field Theory* (PhD thesis, Ruhr-Universität, Bochum 2000).

- [226] R. Bukowski, R. Jeziorski, B. Mozynski and W. Kołos: Int. J. quant. Chem. **42** (1992) 287.
- [227] H.B.G. Casimir, D. Polder: Phys. Rev. **73** (1948) 360.
- [228] C. Cohen-Tannoudji, J. Dupont-Roc, G. Grynberg: *Processus d'interaction entre photons et atomes* (InterEditions CNRS, 1988) 119.

Abstract

In this thesis quantum mechanical non-relativistic few-body problem is discussed. Basing on fundamentals ideas of Faddeev and Yakubovski three and four body equations are formulated and solved for fermionic atomic and nuclear systems. Former equations are modified to include long range interactions. Original results for nuclear and molecular physics were obtained :

- Positively charged particle scattering on Hydrogen atoms was considered. Predictions for π^+ -H, μ^+ -H and p^+ -H scattering lengths were given. Existence of an unknown, very weakly bound H_2^+ bound state was predicted.
- Motivated by the possible observation of bound four neutron structure at GANIL we have studied compatibility of such an existence within the current nuclear interaction models.
- 4 nucleon scattering at low energies was investigated. Obtained results for n-³H, p-³H and p-³He systems were compared with the experimental data. Validity of realistic nucleon-nucleon interaction models is questioned.

Keywords: Few-body, four body, scattering, Coulomb scattering, bound states, resonant states, tetraneutron, hydrogen molecular ion

Résumé

Cette thèse est consacrée à l'étude numérique de systèmes quantiques non-relativistes à trois et quatre particules.

Les équations de Faddeev-Yakubovski ont été modifiées pour pouvoir inclure les interactions à longue portée et ont été appliquées à l' étude des nombreux systèmes physiques. Des résultats originaux ont été obtenus pour les systèmes nucléaires et moléculaires :

- Dans le cadre de la physique moléculaire, la diffusion des particules chargées sur les atomes d'hydrogène a été étudiée. Les longueurs de diffusion pour les systèmes π^+ -H, μ^+ -H et p^+ -H ont été prédites. L'existence d'un nouvel état, très faiblement lié de l'ion moléculaire H_2^+ a été prédit.
- Suite à l'annonce d'une possible mise en évidence expérimentale du tetraneutron (état lié à 4 neutrons) au GANIL, nous avons étudié la compatibilité d'une telle existence avec nos connaissances des forces neutron-neutron.
- La diffusion des systèmes à 4 nucléons (n-³H, p-³H et p-³He) à basse énergie a été examinée. Les résultats sont comparés aux résultats expérimentaux. La validité des potentiels nucléon-nucléon a ainsi été remise en cause.

Mots-clés: Few-body, quatre corps, diffusion, diffusion Coulombienne, états liés, états de resonance, tetraneutron, ion moléculaire d'hydrogène